On the performance of fuel cell supercapacitor hybrid propulsion system for city bus use

Wei Wu

A thesis submitted for the degree of Doctor of Philosophy

Department of Mechanical Engineering
University College London

2018

Statement of originality

I, Wei Wu confirm that the work presented in this thesis is my own. Where information has been derived from other sources, I confirm that this has been indicated in the thesis.

Wei Wu
University College London

Date:

Signed:

Abstract

Fuel Cell (FC) buses have been developed as a long term zero emission solution for city transportation and they have now reached levels of maturity to supplement the coming London 2020 Ultra Low Emission Zone implementation. A critical review of previous research in this field has highlighted promising potential for FC technologies applied to bus applications and also identified the associated challenges.

This research analysed the current FC bus industry and addressed the most recent trend of applying FCs with hybrid technologies for city buses. This research developed a scaled laboratory Fuel Cell and Supercapacitor hybrid drivetrain model for investigating the design and performance of a low emission propulsion systems for city bus applications in its dynamic environment. The laboratory system has been used to validate a computer model to ensure it is suitably representative of practical and full sized FC bus power systems. A novel hybrid control strategy was developed for a FC hybrid system and evaluated with actual bus driving cycles. The power balancing strategy between multiple power sources in the FC hybrid system has been explored and investigated.

The key finding of this research is that hybridising the FC with an energy storage medium showed superior performance over FC only system. Additionally, existing FC hybrid buses generally have an over-sized FC on-board which significantly increases the capital cost. A series of steps have been identified to determine the required FC / energy storage degree of hybridisation. An optimised degree of hybridisation for FC hybrid bus can potentially improve the system performance, reduce the size of the FC on-board and propulsion system costs.

Impact statement

This research investigates the application of Fuel Cell (FC) hybrid city bus to deliver a potential zero emission solution for city bus. This research analyses the current FC bus industry and highlights the potentials and challenges associated with FCs. This research provides a depth analysis of the characteristics of the FC and investigates a suitable strategy to integrate FC hybrid technology for city bus use. The findings of this research can be used for FC bus design and development.

The novel contribution of this research is the proposition of two FC / Supercapacitor hybrid operation strategies aimed at tackling the challenges addressed for the current FC bus industry. Both strategies have been compared and demonstrated with dynamic driving cycles collected from practical buses. Advantages and disadvantages of the two operation strategies have been summarised and the more appropriate strategy has been recommended.

A computer model has been developed to determine the required degree of hybridisation between the FC and Supercapacitor with the aid of a laboratory test bench. Further optimisation strategy on the identified degree of hybridisation has also been considered as a list recommended steps. The optimised degree of hybridisation holds the promise of extending FC life, downsizing power systems and improving overall efficiency.

Dedications

To my parents,

Wu Dao Fan and Zhang Xiao Rong,

Who have offered me unconditional love and support.

Acknowledgements

First of all, my supervisor Prof Richard Bucknall who have supported my academic research and offered me valuable opportunities to engage in engineering world. He taught the importance of independent thinking and problem solving to me who still thought learning was about teacher telling what to do when I first started this PhD. This will accompany me to whatever engineering path I am going to take in the future.

Dr Julius Partridge, who spent almost every day with me for the past three years in the underground laboratory running experiments, testing components, wiring cables, drilling screws and doing all the hard work. I am proud to say that we made this laboratory.

David Ashmore and Cedrick Lin who also worked in the HyFCap project. Their works on the data collection and analysis played an important role for this research, and more importantly, they supplied a London bus.

Dr Adam Wojcik, who is my second supervisor, he supported me throughout my transfer exam and gave me important feedbacks for my research. David Yorke from London Tower transit for arranging three RV1 FC bus workshop visits for me and answering all my email questions.

Dr Christopher Nightingale for giving up his own time to discuss ideas and answer questions. The technical team from UCL mechanical main workshop, particularly Peter, Kee and Phil for their recommendations on the laboratory mechanical design work.

Thanks to the PhD examiners Prof Nick Tyler and Prof Hua Zhao for their additional comments and recommendations that have helped improve this thesis. Konrad Yearwood for reviewing my research, contributing ideas and proof reading this thesis.

Last but not least, my wife Min Liu, for her consistent support and homemade Chinese food for the past four years of this PhD; and small Dou-Ya, the latecomer to the party.

Contents

List of figures

List of tables

Nomenclature

A	PEMFC active area	(cm^2)
B	Parametric constant based on cell type	(-)
C	Capacitance of a SuperCapacitor	(F)
C_{O2}	Concentration of oxygen in catalytic interface	(ppm)
C_{tire}	Circumference of tyre	(m)
E	Energy stored	(J)
E_{nernst}	Nernst voltage	(V)
I	Current	(A)
I_{dc}	Direct current	(A)
I_{ac}	Alternating current	(A)
I_{fc_in}	Output current from the FC	(A)
I_{fc_out}	Output current after the FC boost converter	(A)
I_{sc_in}	Output current from the SC	(A)
I_{sc_out}	Output current after the SC buck/boost converter	(A)
I_{load}	Current in/out of the load simulation system	(A)
J	Current density	(A/cm^2)
l	Membrane thickness of PEMFC membrane	(cm)
L	Inductance	(H)
m	Mass	(kg)
n	Number of electrons per molecule of hydrogen	(-)
N_{avg}	Number of molecules per mole	(molecules/mol)
P	Power	(W)
P_{FC}	Power of the FC and boost converter	(W)
P_{H2}	Partial pressure of hydrogen	(atm)
P_{load}	Power of the load	(W)
P_{mech}	Motor mechanical power	(W)
P_{O2}	Partial pressure of oxygen	(atm)
P_{SC}	Power of the SC and buck/boost converter	(W)

q	Stored charge in an energy storage	(C)
q_{e1}	Charge of one electron	(C)
R	Resistance	(Ω)
R_c	Resistivity to the transfer of electrons	(Ω)
R_m	Equivalent resistance of membrane	(Ω)
$R_{variable}$	Resistance of the variable resistor	(Ω)
SoC	Percentage of charge left in the energy storage	(%)
t	Time	(s)
T	FC cell temperature	(K)
T_{mech}	Motor mechanical torque	(Nm)
v	Bus speed	(miles/hour)
v_{motor}	Motor speed	(rad/s)
V	Voltage	(V)
V_{act}	Activation loss of a PEMFC	(V)
V_{conc}	Concentration loss of a PEMFC	(V)
V_{fc_in}	Output voltage from the FC	(V)
V_{fc_out}	Output voltage after the FC boost converter	(V)
V_{load}	Voltage applied on the load simulation system	(V)
V_{ohmic}	Ohmic loss of a PEMFC	(V)
$V_{open\ circuit}$	Open circuit voltage of FCs	(V)
V_{sc_in}	Output voltage from the SC	(V)
V_{sc_out}	Output voltage after the SC buck/boost converter	(V)
ρ_m	Membrane-specific resistivity to the flow of protons	(Ω/cm)
η	Efficiency	(%)
ΔG_{H2O}	Gibbs free energy for water	(kj/mol)
ΔH_{LHV}	Absolute lower heating values of hydrogen	(kj/mol)
ΔH_{HHV}	Absolute higher heating values of hydrogen	(kj/mol)
ΔS	Change of entropy	(J/K)

Abbreviations

AC	Alternating Current
AFC	Alkaline Fuel Cell
AI	Artificial Intelligence
CAES	Compressed Air Energy Storage
CHIC	Clean Hydrogen in European Cities
CH_3OH	Methanol
CO	Carbon Oxygen
CO_2	Carbon Dioxide
CUTE	Clean Urban Transport for Europe
DC	Direct Current
DfT	Department for Transport
DI water	De-ionised Water
DMFC	Direct Methanol Fuel Cell
Dyno	Dynamometer
ECMS	Equivalent Consumption Minimisation Strategy
EPSRC	Engineering and Physical Sciences Research Council
ES	Energy Storage
ESR	Equivalent Series Resistance
ETC	European Transit Cycle
FC	Fuel Cell
FCH JU	The Fuel Cells and Hydrogen Joint Undertaking
FCPM	Fuel Cell Power Module
FES	Flywheel Energy Storage
HEV	Hybrid Electric Vehicle
HHV	Higher Heating Value
HPES	Hydro Pumped Energy Storage
Hybrid	Electric hybrid

HyFCap	Reducing the cost and prolonging the durability of Hydrogen Fuel Cell systems by in-situ hydrogen Purification and technology Hybridisation
H_2	Hydrogen
ICE	Internal Combustion Engine
JIVE	Joint Initiative for Hydrogen Vehicles across Europe
LEV	Low Emission Zone
LHV	Lower Heating Value
Li-ion	Lithium-ion
MCFC	Molten Carbonate Fuel Cell
NEDC	New European Drive Cycle
Ni	Nickel
Ni-MH	Nickel-Metal Hydride Battery
NO_x	Nitrogen Oxide
NO_2	Nitrogen Dioxide
O_2	Oxygen
PAFC	Phosphoric Acid Fuel Cell
PEMFC	Proton Exchange Membrane Fuel Cell
PHEV	Plug-in Hybrid Electric Vehicle
PM	Particulate Matter
Pot	Potentiometer
PSCAD	Power Systems Computer Aided Design
PSU	Power Supply Unit
Pt	Platinum
RD&D	Research, Development and Demonstration
REEV	Range Extender Electric Vehicle
SC	Supercapacitor
SCR	Selective Catalytic Reduction
SMES	Superconducting Magnetic Energy Storage
SoC	State Of Charge
SOFC	Solid Oxide Fuel Cell
TfL	Transport for London
ULEZ	Ultra Low Emission Zone

Chapter 1 Introduction

1.1 Research motivation

1.1.1 Background

Air pollution, as one of the main causes of global warming and urban public health threats, has been raised as a global priority issue [1.1] [1.2]. The EU has restrictive rules on air pollution quality controls and Britain has been struggling to meet the EU air quality limit [1.3]. Britain failed to meet EU limits in 2010 and has admitted that London cannot achieve this limit until 2025 [1.4] [1.5]. The city of London has some of the worst air quality in the UK [1.5]. The UK Department for Environment Food & Rural Affairs air quality assessment 2013 showed that the London city area has exceeded the limit levels of all Nitrogen Dioxide (NO_2), Particulate Matter 2.5 ($PM_{2.5}$), and Carbon Dioxide (CO_2) emissions [1.6]. Additionally, NO_2 emissions exhibit the worst performance exceeding the EU standard by 50% in some parts of London [1.6]. The Transport for London (TfL) *Transport Emission Roadmap Report 2014* indicated that London's transport is a key contributor to several emission types [1.7] [1.8]. 21% of CO_2 emissions, 63% of NOx emissions and 52% of PM emissions are from transportation activities in London as a result of large scale transportation demands [1.7] [1.8]. The Greater London Authority has been taking actions to mitigate these emissions and introduced the London Low Emission Zone (LEZ) in 2008 as part of their strategy [1.9]. The LEZ is a traffic pollution charge scheme to limit the tailpipe emissions of vehicles operating in London. Vehicles operating in the LEZ must pay charges if they fail to meet the emission standard in London, as Figure 1.1 shows, and is enforced at all times [1.3] [1.8]. One of the main purposes of the LEZ is to reduce the pollution of diesel powered vehicles in central London which is the main source of NO_x emissions [1.8] [1.10].

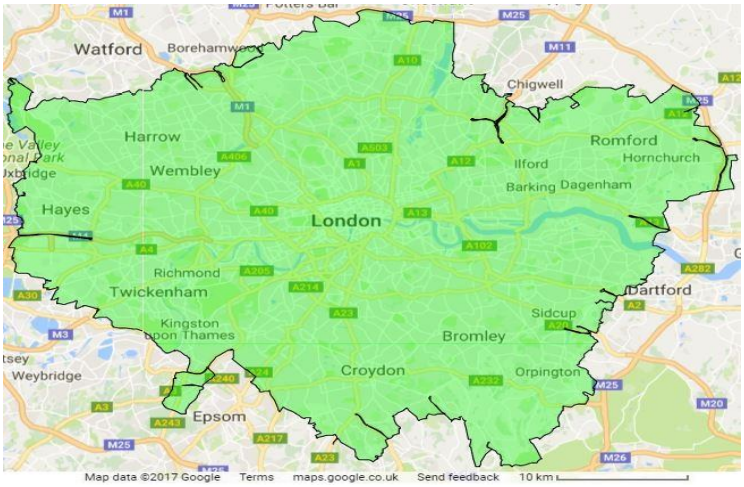

Figure 1.1 LEZ area in London (TfL, 2016)

Urban transportation in London can be divided into two main types: commercial/private vehicles and public transportation. This research will focus on the public transportation aspect. To meet the LEZ standards, TfL has taken emission control actions through different approaches from the public transportation perspective [1.3] [1.6] [1.11]. The public transportation network (bus, tube, rail, taxi) has been improved to be "greener" [1.11]. A detailed action report can be found in the *TfL Transport Emissions Roadmap 2014* [1.7]. Although the implementation of the LEZ has reduced emissions in London, London's air quality is still below the EU standards [1.4] [1.5]. The mayor of London confirmed that a more restricted emission control zone known as the Ultra Low Emission Zone (ULEZ) is to be implemented in 2020 [1.12]. The ULEZ will be a much smaller area compared with the LEZ and it contains some of the areas in London with worst air quality as Figure 1.2 shows [1.10]. The full implementation of the ULEZ is expected to halve emissions of NO_x and should allow 80% of Central London to meet the EU standard [1.12] [1.13] [1.14]. The ULEZ will be located in the transportation Zone 1 of Central London, where public transportation play an important role. Upgrading the public transportation bus fleet could therefore be particularly important for the ULEZ implementation.

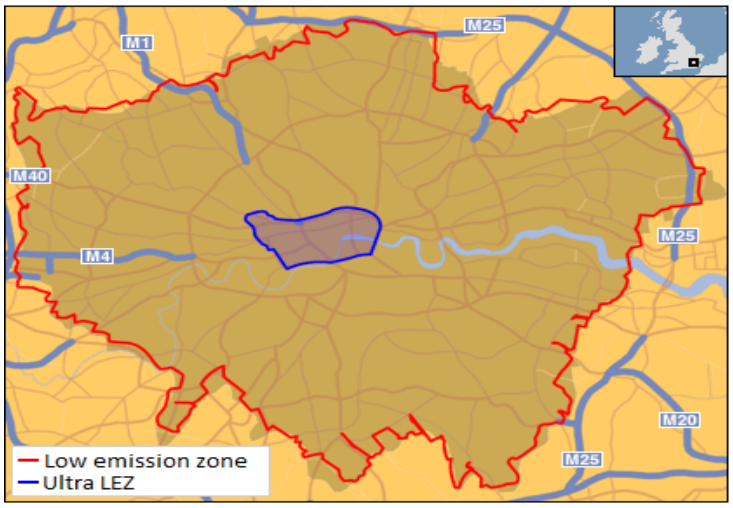

Figure 1.2 ULEZ area in central London (TfL, 2015)

This research will focus on the impact of the bus fleets because London is one of the busiest cities in the world and has an extensive bus transportation network managed by TfL. There are around 7,500 buses providing a total of six million passenger journeys on different routes operating in London each weekday and a significant proportion operate in the ULEZ [1.15] [1.16]. The *London Transport Committee Report 2013* [1.15] showed that bus passenger journeys have grown by 64% from 2000 to 2013 and the demand is expected to continue to rise. Currently the majority of buses operating in the Greater London area rely heavily on diesel engines, which produces

a significant amount of harmful emissions [1.17]. The current diesel powered bus fleet in London would be unable to meet the ULEZ requirement [1.18]. Therefore the transformation of the London's diesel powered buses to buses using a cleaner power source would be a significant factor in realistically achieving the ULEZ requirements.

TfL has implemented measures to improve the bus fleet with the key goal of reducing harmful emissions [1.4]. A major action is the London Hybrid Bus Programme which aims to transform the conventional London diesel bus fleet into a fleet of diesel electric hybrid buses. This transformation programme will be discussed in detail in Chapter 2. The hybrid bus project was set up with the main goal being to cut harmful emissions in the city by 30% [1.19]. The hybrid bus solution has potential to help realise the implementation of the ULEZ. However, these buses will still rely on conventional diesel engine propulsion and as a result continue producing harmful emissions. TfL has also been looking at ultra-low emission buses as a long term solution which leads to the, so called, zero emission bus. Various clean energy bus projects have been carried out in London such as Fuel Cell (FC) buses, bio-fuel buses and wireless charging electric buses [1.19]. With respect to TfL's ULEZ package, the key element for the ULEZ implementation on buses would be the replacement of all diesel only powered double decker buses with diesel electric hybrid buses and to replace all single decker buses with zero emission buses [1.20]. This research will discuss the role that FCs could play in providing a solution for city transportation emissions issues and supporting the ULEZ implementation. Hydrogen and FC applications have the potential to meet the ULEZ requirements and also opens the path to create a future "Zero Emission Zone" as a long term solution for city pollution [1.5].

1.1.2 HyFCap project

What is HyFCap project?

FCs offer a number of advantages for transportation systems and hold the promise of high efficiency and zero harmful emissions. However, these are not yet economically competitive with conventional power systems [1.21] [1.22] [1.23]. The HyFCap project seeks to explore the next generation of FC hybrid vehicle technology with lower cost and higher efficiency as a more viable solution, potentially for the first-ever double decker FC bus [1.24]. The project title of HyFCap Project is Reducing the Cost and Prolonging the Durability of Hydrogen Fuel Cell Systems by in-situ Hydrogen purification and Technology Hybridisation. The HyFCap is a four year project funded by the EPSRC (Engineering and Physical Sciences Research Council, grant number:

EP/K021192/1) and jointly carried out by University College London (UCL) and University of Sheffield. The project started in November 2013 and is expected to end in March 2018.

The Project has been divided into four main Work Packages (WP). WP1 is the development of low cost in-situ hydrogen purification systems with high hydrogen flux for the anode and high oxygen flux for the cathode of a FC which will be carried out by the UCL's Chemistry Department, led by Prof Z. Xiao Guo. WP2 is the development of a mixed ionic liquid based Supercapacitor (SC) to operate in the region of 60℃ to 80℃ specifically designed for FC vehicles which will be carried out by University of Sheffield's Chemical and Biological Engineering Department, led by Prof Peter Hall. WP3 is the investigation of the optimum hybridisation integration of FC and SC in buses by developing models which will be carried out by UCL's Mechanical Engineering Department, led by Prof Richard Bucknall. WP4 is the analysis and specification of a full set of system requirements that the FC/SC technology would have to meet for the application and integration with actual bus profiles which will be carried out by UCL's Civil Engineering Department, led by Prof Nick Tyler [1.24]. Those four WPs work towards the same overall goal from four different but supporting perspectives: Hydrogen purification, energy storage optimisation, power hybridisation and bus system integration.

The project seeks to address the next generation of FC bus systems by:

1. Development of in-situ hydrogen purifiers using highly selective and high permittivity solid-sorbent membranes, to prolong the lifetime of the FC.
2. Development of an improved pouch-style SC based on the optimal combination of ionic liquids specifically for FC bus operation.
3. Investigation of the optimum hybridisation of the FC with SCs, to reduce the transient power demand for FC power capacity and increase efficiency.
4. Specification of the requirements that this FC hybrid technology would have to meet for system integration and understand the viability of this technology [1.24] [1.25].

The expected outcome of the HyFCap Project is a novel FC hybrid bus system design with optimised hydrogen purification, improved energy storage and system hybridisation ready for integration into practical buses which will potentially lead to an efficient, low-cost and low-carbon footprint FC bus system.

Contribution of this research to the HyFCap

This research has contributed to WP3 of the HyFCap Project which is to explore the potential of a more efficient and economic FC hybrid propulsion system. WP3 has been proposed to work as an interlinking package for the other three WPs. WP3 is investigating the integration of FC and SC from a power system perspective, which interlinks the work from WP1 (FC), WP2 (SC) and WP4 (driving cycle).

WP3 has been divided into the following five sub-tasks [1.24]:

1. Task 3.1 to collect and deliver demand profiling data sets and system design.
2. Task 3.2 to deliver an integrated laboratory FC testing platform.
3. Task 3.3 to deliver a software simulation of the integrated test platform.
4. Task 3.4 to deliver an optimised hybrid propulsion control system design.
5. Task 3.5 to carry out performance evaluation.

As part of the HyFCap Project, this research will mainly focus on sub-task 3.2-3.5. The overall goal of tasks 3.2-3.5 is the development of a scaled FC hybrid test platform with both laboratory system and simulated model. The test platform can be used to investigate FC hybrid system performance and identify the method to select the optimised hybridisation and control strategy with potential benefits in terms of cost, efficiency and control. The developed scaled hybrid system allows exploration of the way in which the FC and other power packs can be combined to provide improved overall efficiency, specifically for city bus applications.

A FC laboratory has been developed at UCL which includes a FC power unit and load banks. This research will enhance this FC facility with the addition of a hybrid propulsion system to enable the study of a scaled hybrid bus system configuration. The enhanced model can be used to study the characteristics of the FC hybrid system and test the energy storage to collaborate with WP2 and the model will eventually be evaluated using real bus data from WP4. Therefore, the focus of this research is to build, simulate, evaluate and optimise a FC hybrid propulsion system to allow the study of FC hybridisation for city bus applications.

1.2 Research aims

This research aims to explore the potential of FCs for bus application by developing an optimised laboratory scaled FC hybrid propulsion platform. Hybridising the FC propulsion unit with an energy reservoir could potentially reduce transient power demand applied on the FC which allows efficiency optimisation. Energy storage can satisfy transient peak power demands and exploit regenerative braking energy recovery. This research will address the challenges that need to be solved within the two critical issues: To reduce the FC power requirement through hybrid configuration and to increase efficiency through an optimised control algorithm. The research aims are summarised as follows:

1. Undertake a literature based investigation into available low emission bus technologies focusing on the role that FCs can play in public transport, specifically buses. Provide a critical review of existing literature on FC hybrid bus development to identify the key research challenges.

2. Construct a laboratory scaled FC hybrid platform which is capable of examining FC and energy storage performance. The results obtained from the platform can be used to explore the characteristics of the FC operating as a city bus power source.

3. Simulate the constructed laboratory FC hybrid system through computational modelling and use the laboratory obtained results to validate and verify the model such that the computer model can sufficiently represent the practical system in the laboratory.

4. Evaluate the FC hybrid system model using actual drive cycle data provided by practical buses and investigate any implications and consequences resulting from a system with a downsized FC as the main power source.

5. Identify the method to size the energy storage system for a hybrid system with downsized FC. Explore the method to optimise the FC/energy storage degree of hybridisation for a FC hybrid bus application and support the FC bus power system design through provision of power source integration recommendations for the HyFCap project.

1.3 Thesis outline

This thesis is divided into the following 7 chapters:

Chapter 1 Introduction This chapter provides an introduction to the research project and the motivation behind the research undertaken. The contributions of this research have also been presented.

Chapter 2 Literature review This chapter provides a comprehensive review of related work and general background knowledge of low emission bus technologies and FC system development. A critical review focusing on FC hybrid bus development has been provided.

Chapter 3 Problem formulation This chapter addresses the main research question to be answered through this research. Analysis has been provided to explain how the system that will be developed can contribute to and justify the research question.

Chapter 4 Laboratory system development This chapter describes the construction of a laboratory based FC hybrid system representing the power system of a scaled FC hybrid bus. Experiments have been carried out to gain a better understanding of the characteristics of FCs.

Chapter 5 Computer system modelling This chapter develops a computer model based on the laboratory system. The laboratory obtained results will be used to validate and verify the computer model. Comparison studies between measured laboratory data and simulated data will be made to demonstrate the accuracy of the computer model.

Chapter 6 System optimisation This chapter evaluates the validated model with actual drive cycles to examine the operating strategy of the FC hybrid system for city bus applications. The chapter then investigates the potential for downsizing the FC and explores the method to optimise the degree of hybridisation in a FC hybrid bus.

Chapter 7 Conclusion and further work This chapter summarises the key research findings to the identified research question and presents a general conclusion. This chapter also details specific recommendations for the HyFCap project. Future work has also been discussed in this chapter.

1.4 Research contributions

The author claims the following contributions throughout this research:

1. **Identification of current FC bus industry challenges and trends**
   This research has identified the trend of the current FC bus industry and used laboratory systems to investigate the reasons behind the trends of replacing FC only powered buses with hybrids.
2. **Development of a model and method to identify the degree of hybridisation in a FC hybrid bus system**
   This research developed and validated a computer model that is capable of identifying the degree of hybridisation in a FC hybrid bus system. The method to determine the FC size and energy storage size has been proposed and demonstrated with actual bus collected driving cycle.
3. **Recommendations on the proposed downsized FC operation**
   This research demonstrated the potential for a downsized FC in a FC hybrid bus and showed promising results compared with existing FC hybrid bus systems. Recommendations have been made on sizing the FC for a certain driving cycle.
4. **Recommendations on selection and sizing of the energy storage system for a FC hybrid bus**
   This research reviewed different energy storage systems and recommended the most appropriate option specifically for the FC bus application. The method to size the energy storage has also been presented and tested in the model.
5. **Proposition of two FC/energy storage operation strategies**
   This research proposed two hybrid system operation strategies specifically for FC hybrid buses considering the unique characteristics of FCs. Both strategies have been compared and showed different performance for various driving cycles.
6. **Recommendations on the degree of hybridisation optimisation**
   This research contributed a series of recommended steps to undertake in the identification and optimisation of the degree of hybridisation for any other route that could be used by the HyFCap project. The optimised degree of hybridisation holds the promise of extending FC life, downsizing power systems and improving overall efficiency.

1.5 Contributions to the literature

During the course of this research the following academic papers have been published.

Journal article:

W Wu, J Partridge, R Bucknall, 2018, Stabilised fuel cell output control strategy of proton exchange membrane fuel cell and supercapacitor hybrid propulsion system for city bus application, International Journal of Hydrogen Energy. (submitted)

Book chapter:

J Partridge, W Wu, R Bucknall, 2017, Chapter 2: Development of bus drive technology towards zero emissions: a review. In *Hybrid Electric Vehicles*, Intech press, ISBN 978-953-51-3298-1.

Conference papers:

W Wu, J Partridge, R Bucknall, 2016, Development and modelling of a lab scaled PEM Fuel Cell drive system for city driving application, International Universities Power Engineering Conference, Coimbra, Portugal, DOI: 10.1109/UPEC.2016.8114036.

W Wu, R Bucknall, 2014, Downsizing Fuel Cell capacity in a hydrogen vehicle by regenerative energy capture with Super Capacitor, International Universities Power Engineering Conference, Cluj-napoca, Romania, DOI: 10.1109/UPEC.2014.6934621.

W Wu, R Bucknall, 2013, Conceptual evaluation of a Fuel Cell hybrid powered bus, International Universities Power Engineering Conference, Dublin, Ireland, DOI: 10.1109/UPEC.2013.6714968.

Chapter 2 Literature review

2.1 Introduction

This chapter provides a literature review to furnish the reader with background context of appropriate areas and undertakes an outline review of related aspects of the research. The literature review methodology is mainly based on a search-selection-description strategy. Searches of relevant resources were mostly conducted using UCL's Explore online including Web of science database in the area of mechanical and electrical engineering sciences. The database was searched focusing mainly on works from 2007 to 2017. The Google Scholar search engine was also used to carry out more general searches for peer-reviewed journal articles. Google's search engine was also used, but mainly for industrial and project reports. The selection process included a detailed examination of search results and the selection criteria was mainly based on using journal articles, academic books, industrial reports and government publications. The exclusion criteria was mainly for the works that were insufficiently or ambiguously described or not clearly referenced. The selected works are described in this chapter. The review can be divided into two sections:

1. The aim of the first section is to provide a review of the technologies used in this research and intended to develop an understanding of how and why FC systems can be used for bus applications. This section includes reviews of current London buses, low emission bus propulsion systems, FC systems and energy storage systems. Also included is a comprehensive review of relevant technologies focused on facts that have already been generally established.
2. The aim of the second section is to provide a critical review specifically for the development of FC buses built upon the findings of previous experiments and investigations. This section reviews the methods, findings and conclusions of other research work carried out on FC vehicles. This section will focus on the variety of findings from research carried out in the field.

2.2 London buses

2.2.1 Statistical review

The first motor-powered London buses were introduced in the 1900s and began to be managed by The London General Omnibus Company in 1933 [2.2.1]. After nearly a century of operation, the red London buses have now become a famous iconic image of London as one of the most recognisable British designs in the world. The transport network of London must be analysed separately from the rest of England because it is large and complex enough to provide a basis for viable and representative analysis. Additionally, the transport regulations are also different between London and the rest of England. Transport for London is able to regulate buses in London while no other area has that authority [2.2.2].

The British Department for Transport has been carrying out studies on the London transport operation statistics. The annual bus statistics 2015 report [2.2.2] indicates that there are currently 9,600 buses operating in the Great London area and 26,200 buses operating outside London in England. Although only 36% of buses operating in England are in the London area, London's buses are actually providing over half of the total of England's passenger bus use. A comparison of passenger bus journeys within London and the rest of England from 1983 to 2015 have been plotted in Figure 2.1. The plot shows that London bus use has increased from 1,041 to 2,364 million passenger journey on bus service since 1983 [2.2.2]. On the other hand, the bus use for England excluding London has dropped from 3,596 to 2,284 million passenger bus journey [2.2.2]. Since 2012 there are more bus passenger journeys in London than the rest of England combined including both metropolitan and non-metropolitan areas. The falling number passenger journeys on bus services in London since 2016 is due to more investment in walking and cycling facilities [2.2.2].

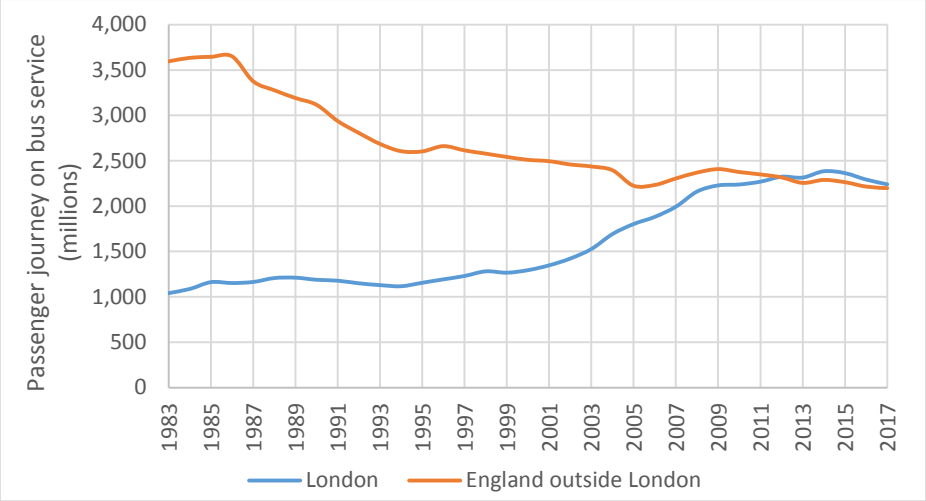

Figure 2.1 Local bus passenger journeys in London and rest of England (Data from DfT public service vehicle survey, TfL 2017) [2.2.2]

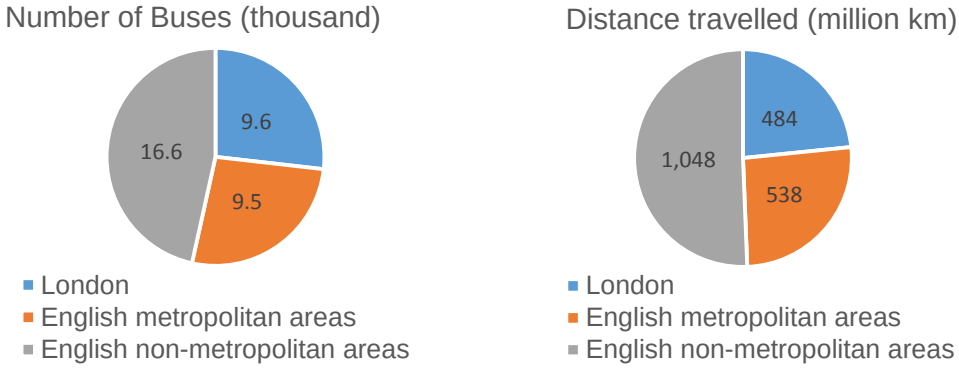

Figure 2.2 Proportion of bus and distance travelled between London and English metro/non-metro areas (Data from DfT public service vehicle survey, TfL 2017) [2.2.2]

Figure 2.2 shows two pie charts of the number of buses and distance travelled comparing London and the rest of England. The number of buses in London are around 30% of the total buses in England including both metropolitan and non-metropolitan areas. It can also be seen from Figure 2.2 that of the total metropolitan fleet over 50% operate in London. The TfL bus report 2016 [2.2.3] shows the buses in London had been scheduled to operate a total of 506.7 million km in 2015/16 and 97.2% of the scheduled operation was completed. The latest TfL study indicates London's buses already account for more than half of all public transport use by London's residents as Figure 2.3 shows. The London bus network has become the single largest road transportation network in the UK in terms of passenger numbers and plays an essential role for the residents of and visitors to London [2.2.4].

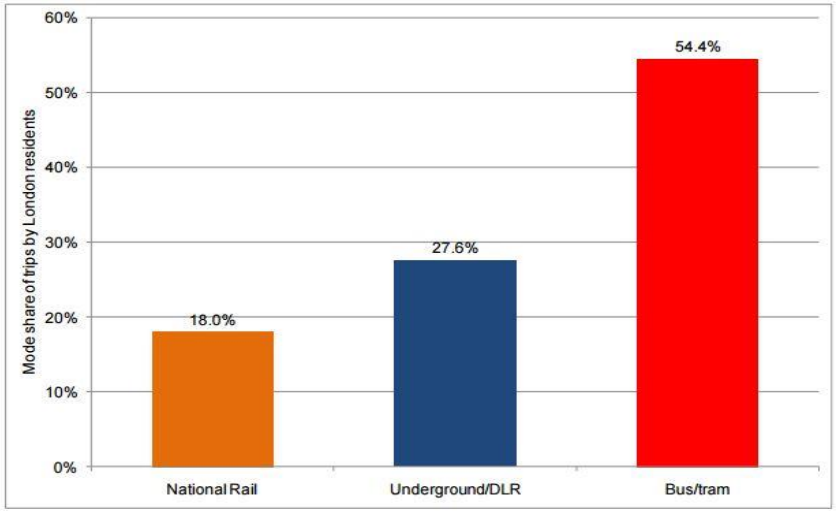

Figure 2.3 Public transportation usage by London residents (Figure from TfL 2016) [2.2.4]

2.2.2 Environmental impact

The harmful emissions from heavy traffic in a city not only contain greenhouse gases contributing to climate change, but can also affect human physical health and well-being significantly in cities like London. The UK government has acknowledged the seriousness of the city pollution issue and have introduced several measurements to help mitigate the impact of road traffic on the environment for decades.

TfL has set a target to reduce CO_2 grams per passenger kilometre by 20% by 2017/18. Public transportation modes generally have a higher passenger capacity per vehicle and thus produce less CO_2 emissions per passenger when compared with cars [2.2.5]. London underground and surface buses are two of the largest contributors of carbon emissions [2.2.5] in the public transport sector. Bus operation has a higher CO_2 emission per passenger due to the much smaller passenger carrying capacity per vehicle compared with underground trains. Although significant progress has been made in meeting overall CO_2 emission reduction requirements through restrictive emission control rules and the low emission zones, the carbon emissions from London's public transportation have been increasing each year over the past decade due to increasing demand [2.2.5-2.2.7]. The TfL health and environment report 2015 summarised that the total CO_2 emission associated with all public transport activities (TfL activities) are 2.2 million tonnes, which is a 2% increase when compared to the 2.13 million tonnes in 2013/14 [2.2.5]. Figure 2.4 shows the total CO_2 emissions from London's public transport sector in the past decade. TfL's surface public transport (excluding taxis and private hire vehicles) and underground produce nearly 90% of all

transport CO_2 emissions. Therefore it can be concluded that London buses are the largest CO_2 emissions contributor among all other London public transportation modes.

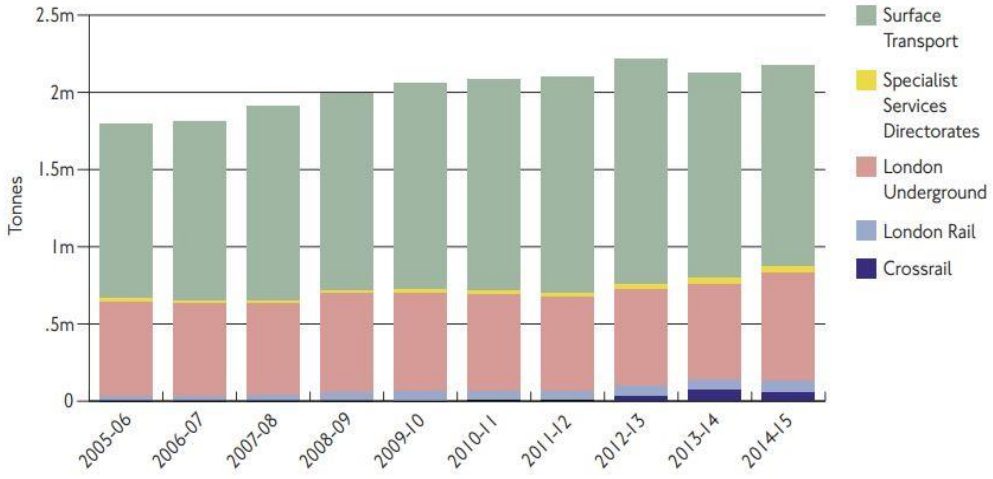

Figure 2.4 Total CO_2 emissions for London public transport from 2005 to 2015 (Figure from TfL 2015) [2.2.5]

In addition to carbon, there are other pollutants within the emissions from transport. The total volume of emissions in London have been reduced. The operation of London's buses emits a number of harmful pollutants such as $PM_{2.5}$, PM_{10} and NO_x (Nitrogen oxide). The continuing introduction of Euro VI diesel buses, which have diesel particulate filters fitted as standard, has greatly reduced the PM emissions from buses. The PM emissions from TfL operations have been decreasing since 2010 [2.2.5]. It must be noted that PM emissions are not just from vehicle exhausts. The biggest contributor to $PM_{2.5}$ for London by far is road transport, however, these emissions are mainly related to tyre and brake wear [2.2.5] [2.2.6]. The implantation of the ULEZ in 2020 is also expected to drive further reduction in PM emissions from road transport [2.2.5].

London's buses are the largest contributor of NO_x emissions which accounts for 72% of all NO_x emissions from TfL operations [2.2.5]. Figure 2.5 provides figures for the total amount of NO_x emission associated with TfL operations along with the target line. TfL has set the target to reduce NO_x from TfL operations by 40% by 2017/18 against 2015/16 levels. The total emission of NO_x from TfL operations has fallen by approximately 25% from 2005 to 2015.

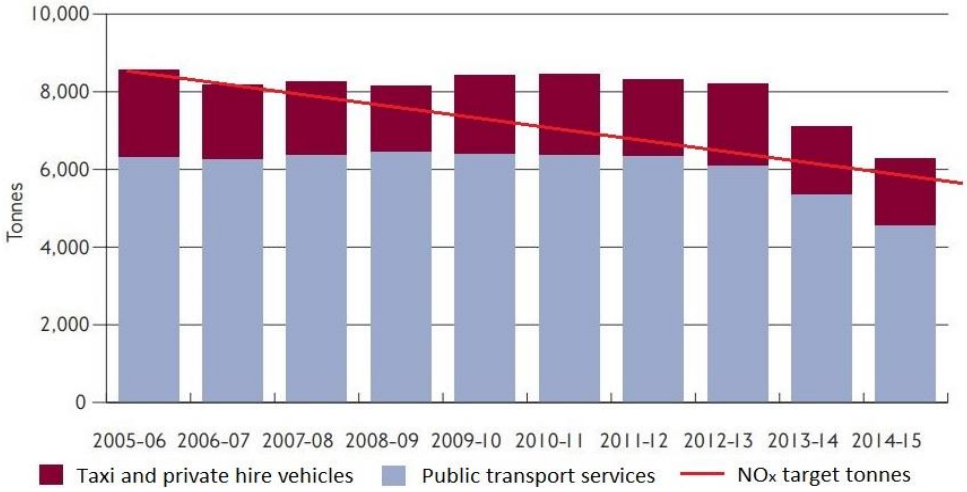

Figure 2.5 Total NOx emissions from TfL operations (Figure from TfL 2015) [2.2.5]

Although the total NOx emission in London has been generally decreasing each year, due to the heavy traffic concentration in city, the emission concentration in recent years has been broadly stable since 2008 [2.2.8]. Figure 2.6 shows the roadside NOx concentration in central London from 2008 to 2016. Each pollutant is calculated based on average values that are measured once per hour across the London air quality network. The non-linear and inconsistent measurement data in the figure is caused by strong seasonal effects and site based conditions [2.2.10] [2.2.11]. Carslaw [2.2.9] [2.2.10] has carried out a detailed study on NOx concentration trends and showed that there was a clear NOx concentration reduction around 2002 that then became stable from 2002 to 2008. As Figure 2.6 shows, the mean value of NOx concentration has remained generally the same from 2008 to 2016.

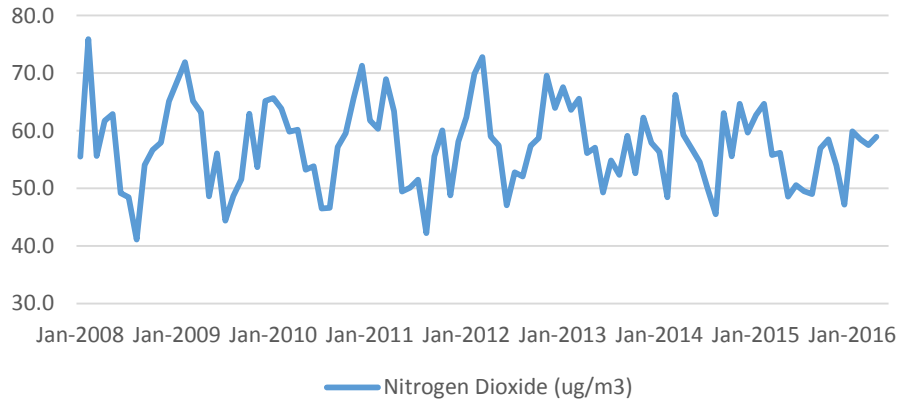

Figure 2.6 London roadside NOx concentration from 2008 to 2016 (Data from London Datastore 2016) [2.2.9]

Although TfL has taken many measures to control and reduce NOx emissions, the concentration level is still above the legal level. TfL provides an overview of NOx emission issues by showing the percentage of the population living in the areas with NO_2 exceedances. As Figure 2.7 shows, there is a significant percentage of people in London exposed to excessive levels of NO_2 emissions. Full implementation of the ULEZ is expected to halve the population exposed to poor air quality in 2020 [2.2.12]. Since London buses are the largest NOx emissions contributor within London's public transports sector, it can be concluded that improving the London bus fleet is an important and essential step to improve air quality in London and supplement the implementation of the ULEZ in 2020.

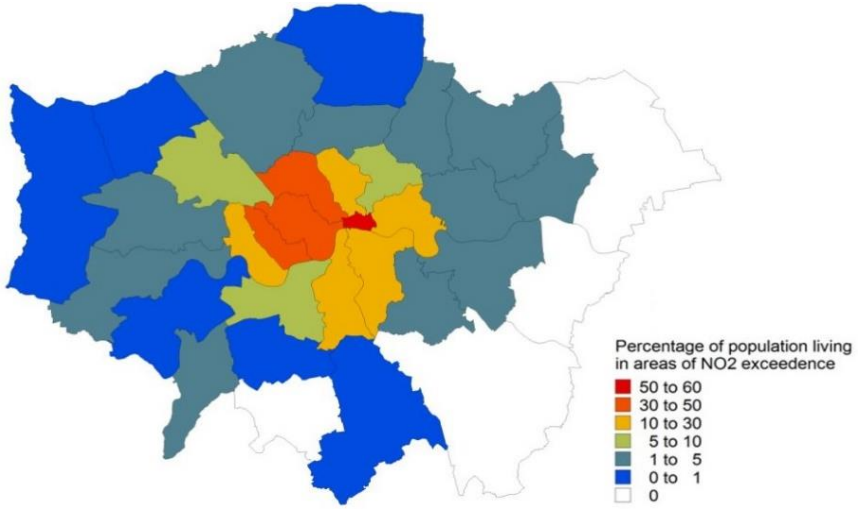

Figure 2.7 Number of people exposed to poor London air quality in 2015 (Figure from TfL 2015) [2.2.12]

The statistical review can be summarised into the following points:

1. London has the largest bus network in the UK and its demand have been consistently increasing since 1990 and is expected to continue to grow.
2. London's buses produce the largest amount of carbon emissions among all other TfL operations in London.
3. London's buses are the largest contributor of nitrogen oxide emissions which is one of the main air quality issues for London.
4. Improving the current London bus fleet is a key step to better air quality and full implementation of the London ULEZ.

2.3 Low emission propulsion bus systems

The UK bus industry has been driving innovative technology in the quest for lower emissions and greater efficiency over the past two decades. Significant progress has been achieved regarding “greener” bus development and the technology is being distributed across the UK [2.3.1] [2.3.2]. Cenex, as the UK’s first centre of excellence for low carbon technologies, forecast the main technologies assisting the transition to low emission propulsion buses in the UK as Figure 2.8 shows [2.3.3]. Cenex summarised the UK low emission bus industry into two phases using 2020 as a key milestone. Before 2020, the mass implementation and distribution of well-developed hybrid propulsion buses will offer relatively rapid payback in terms of emission reductions. After 2020, other technologies that offer further emission reduction over typical hybrid buses will start to be deployed and evaluated as a longer term solution [2.3.3].

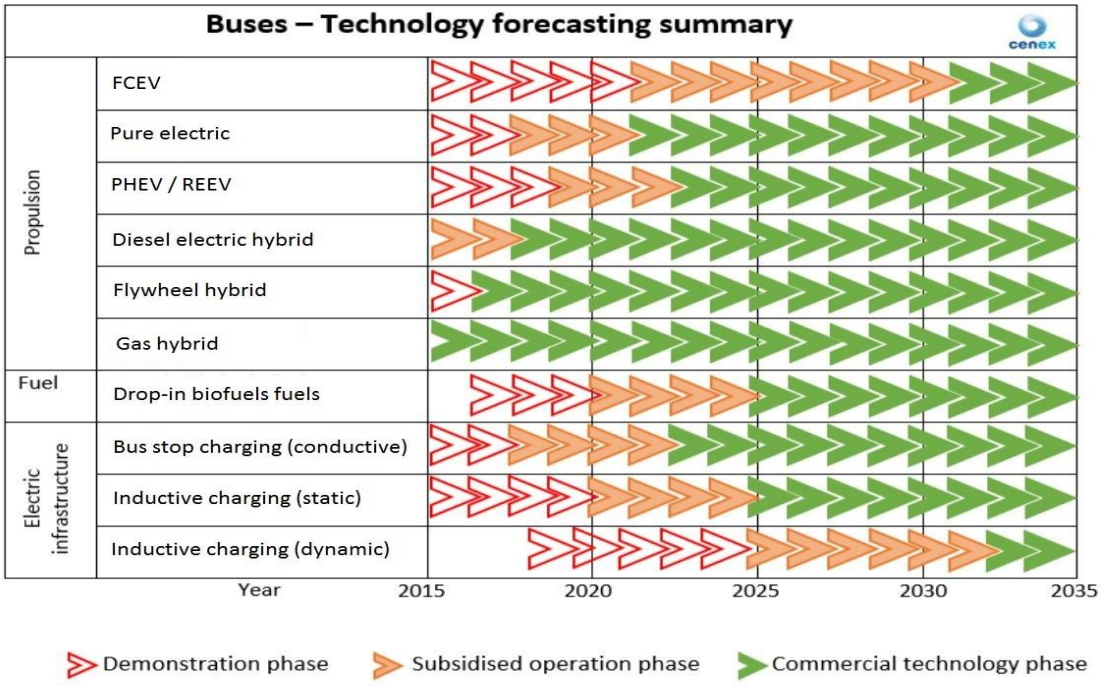

Figure 2.8 Low emission bus technologies forecasting summary in the UK (Figure from Cenex 2015) [2.3.3]

Current London bus technologies

London has a well-developed strategy for improving air quality by 2025, including the implementation of the ULEZ, retrofitting of buses and investing in zero emission capability. There were 9,600 buses operating in the Greater London area in 2016 where the majority of them are conventional diesel powered buses resulting in significant harmful emissions. TfL has set measures to reduce diesel powered buses

from two perspectives: to replace the current conventional technology and to investigate long term zero emission solutions. TfL has carried a review of the number of bus operating by type of buses in London in 2015 as Table 2.1 shows.

Table 2.1 Number of buses by type of bus in London (data from TfL) [2.3.4]

Bus type	Drive train type	2010	2011	2012	2013	2014	2015
New Routemaster	Hybrid	0	0	5	8	168	432
Routemaster	Diesel	18	18	19	20	19	19
Artic	Diesel	320	260	0	0	0	0
Single decker	Diesel	2,676	2,670	2,661	2,608	2,606	2,662
	Fuel Cell	0	5	5	5	8	8
	Hybrid	27	27	33	28	23	23
	Electric	0	0	0	0	2	8
Double decker	Diesel	5,554	5,487	5,787	5,696	5,296	5,026
	Hybrid	29	79	233	352	643	799
	Electric	0	0	0	0	0	0
Total		8,624	8,546	8,743	8,717	8,765	8,977

From the drive train type aspect, the buses can be categorised into four types: conventional diesel bus, low emission hybrid bus, zero emission electric bus and zero emission Fuel Cell bus. Figure 2.9 shows the proportional change of diesel buses in London from 2010 to 2015 using data from Table 2.1.

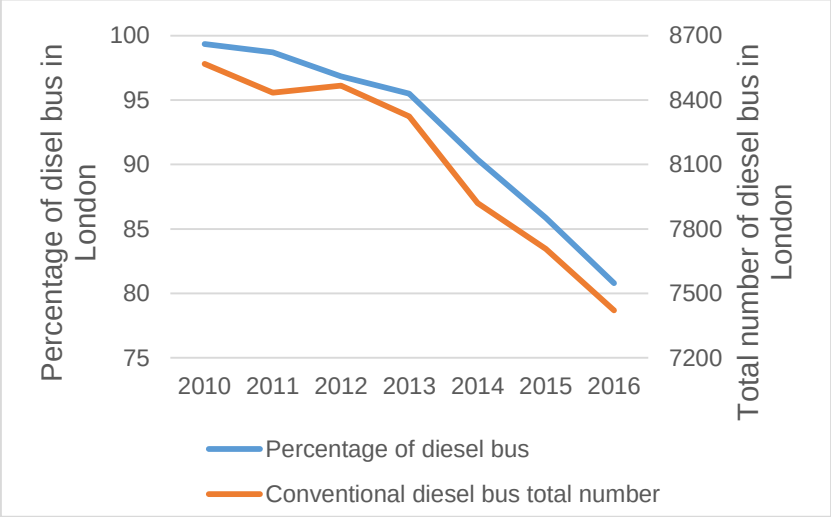

Figure 2.9 Proportional and number change of diesel bus in London [2.3.4] [2.3.5]

As Figure 2.9 shows, London has been working towards reducing the proportion of conventional diesel buses operating in central London from at least 2010. Significant progress has been made in the past five years where 20% of conventional diesel buses in London have been replaced with lower emission technologies in 2016. The introduction of hybrid buses has played an important role in this accomplishment which

will be discussed in detail in the next section. Zero emission technologies such as the battery electric bus and the fuel cell bus have also been trialled for demonstration and evaluation purposes [2.3.6].

2.3.1 Battery electric drive

The battery electric buses, often described as pure electric buses, use an electric motor powered by batteries (lithium based mostly) for propulsion. Electric transit buses have been developed for years and the market share has featured steady growth in recent years. The electric bus market was 6% of global bus purchases in 2012 and it is forecasted to grow to 15% in 2020 [2.3.7]. The electric bus development is being carried out all over the world with the largest shares in China, Europe and North America [2.3.8]. A table summarising key information of some of the most active operating battery electric buses worldwide can be found in Appendix A.

The configurations for electric buses are typically fairly straightforward since it is basically a battery powering an electric motor to propel the vehicle as Figure 2.10 shows. Battery electric buses can normally operate in two different forms: opportunity and overnight. Opportunity e-buses have a smaller energy storage capacity that offers limited range but can be charged much quicker (5-10 min); while overnight e-buses have a much larger energy storage but at the cost of a longer charge time (2-4 hour) [2.3.9]. These two forms represent two different electric bus approaches for the urban environment. The opportunity e-bus minimises the weight of the battery pack through frequent fast recharge at passenger stopping points. This holds the promise of high efficiency and low projected capital cost but requires an effective recharge technology and network. The overnight e-bus uses large energy storage to extend range so that the bus can be in service for the entire route/day without recharge. This holds the promise of high flexibility and convenience but suffers from passenger space loss due to battery size, long recharge time and battery lifetime issues [2.3.10].

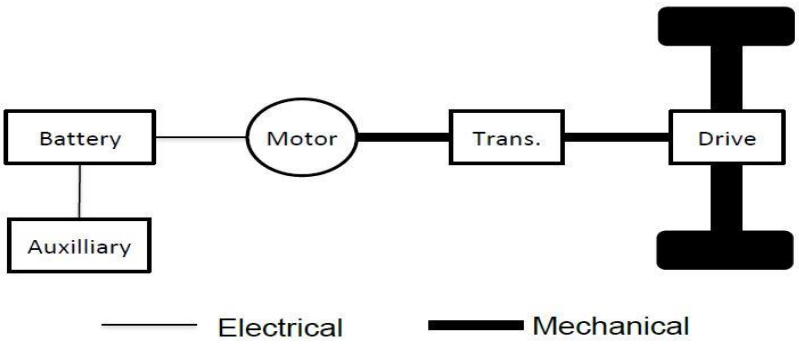

Figure 2.10 Battery electric drive bus configuration

Electric buses are zero emission at the point of use and therefore offers great emission savings particularly in terms of local air pollution. Additionally, the electricity used for charge the buses can be controlled in terms of distribution and renewable energy capability [2.3.6]. However the two approaches need to address the key challenges of expensive capital cost, limited range, long recharge times, infrastructure requirement and battery life issue [2.3.11]. Additionally, the required auxiliary loads such as heating and air conditioning also have a significant impact on the battery bus, particularly in winter time [2.3.11]. Since battery electric buses focus on a different approach compared with FC hybrid buses, this research will not look into details of battery electric systems. More details on battery electric bus development in London can be found in Appendix B.

2.3.2 Hybrid drive

Overview of hybrid bus technology

The diesel engine has been the dominant public transport bus technology due to its fuel economy and efficiency for decades. However, as global pollution issue rise, the diesel engine's harmful emissions have been considered as the biggest drawback of diesel powered buses. To overcome these pollution issues, hybrid systems have been brought into commercial use to seek a lower emission bus system using downsized diesel engines.

An electric hybrid bus combines a conventional internal combustion engine with an electric propulsion system. The overall goal of the hybrid propulsion system is to have the bus providing the same power and range capability as conventional buses with lower fuel consumption and lower emissions [2.3.12]. These types of buses are propelled by an electric motor powered by a combination of a conventional engine and an energy storage system. The energy storage serves two main purposes: to provide power during bus starting and power peaks and to enable energy to be recovered

through regenerative braking [2.3.13] [2.3.14].

The main benefits of hybrid systems for buses can be summarised into the following five points.

a) **Enable regenerative braking**: Significant amounts of energy is lost and dissipated as heat during conventional braking. The electric motor can be operated as a generator to charge the energy storage which can greatly reduce the energy lost in conventional braking, particularly for city buses.
b) **Engine downsizing**: The inclusion of an energy storage system has the additional advantage that the diesel engine can be decreased in size as it will not be required to meet the highest transient peak demands by itself which directly reduces the emissions from the engine.
c) **Engine efficiency optimisation**: Diesel engines function at their lowest efficiency during low load and low speed operations. Energy storage can be used to drive the motor to power the bus during low load and start-up to avoid the diesel engine operating at low efficiency.
d) **Idle off**: The average vehicle idles for around 15% of urban driving time and even more for a bus due to frequent stops [2.3.15]. Since the energy storage in the hybrid bus can be used to power the auxiliaries and provide start up power for the bus, the main engine can be switched off when the bus is stopped to prevent idling [2.3.16] [2.3.17].
e) **Simplify electrical accessories**: The electrical accessories (air conditioning, pump, door, CCTV, light etc.) can be directly powered by electricity and therefore eliminate the need for an extra alternator found in conventional buses [2.3.18].

Classification of electric hybrid drivetrains

Most types of electric hybrid buses share the benefits discussed and they can be further categorised into three major types: series, parallel and series-parallel. Each configuration uses similar main components but differ in drivetrain topology, engine size, electric motor size, transmission technology, control system and applications. Different hybrid configurations also have additional different pros and cons based upon their characteristics, configurations and applications.

In a **series electric hybrid drivetrain**, as Figure 2.11 shows, the mechanical output from the engine has been converted to electrical power via a generator. The electrical power from the generator will be supplemented with a battery to power the electric motor, which drives the wheels.

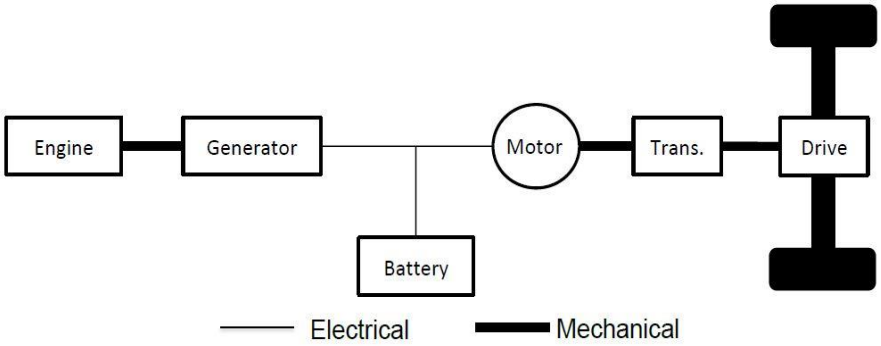

Figure 2.11 Simplified architecture of a series hybrid drivetrain [2.3.19]

Advantages

1. The complete decoupling between engine and wheels means the engine control is not dependent on vehicle speed and brings additional flexibility [2.3.20]. This creates one of the major advantages of series hybrid drivetrain in that the engine can operate at any point on its speed-torque map which is not easily practicable for conventional vehicle drivetrains. Therefore, the engine can be operated at near optimum efficiency which minimises fuel consumption and emissions [2.3.19].
2. The electric motor is the only means of driving the wheels which means series hybrid drivetrains contain the simplest hybrid configuration in terms of mechanical structure and control strategy.
3. The electric motor can operate at very high speed which could eliminate the need for complicated muti-speed transmission and clutch systems i.e. simple gearbox [2.3.19].

Disadvantages

1. Energy from the engine output needs to be transformed from mechanical to electrical and then back to mechanical which causes extra losses during the process [2.3.19].
2. The requirement of an additional generator/motor adds extra cost and weight.
3. Series hybrid buses require a powerful motor as it is the only powerplant directly propelling the vehicle.

In a **parallel electric hybrid drivetrain**, as Figure 2.12 shows, the mechanical output from the engine and motor output powered by battery are connected in parallel to the transmission and directly drive the wheels. This drivetrain can be considered as a conventional diesel bus drivetrain with an additional battery/motor system.

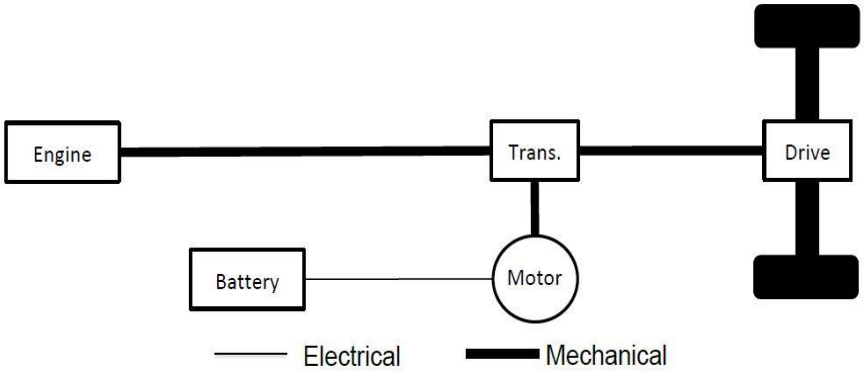

Figure 2.12 Simplified architecture of a parallel hybrid drivetrain [2.3.19]

Advantages

1. The mechanical power from the engine is utilised directly without additional conversions making the parallel hybrid system generally cheaper and higher transmission efficiency than the series hybrid system [2.3.13].
2. The electric motor can be selected to be less powerful than that for the series hybrid drivetrain as the battery powered motor can simply be used to supplement peak load and be used as a generator to recharge the battery via the engine output.
3. Does not require additional generator because of the mechanical coupling.

Disadvantages

1. Like conventional engines, engine speed is dependent on vehicle speed which resulting the engine being unable to operate in a narrow or constant speed range, thus efficiency reduces at low rotation speed [2.3.21].
2. Computer control is required to coordinate the balance between engine and motor and this depends upon the load power demand.
3. The battery can only be charged during regenerative braking or cruising, and is therefore unable to be charged at standstill when the bus is stationary [2.3.21].
4. The mechanical system is more complicated because of the two axle torque coupling design [2.3.18].

In a **series-parallel electric hybrid drivetrain**, as Figure 2.13 shows, which is also called power split drivetrain. This kind of system, a combination of the series and parallel hybrid drivetrains, has both mechanical and electrical coupling working either individually or simultaneously. The mechanical power from the engine is divided into two power flows which are used to directly drive the wheels through transmissions and to electrically power the electric motor with the battery.

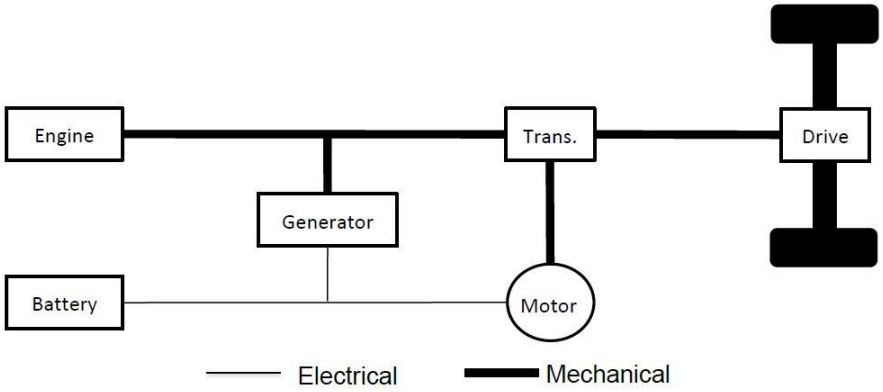

Figure 2.13 Simplified architecture of a series-parallel hybrid drivetrain [2.3.19]

Advantages

1. Series-parallel hybrid drivetrain can work as either a series hybrid system or a parallel hybrid system so it has most of the advantages of both the series and parallel systems. This type of drivetrain uses a controller to select the more efficient operation mode, dependent upon the power allowing the overall system to operate at near optimum efficiency more often than either the series or parallel system alone [2.3.22].
2. High flexibility to switch between engine power and electrical power.

Disadvantages

1. Merging the series and parallel drivetrains can gain both of their advantages but at the same time it also greatly increases the system complexity in terms of both configuration and control.
2. The need for an additional generator, a large electric motor and complicated control system makes the cost increase significantly.

The three main hybrid drivetrains have their own characteristics which results in additional pros and cons. There is no clear answer as to which drivetrain is better than the others, but it can be determined which system would be more suited for certain applications. This research will only consider city bus driving applications where a typical city bus environment, such as London, has a start-stop traffic pattern with generally low speed operation. As discussed before, one of the major drawbacks of

parallel hybrid systems is low efficiency at low speed operations and series-parallel hybrid systems are still not a viable solution for public transport due to high capital cost and engineering complexity [2.3.23]. Muncrief and Ehasani [2.3.24] [2.3.25] have provided detailed comparisons between series hybrid and parallel hybrid drivetrains and concluded that series hybrid is generally more efficient for low speed applications over short distances while parallel hybrid is more efficient at higher speed and longer distance. Hence, it can be concluded that a series hybrid drivetrain would be more suitable for city transport bus applications because it is more efficient during low speed operations and can also exploit the benefit from frequent regenerative braking in city driving conditions due to the direct battery electrical connection. For these reasons this research will only consider series hybrid propulsion systems. Please note all hybrid systems discussed hereafter are referring to electric hybrid systems.

London hybrid bus programme

Through worldwide ongoing hybrid bus trial programmes, London has implemented the London hybrid bus programme that aims to set a positive example of a green public transport [2.3.26]. The London Hybrid Bus programme first introduced in 2005, aims to transform part of the conventional diesel powered buses into diesel electric hybrid buses with the main benefits of reducing both fuel consumption and harmful emissions. The hybrid buses utilise series hybrid configuration powered by a combination of a conventional diesel engine/generator and lithium-ion (Li-ion) battery pack. The first trial bus fleet had eight buses operating on different routes in 2007 and the follow up customer interviews showed 96% of customers supported hybrid bus technology [2.3.27]. After investigation and analysis of the first trial bus fleet, hybrid buses started to be officially deployed in Central London from 2010. The hybrid bus deployment timeline is shown in Figure 2.14 using the TfL bus data from Table 2.1.

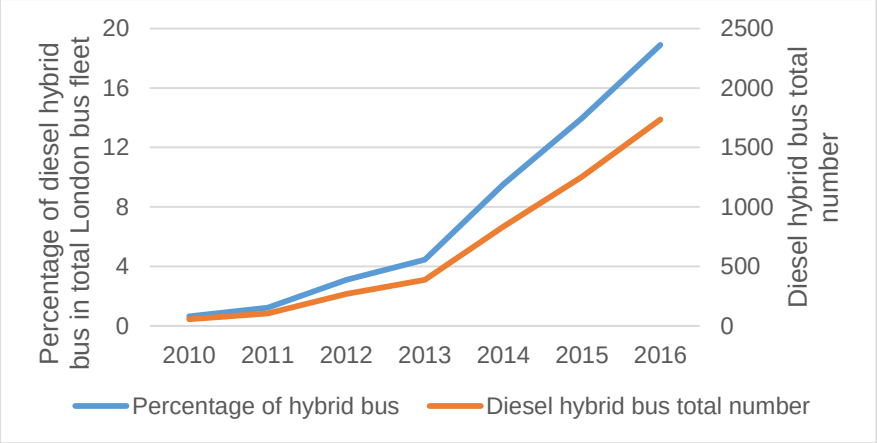

Figure 2.14 Proportional and number change of diesel hybrid bus in London [2.3.4]

As Figure 2.14 shows, the total number of diesel hybrid buses has increased from 56 in 2010 to 1700 in 2016 which is 20% of all London's entire bus fleet making London buses the largest hybrid bus fleet in the world [2.3.28]. This leads the bus fleet to the ultimate objective by 2020 which is to make sure every double-decker bus (~3000) entering the ULEZ are low emission diesel hybrid buses and every single-decker (~300) to be zero emission buses [2.3.29-2.3.31].

The double-decker hybrid buses in London currently cost approximately £300,000 each, while a conventional diesel bus costs £190,000 which is approximately 50% less expensive [2.3.32-2.3.35]. Therefore the overall hybrid bus investment to reduce emission and fuel consumption is 50% more expensive [2.3.32]. Compared to a conventional double-decker diesel bus, the TfL test hybrid bus revealed reductions of 80% in nitrogen oxides and carbon monoxide; and 30% in carbon dioxide and fuel consumption [2.3.36]. TfL has provided a study on the London bus emission reduction roadmap trend as Figure 2.15 shows.

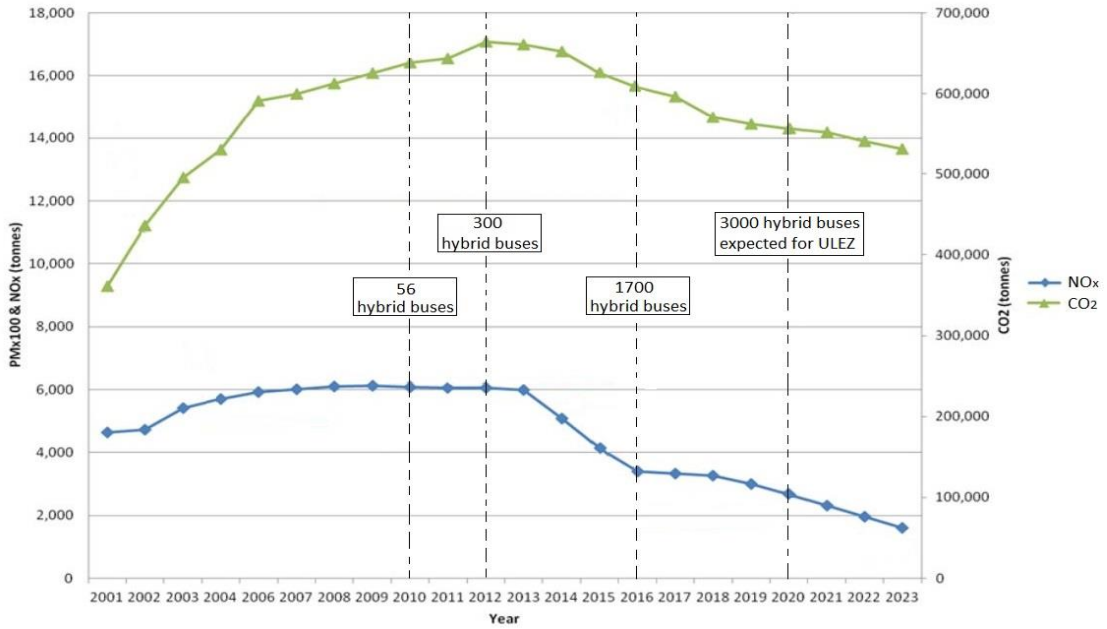

Figure 2.15 London annual bus emission trends (Figure from TfL) [2.3.36-2.3.38]

The mass production and distribution of hybrid buses have played a key role in the carbon and nitrogen oxide reduction roadmap. The hybrid bus programme showed significant payback in terms of fuel economy and environmental impact from 2013. The latest total bus target and emission reduction in 2016 have shown the trend generally matching the forecast [2.3.39] [2.3.40].

Considering fuel economy and emission reduction, hybrid buses operating in London have shown promising results and have been widely accepted by the travelling public. It can be concluded that hybrid drivetrain technology, when applied in city driving buses, can effectively bring environmental benefits. However the hybrid buses will eventually reach an emission reduction threshold because they are still diesel-based. TfL has also been looking at another long term solution and that is the Fuel Cell technology.

2.3.3 Fuel Cell drive

Overview of Fuel Cell bus technology

The Fuel Cell (FC) is a clean energy source with the main benefits of zero harmful emissions and relatively high efficiency. The FC uses hydrogen as a fuel and generates electricity with water as a waste product through electrochemical processes. By replacing the internal combustion engine of conventional buses, FCs can be used to power the buses using electrical energy only, therefore achieving zero operating emissions [2.3.41]. The drivetrain of FC buses is similar to that of the battery electric bus with the batteries replaced by a FC because they are both electrically driven as Figure 2.16 shows. FC buses can be configured in series hybrid propulsion systems with some form of energy storage to reduce the size of the FC stack [2.3.41]. Currently, most FC buses have pure FC drivetrains or series hybrid drivetrains.

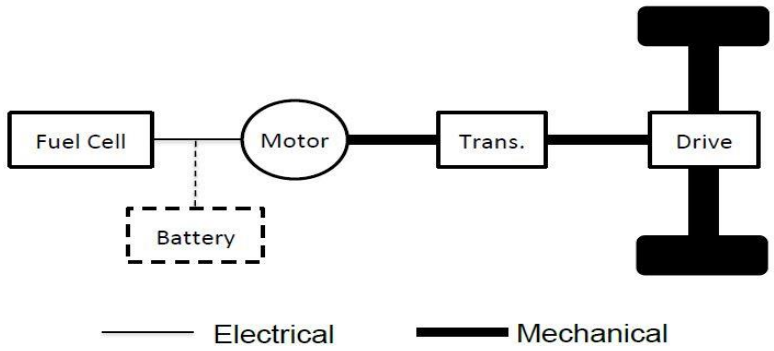

Figure 2.16 Simplified architecture of a FC drivetrain

Both FC and battery electric buses have been developed as long term solutions to zero emission bus systems. The Fuel Cells and Hydrogen Joint Undertaking (FCH JU), which is one of the largest FC research, technological development and demonstration organisations in Europe, has done a comparison study between these two future zero emission bus concepts and the study concluded both systems hold promising futures based on their demonstration performance but have their own challenges to overcome. A summary of some of the key comparison conclusions between the two technologies can be found in Appendix C.

There have been a number of hydrogen bus projects in the last 17 years in Europe to demonstrate FC technology performance in practice. Details of the FC bus demonstration projects in Europe from 2001 to 2019 can be found in Appendix D. An up to date summary of the majority of active fuel cell bus demonstration projects worldwide can be found in Appendix E.

The FC bus technology has significantly improved through demonstration projects from 2001 to 2017. Some of the key achievements by 2017 throughout the FC bus demonstration projects can be summarised as follows [2.3.42-2.3.44].

1. Bus daily range extended from 60 km to up to 450 km.
2. Fuel economy improved from 25 kg H_2/100 km (3,550 MJ/100 km) to 9 kg H_2/100 km (1278 MJ/100 km).
3. Refuelling time reduced from an average 25 min to below 10 min.
4. Purchase cost reduced by 76% compared to the first deployment in 1990s.
5. Achieved an equivalent energy consumption performance to diesel vehicles (Typical diesel vehicle: 62 miles per gallon [2.3.45]; FC vehicle: 67 miles per gallon equivalent [2.3.46]).

Significant progress have also been made for commercial FC vehicles e.g. cars, vans and trucks. Large companies such as Toyota, Honda and Hyundai have also shown growing interest in FC vehicles for commercial use [2.3.42]. The main challenge for commercial FC vehicles is the requirement of an infrastructure network for hydrogen fuelling; for FC buses this can be centralised and thus does not need to be as comprehensive [2.3.43]. Owing to differences in the application between buses and commercial vehicles, this research will not look into details of commercial FC vehicles but instead focus on FC buses.

London FC bus development

TfL has been working in FC bus demonstration projects since the first major European FC bus project in 2001. The first FC bus fleet consisting of five FC buses were in service from 2004 to 2009 and then the fleet was extended to eight FC buses from 2010 to 2017. All the FC bus activity in London has been carried out on route number RV1, which is a 9.7 km route travelling in Zone 1 of London. Details of the development history of the London RV1 FC bus can be found in Appendix F.

Figure 2.17 shows an elevated view of the FC bus, and Figure 2.18 shows a 3D drawing with the main components of the bus labelled. Table 2.2 summarises some key specifications and information for the London RV1 buses.

Figure 2.17 RV1 FC bus operating in London (Photo from zaplog.nl, 2012)

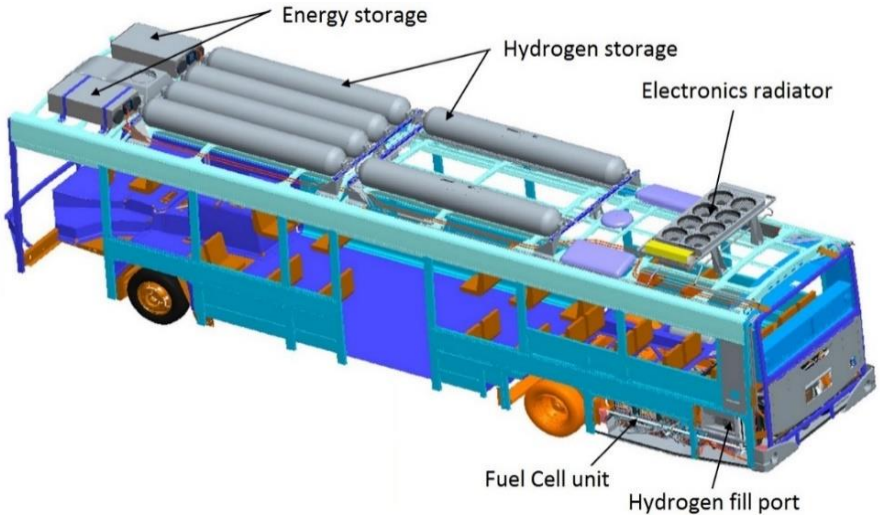

Figure 2.18 London FC bus design and main components (Figure from Bluways, 2011) [2.3.47]

Table 2.2 Specifications of London FC bus RV1

[2.3.47-2.3.49]

RV1 bus mechanical design specification			
Body	Wrightbus Pulsar	Chassis	12m VDL Chassis
Information of Route RV1			
Length	9.7 km	Journal time	24-33 min
Total stops	19	Road condition	Mainly flat*
Daily duty	16-18 hours	Average speed	12 km/h
FC hydrogen bus specification			
Max range	300 km with 4 cylinder	Weight	11 ton (unloaded)
Top speed	56 km/h	Approx. cost	4-5 times of a diesel conventional bus
Bus electrical information			
FC stack	Ballard 75 kW	FC output voltage	350 V
Bus electrical voltage	700 V	Hybrid drive	Siemens series ELFA
Energy storage	Maxwell supercapacitor 0.5 kWh	Energy storage unit	BCAP3000P
Hydrogen information			
Hydrogen supplier	Air product	Refuelling time	< 10 m
Cylinder bottle number	4-6 adjustable	Cylinder bottle type	3
Cylinder bottle weight	32 kg with 4 cylinder	Cylinder condition	350 bar, 15℃

*RV1 route information has been recorded with GPS from Google maps and gradient along the route has been calculated from elevation data and plotted in Figure 2.19.

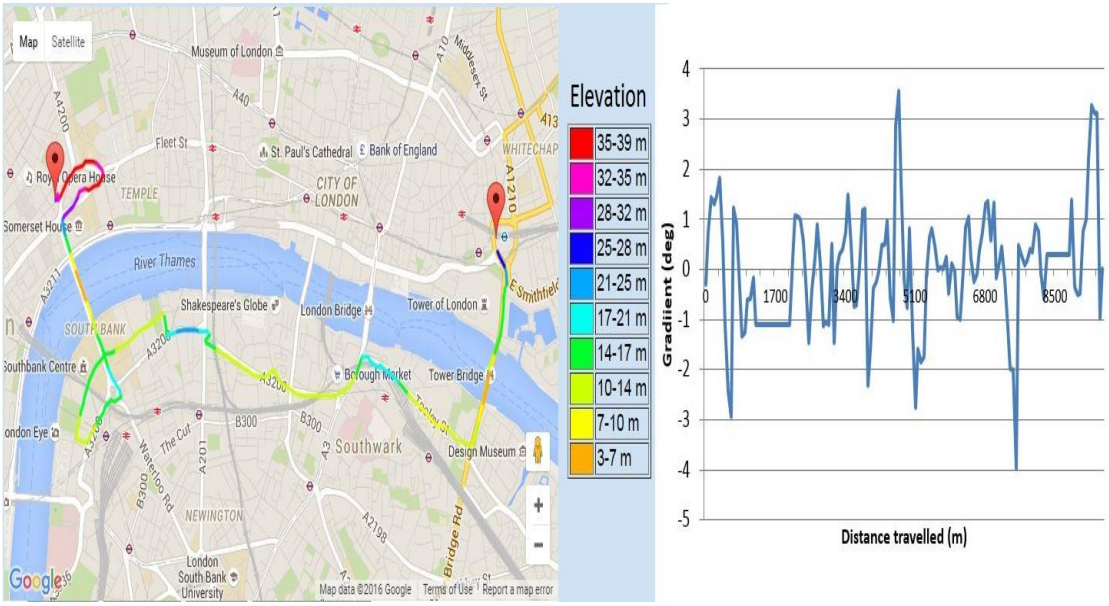

Figure 2.19 London RV1 route elevation and gradient

(Elevation data from Google map and Maplorer, 2016)

The London RV1 FC buses have been in daily service since 2011. The buses leave the depot at 06:00 and return for hydrogen refuelling around 01:00. The buses are capable of covering a full day's service with no requirement to refuel. After service, the buses then return to the depot for refuelling, which takes less than 10 minutes. The depot, where routine maintenance and hydrogen management is carried out as Figure 2.20 shows, was specifically designed and built for hydrogen FC buses and is located next to the main depot for conventional diesel buses. The route of RV1 is a specialised route selected for FC bus demonstrations. The route is a mainly flat route without significant gradient changes along the river as Figure 2.19 shows.

Fuelling station **Maintenance workshop**

Figure 2.20 RV1 FC bus depot located in London

(Photos taken from London FC bus workshop site visit at 17/12/2014)

Over the past five years of daily operation in London, the RV1 FC buses have covered more than a combined 1.1 million kilometres operation [2.3.50]. Additionally, a number of the buses have achieved the important milestone of 20,000 hours of continuous operation without replacement or major repairs by 2016 [2.3.51]. The eight FC buses were operating under the CHIC (Clean Hydrogen in European Cities, 2010-2016) project which is one of the largest European FC bus demonstration projects. One of the most significant results of the CHIC project in London is the improvement in fuel economy.

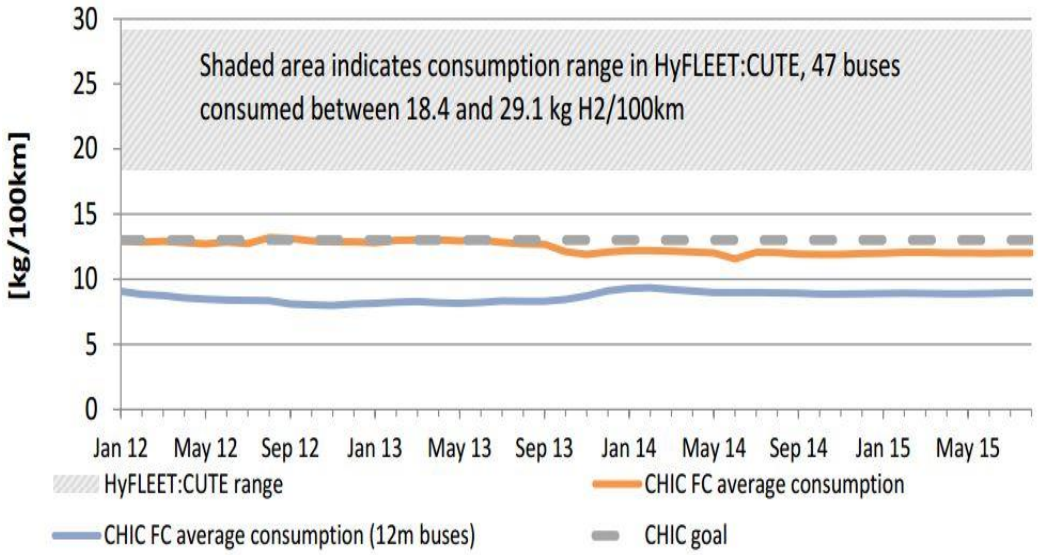

Figure 2.21 Average fuel consumption of FC buses in the CHIC project (Figure from FCH JU, 2016) [2.3.52]

As Figure 2.21 shows, fuel economy of the CHIC FC buses has improved markedly compared with the FC buses in the CUTE (Clean Urban Transport for Europe, 2001-2009) project. The blue line representing the 12m FC buses fuel consumption, which is the RV1 FC buses in London, shows nearly 50% fuel economy improvement over the CHIC target line and average of other CHIC FC buses across Europe [2.3.52].

However, the main barrier to FC powered buses is still the high capital cost [2.3.53] [2.3.54]. A FC powered bus costs approximately five times that a conventional diesel bus with similar power output [2.3.53] [2.3.54]. The cost issue is mainly a consequence of the expensive FC stack unit along with the small amount of component production for FC systems impacting economies of scale. The current FC bus system still needs improvement both technically and economically to overcome this barrier.

The low emission bus section of the literature review can be summarised as follows:

1. London has focused on low emission bus development. London's buses have been developed from two perspectives: low emission buses as a transition solution and zero emission buses as a long term solution.
2. Diesel-electric hybrid buses are at the mass deployment period in London. The initial payback, which is emission and fuel consumption reduction, has been noted indicating hybrid propulsion buses are a viable low emission transit solution.
3. Fuel Cell electric buses have been developed and tested in the past decade. The trial buses have shown great improvement over time in terms of fuel

economy. FC buses have been proven to be capable of providing a potential long term zero emission bus system. The system, however, still needs to be further improved both technically and economically.

2.4 Fuel Cell technology

2.4.1 Fuel Cell overview

A Fuel Cell (FC) is an electrochemical energy converter producing DC electricity directly through a chemical reaction. The FC is a clean and efficient power unit that has undergone substantial development and is now commercially available offering a potential clean power source solution. The FC circumvents all the combustion and mechanical processes of a conventional internal combustion engine into a single chemical step to generate electricity. The electrochemical reaction can be simplified into one step which is to supply fuel and oxygen to the FC and generating DC electricity and water as Figure 2.22 shows. The FC can use different kinds of fuels when using a reformer but the reaction of importance is between hydrogen (H_2) and oxygen (O_2) to form water and free electrons used for electrical power, hence compressed H_2, as a fuel, is usually preferred [2.4.1].

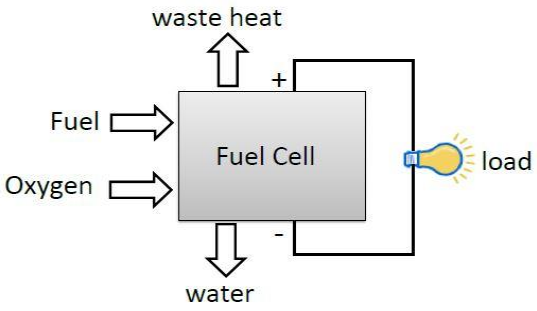

Figure 2.22 Simplified generic FC operation configuration [2.4.2]

Compared with the typical internal combustion engine (ICE) the FC offers benefits of high efficiency and zero greenhouse gas emissions. The FC also offers additional benefits such as simplicity, flexible modular construction, low noise, small size and small weight as a consequence of the simple chemical process. On the other hand, the FC has drawbacks such as low power density, is still a developing technology, slow reaction rate, short lifetimes and expensive purchase cost [2.4.3].

2.4.2 Types of Fuel Cells

Various fuel cell technologies exist, where each technology has its own specific advantages, disadvantages and applications. The different fuel cell types are usually distinguished by the electrolyte used and six of the most commonly used FC types have been selected and summarised in Table 2.3.

Table 2.3 Comparison among six common FCs [2.4.2, 2.4.4, 2.4.5]

	PEMFC	DMFC	AFC	PAFC	SOFC	MCFC
Main Fuel	H_2	CH_3OH, H_2	H_2	H_2	CO, H_2	CO, H_2
Electrolyte	Polymer membrane	Polymer membrane	Potassium hydroxide	Phosphoric acid	Nonporous metal oxide	Alkali carbonate
Temp(℃)	30-100	20-90	50-200	~220	800-1000	~650
Oxidiser	Air/O_2	Air/O_2	O_2	Air	Air	Air
Catalyser	Pt	Pt	Pt, Ni	Pt	Ni	Ni
Efficiency	50-70 %	20-30 %	60-70 %	55 %	60-65 %	55 %
Estimated cost	£ 2000 / kW	£ 8,000 / kW	£ 5,000 / kW	£ 3,000 / kW	£ 1,000 / kW	£ 2,000 / kW
Lifetime (h)	100,000	100,000	10,000	15,000	7,000	12,000
Start-up time	≤5 minutes	≤5 minutes	≤5 minutes	1~4 hour	≥10 hour	≥10 hour
Target power	10 W-100 kW	1 W-100W	1 kW-100 kW	100 kW-10 MW	1 kW-100MW	1 MW-100 MW
Promising application	Portable, transport	Portable, stationary, transport	Stationary, transport	Stationary	Stationary	Stationary

PEMFC: Proton exchange membrane fuel cell	O_2: Oxygen
AFC: Alkaline fuel cell	CH_3OH: Methanol
PAFC: Phosphoric acid fuel cell	CO: Carbon oxygen
MCFC: Molten carbonate fuel cell	H_2: Hydrogen
SOFC: Solid oxide fuel cell	Pt: Platinum
DMFC: Direct methanol fuel cell	Ni: Nickel

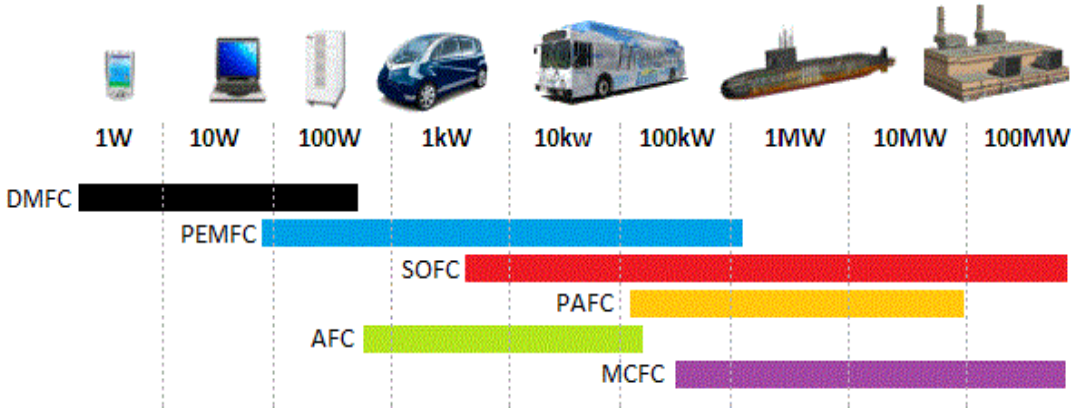

Figure 2.23 Power scale targets for different FC applications [2.4.5]

Antig [2.4.5] provided a graphic demonstration of the applications for the six types of fuel cells in terms of general power range as Figure 2.23 shows. All the FCs discussed above have their own specific optimum applications. More description of these six FC types in terms of operation, theory, advantages and disadvantages can be found in Appendix G. This study will only consider the FC for transportation applications, more specifically, for buses. The DMFC has a very obvious benefit that it can use cheap liquid methanol as fuel, however, it has the lowest efficiency among other FC types. The AFC has the problem of leakage risk of highly corrosive electrolyte material which is not ideal for public transportation. The PAFC stack needs to be kept above 42 °C at all time to prevent freezing which makes it more beneficial for larger scale power plant. The SOFC and the MCFC have very high operating temperatures and extremely long start-up time which makes them unsuitable for transportation applications. That leaves the most appropriate FC option for city transportation application to be PEMFC which is why the majority of FC buses discussed before are PEMFC based. The PEMFC has relatively high power density and low weight; it can achieve high efficiency and operates at low temperature, which makes it ideal for transportation applications [2.4.2]. However, certain barriers need to be overcome as regards of PEMFC such as high cost and slow response rate. This research will only consider PEMFC for bus application, hence all description of the FC afterwards would be the PEMFC.

2.4.3 PEMFC operation principle

The proton exchange membrane fuel cell, also known as polymer electrolyte membrane fuel cell, was first developed by General Electric in the 1960s for their first manned space vehicle. Despite the aerospace applications, the PEMFC was not a practicable option for wider applications until the early 1990s because of the extremely expensive materials. Important advances for the PEMFC have been achieved such as reducing the platinum catalyst loading from 25 mg/cm^2 to 0.05 mg/cm^2 [2.4.6]. The cost

of the PEMFC has dropped significantly since 2000 which makes the PEMFC a viable solution for other applications apart from space programs [2.4.7]. The primary conceptual difference between the PEMFC and conventional engines is that conventional engines involve mainly combustion and mechanical processes while the PEMFC involves mainly chemical and electrical processes [2.4.8].

A PEMFC typically consists of a series of elementary fuel cells; and individual cells can be stacked together to provide a higher output owing to the simple concept of the FC [2.4.9]. A single FC can be divided into two main parts: bipolar plates (collector plates) and membrane electrode assembly as Figure 2.24 shows [2.4.10]. The operation process of PEMFC can be simplified into four steps.

a) The H_2 is fed to the electrode and the reaction, shown on the left ("$H_2 \rightarrow 2H^+ + 2e^-$ ") will occur by catalyser.
b) The protons ($2H^+$) created will travel through the membrane to the other electrode of the membrane.
c) The electrons ($2e^-$) created will travel via a conductive path, via the external load, to the other collector plate, thus providing power to the external load.
d) Oxygen is fed to the other electrode reacting with the protons and electrons through the following reaction "$0.5O_2 + 2H^+ + 2e^- \rightarrow H_2O$" to produce water [2.4.7] [2.4.11].

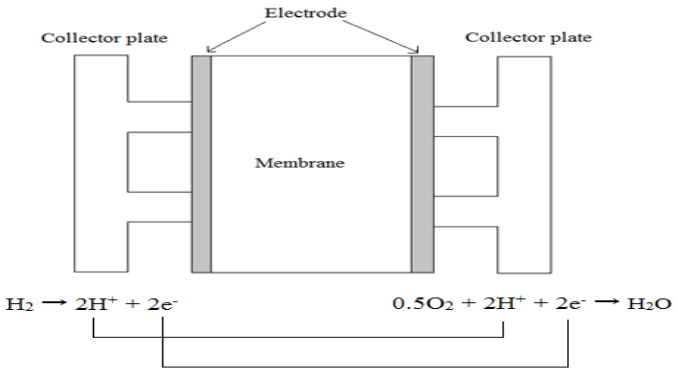

Figure 2.24 Simplified chemical principle of PEMFC operation

The plates uniformly distribute air and fuel to supply each individual cell, allowing the reaction to occur simultaneously in each cell. The actual chemical reactions within the membrane are much more complicated than the basic principle and involves power conditioning, water management, heat transfer, gas diffusion and material selection. This research will not discuss the details of PEMFC chemical characteristics (further reading can be found in [2.4.12]), however, it is important to understand the electrical characteristics of PEMFC outputs.

Theoretical PEMFC efficiency

The PEMFC holds the promise of very high theoretical efficiency. To calculate the efficiency of the PEMFC, the higher heating value (HHV) and lower heating value (LHV) need to be introduced. The difference between the two heating values depends on the chemical composition of the fuels. The HHV is defined as the LHV plus the addition of the vaporisation heat of water content in the fuel [2.4.13]. The two heating values are almost identical for certain fuels such as carbon, but more significant for hydrogen because of the water product temperature is between 100 and 150 °C. It is important to clarify which heating value is used when calculating the efficiency. A look-up table of LHV/HHV for different gaseous/liquid/solid fuels can be found in [2.4.14]. The heating values of hydrogen can be represented with the absolute value of the reaction enthalpy which has been calculated as [2.4.15]:

$$H_2 + \frac{1}{2}O_2 \rightarrow H_2O \text{ (steam form)} \quad (2\text{-}1)$$

$$\Delta H_{LHV} = -241.82 \frac{kj}{mol}$$

$$H_2 + \frac{1}{2}O_2 \rightarrow H_2O \text{ (liquid form)} \quad (2\text{-}2)$$

$$\Delta H_{HHV} = -285.83 \frac{kj}{mol}$$

To calculate the efficiency, the FC theoretical potential needs to be deduced. Barbir [2.4.16] provides a detailed derivation of PEMFC potential as shown below. The general electrical work is a product of charge and potential which is:

$$W = qE \quad (2\text{-}3)$$

where:

W is electrical work in $Jmol^{-1}$

q is charge in coulombs mol^{-1}

E is potential in Volts

The total charge transferred in a PEMFC reaction can be calculated as:

$$q = nN_{avg}q_{e1} \quad (2\text{-}4)$$

where:

n is the number of electrons per molecule of hydrogen (which is 2 for H_2)

N_{avg} is the number of molecules per mole which is Avogadros' number (6.022×10^{23} molecules/mol)

q_{e1} is the charge of 1 electron which is 1.602×10^{-19} Coulombs/electron

where the product of N_{avg} and q_{e1} is the Faraday's constant, F=96,485 Coulombs/electron-mol.

Hence the equation (2-3) becomes:

$$W = nFE \tag{2-5}$$

To determine the electrical work of the PEMFC, another thermodynamic term, Gibbs free energy (ΔG), needs to be introduced. Gibbs free energy is defined as the energy associated with a chemical reaction that can be used to do work, in other words, the energy that can be converted into useful work – electricity [2.4.17]. Therefore the Gibbs free energy equations in terms of electrical work of PEMFC can be calculated as:

$$W = \Delta G = \Delta H - T\Delta S \tag{2-6}$$

where:

ΔH is the change of heat content (enthalpy) in joule/kilogram

T is the absolute temperature in Kelvin

ΔS is the change of entropy in joule/Kelvin

The Gibbs free energy for water (H_2O) can be calculated from the thermodynamic properties of selected substances look up table available in [2.4.18].

$$\Delta G_{H_2O} = -228.57 \frac{kj}{mol} \text{ (steam form, LHV)}$$

$$\Delta G_{H_2O} = -237.13 \frac{kj}{mol} \text{ (liquid form, HHV)}$$

Therefore equation (2-5) can be substituted into (2-7) providing the theoretical FC potential for LHV and HHV.

$$E = \frac{-\Delta G}{nF} \tag{2-7}$$

$$E = \frac{228.57}{2 \times 96.48} = 1.185\ V \text{ (steam form, LHV)}$$

$$E = \frac{237.13}{2 \times 96.48} = 1.229\ V \text{ (liquid form, HHV)}$$

Considering the thermodynamic properties for water entropy under different conditions where $\Delta H_{steam} = -241.83$ kj/mol and $\Delta H_{liquid} = -285.83$ kj/mol, the FC theoretical efficiency can be calculated as:

$$\eta = \frac{\frac{-\Delta G}{nF}}{\frac{-\Delta H}{nF}} = \frac{1.185}{1.253} = 94.5\% \text{ (steam form, LHV)}$$

$$\eta = \frac{\frac{-\Delta G}{nF}}{\frac{-\Delta H}{nF}} = \frac{1.229}{1.482} = 83.1\% \text{ (liquid form, HHV)}$$

The voltages 1.253V and 1.482V correspond to hydrogen's LHV and HHV, which are also called thermoneutral potential. Those two potential values can be used to calculate the actual electrical efficiency because they only correspond to hydrogen fuel conditions.

Therefore the actual FC electrical efficiency can be calculated as:

$$\eta = \frac{Average\ Cell\ Potential}{1.253}\ \textit{(steam form, LHV)} \quad (2\text{-}8)$$

$$\eta = \frac{Average\ Cell\ Potential}{1.482}\ \textit{(liquid form, HHV)} \quad (2\text{-}9)$$

[2.4.16] [2.4.19]

Although using both heating values to express the efficiency is appropriate, the use of LHV/HHV can be confusing. Since LHV does not account for the latent heat of condensation of the water produced, it is thermodynamically more accurate to use the HHV expressing PEMFC efficiencies [2.4.16] [2.4.20]. Therefore the efficiency will be calculated using HHV in this research as it accounts for all the energy available.

PEMFC voltage losses

As the efficiency calculation indicates, the PEMFC has a very high theoretical efficiency. However, this theoretical efficiency can be achieved only if all the Gibbs free energy (electrical work) has been fully utilised, which is scientifically impossible. There will always be energy losses during the process, in this case, voltage losses of the electrical work. There are three types of main voltage losses for PEMFC: Activation loss, Ohmic loss and Concentration loss [2.4.21]. Figure 2.25 provides graphical representations of the three major voltage losses. Please note the three plots are not on the same scale in Figure 2.25 and they will be plotted on the same scale in Figure 2.26 later.

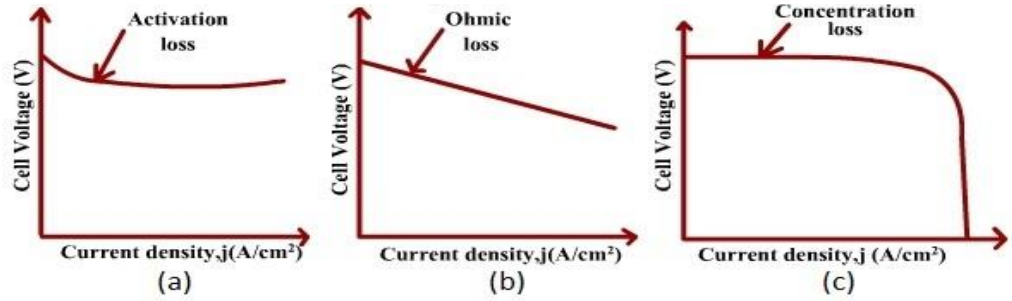

Figure 2.25 Graphical representation of three major voltage losses for PEMFC (Figure edited from NPTEL, 2012) [2.4.22]

A certain amount of energy is needed to start the chemical reaction and sustain the reaction which produces a non-linear potential drop called activation polarisation [2.4.22]. Activation losses occur at both anode and cathode and are associated with electrode kinetics [2.4.23]. This type of loss causes a voltage loss as soon as the FC is turned on to initiate and maintain the reaction. The activation polarisation effect on an individual cell has been plotted in Figure 2.25 (a).

The Ohmic losses are due to the resistance of membrane ionic conductivity and flow of electrons through the fuel cell components. Although the internal resistance is subject to change dependent on water concentration and membrane temperature, the resistance change is usually negligible due to the small temperature range of PEMFC [2.4.16] [2.4.24] [2.4.25]. This type of loss obeys Ohm's Law providing a generally linear relationship curve as Figure 2.25 (b) shows.

The concentration losses occur if a reactant is rapidly consumed and the reactant cannot be delivered at constant pressure due to flow resistance [2.4.26]. This type of loss usually associated with mass transport of reactant and occurs by both the processes of convection and diffusion [2.4.27]. The concentration losses generally have a very small effect until the current density reaches a certain higher threshold and then starts to increase rapidly as Figure 2.25 (c) shows. This also determines the maximum output limit that a FC stack can achieve. If a FC stack is requested to provide a higher power (hence high current density is required) than the stack can provide, the concentration loss would be a significant contributor to the FC voltage loss. This would cause the FC to fail. (Detail deductions and calculations of all three losses can be found in [2.4.16])

The actual FC potential can be calculated as:

$$V_{out} = number\ of\ cell \times V_{cell} = E_{theoretical} - V_{act} - V_{ohm} - V_{conc} \qquad (2\text{-}10)$$

The result of equation (2-10) would then produce the actual FC output voltage which is the actual FC curve shown in Figure 2.26. Figure 2.26 shows an idealised and actual performance of a fuel cell with respect to the potential current response at 25 °C and 1 atm (101 kPa). This actual PEMFC voltage curve represents a generic voltage characteristic of FC output voltage under all three losses. This would be the PEMFC output voltage from an individual cell which can be multiplied to form a larger power source with the same voltage curve [2.4.28].

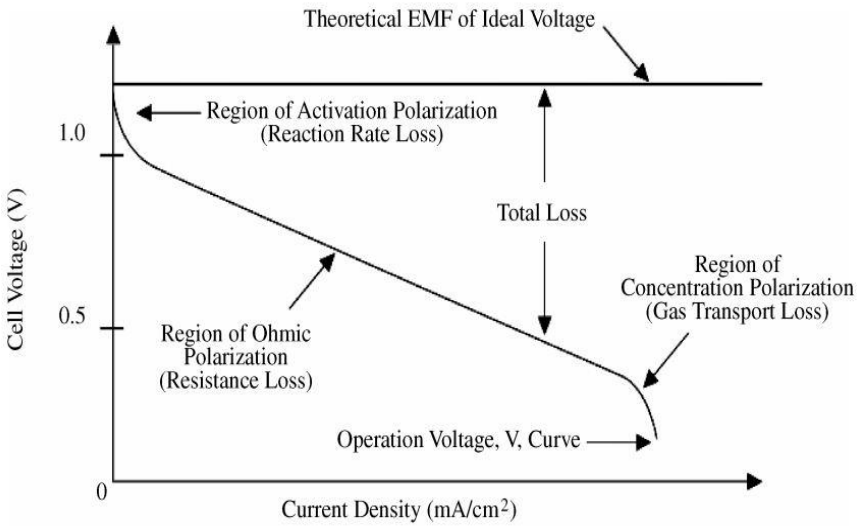

Figure 2.26 Generic theoretical and actual FC voltage curves (Figure from Pilatowsky, 2011) [2.4.21]

2.4.4 PEMFC for bus application

PEMFCs have been developed and trialled in a wide range of applications since 2002. Because of their applicable properties, PEMFCs have been used mainly in three application fields: transportation (automobiles, scooter/bicycles, boat and airplane), stationary (power plant) and portable (backup power, uninterrupted power supply and portable devices power supply) [2.4.29]. Depending on the application requirements, various PEMFC applications have been developed for different uses requiring a wide power range (1 kW – 300 kW) [2.4.30]. This research will focus on the field of transportation applications for PEMFCs, in particular, bus applications. PEMFC technologies for bus applications have been developed since the 1980s and the first demonstration fleet entered the public domain in the early 2000s. After 17 years of research, development and demonstration (RD&D), PEMFC technologies have been greatly improved since the first aerospace applications and have become a much more commercially viable solution for automobiles [2.4.16] [2.4.31]. The improvement over time and efficient performance have made FC buses a promising potential zero emission bus solution. A summary of the main advantages and key challenges of PEMFC for bus application has been provided as follows.

Advantages for FC bus

1. Environmentally, as the most desirable option. FC buses produce no harmful operating emissions and hold the potential of total zero harmful emissions as the clean hydrogen production industry grows.
2. High efficiency. The overall efficiency is much higher than that for conventional internal combustion engines because FCs are free of associated enthalpy and frictional losses. The superior theoretical efficiency of PEMFCs also has the potential for improved performance efficiency as the technology becomes more mature [2.4.16].
3. Fast start up. Unlike other FCs, PEMFC can be quick start and meet the requirements of bus applications with respect to start-up time [2.4.32].
4. Low operating temperature. The operating temperature of PEMFC is around 80℃ which makes it more suitable for transportation usage compared with alternative FCs.
5. Fast refuelling time. Hydrogen fuel can be refuelled much quicker compared with battery electric powered vehicles because the fuel is usually stored in highly compressed gas.
6. Simplicity. PEMFCs have a very simple working concept because they are made in layers of identical cells [2.4.16]. This modular system configuration gives PEMFC buses extra flexibility in terms of bus design, system change and maintenance.
7. Quiet and less vibration. The FC stack itself does not have moving parts and is completely based on the chemical reaction to provide electrical transmission. Therefore, they make much less noise and vibration when compared with conventional buses.
8. Less size and weight. PEMFCs can be made in a variety of sizes, depending on the application requirement. The small size and weight of PEMFCs not only offers more flexibility but also provides additional benefit when competing with other zero emission buses such as battery electric buses [2.4.16].

Challenges for FC bus

1. Expensive. Although the cost of the PEMFC has reduced throughout the development, PEMFC buses currently still cannot compete economically with conventional technologies. This is an issue for most new technologies and they are expected to continually diminish with the development and maturing of the technology itself [2.4.33].
2. Slow response rate. FC power output is limited by an inability to react quickly to sharp power demand transients because of the low power density characteristics

and the hydrogen fuel control system.

3. Hydrogen issues. First, hydrogen, which is the most common fuel for FCs is not a primary fuel, is usually produced from hydrocarbon reforming or water electrolysis. Therefore, in order to accomplish true zero emissions, the hydrogen fuel has to be produced from clean energy instead of fossil fuels [2.4.34]. Hence the FC bus technology would also need to be based on the clean hydrogen production development. Second, the most common way to store hydrogen on-board a vehicle is by using compressed gas cylinders, which creates extra cost and space-demand.
4. Infrastructure required. Widespread use of hydrogen vehicles would require the establishment of new hydrogen infrastructure. However, this problem can be lessened for bus applications because buses are generally centrally managed and distributed [2.4.35].
5. Water management required. Although water produced during FC bus operation is usually emitted as vapour, managing the waste water produced in the PEMFC is also essential as moisture can be an important factor in chemical reactions [2.4.36].

The PEMFC section of the literature review can be summarised into the following points:

1. PEMFCs stand up as the most suitable for applications to buses because of their high efficiency, short start-up time and relatively low operational temperature range compared to other FCs.
2. The working principle of the PEMFC is relatively simple and is based on a chemical reaction to provide electrical output.
3. The PEMFC has superior theoretical efficiency. Additionally PEMFC applications still have potentials for improvement.
4. The PEMFC has many unique advantages that are especially beneficial for bus applications, but there are also challenges to address and barriers to overcome such as expense, slow response and hydrogen infrastructure.

2.5 Energy storage options

2.5.1 Energy storage overview

An energy storage device is a device with the ability to store energy in one form or another. Electrical energy can be stored directly in electrical form or converted to other forms depending on the type of storage medium [2.5.1]. The current energy storage technologies are generally divided into three main groups: electrostatic, mechanical and electrochemical storage [2.5.2]. The three groups represent three major storage processes with different technologies as Figure 2.27 shows.

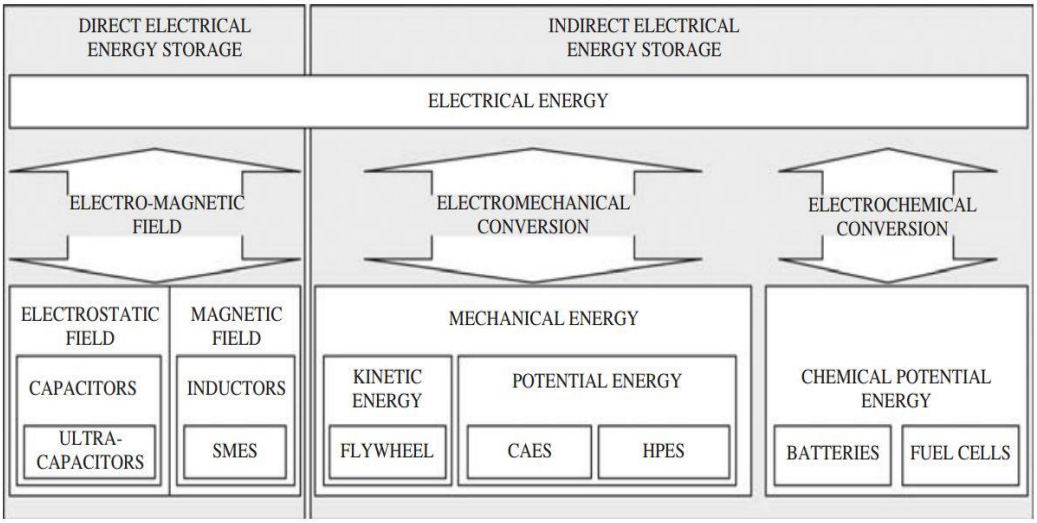

Figure 2.27 Three main groups of energy storage technologies and devices (Figure edited from Grbovic, 2013) [2.5.1]

- The electro-magnetic storage group represents a direct electrical energy storage where energy will be stored and used in electrical form directly. The two most commonly used direct electrical energy storage method are capacitors, which store energy in electrostatic field, and inductors, which store energy in magnetic field [2.5.1]. These means of storage are commonly used in supercapacitors and super-conducting magnetic energy storage (SMES).
- The mechanical storage group represents indirect electrical energy storage where energy will be stored and converted between electrical form and mechanical form. In the mechanical energy storage format the energy is normally stored as kinetic energy using flywheels or potential energy using CAES (compressed air energy storage) and HPES (hydro pumped energy storage).
- The electrochemical storage group represents another indirect electrical energy storage where energy will be stored and converted between electrical form and chemical form. This type of technology is being commonly used in batteries [2.5.1].

2.5.2 Energy storage for transportation applications

Energy storage is being widely used in transportation applications at present. The aim of this section is not to present in detail the electrochemistry of different energy storage technologies, but to focus on the general characteristics and performances of the types used on buses. The energy storage system in hybrid buses generally serves two purposes: to deliver energy to supplement the engine and to absorb energy from regenerative braking. The energy storage specification requirement for hybrid buses differ from those for pure electric buses where energy storage is the only power source. Pistoia [2.5.3] summarised some key general requirements for energy storage used in hybrid buses as follows.

1. Designed to maximise total power delivered and recapture regenerative energy.
2. Must deliver high power in repetitive shallow charge/discharge.
3. Need to be light weight, safe and having extensive life cycle.
4. Need to avoid reaching full discharge or full charge during bus operation.
5. Need for a controller to interface with overall vehicle energy management.
6. Can have a smaller operating range in terms of state of charge (SoC) while energy storage for pure electric bus must be capable of regular deep charge/discharge [2.5.3].

The power/energy capacity of storage depends on the specific application requirement. Energy storage for transportation applications can be loosely divided into two primary categories: high power/fast discharge and high energy/extended discharge [2.5.4]. Those two categories represent two important parameters: power density and energy density. Power density indicates how fast energy can be delivered or absorbed while energy density describes how much energy can be held in storage. A Ragone plot can be used to explain the relationship between power density and energy density. Figure 2.28 shows a Ragone plot summarising some of the more commonly used energy storage technologies used in transportation.

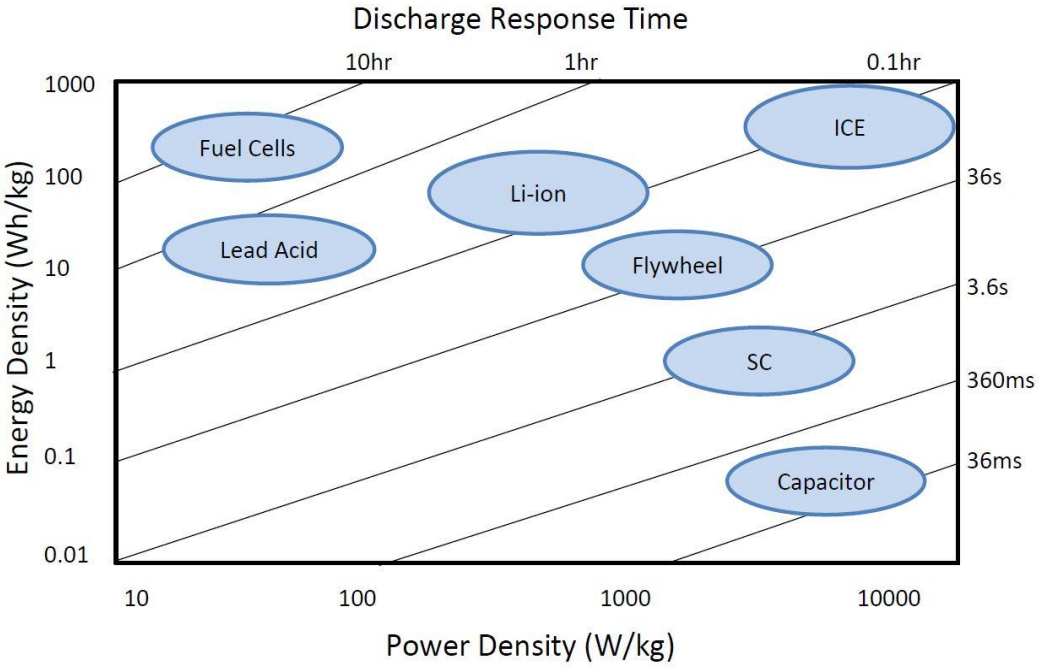

Figure 2.28 Ragone plot of main energy storage devices for transportation applications [2.5.5]

- **Fuel Cell**: FCs have a very high energy density but very low power density meaning it can store a lot of energy but are not designed to release the energy quickly. As discussed before, FCs can and do work as the sole source to drive a bus but the FC has to be high power or hybridised with different sources allowing a smaller FC.
- **Lead Acid**: The Lead-acid battery is the oldest type of rechargeable battery and is also one of the cheapest and most widely used battery systems due to wide use in the automotive industry [2.5.6]. Although there are hybrid buses using lead acid batteries for energy storage, they are generally not considered in the model [2.5.7]. The relative low specific energy of lead-acid batteries make them unsuitable for bus applications due to the weight requirement (e.g. It would require approximately 9,000 kg of lead acid batteries to meet a busy city's transit authority performance and range requirement in an electric bus) [2.5.8] [2.5.9].
- **Flywheel**: The flywheel is a device that stores energy in mechanical form through kinetic energy in a rotating inertial mass. It is environmental friendly and has both reasonably high energy density and power density. However flywheels are not suitable for city transit bus system as a mass energy store due to their large space demand and complicated technology requirement.
- **ICE:** The internal combustion engine, has the highest power density and energy density among the energy storage technologies shown in the figure. The superiority of this mature technology is the reason why ICEs have dominated the heavy

vehicle industries. However, ICEs will need to be greatly improved or completely replaced due to them being heavy polluters.

- **Li-ion:** Ehsani [2.3.33] provides a detailed characteristic comparison of fifteen types of electrochemical battery. The environmental impact of batteries is an important concern that needs to be addressed even though the primary objective of green transport technology is to reduce hydrocarbon use. Beliveau [2.5.10] carried out a study showing that the Lithium-ion (Li-ion) battery and Nickel-metal hydride (Ni-MH) battery are comparatively environmental friendly against other types by evaluating the material, mass, emission of batteries. Li-ion batteries have good energy density and reasonably good power density makes them one of the most commonly used technologies for hybrid bus applications.
- **Capacitor:** The capacitor is a passive two-terminal electrical component used to store electrical energy in the form of static charge. They have high power density but very low energy density. Standard capacitors are generally not considered for large scale energy storage for vehicles because of their energy capacity and weight limitation.
- **SC:** The supercapacitor is a derivative of standard capacitors with increased energy density. The SC works by separating charge between electrode and electrolyte to store the electrical energy in double-layer capacitance [2.5.11] [2.5.12]. SC have very high power density and a reasonably high energy density which makes them a good option for hybrid bus applications [2.5.13].

Based on the comparisons and discussions, although there are recent studies that addressed the potential of SCs, the most dominant type of energy storage for hybrid bus applications is still the Li-ion batteries [2.5.14] [2.5.15]. From the Ragone plot, both Li-ion and SC had relatively good energy density and power density. The largest difference in terms of electrical output is that Li-ion batteries generally have more specific energy while SCs generally have more specific power [2.5.15] [2.5.16]. Both technologies are relatively mature and are widely used in the automotive industry. Their different energy storage methods provide different characteristics and performances in hybrid bus applications. They are both considered as suitable solutions for energy storage in hybrid buses. Details of Li-ion battery and SC as energy storage in this research will be discussed in detail in Chapter 4.

The energy storage section of the literature review can be summarised as follows:

1. FCs have very high energy density and relatively low power density compared to other energy storages.

2. Energy storage by electrostatic and chemical means are better suited for portable applications that can be used in transport applications.
3. Li-ion battery and SC are considered as two of the better energy storage options for hybrid bus applications.

This research will follow up the recent FC bus developments by carrying out a critical review of FC buses in the next section to help further understand the role of FCs for public transportation.

2.6 Critical review of FC hybrid bus development

This section provides a methodological review of past literature mainly focusing on FC hybridisation technology in the transportation industry.

2.6.1 Drivetrain configurations

As discussed before, the series hybrid configuration is more advantageous for city bus applications. For a FC bus, the electrical output from the FC can be directly supplied to the propulsion motor and supplemented from an energy source, which eliminates the need for an additional generator and conversion process for diesel electric series hybrid buses [2.6.1] [2.6.2]. For this reason the majority of FC hybrid buses use series hybrid propulsion configuration [2.6.2] [2.6.3]. Initial feasibility assessments of integrating series hybrid technology with FCs have been presented since 2005. Research on the types of series hybrid configuration have been detailed in a number of researches. Figure 2.29 summarised some of the more representative configurations suggested in the researches.

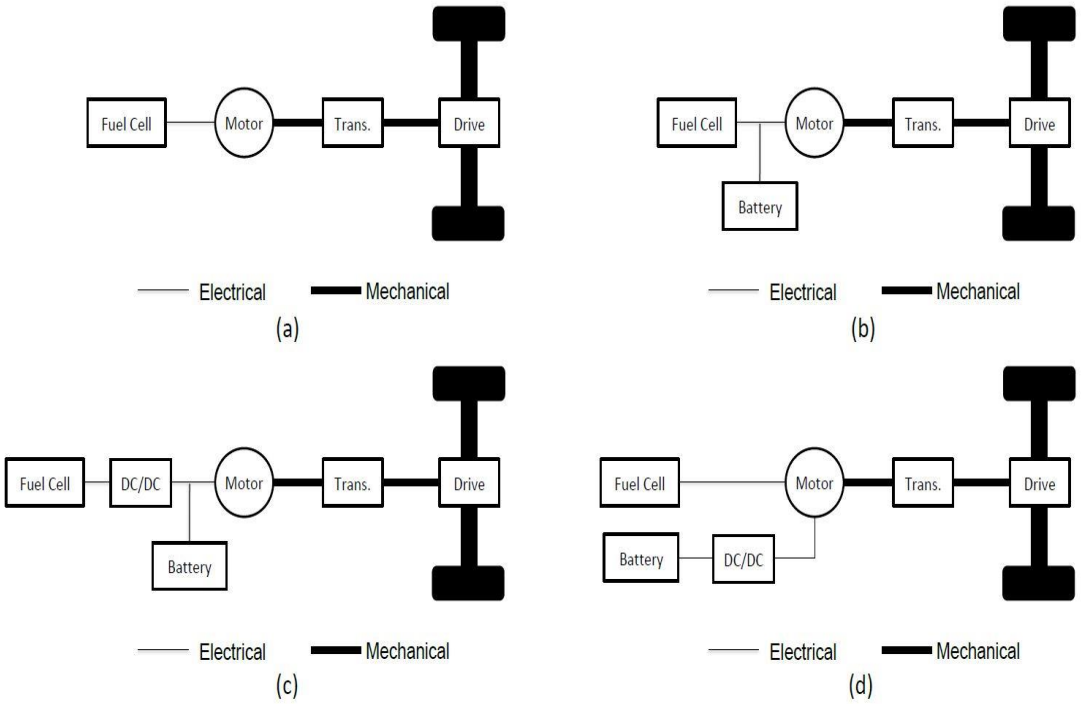

(a) FC direct drivetrain
(b) FC/Battery series hybrid drivetrain
(c) FC/Battery series hybrid drivetrain with converter for FC
(d) FC/Battery series hybrid drivetrain with converter for battery

Figure 2.29 FC bus alternative system configurations

[2.6.2] [2.6.3] [2.6.4]

The first three types (a, b, c) are direct FC configuration, series hybrid configuration and series hybrid with converter configurations respectively. These were assessed and compared experimentally in Wang's (2006) work [2.6.2]. These three configurations were integrated to prototype buses and were road tested for performance evaluation. Results from the Type a and Type b were compared. Apart from the propulsion systems the buses were otherwise identical. The result of the Type a configuration bus showed slightly higher fuel consumption rates and much higher FC power variation rates which could be detrimental to FC stack life and performance. The result of the Type b configuration showed approximately 20% less power variation in FC output and slightly higher efficiency. The second experiment was carried out by comparing the performance of integrating Type b and Type c configurations on the same bus respectively. The results showed Type c configuration had higher fuel consumption and a reduction in FC power variation rate than Type b. The authors also stated the DC/DC converter can be used to adjust the SoC of the battery and control the power distribution between FC and battery. The authors concluded that series hybrid configuration with FC would perform better than the FC direct driven system and the hybrid system with DC/DC converter would enable easier control of power flow.

Although this piece of work is relatively dated and the buses were not operated for long distance or duration, it still produced useful results for FC hybrid bus development and has been considered in this research. The FC direct driven prototype bus had higher and quicker power variations since the FC, as the only power source in the bus system, needs to manage all the power demand. The lower efficiency of the Type a bus is because all the braking energy had gone to waste when some of this energy could be recovered with recovery and storage. The reduced efficiency of Type c bus when compared to Type b was due to the additional losses within the DC/DC converter. However, the converter plays an important role in both controlling FC output and battery SoC.

The Type c and Type d configurations were also analysed and compared in Li's (2014) work [2.6.3]. The main difference between Type c and Type d is the location of the DC/DC converter. The authors carried out a comparison study on advantages and disadvantages of the two configurations and concluded Type c could better match the power demand of a bus. Although there were no simulation or experimental results supporting the authors' argument, the theoretical analysis still provides an understanding of converters for FC buses. The locations of the DC/DC converter in the FC bus system serve different functions. The FC output converter is needed in the system to control output power and voltage, which also reflects Wang's work discussed before. On the other hand, the requirement of a Battery output converter would depend upon the type of energy storage and the hybrid system control strategy. For example, as Figure 2.30 shows, a converter might not be needed for lithium batteries if it can match the output voltage of FC because it can keep the variation in voltage relatively small until it exceeds 80% of the discharge capacity [2.6.4]. On the other hand, a converter is needed for supercapacitors to boost the voltage because the voltage of supercapacitor is direct proportional to the SoC [2.6.4].

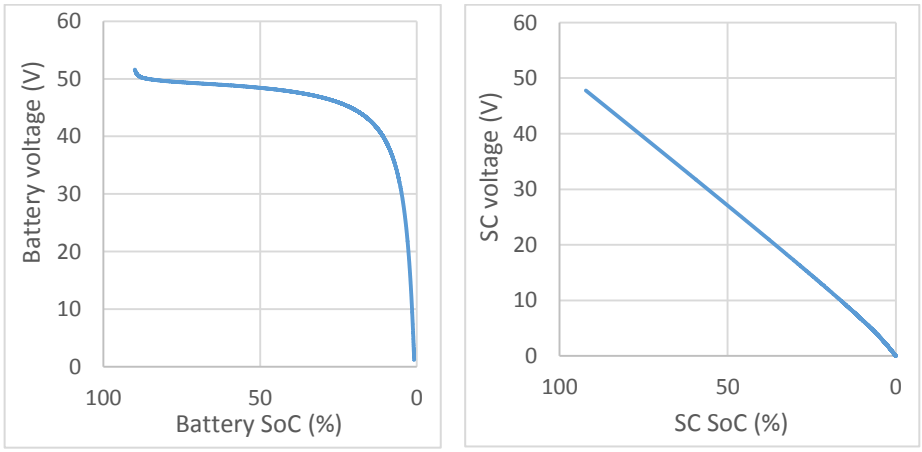

Figure 2.30 Typical battery and SC discharge curve

The hybrid configuration section of the critical review can be summarised as follows:

1. FC series hybrid drivetrain can achieve higher efficiency and better fuel economy than a FC only drive train system because of better control and enabling regenerative braking.
2. In a FC hybrid drivetrain, a DC/DC converter is required for the FC to boost and control the FC output voltage and power. However whether a converter is needed for energy storage would depend on the energy storage type and requirement for power conditioning.

2.6.2 Hybrid control system

An energy management system is normally required to control, balance and optimise the output of each power source in a hybrid system. A significant amount of research has been carried out on hybrid system control whereas the majority of researches were for diesel electric hybrid systems. Control system development for FC hybrid buses has been carried out more recently. Although the control system of FC hybrid systems were originally applied to other non-FC hybrid bus systems, these control systems are worth investigation due to the different characteristics of FCs.

Panday et al (2014) [2.6.5] provided a comprehensive review of most of the existing hybrid vehicle energy management strategies and provided a classification method as Figure 2.31 shows. In Panday's work, energy management strategies for hybrid electric vehicles (HEV) has been divided into two main categories: rule-based strategy, where control schemes are based on operation modes, and optimisation-based strategy, where control schemes prioritised in terms of system optimisation. Each category can be further sub-divided into different classes of types having different methodologies. The authors did a conceptual review of all types of control strategies in the Figure and compared them in terms of complexity, computation time and optimisation type. The authors concluded that each control strategy has its own advantages and disadvantages depend upon the applications. Additionally, Panday et al also suggested that rule-based controllers are generally easily implementable but less optimal in terms of fuel economy and efficiency while optimisation-based controllers generally produces better result but are more complex.

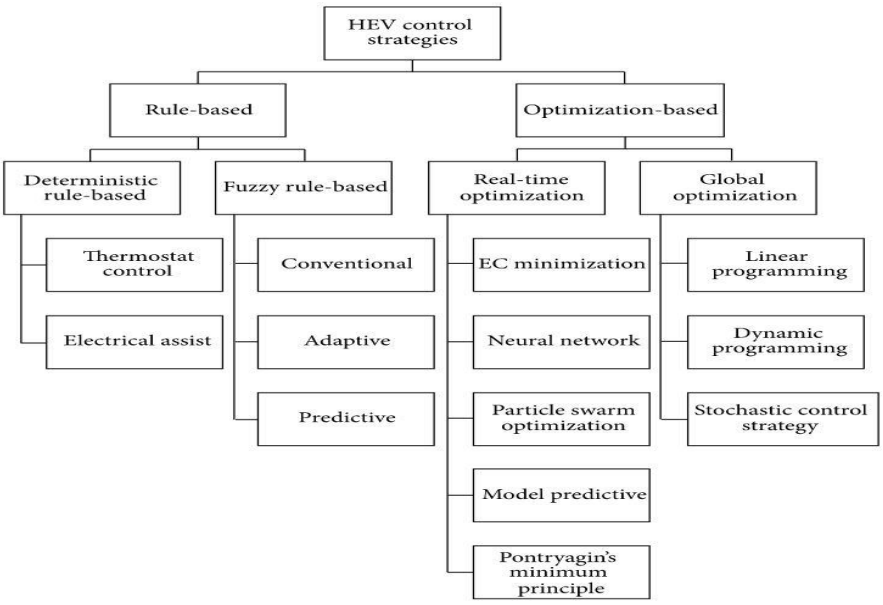

Figure 2.31 Hybrid electric vehicle energy management strategies [2.6.5]

There has also been recent research focusing on energy management specifically for FC hybrid applications. In Garcia's (2012 and 2013) [2.6.6-2.6.8] works, five of the more promising control systems have been investigated for FC hybrid vehicle application. The five control strategies are operation mode control, cascade control, equivalent consumption minimisation strategy control, fuzzy logic based control and predictive control. Operational mode control determines the operation mode of the vehicle by generating a reference value for power or SoC to control the power flow and this is also called deterministic rule-based control in Panday's work. Cascade control, which is one of the real time optimisation strategies, works by controlling two cascade control loops where the outer loop uses a simple proportional controller to generate a reference battery current and the inner loop to adjust the current to match the outer loop defined current.

Equivalent consumption minimisation strategy (ECMS) control focuses on obtaining the minimum hydrogen consumption for the FC based on power demand and energy storage SoC in real time. Fuzzy logic based control is one of the most widely used control strategies for different applications which is a rule-based control that determines reference power values depending on the vehicle specification. Predictive control focuses on obtaining a global optimum solution if there is prior knowledge of the route and the route is planned in advance. The authors applied all five control strategies on actual FC hybrid tramways to evaluate and compare their performances. The results showed that all five control strategies showed similar outcomes, with the following exceptions. ECMS achieving the lowest hydrogen consumption, as expected,

while fuzzy logic and predictive controls require much longer computation time and require a more complex control system. The operation mode control and fuzzy logic control are the simplest rule-based control strategies to design and implement, but suffers from lower accuracy and more variation where similar arguments were also conducted in other works [2.6.9] [2.6.10] [2.6.11]. The authors concluded that ECMS control to be the most suitable control strategy for FC hybrid electric vehicles.

Similar conclusions regarding ECMS control have also been drawn in works from Xu (2009 and 2015) [2.6.12], [2.6.13] and Zhang (2013) [2.6.14]. Xu (2009) applied ECMS controls on several actual FC hybrid buses and put them in daily service during the 2008 Beijing Olympic Games. The recorded data indicated a 17.8% reduction in fuel consumption using ECMS when compared with a rule-based strategy. It was found the fuel cell system efficiency was improved from 48.3 % to 49.5 % and the total hydrogen energy consumption was reduced from 67 MJ to 50 MJ with the ECMS control. The authors provided an energy flow Sankey diagram showing this 17.8% reduction consisted of 2.5% from ECMS control and 15.3% from the braking energy regeneration strategy brought about by ECMS control. In Xu's (2015) work, the authors developed an optimal energy management strategy based on mean value calculation and showed it can achieve longer driving mileage than conventional controllers. Xu's conclusions were also verified in Zhang's (2013) work showing that effective regenerative braking control can significantly reduce the hydrogen consumption. The authors also concluded that regenerative braking can work independently without affecting the anti-locking braking system.

The hybrid controller section of the critical review can be summarised as follows:

1. Some aspects of the diesel electric hybrid energy management system can also be used for FC hybrid systems. However, due to the different characteristics of FC, an optimised FC hybrid controller needs to be designed.
2. Five types of common hybrid control systems have been tested in FC hybrid systems. The equivalent consumption minimisation strategy showed best fuel economy while also reasonably meeting the performance of the other four control strategies.

2.6.3 FC/battery degree of hybridisation

The degree of hybridisation between engine and energy storage has an important role in component sizing and system optimisation in terms of configuration and performance [2.6.15]. Significant research has been carried out on diesel engine hybrid technologies but a very limited amount of literature work has been found on how the FC/battery degree of hybridisation would affect the system performance. Since FCs have a different characteristic curve from conventional engines, it is important to specifically investigate the effect of varying FC/battery degree of hybridisation.

In Zheng's (2014) [2.6.16] work, the authors presented a power source sizing methodology for FC hybrid vehicles. The authors presented a generic FC/battery combination plot as Figure 2.32 shows. For a FC hybrid vehicle, they suggested there is a minimum FC and battery size in the hybrid configuration to be determined by the maximum vehicle speed and acceleration requirement. The authors simulated 72 power source sizing combinations of FC (20 – 100 kW) and battery (7 – 56 battery module, 6.5 Ah each) and modelled the hydrogen consumption and system cost under each circumstance. After applying all 72 combinations to two different driving cycles, the authors filtered out 51 ineffective combinations and selected the two best combinations out of the 19 combinations for optimum fuel consumption and cost respectively. The authors concluded that an optimum degree of hybridisation range can be found for FC hybrid vehicles depending on the application requirements and the size of FC stacks plays a vital role in cost optimisation. However the authors did not specify how the hydrogen consumption calculations were made and how the power combinations were going to be varied with driving cycles.

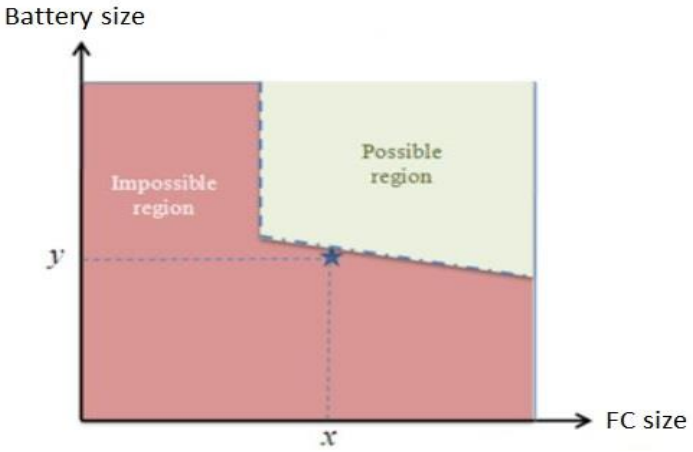

Figure 2.32 Generic FC hybrid vehicle power source sizing combination [2.6.16]

In Xu's (2013) [2.6.17] work, the authors presented a theoretical model describing the relationship between power source size and vehicle performance. The authors suggested the optimal sizing between power sources needs to be evaluated from five main factors: maximum speed, acceleration rate, maximum climbing angle, maximum mileage and hydrogen consumption. The authors demonstrated two prototype buses with different FC/battery power source size combinations using both theoretical calculation and on-road experiments. The two prototype buses are Bus 1 (40 kW FC, 180 A.h battery and 330 V battery voltage) and Bus 2 (80 kW FC, 100 A.h battery and 280 V battery voltage). The results showed Bus 1 achieving 23% higher maximum speed, 37% shorter time to accelerate to 50 km/hour, 18% greater mileage and 2% less hydrogen consumption and exactly the same maximum climbing angle as Bus 2. Although the authors did mathematically formulate an optimal power source ratio for FC/battery hybrid, this ratio can only be considered as an optimal solution when it is used for this specific bus on the specific driving cycle selected. However, the comparison study between Bus 1 and Bus 2 showed some very interesting results in that the Bus 1, with a smaller FC and larger battery, actually surpassed Bus 2 for most of the degree of hybridisation optimising factors.

In Hosseinzadeh's (2013) [2.6.18] work, the authors simulated a FC/battery hybrid forklift truck and focusing on the effect of FC and battery size on vehicle hydrogen consumptions. The authors compared different sets of power source combinations and reached similar conclusions to Xu's (2013) work. The authors also compared two different control strategies for power balancing between the FC and battery, first using average hydrogen consumption based on previous driving cycles, and second focusing on keeping FC output constant at its peak efficiency point. The result showed the second strategy reduced hydrogen consumption by 22% when compared with the first strategy. However, the authors did not specify clearly how the battery SoC was affected by the two strategies.

Melo et al (2014) [2.6.19] and Ribau et al (2014) [2.6.20] [2.6.21] conducted a similar approach on FC hybrid vehicle hybridisation degree study by investigating the effect of driving cycle on FC hybrid systems. The authors analysed two cases. One case focussed on a cost-optimised system. The other case focussed on a hydrogen consumption optimised system. Both optimised systems have been simulated each using two different driving cycles: Porto metropolitan area and ETC (European transit cycle) for heavy duty vehicles. The Porto cycle represents a typical busy city driving environment which has a low average speed, high average acceleration and longer

idling time due to frequent start-stop. The ETC cycle represents a heavy duty driving cycle outside the city which has a higher average speed and reduced idling time and accelerations. The comparison results presented by the authors have been summarised in Table 2.4.

Table 2.4 Comparison between cost-optimised and fuel-optimised models [2.6.19-2.6.21]

Driving cycle	Optimised by	FC (kW)	BAT (kWh)	Bus mass (kg)	Cost (1000$)	H2 cons. (MJ/km)	Max. speed (km/h)	Time (s) 0-50km/h
Porto	Min Cost	82	9	12730	39.3	17.2	99.6	12.0
	Min fuel	25	306	17140	298.9	11.2	155.0	8.4
ETC	Min Cost	125	36	13883	84.9	8.2	148.6	7.1
	Min Fuel	83	267	16742	271.9	7.5	161.0	7.2

In the Porto metropolitan driving cycle, the fuel-optimised model showed 65% less fuel consumption and was 87% more expensive than the cost-optimised model. The degree of hybridisation between FC and battery output varies significantly for the two optimisation methods which affect the fuel economy and cost directly. In the ETC driving cycle, the fuel-optimised model showed 9% less fuel consumption and was 69% more expensive than the cost-optimised model. The authors concluded two points from these comparison studies. The optimised system has to find the balance between cost-optimisation and hydrogen consumption-optimisation. Secondly, the system optimisation is heavily dependent on driving cycles.

Similar arguments regarding the driving cycles have also been verified in Cipollone's (2014) [2.6.22] and Xu's (2015) [2.6.23] work. Cipollone (2014) presented a mathematical model of a fuel cell hybrid vehicle and tested it on different driving cycles. The authors selected the fuel cell and battery capacity by finding an optimum balance between designed energy flows and power required for a specific driving cycle. The authors pointed out that the power source balance of other FC vehicles are usually carried out by simply considering the power requirement throughout the bus operation which could over-size the power sources. Over-sized FC/battery capacity could cause the FC to regularly turn on and off because of the generally high SoC in the battery. In Xu's (2015) work, the authors proposed a dynamic programming strategy for power source optimisation problems and suggested it is very important to define the driving cycle in advance. The authors concluded that the degree of hybridisation optimisation between FC and energy storage is not only about power source capacity and control strategies, but is also closely related to the specific driving cycle.

The previously discussed work and most of literature on FC degree of hybridisation studies are for FC/battery hybrids. There are a few papers presenting work on FC with Supercapacitor (SC) degree of hybridisation research. In Lachhab's (2014) [2.6.24] work, the authors used MATLAB to simulate two kinds of hybrid strategy between the FC and SC. The first one is full sizing where the SC is expected to supply all the power for maximum acceleration while the second one is optimal sizing where SC and FC will work together to supply the acceleration power. Although the authors suggested using the full sizing SC design because optimal sizing has slightly more FC output power variation and higher hydrogen consumption, it is clear that the full sizing FC vehicle would require a much larger SC on-board.

In Bubna's (2012) [2.6.25] work, the authors decided to combine SCs with batteries in a fuel cell hybrid transit bus to make use of the high specific power of SCs. The authors pointed out batteries typically lose their effectiveness after a few thousand charge-discharge cycles while SCs can maintain performance for about one million cycles. This drives the thought of applying SCs on FC hybrid buses as frequent charge-discharge cycles are expected to occur. The authors compared six combinations of battery and SC as the energy storage of the FC hybrid bus system. The authors have compared the effect of this hybrid energy storage mathematically. The results showed that the more SCs were integrated in the energy storage, the less current load, energy throughput and heat generation there were. The authors suggested SCs are much more effective in shielding batteries from high current load, reducing energy throughput and prevent heat generation which thereby reduces battery stress and extends battery lifetime. However the more SCs were used in the system, the more cost and weight would be added to the energy storage system. The authors concluded integrating SC with battery in FC hybrid buses is an effective solution to improve the energy storage system for FC applications.

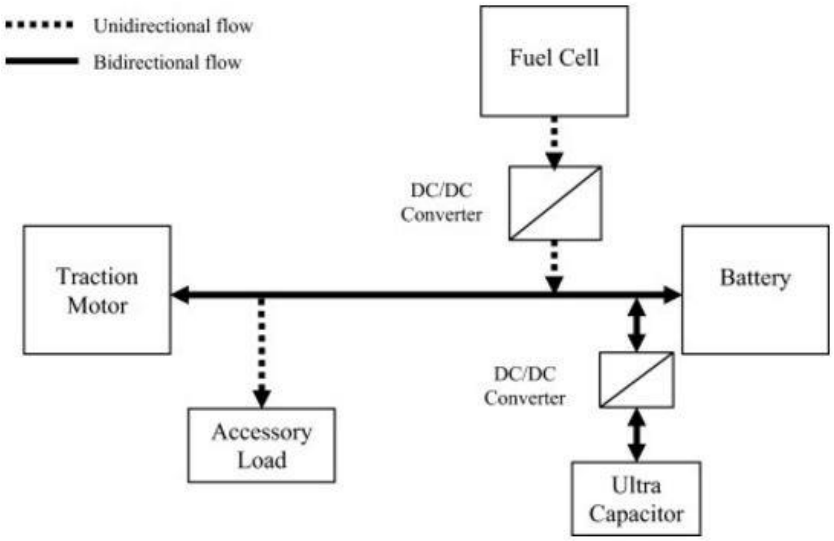

Figure 2.33 Direct parallel FC/BAT/SC structure [2.6.25] [2.6.26]

Similar arguments have also been presented in Xie's (2015) [2.6.26] and Odeim's (2015) [2.6.27] works where the authors built up a direct parallel connected structure test platform of FC, SC and batteries as Figure 2.33 shows. The authors focused on investigating how the three power sources react to dynamic power changes. The results indicated FC has the narrowest power distribution during dynamic cycle to satisfy the slow dynamic power variations. The response of the battery pack power output to dynamic loads is also relatively slow. The SC bank met the fast dynamic load requirements well. Owing to the different charge/discharge characteristics of batteries and SCs (as showed in Figure 2.30 before), the batteries and SCs have been used to meet different demands in this direct parallel structure. The authors also suggested that using DC/DC converters for the three sources can not only effectively control the energy flow but also protect the FC and energy storage system.

The degree of hybridisation section of the critical review can be summarised as follows:

1. An optimal balancing range between FC size and battery size can be found after evaluating five factors: maximum speed, acceleration time, maximum climbing angle, maximum mileage and hydrogen consumption.
2. The optimised system has to find the balance between cost-optimise and hydrogen consumption-optimise and system optimisation is heavily depending on driving cycles.
3. SCs are more effective than batteries in hybrid systems in terms of shielding high current load, reducing energy throughput and preventing overheat.
4. SCs have a quicker response to dynamic load than batteries, but would also add extra cost to the vehicle.

2.6.4 Experimental FC hybrid vehicles

This section will focus on reviewing past research carried with FC experimental test vehicles and real bus systems since most of the existing work is based on theoretical analysis and simulation. Developing an experimental prototype FC system is an important approach to evaluate the performance of a FC system in realistic conditions which can be different from conceptual analysis. Owing to the fact that building a full size FC vehicle is costly, there is not a large amount of research literature available.

In Wu's (2014) [2.6.28] work, the authors built a 9.5 kW FC, 1500 F SC hybrid prototype scaled test vehicle to investigate the FC response under dynamic loads. The authors integrated the FC and SC on a test vehicle equipped with corresponding conditioning systems. The integrated test vehicle has then been tested under step load to evaluate the performance of FC/SC hybrid systems and the results are shown in Figure 2.34. The results showed the FC (red line) requires more time to adjust to the power demand while the SC (dash line) showed much quicker response and compensates for the FC, which takes longer to respond to changing power demands. The authors concluded rapid load cycling is one of the main causes of FC inefficiency and passively coupling SCs with the FC allows hybrid systems to satisfy quick dynamic load adjustment easily. The authors also suggested the size of the SC in a FC hybrid vehicle should be kept at a balance point between large enough to cover maximum acceleration power demand and small enough to ensure the FC does not overcharge the SC under low loads.

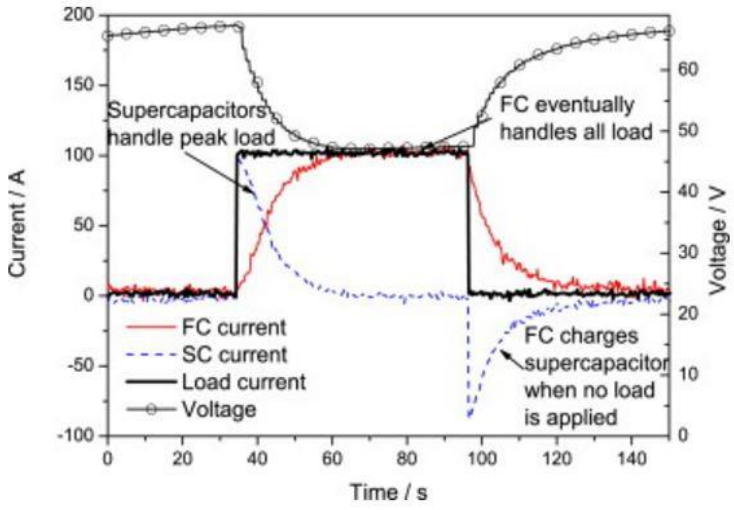

Figure 2.34 Response of FC/SC hybrid test vehicle under pulse load [2.6.28]

Similar points were also addressed in Li's (2016) [2.6.29] work where a FC/energy storage hybrid system was applied on a tramway under actual driving cycle. The hybrid tramway used two 150 kW FC as the main power source and had an energy storage

system consisting of two batteries and two SCs. The power balance between power sources and energy storage system have been controlled through two unidirectional DC/DC boost converters for the FCs and two bi-directional DC/DC boost/buck converters for the energy stores. The authors proposed a control approach where a reference power and voltage command is determined to match the load requested according to the tramway driving cycle. In the actual driving cycle test, the FC showed relatively stable output as the main power source while the energy stores showed more dynamic change response both discharge during acceleration and charge during low load. The authors also determined that it is important for the strategy to be able to maintain stable operation of the FC. Although the authors did not mention it in the study, there is another interesting point that can be observed from the results. The charge/discharge power and current of the SC are much larger than those for the batteries meaning the SCs are reacting to dynamic power demand changes much quicker than the batteries. This can be explained from the energy storage review section carried out previously, that the power density of SCs is much higher than batteries.

There is also research on applying FC hybrid systems on real bus systems. In Bubna's (2010) [2.6.30] work, the authors presented the operation experience of one of the earliest FC hybrid bus in daily services. The FC/battery hybrid bus was designed in 2005, delivered to University of Delaware in 2007 and officially entered daily service. The bus itself was more like a battery electric bus with the FC acting as a range extender as the FC will only be turned on when the battery SoC reaches 0.65 if its threshold as Figure 2.35 shows.

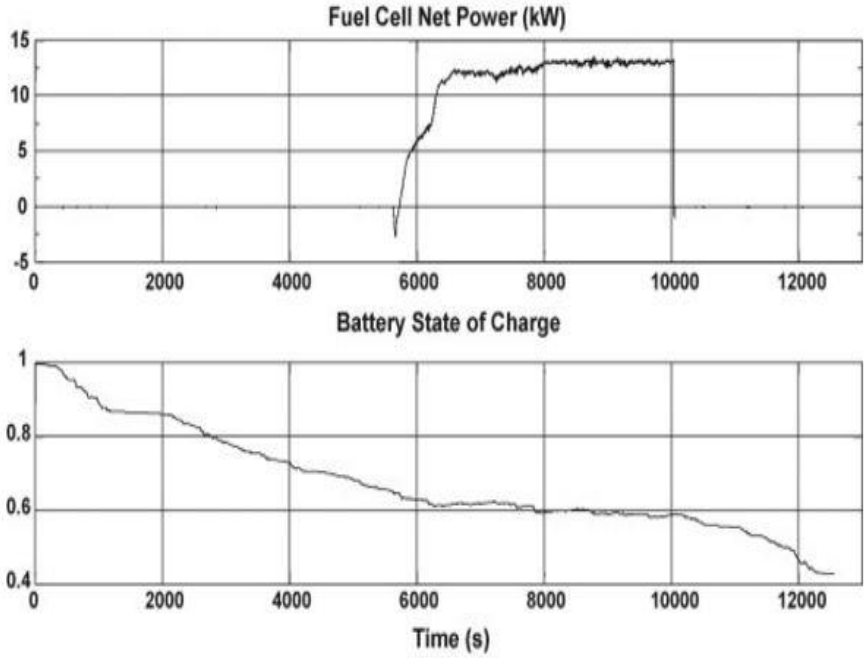

Figure 2.35 Correlation between FC power and battery SoC [2.6.30]

On a typical run of the bus, the FC stack was only used as a secondary power source that only works with the battery as a series hybrid system on the second half of the journey. The bus had been in service for two years and provided valuable operating experience for FC and battery buses. The authors suggested the average efficiency over all days weighted by the hours of operation per day was 32.4% which gives an average 10 kW net power. There were some low efficiency periods which were suggested to be caused by the lingering effect of freeze damage sustained during shipment. The authors pointed out that the FC efficiency plot has shown a generally rising trend because more FC issues have been tracked and more fault diagnosis experiences. The other important metric the authors presented is the regenerative energy ratio which varies from 0.2 to 0.4 in a busy city driving environment. The authors suggested the reason for variations in the regenerative ratio is because of the changes in ridership and road conditions. The authors suggested the vehicle problem occurrence reduced markedly as more operating experience was gained. The authors concluded that regenerative energy is an important contributor to improve efficiency in city driving for FC hybrid buses and the operating issues can be reduced greatly as more FC bus problem-solving experience is gained.

In Sergi's (2013) [2.6.31] work, a pure battery electric city bus was retrofitted as a FC/battery hybrid bus and tested on road. The hybrid system used a series hybrid configuration where both FC and battery pack power the bus. This bus design tried to keep the FC as a constant power source which will be used both propel the bus with

the aid of the battery and increase the battery SoC while the bus is stationary. In this design, instead of using the FC to supplement dynamic load change, the FC output power was controlled by DC/DC converters to only provide three outputs: 1.5 kW (when the battery is overcharged), 2.5 kW (during FC warm up) and 5 kW (all other cases). The authors pointed out that this type of operation can eliminate the issue of FC slow response rate and enables easier control of FC output. Although this test bus was a battery-heavy hybrid system, this type of control strategy has the potential to solve the FC dynamic load problem and keep the FC at near optimum operation.

The experimental FC vehicle section of the critical review can be summarised as follows:

1. FC could have slow response to step loads. SCs have been suggested to be integrated with the FC to compensate for any potential power gaps from dynamic loads. The size of SC in a FC hybrid vehicle should be kept at a balanced range between large enough to cover maximum acceleration power demand and small enough to ensure the FC does not overcharge the SC under low loads.
2. Regenerative braking control plays a vital part in optimising fuel economy and system efficiency of the vehicle, particularly for the city driving environment.
3. Keeping the FC as a constant power source while using the battery to cover any transient power demand in a FC hybrid bus can compensate for the FC slow response issue and potentially extend the FC stack life.

2.7 Summary

In a large city like London, air pollution is one of the most significant environmental and public health issues. Research and studies have been carried out for tackling the air pollution crisis and found one of the largest contributors to air pollution in London is from public transport buses. The government has introduced several measures to help mitigate the impact of bus transportation on the environment. Among all the low emission technologies, FC technology shows great potential to become a long term clean energy solution for city transportation. The FC technology itself has evolved significantly and demonstrated great improvement over time. This research will further explore the role FCs could play in terms of mitigating the impact of pollution from buses.

Lastly, a summary timeline of London low emission bus development milestones of the literature review is presented in Figure 2.36.

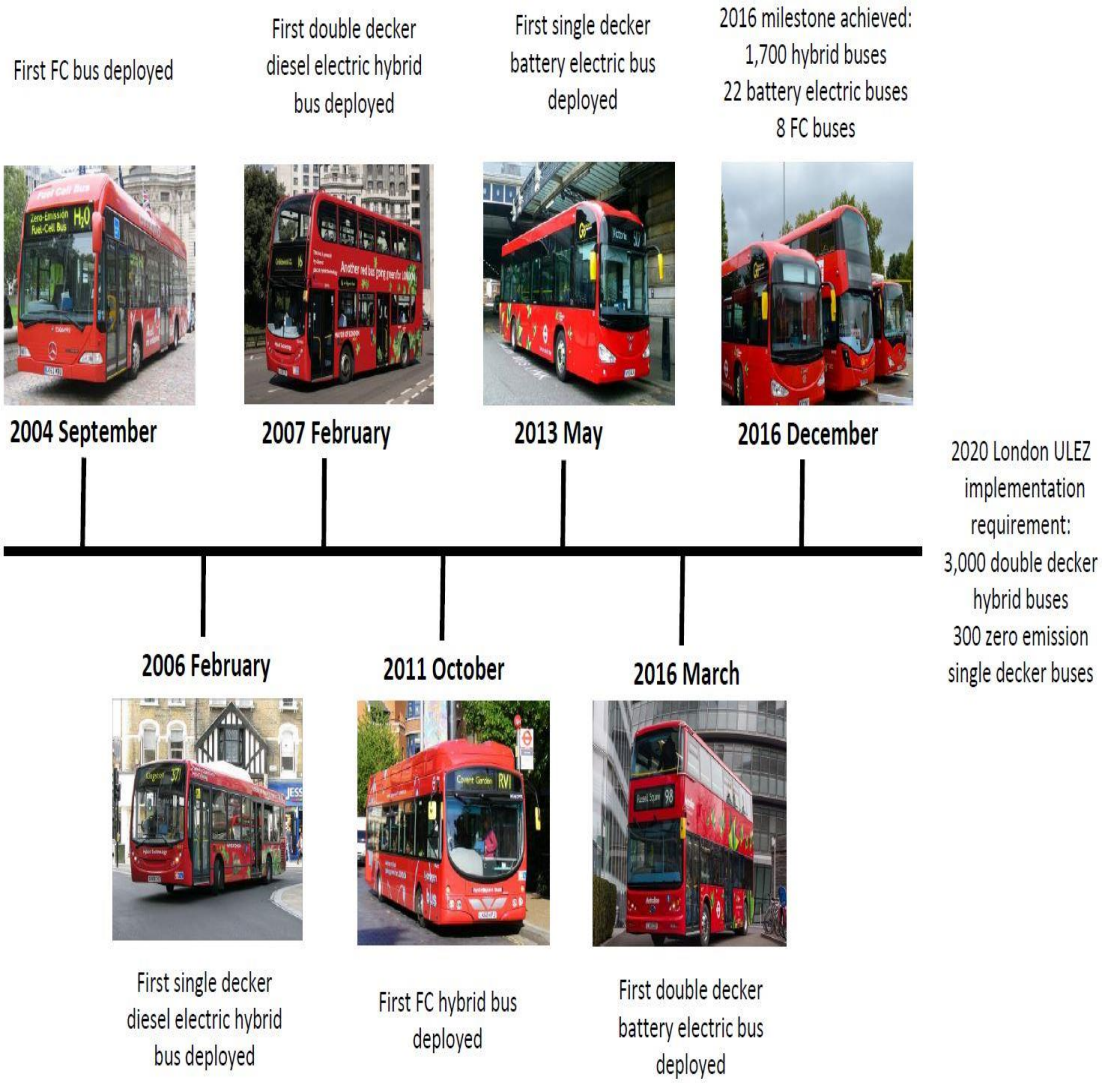

Figure 2.36 Timeline of London low emission bus development milestones

Chapter 3 Problem formulation

3.1 Introduction

This chapter provides a conceptual analysis of how the research problems have been formulated through literature reviews and research gaps identified. The FC bus industry has been in development for nearly 15 years. After analysing the current FC bus industry and the issues addressed from critical reviews in Chapter 2, a number of gaps can be identified which lead to the research questions of this work.

The problem formulation can be presented in three distinct sections.

1. The first section aims to identify the gaps of the FC bus industry and technology development.
2. The second section aims to formulate the research questions this work intends to investigate in order to bridge the gaps.
3. The third section explains the proposed justification method for the identified research questions and also explains how this work could contribute to the research motivations and FC bus industry.

3.2 Gap analysis

Current state of FC buses

FC buses have shown great potential for providing a zero emission bus solution for city public transport. However, unlike battery electric buses, FC buses are still under trial and nearly all commercially operating FC buses are within demonstration projects. The FC bus technologies under trial have been evolving since the first trial FC bus from the CUTE project in 2000. Different system configurations have been integrated and investigated to seek the optimum FC powered bus over the past 16 years. The fuel economy of FC buses has shown a generally improving trend over time with system developments from both academia and industry. Table 3.1 shows some of the more commonly used, commercially available FC bus models worldwide used under different demonstration projects. All these buses have been in passenger service in commercial use for a relatively long period of time. These bus models represent the majority of commercially available FC buses where a significant amount of them are retrofitted from conventional single-decker buses. The operation and evaluation of those FC demonstration buses have provided valuable experience and information for FC bus development.

Table 3.1 Comparison between FC bus models specification and configuration

Bus model	Year	FC power (kW)	Energy storage capacity (kWh)	Energy storage peak power (kW)	Energy storage type	Fuel consumption (kg/100km)	Ref
Citaro Fuel Cell bus	2000-2009	250	n/a	n/a	n/a	20~24	[3.2.1] [3.2.2] [3.2.3]
TriHyBus	2009-2012	48	27.4	200	Li-ion	8.5~12	[3.2.4] [3.2.5]
TX Proterra	2009-2012	32	54	not available	Li-ion	8.43 (plug in)	[3.2.6] [3.2.7]
Citaro Fuel Cell Hybrid	2010-present	120	26.9	180	Li-ion	10-14	[3.2.1] [3.2.8]
Sunline AT FCB	2010-2012	150	47	not available	Phosphate Li-ion	11.55	[3.2.9] [3.2.10] [3.2.11]
Van Hool A300L	2011-present	120	17.4	250	Li-ion	9.7	[3.2.12] [3.2.13] [3.2.14]
Bluways/ Wrightbus	2011-present	75	0.5	240	SC	8~9	[3.2.15] [3.2.16] [3.2.17] [3.2.18]
Van Hool A330	2012-present	150	17.8	not available	Phosphate Li-ion	8 (claimed)	[3.2.19] [3.2.20]
ElDorado National	2012-2015	150	11	200	Li-ion	10.46	[3.2.9] [3.2.21] [3.2.22]

Identifying the gaps

As Table 3.1 shows, various FC bus system configurations have been developed and demonstrated in practical buses. Although the fuel economy has generally seen improvement since 2000, fuel economy cannot be the sole factor in determining an optimum FC system. It also depends on factors such as driving cycle, system control, mechanical framework, capital/operating cost etc. It is therefore hard to determine which type of FC bus configuration is the “future generation of FC buses” as different manufacturers all make different claims. However, there are some points that can be addressed after analysing the table.

It can be seen from Table 3.1 that all FC buses after 2009/2010 were hybridised with some means of energy storage (ES). One of the earliest commercially available FC buses was the Citaro Fuel Cell bus in the CUTE project where a 250 kW FC was the only power source in the vehicle. The fuel consumption of this FC only bus was around 20~24 kg/100km which is nearly double that of the more recent FC hybrid buses. Comparing the Citaro FC bus with FC hybrid buses, FC hybrid drivetrains can enable regenerative braking which significantly improves system efficiency, but at the cost of

extra energy storage and control systems. The FC technology was under initial assessment with immature design and limited operational experience in the early 2000s which could be the reason for poor fuel economy. The majority of FC powered buses today are FC hybrids. This was also reflected in the critical reviews of FC drivetrains in section 2.6.2 where arguments of FC hybrid drivetrain can potentially achieve higher efficiency and fuel economy than FC only powered drivetrain were presented.

The other point that can be noted from Table 3.1 is the large variation in the FC/energy storage hybridisation ratio of different FC buses. It can be seen that the size of the FC and energy storage varies from different bus models. The fuel economy of the FC hybrid buses presented in the table varies from 8 to 12 kg/100km due to different component configuration and driving cycles. The FC/ES hybrid ratio determines the system configuration and control strategy which plays an important role in the bus performance [3.2.23]. As the table shows, the peak power ratio varies from 0.5 to 0.8 showing the ES is capable of contributing a significant amount of power to the hybrid system. However, the ES capacity varies in a much wider range for the current FC bus industry. It is clear that a smaller capacity ES can only be used to cover peak power demand for a very short time. It can be seen that the current FC hybrid bus industry has a lot of variation in terms of FC/ES hybrid ratio. Although they have different fuel economy, that does not necessarily determine which type of hybridisation is better as each bus used different systems and operated under different driving cycles. Since the driving cycle plays a vital role in fuel economy, which was also supported in critical reviews of hybridisation degree research, it is difficult to determine which hybrid concept achieves the best performance among others in a given scenario.

The demonstrated FC buses also showed very different performance. Taking London as an example, two different types of FC buses have operated on the same route with a third FC bus type joining the fleet in 2017. The first FC bus fleet operated in London from 2004 to 2009 was the old RV1 which is the Citaro Fuel Cell bus in the table, and the second FC bus fleet that replaced the old RV1 was the current RV1 bus fleet operated from 2010 to present which is the Bluways/Wrightbus in the table. The two extra Van Hool A330 buses will use a different FC hybrid configuration and will also join the current RV1 fleet for demonstration purposes. Since all three FC bus types used different FC configurations and operated on the same route RV1, these buses could reasonably demonstrate the effect of degree of hybridisation on FC bus performance. Since the details of the two new Van Hool FC buses have not yet been

unveiled, this research will only focus on the present FC bus fleet.

The old RV1 fleet as the first generation used a 250 kW FC to directly power an electric motor. The current RV1 fleet uses a 75 kW FC and a 0.5 kWh ES series hybrid configuration and significantly reduced the fuel consumption on the same route (The driving cycle was assumed to be the same between present route RV1 and old RV1 fleet). The current RV1 FC bus fleet is one of the bus fleets in the CHIC project. This fleet also achieved one of the best fuel economies when compared with other FC hybrid buses. Unlike other FC/battery buses, the ES system in the current RV1 bus is a 0.5 kWh SC and has the smallest ES capacity among other operational FC hybrid buses, but is capable of providing high peak power due to the high power density characteristic of SCs. The current RV1 FC buses have already achieved nearly 50% better fuel economy than the target values of the CHIC project which is significantly better than any other CHIC FC buses (Figure 2.21). The current RV1 fleet uses a relatively small FC stack and the smallest energy storage capacity and achieved one of the best fuel economies. This suggested the combination of a FC hybridised with a high power density SC could potentially provide a more efficient FC bus solution. Also, a smaller FC stack, compared with other current FC buses, could be sufficient to cover certain city driving requirements. Ballard, which is one of the largest FC companies in the world, has announced they are developing two smaller sized FC stacks (30 kW and 60 kW) to meet the largest FC bus order to date from China which is a planned deployment of 300 FC buses in 2017 [3.2.24] and further proves the promising future of smaller FC stacks for city buses.

Following the discussion of current FC bus developments, the question this research aimed to answer can be formulated. To bridge the identified gap this research will:

Explore the potential of integrating a SC with a downsized FC for a FC hybrid bus application and investigate the method to identify an appropriate degree of hybridisation between the constituent power sources.

3.3 Justification for research question

3.3.1 Justification method

Following the identified research question, this section will explain the proposed methods to answer the questions and justify the work of this research. The purpose of this research is to investigate the performance of FC powered bus systems with the ultimate goal being to design the next generation of FC buses from the power system engineering point of view. The initial validation of the design concept has been proposed to be carried out by computer simulation to use the advantage of time and cost provided by modelling. However, as discussed in critical reviews, simulation only, although a powerful tool in itself, would allow rigorous evaluation of the concepts, but to gather empirical performance data a practical test rig would need to be constructed, the design of which would be based on the output from the simulation results.

It is difficult to build a full sized FC bus system in the laboratory. This is not only due to the power, scale and mechanical size demand of a bus system, but also constraints imposed by the HyFCap project requirements and scopes. This research will therefore be carried out using a scaled FC system to investigate the drivetrains. The scaling factor has been selected to be an approximately 10% of the power systems in London RV1 FC bus. The RV1 was selected as the template to develop the models for this research. The scaled FC bus system means all the components will need to be scaled to simulate a completely down-sized FC bus power system in the laboratory. All components would need to be designed, purchased and assembled in a laboratory space where they can be changed relatively easily in a simulation model afterwards. Hence this scaled FC bus system development will follow the “design-build/simulation-optimisation” process for different systems. The computer model can be scaled up to a full sized FC bus level for optimisation once the scaled model has been validated to be representative of the laboratory test bench.

3.3.2 Justification of FC basic drivetrain

A FC only powered bus system has one of the simplest bus drivetrain configurations, consisting of a power conditioned FC driving an electrical motor. The first step has been proposed to build and simulate a basic drivetrain as Figure 3.1 shows. The FC only driving system will be denoted as the FC basic drivetrain in this work.

Figure 3.1 Top level block diagram of the FC basic drivetrain

The FC basic drivetrain system will be built in the UCL electrical laboratory and simulated with computer models. Simulating and building this FC basic drivetrain will serve the following purposes:

1. Test the FC stack to better understand the specific characteristics of PEMFCs.
2. Develop the power conditioning system for FCs.
3. Apply an electrical load system to the FC to simulate different power demand conditions and evaluate the performance of the FC under different power profiles.
4. To investigate the reaction of the FC under worst case scenarios when subjected to fast transient and large step changes in power demand.

3.3.3 Justification of FC hybrid drivetrain

A FC hybrid bus consists of a FC system as the main power source and an energy storage system. In order to build and simulate a FC hybrid bus system, an energy storage system is required to be integrated with the FC system. The next step aimed to enhance the developed FC basic drivetrain into a hybrid drivetrain to investigate the drivetrain of a FC hybrid bus. This section has been divided into two sections: to develop a load system and to develop an energy storage system.

Load system development

In the FC basic drivetrain, only simple electrical loads will be applied on the FC stacks mainly to investigate the reaction and performance of the FC. In this section, in order to simulate an actual bus driving environment, representative static and dynamic loads needs to be integrated in the system to simulate a FC bus more accurately. In an actual driving conditions, the FC bus would have to overcome various loads (windage, friction, inertia and change of gradient) while in operation. It is necessary to develop a load system to be applied on the FC drivetrain to enable simulating actual driving conditions

in a laboratory. The first step in the upgrade of the FC basic drivetrain will be the integration of a driving motor and a load system for the motor as Figure 3.2 shows.

Figure 3.2 Top level block diagram of the FC load system

The load system will be built in the laboratory and also simulated with computer models. Simulating and building this load system can serve the following purposes:

1. Analyse the FC performance when it is directly driving a motor to simulate more realistic FC bus performance.
2. Enable load control (power, speed and torque) on the motor so that different realistic driving conditions (acceleration, braking, uphill, overloaded etc.) can be applied to the FC via the motor.

Energy storage development

The second step will be the integration of an energy storage system to the FC hybrid drivetrain. As discussed in the literature review, the series hybrid propulsion system has been determined to be the most suitable solution for FC bus applications. The parallel hybrid propulsion system will not be considered for FC bus application in this research, hence all discussion on the FC hybrid system will relate to the series hybrid propulsion systems hereafter. A series hybrid system as Figure 3.3 shows has been proposed for the computer simulation and laboratory model FC powered drivetrain. As discussed in literature reviews, supercapacitor and lithium battery technology have been recommended as the two most promising energy storage options for hybrid buses. One of these options will be selected as the energy storage for this FC bus application. The two energy storage options will be analysed in detail in Chapter 4.

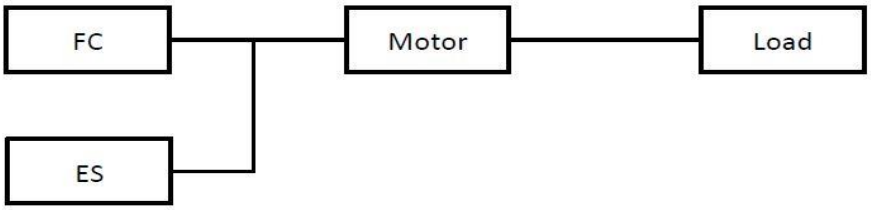

Figure 3.3 Top level block diagram of the FC hybrid drivetrain

Again, the energy storage system for the FC hybrid drivetrain will be built in the laboratory and also simulated with computer models. Simulation and building this energy storage system will complete the FC hybrid drivetrain which can serve the following purposes:

1. Identify the appropriate ES system for this FC hybrid drivetrain application and explain why it is more appropriate than other ES options.
2. Design the control system and conditioning system for the ES for better integration with the FC hybrid drivetrain.
3. Investigate the performance of the FC hybridised with the energy storage under different load conditions.

3.3.4 Justification of FC control optimisation

The controller will be responsible for managing the power between the FC and the ES in response to the load power demand from the motor. The controller will first be designed as a computer simulation model which can be validated with the completed laboratory FC hybrid drivetrain. In this section, the proposed design concept will be evaluated with actual driving cycle and identify the method to find the optimum degree of hybridisation for FC hybrid buses for this specific configuration.

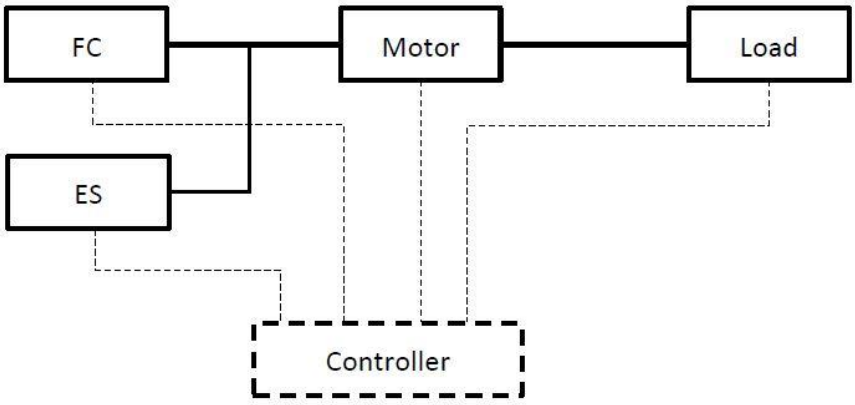

Figure 3.4 Top level block diagram of the FC hybrid drivetrain control system

Simulating and building this control system for the developed FC hybrid drivetrain can finalise the simulation of the scaled FC hybrid bus which can serve the following purposes:

1. Scale up the computer model to represent the power levels of a full scale practical bus.
2. Investigate the effect of degree of hybridisation between the FC and the ES in this hybrid drivetrain and identify the strategies to determine an appropriate hybrid ratio for a FC hybrid bus.
3. Understand how the control strategy would influence the FC hybrid drivetrain.
4. Evaluate performance of the FC hybrid drivetrain under different FC/ES degree of hybridisation and test the viability of a FC hybrid configuration with a downsized FC and identify the optimum control strategy for this design.
5. Evaluate the feasibility of this downsized FC hybrid system design and

compare this design with existing FC hybrid bus systems.

3.4 Summary

This chapter provided analytical analysis into the problem posed by the FC bus development and applications. A gap analysis of the current FC bus industry was presented and gaps have been identified after analysing the commercially available FC buses over the past 16 years. Three points have been observed from the existing FC buses. The first is FC only powered buses have started to be replaced by hybrid ones. The second is FC hybrid buses have large variation in terms of degree of hybridisation. The third is the size of FC stacks shown a downsizing trend. The gaps lead to the research questions which are intended to bridge the gaps by developing a scaled FC hybrid system by both building a laboratory system and computer simulation model.

The justification method has been proposed to both build and simulate a FC hybrid drivetrain to investigate the research question. The justification process has been divided into three steps: to develop a FC basic drivetrain, to develop a FC hybrid drivetrain and to develop the controller. The purposes of each step have been identified which leads to the investigation into the feasibility of the FC hybrid bus design concept. The final expected outcome of this study would be an optimised FC hybrid system validated with both laboratory and computer models and evaluated with different duty cycles. This system can help in understanding the design and development factors specifically for FC hybrid bus applications from a power system point of view and hence support the FC bus development for the HyFCap project.

Chapter 4 Laboratory system development

4.1 Introduction

This chapter describes the design and construction of the proposed FC laboratory test bench. The laboratory system will be a test bench of the power system of a FC hybrid bus. The development of the laboratory system has been divided into two main activities: the development of a FC basic drivetrain and a FC hybrid drivetrain.

First, a basic drivetrain consisting of a FC, a boost converter and an electrical load system will be developed and constructed. After the system is assembled, a number of experiments will be carried out to analyse the system's performance. Second, the basic FC drivetrain will then be integrated with an energy storage system, motor and load system to build up the proposed hybrid drivetrain. The development of the basic and hybrid drivetrains will be described in stages.

4.2 PEM Fuel Cell stack

4.2.1 FC system design

The main component, which is also the most important part of a FC bus, is the PEMFC as the primary energy source. The proposed FC hybrid system is intended to be an approximately 10% scaled model of a FC bus power system using the current London RV1 as the template. The FC stack power utilised for the RV1 bus is a 75 kW PEMFC from Ballard which makes the required power of the scaled FC unit to be 7.5 kW. There are only a limited number of options that satisfy this power requirement and application. After comparing the FC products from some of the largest FC companies (Ballard, Hydrogenics and Intelligent Energy), a 8.5 kW PEMFC unit from Hydrogenics was selected as the closest option to meet the 7.5 kW power requirement.

FC specification

The Hydrogenics 8.5 kW PEMFC selected is a HyPM HD 8 FC which has been designed for high durability and mobile power applications [4.2.1]. This FC system uses gaseous hydrogen as the fuel and generates electricity with water as a waste product. Table 4.1 summarises the key specifications from the product manual and datasheet for the HyPM FC. Figure 4.1 is a schematic of the HyPM HD 8 FC with the main components and interface connections. As it can be seen from the Figure, certain conditioning systems such as regulator, pump, valve, blower etc. are also required to control the reactions within the stack.

Table 4.1 FC and hydrogen supply specifications (@ 21℃ 101.3kPa)

Model	HyPM HD 8	Rated power (kW)	8.5
Dimensions (mm)	785x446x301	Operating current (A)	0-380
Mass (kg)	78	Operating voltage (V)	20-40
Volume (L)	105	Peak efficiency (%)	51
Coolant temperature (℃)	50-60	Consumption (L/min)	≤130
Maximum air flow rate (L/min)	800	Start-up electrical input (V)	12-13 dc

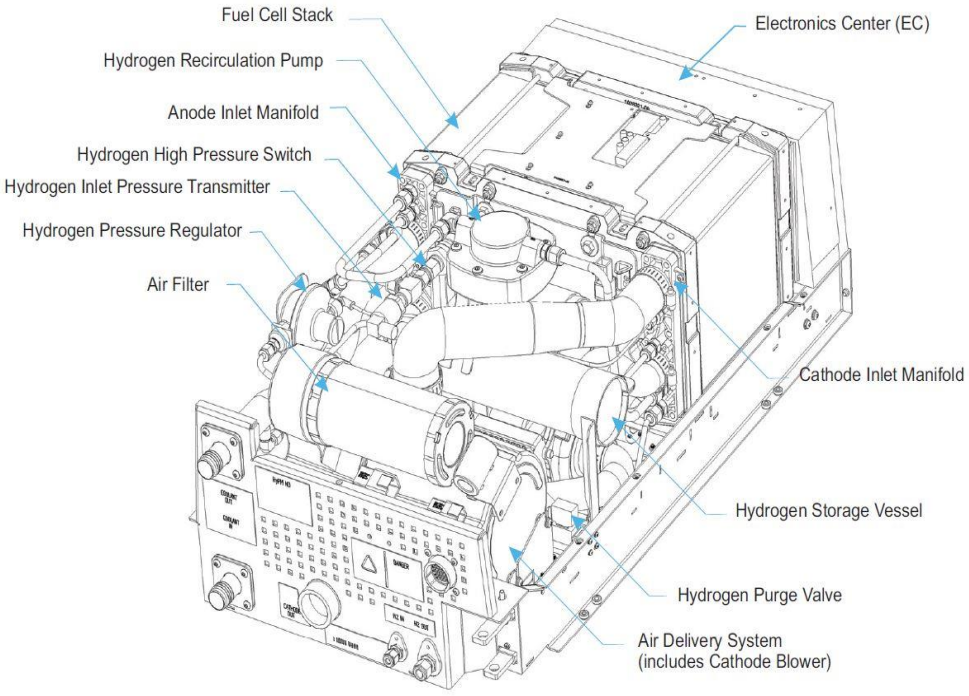

Figure 4.1 HyPM HD 8 FC drawing

(Drawing from HyPM HD 8 FC installation and operation manual)

Further information of this FC can be found in Appendix H including a full technical specification table, physical dimensions information and more drawings of the stack.

FC operation

As discussed in the literature reviews, FCs generate electricity by electrochemical reactions. Figure 4.2 shows the general operating process of the HyPM HD 8 FC. As Figure 4.2 shows, the FC requires the input of hydrogen supply, ambient air, coolant and start-up power and produces the output of exhaust from anode/cathode and electricity. The generated electricity will be supplied to the load system through the load bus bars. The H2X PEM Fuel Cell Stack box in the centre of Figure 4.2 represents the FC stack itself while the other components represent the internal conditioning systems for the stack which are also presented in Figure 4.1. The solid box in Figure 4.2 indicates the components that have been included in the HyPM HD 8 FC while the dashed boxes indicate the ones that needs to be externally supplied by the user.

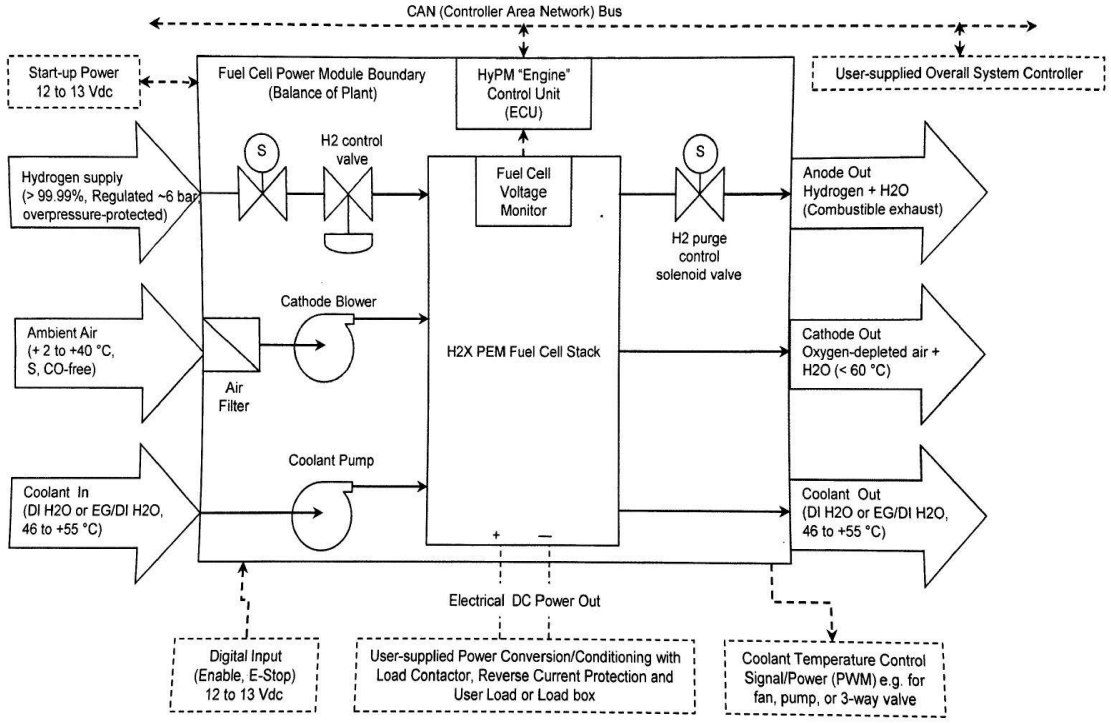

Figure 4.2 Simplified representation of HyPM HD 8 FC flows and interfaces (Figure from HyPM HD 8 FC installation and operation manual)

FC sub-systems

Figure 4.3 provides an upgraded version of the simplified FC representation shown previously. This Figure better illustrates the external sub-systems that are required for the HyPM HD 8 FC.

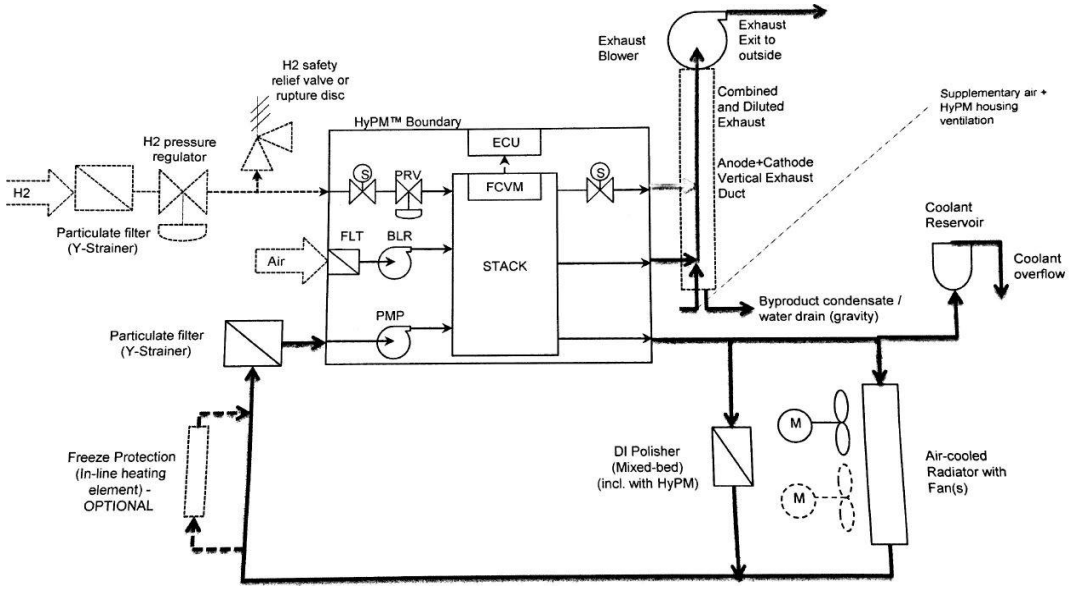

Figure 4.3 Typical balance of system component for HyPM HD 8 FC

(Figure from HyPM HD 8 FC installation and operation manual)

From Figure 4.2 and 4.3 the subsystems are as follows.

- A 12-13 V_{dc} start-up power source. This power is required to start up the FC unit by using external batteries.
- Hydrogen supply control. This is required to safely control the fuel flow to the FC stack using hydrogen regulators and control valves.
- Overall system controller. This is required to control the operation mode of the FC stack using the manufacturer-supplied FC control software. The software not only controls the FC but also enables real time monitoring of the FC unit.
- Ventilation system. This is required to ventilate the exhaust gas and dust safely by integrating an external blower.
- Cooling system. This is required to keep the FC under safe and optimum operating temperature using a combination of air-cooled radiators and water-cooled coolant.
- An external emergency stop (e-stop) digital input. This is required for safety reasons. A manually controlled emergency button to the controller was used for this function.
- Hydrogen sensor. It is a very important safety measure to detect any hydrogen leaks. This was done by installing hydrogen detectors in the laboratory.

This summarises the main sub-systems for the HyPM HD 8 FC which would also be required for most FC applications.

4.2.2 FC system installation

FC installation

The HyPM HD 8 delivered by Hydrogencis comes as a complete unit as shown in the drawing from Figure 4.1. Since the FC installation is static, the FC unit was simply screwed on a standard table as Figure 4.4 shows. The FC was placed adjacent to the hydrogen cabinet and laboratory wall to enable easier connection to the fuel supply and ventilation systems. All the connections are on the same side of the FC via a connector interface as shown in Figure 4.5.

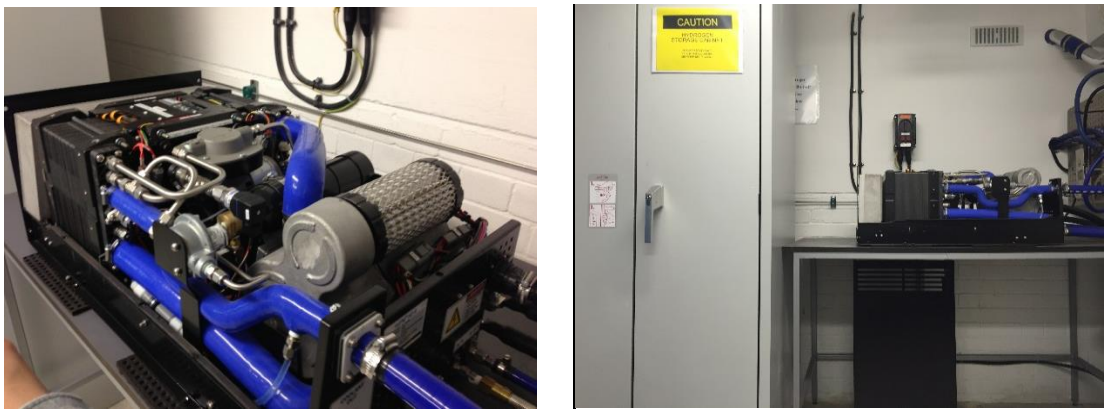

Figure 4.4 The HyPM HD 8 FC and placement

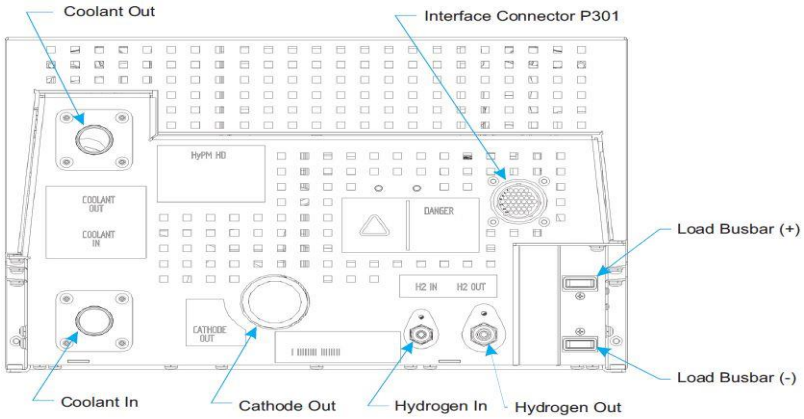

Figure 4.5 Connection interface of the HyPM FC
(Drawing from HyPM HD 8 FC installation and operation manual)

The “Hydrogen in” connection is for the fuel flow controls. The “coolant in/out”, “hydrogen out (anode)” and “cathode out” connections are for the FC cooling and air flow controls. The “Interface connector P301” connection is for the FC overall controls and start-up power. The “load bus bar (+/-)” connections are for the external load which are basically the positive and negative connections of the electrical output of the FC.

Hydrogen supply system installation

The hydrogen supply and delivery system for this study was designed and built in association with external industrial companies (BOC for the hydrogen controls and Asecos for the hydrogen cabinet). The hydrogen fuel will be delivered to the “hydrogen in” connection. The hydrogen fuel supplied to the FC stack needs to be regulated and controlled at the required pressure for the FC. Table 4.2 shows the fuel system requirements as provided by the FC manufacturer.

Table 4.2 FC hydrogen fuel system requirement and design

Fuel system requirement		
Gaseous hydrogen	%	≥99.99
Supply pressure (absolute)	kPa	515-690 (5.15 -6.90 bar)
Stack operating pressure (absolute)	kPa	≤120 (1.2 bar)
Hydrogen temperature	℃	2-40

Due to the laboratory height limit (2.15 m height), the hydrogen cylinders for the FC have been selected as standard size K (1.46 m height) at 175 bar pressure at 15 °C. For safety and monitoring purposes, cylinder cabinet and flow control valves were installed with the hydrogen supply system. The hydrogen supply system design is shown in Figure 4.6 and a photo of the actual hydrogen supply system is shown in Figure 4.7.

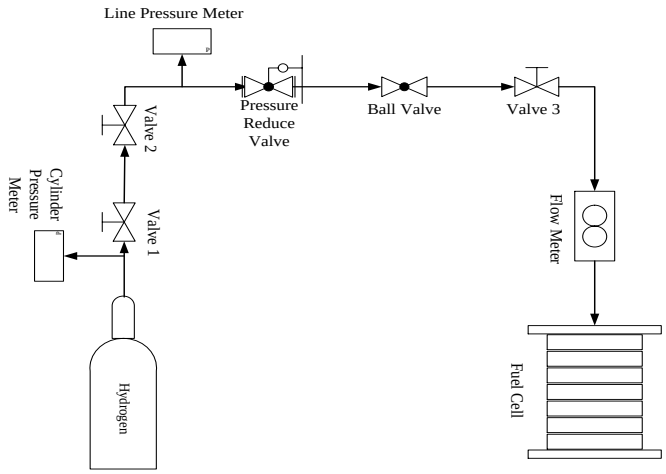

Figure 4.6 Hydrogen fuel supply system design for HyPM FC [4.2.2]

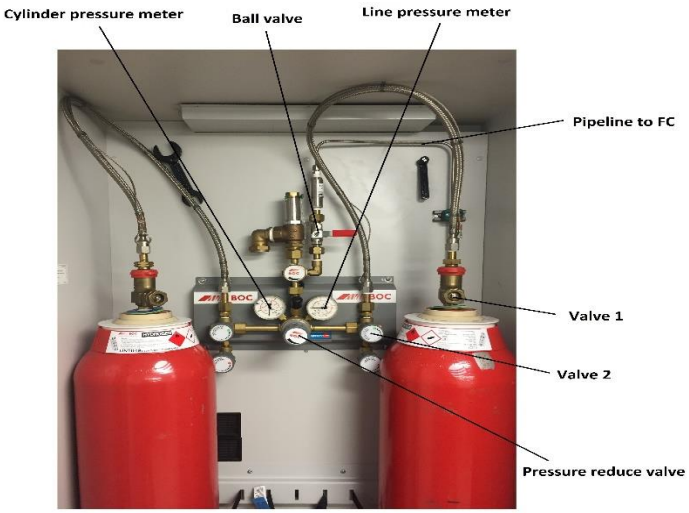

Figure 4.7 Actual hydrogen fuel supply system inside cylinder cabinet

Ventilation system installation

The ventilation system consists of a set of pipeline connections and an exhaust blower to vent the anode and cathode exhausts. The anode exhaust consists of warm hydrogen and water expelled via the “hydrogen out” connection. The cathode exhaust consists of warm, oxygen-depleted air and water which is expelled via the “cathode out” connection. The ventilation system has been designed to use a dilution blower system to vent both exhausts.

Cooling system installation

The cooling system consists of a set of pipeline connections and a coolant flow system. The FC temperature is estimated based on the FC output current to determine the cooling requirement. A current-temperature correlation look up table has been provided by the manufacturer as Table 4.3 shows.

Table 4.3 General current-temperature correlation look up table

Current	Temperature (℃)
>125	65 (±2)
75-125	60 (±2)
55-75	55 (±2)
<55	50 (±2)

The cooling system for the FC keeps the FC inner temperature within the range indicated by the look up table. Deionised water (DI water) is used as the coolant for the FC and is stored in a coolant reservoir. The coolant will be delivered to the “coolant in” connection on the FC connector interface through a DI polisher. The warm coolant will be recycled to the coolant reservoir and cooled with a PWM-controlled external

radiator to ensure the continuous delivery of cold coolant. The cooling system has been set to turn on simultaneously with the exhaust blower so that both ventilation system and cooling system are on whenever the FC is operating. The ventilation and cooling systems are shown in Figure 4.8.

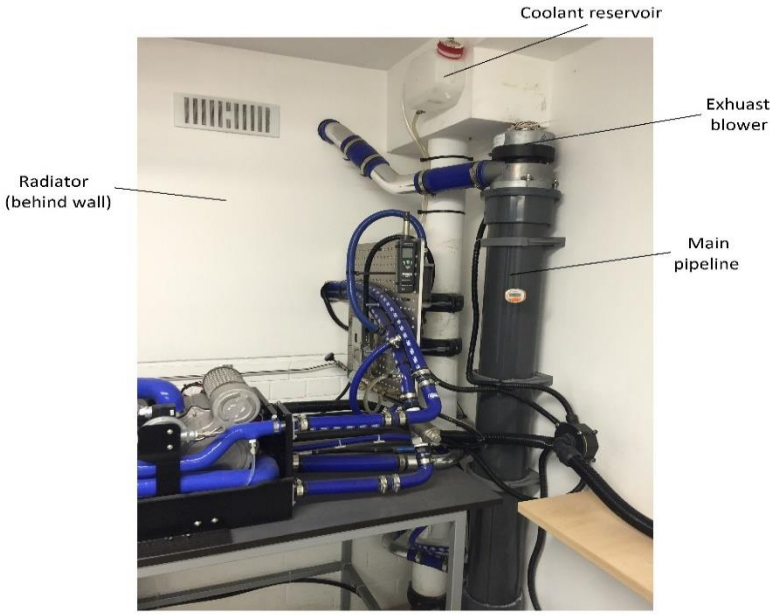

Figure 4.8 Ventilation and cooling system for the FC

4.2.3 FC evaluation test

After the components and safety measures for the FC are installed and tested, the next step is to carry out a set of evaluation tests for the FC. The evaluation tests test the performance of the FC and sub-systems and can be used to provide comparison with the performance stated in the manufacturer's data sheet. The factory acceptance test results of the HyPM HD 8 FC have been presented in Figure 4.9 and will be the benchmark for the laboratory FC.

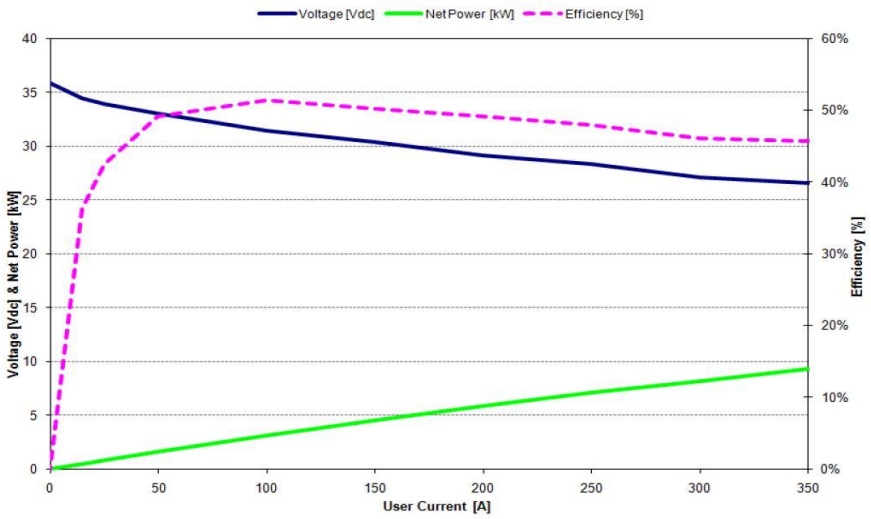

Figure 4.9 HyPM HD 8 factory acceptance test performance curve (Figure from HyPM HD 8 FC installation and operation manual)

FC resistive load design

In order to evaluate the FC unit with different power ranges, a load system needs to be applied on the FC. The simplest method to apply a load on the FC is to apply a controlled DC electrical resistive load system because the output from the FC is DC. The resistive load for the FC evaluation test has been selected as ten parallel connected variable resistors (0-1 Ω). Based on the performance graphs provided by the manufacturer, the resistance required can be calculated for different power levels. Each resistor is controlled by a separate switch, therefore the total load resistance can be easily controlled by changing the number of resistors parallel-connected in the circuit. The resistance values were computed based on the FC performance graph. The power distribution and resistance requirements have been shown in Table 4.4.

Table 4.4 Power distribution of the resistive load banks for FC evaluation test

No of Parallel R Connected	FC output voltage (V)	Ideal resistance (Ω)	Ideal power (W)	Percentage of full power
1	34	0.858	1347	16%
2	33	0.429	2538	30%
3	32	0.286	3580	42%
4	31	0.214	4490	53%
5	30.5	0.172	5408	64%
6	30	0.143	6294	74%
7	29	0.123	6837	80%
8	28.5	0.107	7591	89%
9	28	0.0953	8227	96%
10	27	0.0858	8497	100%

The actual resistive load system has been shown in Figure 4.10.

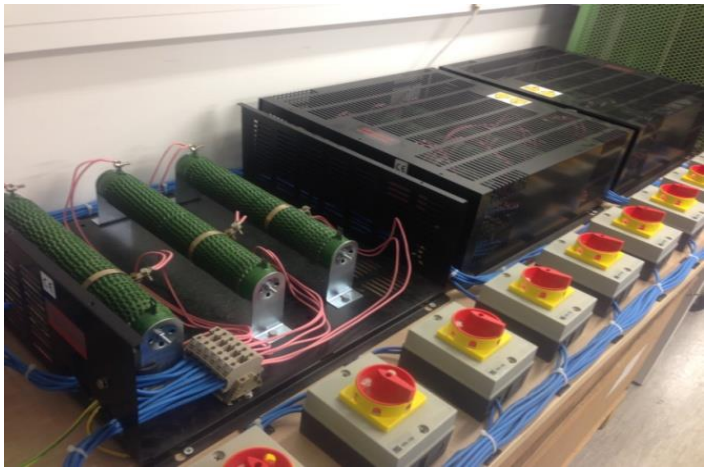

Figure 4.10 Electrical resistive load for FC evaluation test

FC performance test

To evaluate the performance of the FC against the factory acceptance test, similar tests were carried out. The FC output power is increased from no load to full load in steps. Although step responses of the FC are expected to be observed instead of ramp responses, it can be used to evaluate the voltage/current/power/efficiency performance of the FC. The general method for this evaluation test is to switch on one more resistor to be connected in parallel every 210 s to take the FC from no load to full load to allow the FC to settle down between steps. The comparison results between FC test and factory acceptance test have been plotted in Figure 4.11.

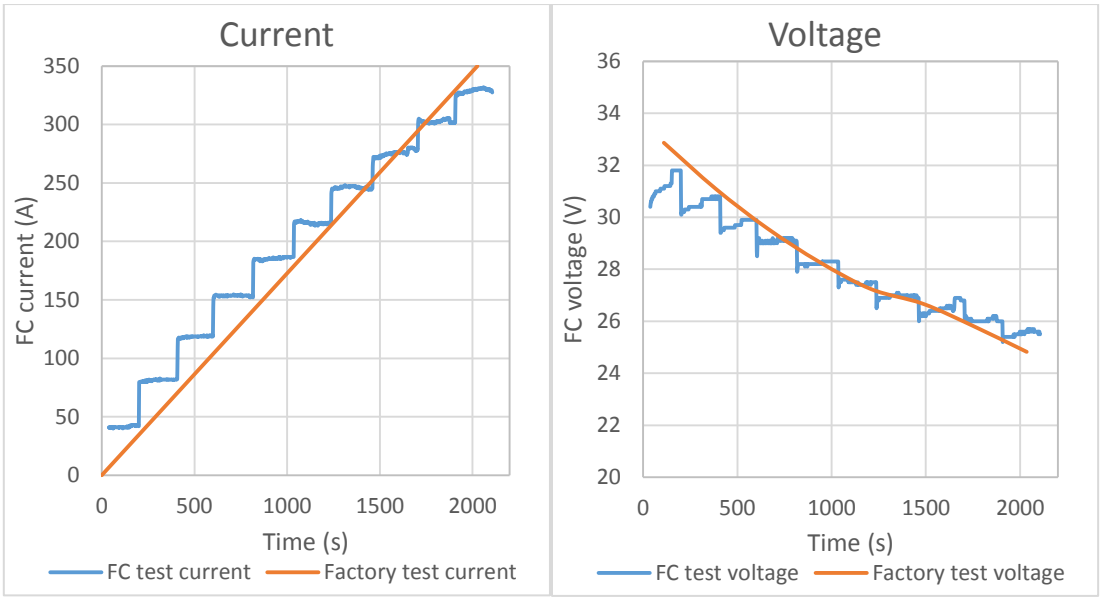

Figure 4.11 FC performance comparison for current and voltage

As Figure 4.11 shows, the FC output terminal voltage drops as the output current increases. Although the FC test was carried out with step change, it can be seen that the performance reasonably matches the results of the factory acceptance test. The other main performance parameter that was measured for this FC was efficiency. As described in section 2.4.3, the method to calculate the FC electrical efficiency is formulated as:

$$\eta = \frac{Average\ Cell\ Potential}{1.482}\ (corresponding\ to\ HHV) \qquad (4\text{-}1)$$

The actual FC efficiency can be determined by the real time cell potential. The monitoring software for the FC is capable of real time monitoring of individual cell potentials. Hence the FC efficiency can be calculated and is plotted in Figure 4.12.

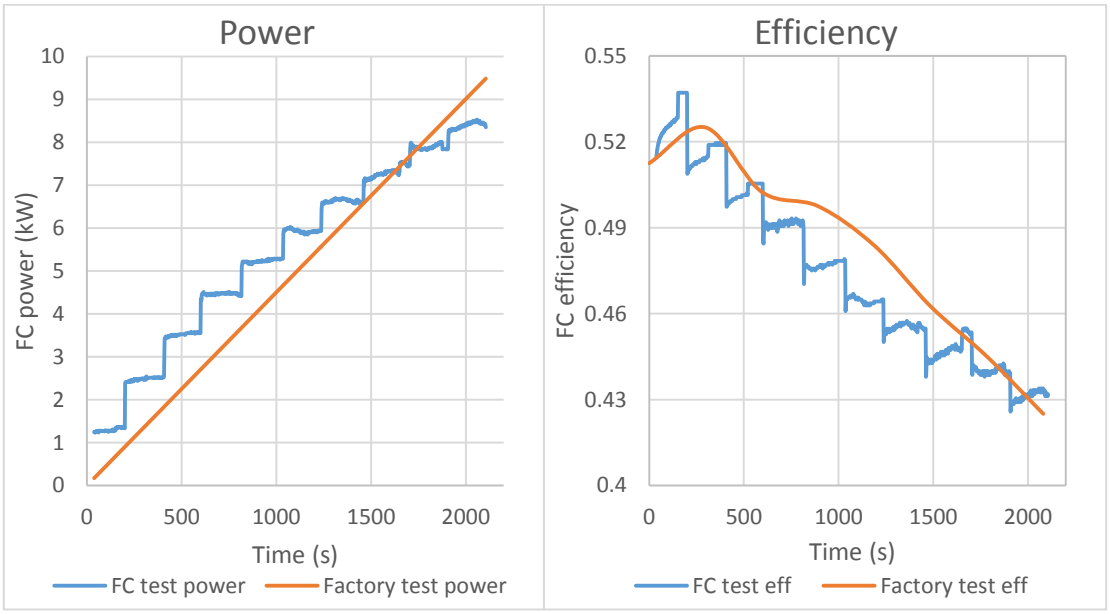

Figure 4.12 FC performance comparison for power and efficiency

As Figure 4.12 shows, the efficiency drops as the FC power increases and both parameters reasonably match the factory test curves. The efficiency curve can be explained by the FC voltage curves discussed in 2.4.3. For a FC, as the output current increases the output terminal voltage decreases as a consequence of losses (Figure 2.25 and 2.26). The efficiency of PEMFCs generally decreases as the power requirement increases. It can be seen that FCs have better efficiency performance under lower loads which is completely different from the parabolic efficiency curve of a conventional diesel engine. This unique efficiency characteristic brings additional opportunities for FC bus applications which will be explained later.

Another point that can be observed from the efficiency curve is that there is a small efficiency change after the load is changed. This is particularly obvious for the first four resistor number changes. This can be observed in Figure 4.11 as well where the FC voltage increases slightly over time after the resistance is changed. This trend was caused by the temperature change of the FC. In order to investigate the effect of temperature on efficiency, efficiency and real time temperature of FC have been plotted in Figure 4.13.

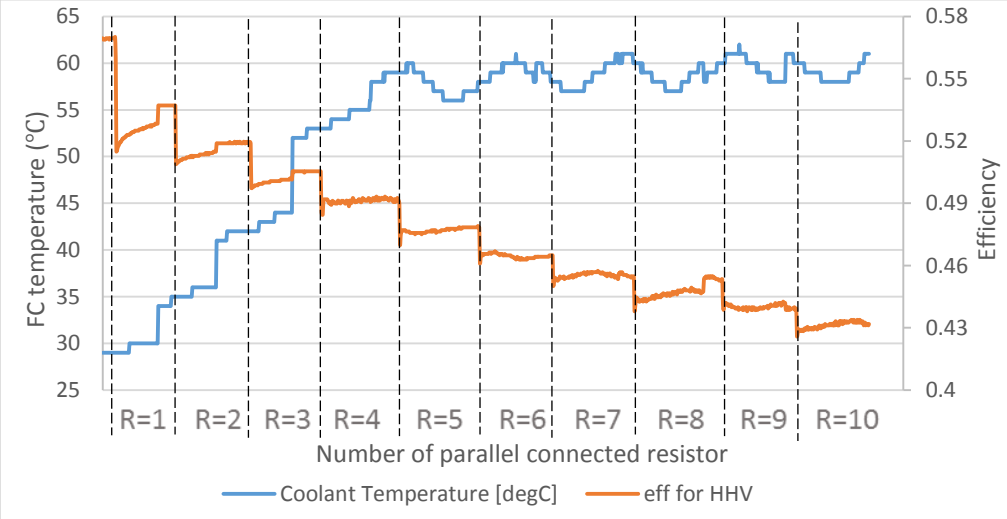

Figure 4.13 FC efficiency change affected by temperature in increasing load

As Figure 4.13 shows, in the first four zones (R=1~4), the efficiency is proportional to the coolant temperature. In the next six zones (R=5~10), the coolant temperature varies around 60 degrees so that the efficiency became more stable. Two points can be addressed from this plot. First, the FC stack is required to warm up to a certain temperature to achieve optimised efficiency. Second, the cooling system will keep the FC temperature around 60 Celsius to prevent over-heating.

The decreasing load tests were also carried out and showed similarly reversed results as the increasing load tests. The efficiency and temperature results of the decreasing load test are plotted in Figure 4.14. The main difference observed was the decreasing load tests had generally higher efficiency. The efficiency also became more stable in each zone for the decreasing load test. This is because the FC started from a higher temperature which also verified the points regarding temperature.

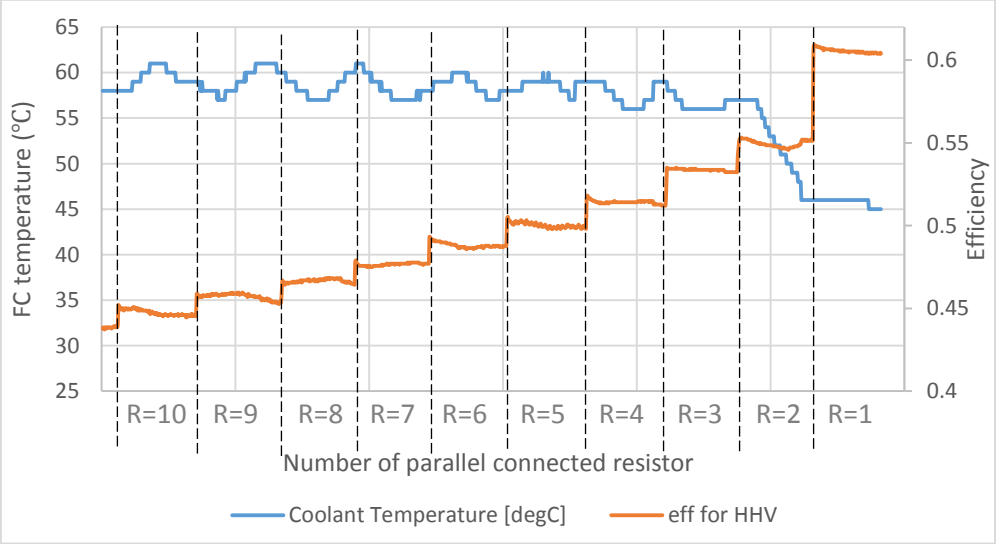

Figure 4.14 FC efficiency change affected by temperature in decreasing load

Please note the results from these evaluation tests were used to inform the design of the FC computer simulation. From this point the computer simulation and laboratory system were developed in parallel and validated against each other. The computer simulation will be discussed in Chapter 5.

4.3 Boost converter for FC

As the FC characteristic curve shows, the FC output voltage drops as the power output increases. This reduction in terminal voltage may not be an issue for purely resistive loads, but could be a problem for motor loads. Motor controllers and motors are normally designed to operate within a reasonably specific supply voltage range. Operation of a motor outside its design voltage supply range could lead to motor and/or controller damage or the safety devices could cause the motor to trip. For FC bus applications, the motor will be powered by the FC output. This is the reason why many FC bus designs have a DC/DC converter to adjust the voltage level to within the motor operating voltage range. This argument was also presented in many works discussed in the critical review in section 2.6.1 where they emphasised the importance of DC/DC converters for FCs.

4.3.1 Boost converter design

Boost converter theory

Since the FC output voltage drops as the power increases, there is a need to maintain a near steady output voltage at the bus bar. The DC/DC converter used for FC applications is normally a boost converter. A boost converter consists of two semiconductors (a diode and a switch), an inductor and a capacitor as Figure 4.15 shows.

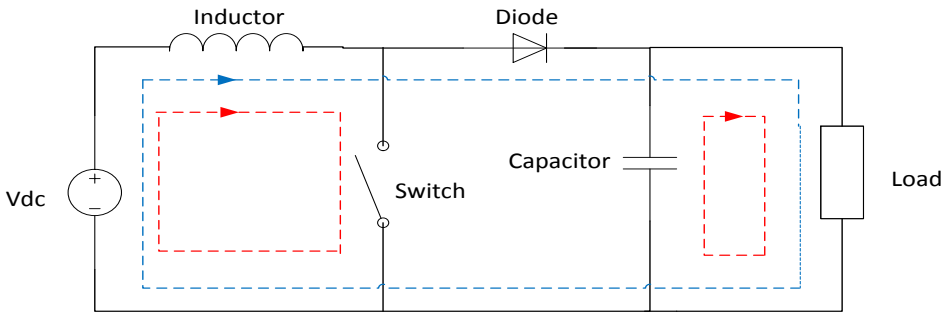

Figure 4.15 Typical boost converter configuration and operation

a) When the switch is closed, the current flows via the red loop. The inductor will be charged by the voltage source. The capacitor also discharges to the load simultaneously [4.3.1].

b) When the switch is open, the current flows via the blue loop. The inductor discharges to the capacitor and the load. The inductor discharge potential is in series with the voltage source and works as a temporary second source. As a consequence of the inductor discharge the load terminal voltage will be greater than the source terminal voltage [4.3.1]. The level to which the load voltage needs to be boosted can be controlled by adjusting the switching duty cycle of the switch [4.3.2].

Boost converter design for FC

The HyPM FC shows the output performance to be 0-380 A, 40-20 V and 0-8.5 kW. The University and the HyFCAP project required the laboratory DC voltage to be no more than 50 V_{dc} for safety reasons. Therefore the maximum system voltage level for the laboratory FC system was set at 48 V_{dc} (all voltages stated hereafter are dc unless specified). The boost converter would then need to regulate the 20-40 V FC output voltage to 48 V.

Since most low voltage boost converters available in the industry are for relatively low current applications, several converters need to be connected in parallel to split the high currents delivered by the laboratory FC. Three companies were approached who

may be able to provide a custom design. These were CTP Power Automation, Traco Electronic and Custom Power Design Ltd. Custom Power Design Ltd provided a solution with the least number of required converter units.

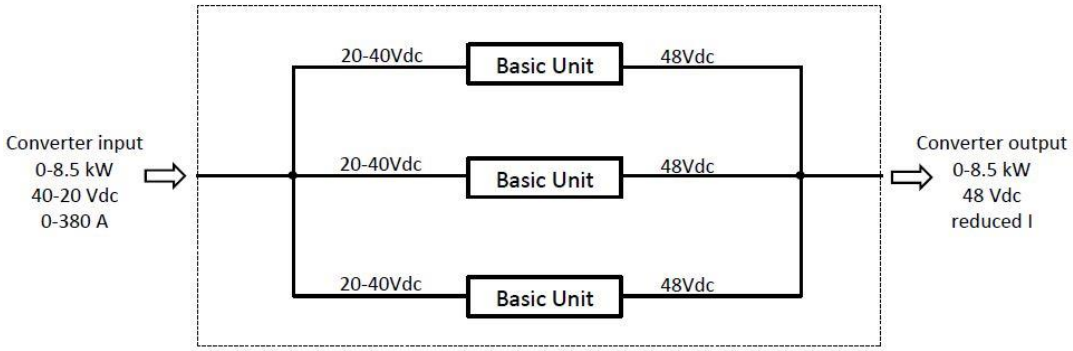

Figure 4.16 Boost converter for HyPM FC design

Figure 4.16 presents the design of the boost converter for the FC. The FC output power will be equally divided into three paths to three identical converter units. Each unit will boost the varying input voltage to a fixed 48 V output. The conversion efficiency of the boost converter varies with the magnitude of power output and amount of regulation. A manufacturer datasheet for the converter unit and a detailed schematic drawing can be found in appendix I.

4.3.2 Boost converter installation

The installation of the boost converter for the FC is relatively straight-forward as it simply requires an input and an output connection as Figure 4.17 shows. The three converter units have been assembled as one complete rack mount with corresponding input and output connections. The three converter unit input/output connections have been assembled on bus bars for easier connection from the FC or to the load. A toggle switch has been installed to control the on-and-off of the boost converter.

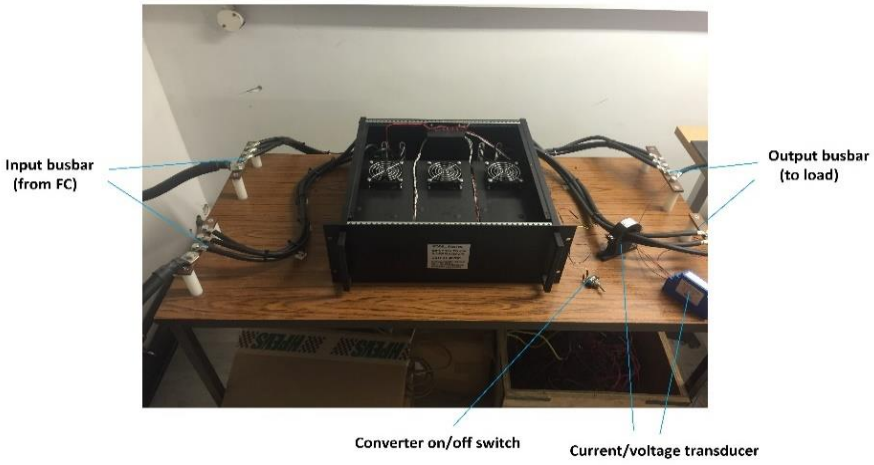

Figure 4.17 Boost converter unit configuration and connections

4.3.3 Boost converter test

Load design for boost converter test

The boost converter test aims to evaluate the performance of voltage boosting and investigate the conversion efficiencies. The same resistors as used in the earlier FC performance test have been connected at the output of the converter as the load. However, the resistors would have to be rewired to account for constant 48 V output. A resistive load with a combination of series and parallel connected resistors has been designed as Figure 4.18 shows. Each variable resistor has been adjusted to match the total resistance calculation as summarised in Table 4.5. The total resistances are calculated to ensure the power to be dissipated does not go beyond the power rating of the resistors. Only four levels of load conditions can be produced for this boost converter test because of the limit of resistors available in the laboratory.

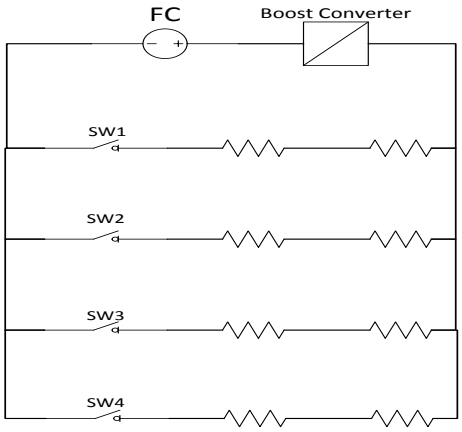

Figure 4.18 Resistive load configuration for boost converter test

Table 4.5 Look up table of resistive load design for boost converter test

Load condition	Switch closed	Number of resistors used	Total resistance (Ω)
open circuit	none	0	n/a
1	sw1	2	2.05
2	sw1, sw2	4	0.9669
3	sw1, sw2, sw3	6	0.6253
4	sw1, sw2, sw3, sw4	8	0.4681

Boost converter test result

The proposed system set up has been tested for a 20 minutes run with 5 minute intervals between each switch being closed (load condition open circuit to 4). The input and output voltage and current have been plotted in Figure 4.19 against the load conditions presented in Table 4.5.

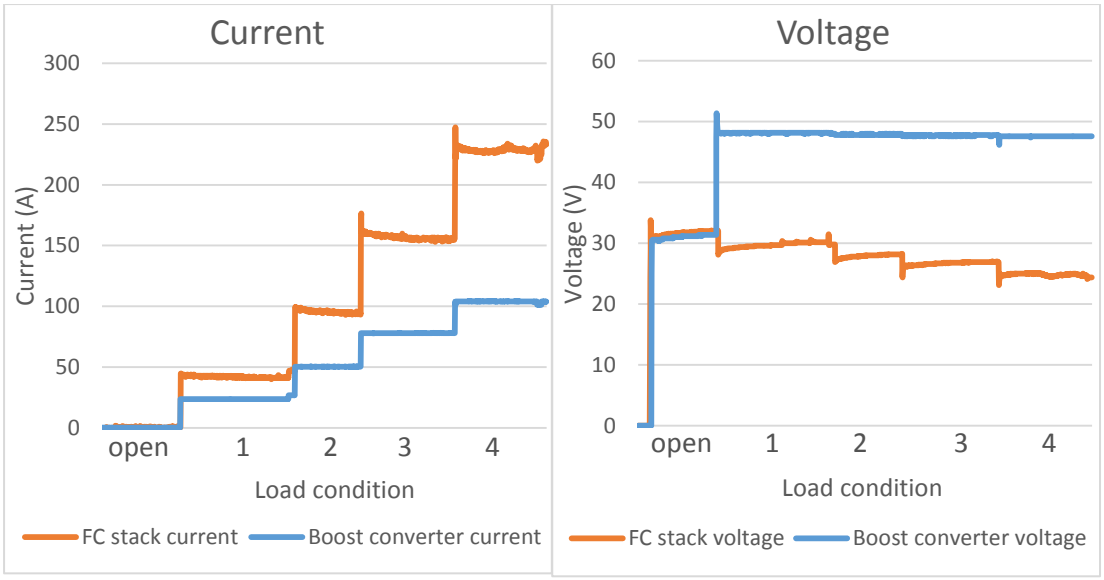

Figure 4.19 Output current and voltage of FC with and without boost converter

The FC stack voltage/current indicates the input voltage/current to the boost converter in Figure 4.19. As the voltage plot shows, the boost converter has functioned as expected to regulate the output voltage at a near constant 48 V (47.6-48.2 V) as the FC output voltage decreases with increasing load. It can also be observed that the amount of current drop increased significantly as the voltage boosting requirement increases. The input and output power can be calculated to test the conversion efficiency. The power and conversion efficiency plots have been plotted in Figure 4.20.

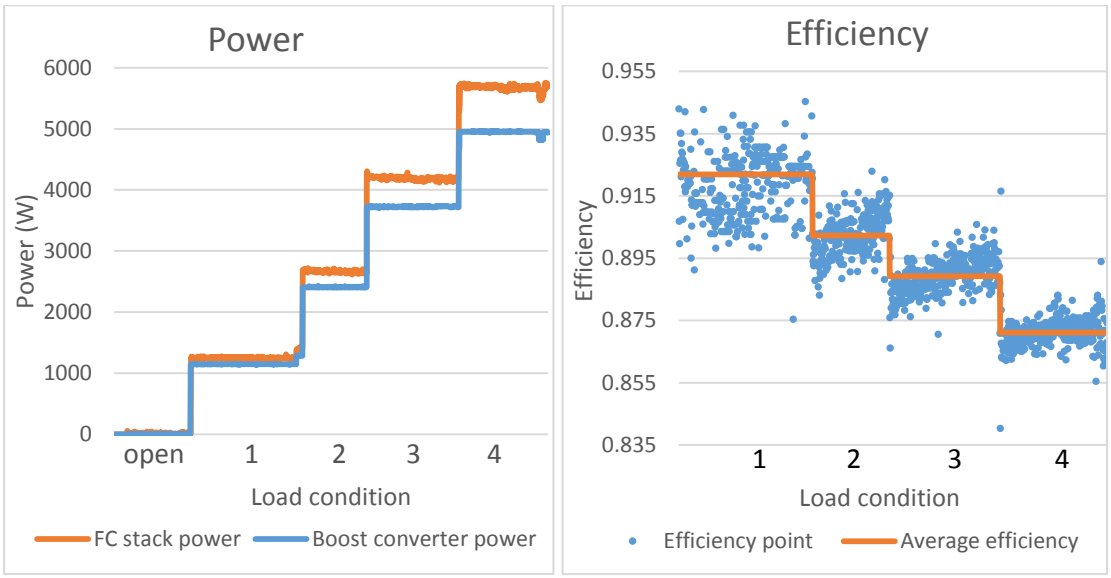

Figure 4.20 Input and output of boost converter for power and efficiency

As Figure 20 shows, the average efficiency varies from 85% to 92% and the efficiency drops as the power increases. This can be explained by the boost converter theory discussed before. The more voltage required to be boosted, the boost converter would have to further adjust the duty cycle by increasing the switching frequency and thus

creates more switching losses. Based on the obtained efficiency of the FC and boost converter, it can be calculated that the overall combined efficiency of the FC and the boost converter would be vary from 46 % to 36 % dependent on power output. It can be seen that FCs hold slightly better performance when compared with a diesel engine (30%-45%). Although the FC produced only 6 kW in this test which is less than the full power of 8.5 kW due to the limit of resistors, this test still sufficiently demonstrated the operation of the boost converter.

4.4 FC under transient peak load

Start and stop frequently occurs in a typical city bus driving cycle, which leads to constant changes in the power demand. It is important to investigate how the FC responds to changes in power demand, which was also highlighted in the critical review section 2.6.4 where a number of past works suggested FCs struggled to handle peak loads quickly.

A set of step changing load tests (0%-10%-20%-30%-40%-50%-60%-70%-80%-90%-100%) have been carried out in the FC evaluation test described and showed the FC functioned as expected. This section aims to observe the reactions of FC under more transient load changes. The boost converter was temporally disabled for this set of experiments because of the lack of resistive loads. The same resistive load used for the FC evaluation test was used for the transient peak experiments.

The first set of experiments were carried out when the power demand from the FC had step increases from: 0-25%, 25-50%, 50-75% and 75-100% to observe the transient response of the FC. The FC was allowed to settle for approximately 10 minutes after each test before switching to the next load test. A large amount of data was logged during the experiments such as hydrogen flow, stack current/voltage, output power, efficiency, air flow, coolant temperature etc. Two of the more important parameters, which are hydrogen fuel flow rate and FC stack output power, have been selected and plotted in Figure 4.21.

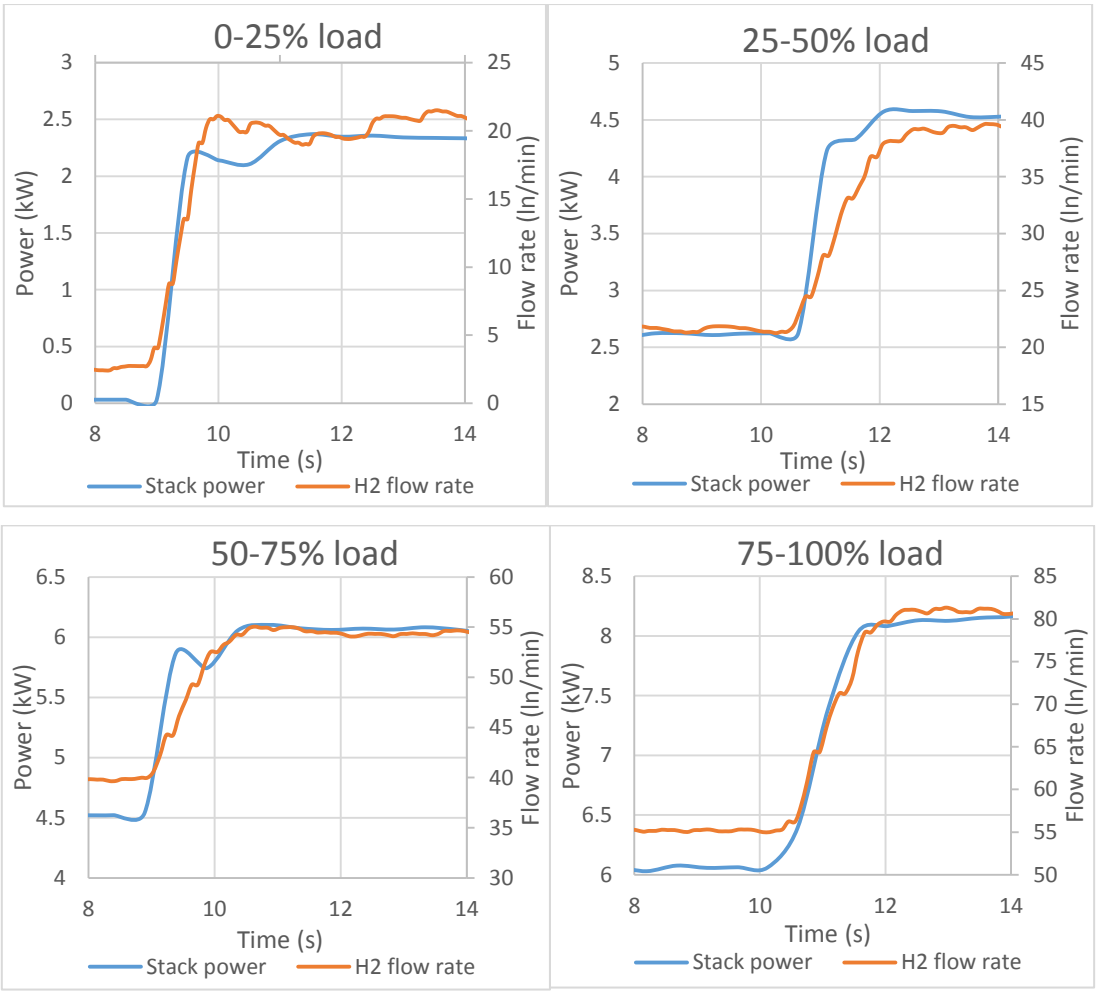

Figure 4.21 FC transient response to 25% step change load

As it can be seen from the figures, the FC power and hydrogen flow rate both respond to the resistive load change to meet the new power demand. It takes approximately 2 to 3 s for the FC output power to become relatively stable. It can also be seen that the hydrogen consumption always slightly lags the FC power in terms of response. It can also be observed the transient response to load change becomes smoother as the FC warms up and reaches the higher power level.

It can be seen that the FC can respond to 25% power change reasonably quickly. The next set of experiments have been carried out to investigate the FC response under much larger power changes to simulate worst case scenarios. The experiments have been carried out with load change from 0-25%, 0-50%, 0-75% and 0-100%. The results have been plotted in Figure 4.22.

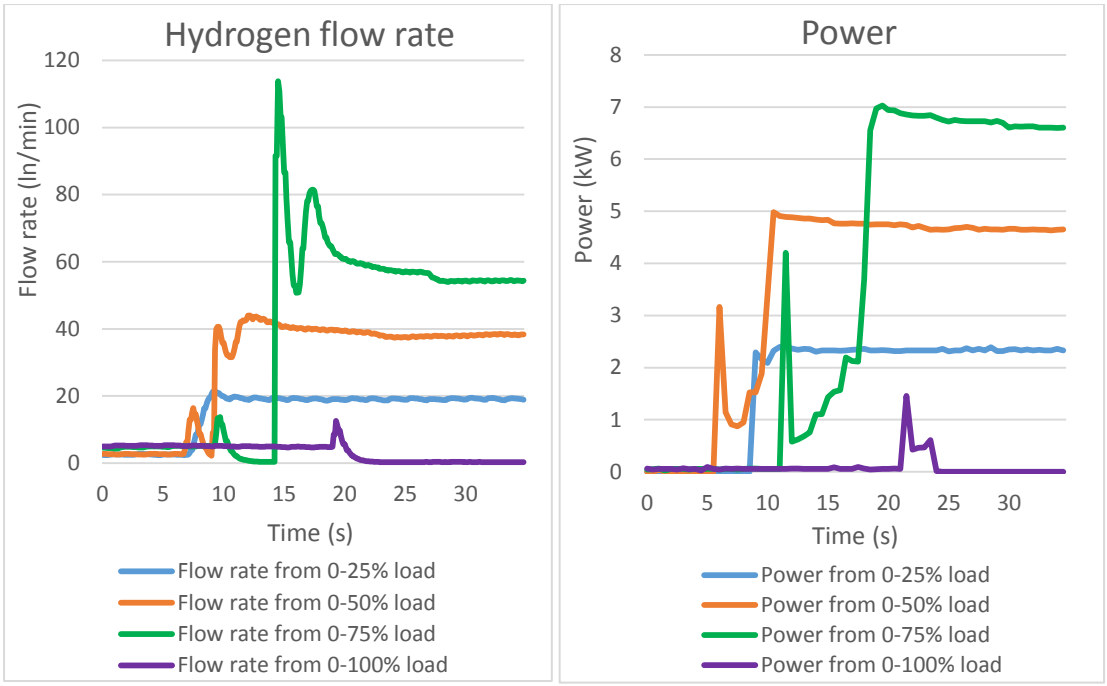

Figure 4.22 FC transient response to large step change load

When the step load occurs, the FC current demand is high. Since the FC is a passive energy source that just reacts, the only control source is the hydrogen flow valve. The valve opens but the hydrogen flow is greater than the FC can absorb as the FC itself does not respond instantaneously. As a result the hydrogen flow valve then throttles back. The oscillations seen in the waveforms reflect the degree of damping that the controller is set at.

The 0 to 25% step load is such that the hydrogen valve control provides a critically damped response. The hydrogen flow and stack power both respond to the load change reasonably quickly. The 0 to 50% step load is such that the valve control provides a quarter amplitude damping. Hydrogen flow rate takes approximately 8 s to become stable at the required flow rate because of the controller tuning. The FC output power reacts immediately after the load demand has been changed, however, it soon dropped because there is not sufficient hydrogen being delivered to match the power demand. The 0 to 75% step load is such that the valve control provides an underdamped response. Hydrogen flow rate takes approximately 20 s to become stable. The FC stack power also has a power drop and then rises to the required power. During this process, the HyPM FC reported the ‘Hard Recovery Alarm’ but recovered to produce power. The hard recovery alarm has been defined as a transitional state when the stack becomes unstable during running and the system attempted to recover the stack. This type of operation is suggested to be avoided to prolong the FC stack life. In the 0 to 100% step load the hydrogen flow rate and stack power both attempted

to increase but failed and drop to zero. HyPM system reported 'Cell Low Voltage Alarm' and 'Hard Recovery Alarm'; the system recovery failed and tripped.

It can be seen from the results that the FC was unable to respond quickly and even failed to reach the required power should very large load changes occur. There are two main reasons for this slow response issue: one is the small power density of FCs as addressed previously, the other one is that the hydrogen fuel flow controller would be unable to adjust fast enough if the change in demand is too large. It has been determined that the FC unit has a slow response issue when large transient peak load change occurs. This type of large step change should be avoided for FC operation.

Step unload tests (25-0%, 50-0%, 75-0% and 100-0%) in reverse of the loading tests have also been carried out. It was found unloading the FC from full load to no load can be achieved reasonably fast (<1 s). It can be seen step unloading is not a significant factor for FCs.

More plots (hydrogen flow rate, stack current, stack voltage, stack power, FC efficiency, air flow and coolant temperature) of the FC under large step transient loads for both loading tests and unloading tests can be found in Appendix J.

4.5 Discussion on FC basic drivetrain justification

As identified in section 3.3.2, the justification purpose of the FC basic drivetrain was:

1. Test the FC stack to better understand the specific characteristics of PEMFCs.
2. Develop the power conditioning system for FCs.
3. Apply an electrical load system to the FC to simulate different power demand conditions and evaluate the performance of the FC under different power profiles.
4. To investigate the reaction of the FC under worst case scenarios when subjected to fast transient and large step changes in power demand.

The FC evaluation tests detailed in this chapter showed the unique efficiency characteristics of the FC where the efficiency generally drops as the power requirement increases. The FC bus will operate at a lower efficiency during higher power operations such as high speed operation and bus acceleration. This would reduce the overall efficiency of the FC bus. Additionally, the FC as the only power source in this configuration, has to be able to satisfy all power demands. Hence, the FC in this drivetrain would have to be powerful enough to cover the vehicle under the highest power demands where it actually has the lowest efficiency. This would

significantly increase the size of the FC on-board the bus.

The FC tests showed slow response under step transient loads. This slow response would affect the dynamic performance of the vehicle such as acceleration rate and hill climbing ability. Additionally, in the worst case scenario, such as a fully loaded bus trying to accelerate to top speed while climbing a hill, the FC could cut out in the middle of the road. Although the slow response here is seen for step changes, for a real bus drive this is more likely to be a ramp change, this is still a potential risk to be noted.

The single drivetrain configuration is simply a FC-motor-wheel connection. The unidirectional drivetrain means the regenerative braking energy cannot be reused and would be dissipated as waste heat. This would reduce the system efficiency, particularly in city driving.

Therefore the results gathered highlight the main drawbacks of this FC basic drivetrain as summarised as bellow:

1. Low efficiency under high load operations.
2. Require an oversized FC stack.
3. Slow response under step change.
4. Lack of ability to recover braking energy.

By utilising hybridised technology, the system can potentially take advantage of the FC characteristics while eliminating or mitigating the problems identified for the FC-only systems.

1. Low efficiency under higher load operations issue.
   - Energy storage can supplement the FC under higher loads to eliminate FC operation at lower efficiency.
2. Large FC stack requirement issue.
   - The FC does not have to be able to cover the worst case scenario (highest power demand) on its own, reducing the maximum FC size requirement.
3. Slow response under step changes issue.
   - Ability to use energy storage to satisfy any transient peak demands to eliminate the FC slow response limitation under large varying loads.
   - Reducing the amount of variation in terms of the FC output power can potentially extend the FC lifetime as well.
4. Lack of ability to reuse wasted energy limitation.

- The hybrid configuration can enable regenerative energy harvesting to charge the energy storage which is a significant benefit for city buses.

4.6 Hybrid drivetrain integration steps

Step 1: FC basic drivetrain

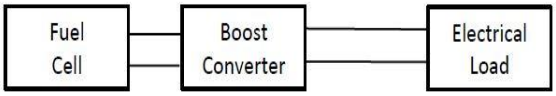

Figure 4.23 FC basic drivetrain block diagram

The previously developed basic drivetrain as Figure 4.23 shows has been used as the fundamental structure of the proposed hybrid system. The FC along with its conditioning system and boost converter will remain as the primary power source of the system. However, the resistive load needs to be replaced with a load system more representative of a practical bus load model.

Step 2: FC drivetrain using traction motor load

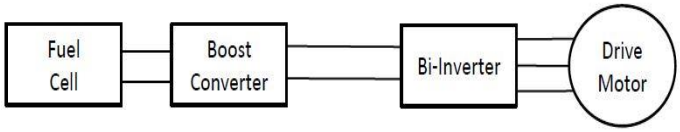

Figure 4.24 FC drivetrain using traction motor load block diagram

The second step, as Figure 4.24 shows, is to replace the resistive load with a motor system to enable a more realistic simulation of driving cycles. An AC motor system and the inverter (motor controller) has been used to simulate the driving motor of a bus. In an actual operating FC bus, the motor driving the wheels (via the transmission) will be loaded by forces generated by gradient, windage, friction and passenger loads which are difficulty to generate in a laboratory environment. Therefore, an additional load system would have to be designed to be able to apply a controlled load to the drive motor.

Step 3: FC drivetrain with motor/generator load system

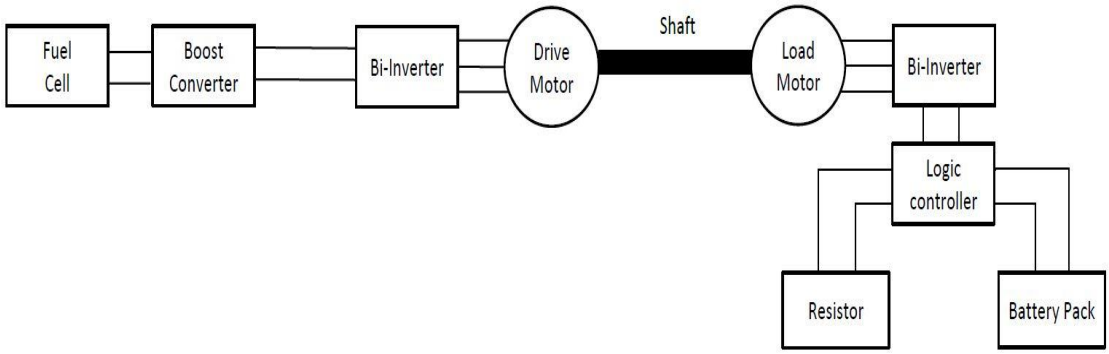

Figure 4.25 Motor/generator load design block diagram

As Figure 4.25 shows, the designed load system for the FC drivetrain consists of two main parts: a motor/generator set and the controlled load system for the set. The drive motor for the FC drivetrain will first be mechanically coupled with another identical motor which works as a load motor. The load motor will be controlled to work as a motor or a generator through the logic controller. The logic controller controls the load that will be used to determine how much power is to be dissipated or delivered from/to the load motor to enable the simulation of different driving conditions.

Step 4: FC hybrid drivetrain with energy storage and load system

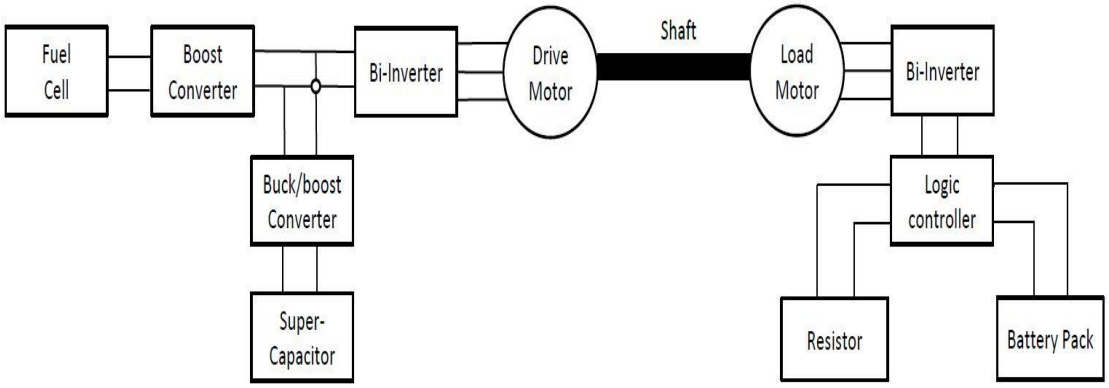

Figure 4.26 Complete FC hybrid drivetrain block diagram

As Figure 4.26 shows, an energy storage system along with its conditioning system will be integrated to form the series hybrid configuration. Both FC and energy storage will be connected through power conditioning systems which have been used to control the corresponding sources. The components on the left of the coupling shaft directly mimic the real bus power systems. The components on the right of the shaft form the laboratory model which does not exist in a real bus system but they do mimic the load without the inertial component.

4.7 Motor/generator load system

4.7.1 Motor selection

The drive motor will be directly powered by the FC through the boost converter which is designed to provide a near stable 48 V output voltage. The controller selected would need to be a model that can operate at 48 V as well. After a number of motor comparisons and company negotiations, the motor for this FC drivetrain was selected to be the AC-9 motor kit manufactured by HPEV. The AC-9 motor kit consists of a drive motor and a 48 V motor controller which also works as an inverter. The peak power graph of AC-9 motor has been shown in Figure 4.27. The peak power of the motor has been sized to be of greater magnitude than the 8.5 kW FC can provide because the motor is expected to be powered by both the FC and energy storage device during peak load operation.

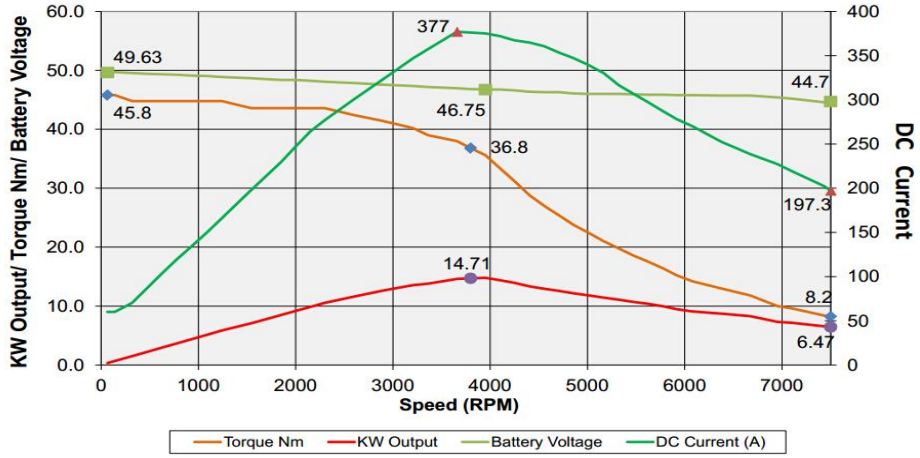

Figure 4.27 HPEV AC-9 motor kit peak power graphs

(Figure from HPEV manufacturer datasheet)

The motor parameters can be monitored in real time and controlled via computer software (1314 PC Programming Station). The motor itself can be operated in speed control mode or torque control mode. The user control is carried out via two potentiometers where one represents the motor throttle and the other represents the motor electrical brake (regenerative brake). These potentiometers were initially manually controlled wire wound potentiometers which can be replaced with digital potentiometers later for more accurate speed/torque control.

4.7.2 Motor/generator set installation

An identical AC motor (and controller) have been selected for this motor/generator set. Using two identical motors to develop a back-to-back system can greatly simplify the dynamic calculations between the two motors. Since the motor manufacturer does not supply the motor holder with the motor kit, the mount to hold the motor would have to be designed and built in the laboratory. The motor holder and the coupling components design are shown in Figure 4.28.

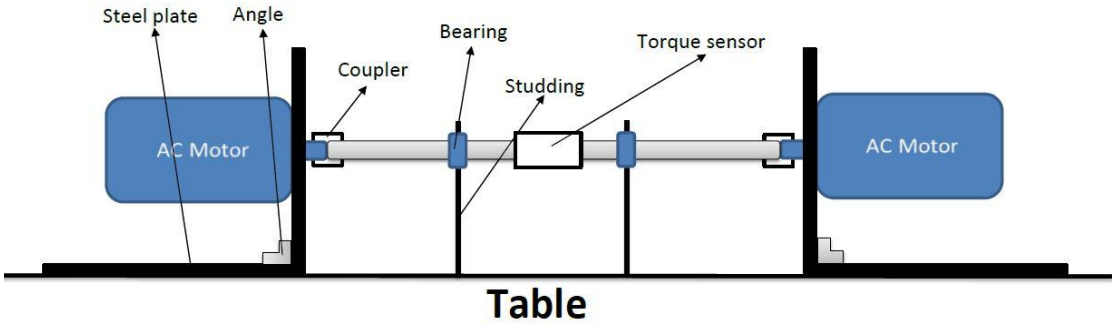

Figure 4.28 Motor/generator set coupling structure design

- Steel plates (for L bracket): heavy duty plates to be screwed on table and motor front panel.
- Angle: steel heavy duty 90 degree angle to secure the steel plates.
- Coupling: both couplings (one spider coupling and one metal bellow coupling) have been sized based on motor specifications for mechanical coupling between motors and shaft (iron bar).
- Bearing and studding: used to hold the shaft (iron bar).
- Torque sensor: used to measure the torque in real time while the motors are operating.

The designed structure was built with the assistance of the UCL mechanical engineering main workshop and the completed structure is shown in Figure 4.29. This motor/generator set system was placed on a solid table between the boost converter for FC (left motor) and the load system for the load motor (right motor).

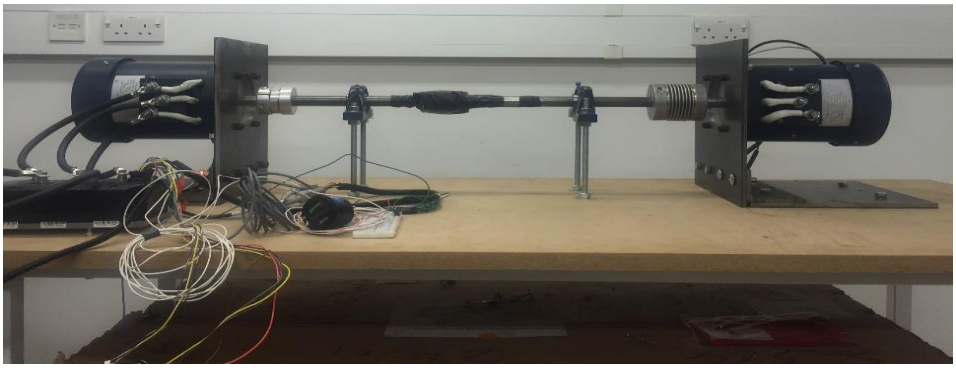

Figure 4.29 Photo of the completed motor/generator set structure

4.7.3 Laboratory motor load system

The concept of load design considers practical driving loads for buses applying a specific positive or negative torque on the drive motor. The load motor could work as a generator to apply a negative torque on the shaft if the bus is going uphill or flat road (for windage and friction). On the other hand, the load motor could work as a motor to apply a positive torque if the bus is going downhill. The amount of torque applied on the shaft can be determined based on the bus/road conditions such as road gradient, bus load, vehicle speed etc. The load system design has been shown in Figure 4.30.

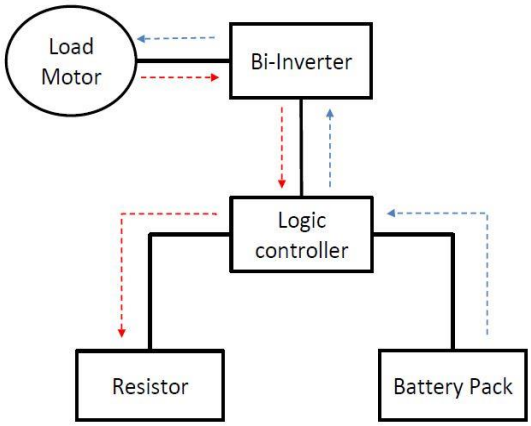

Figure 4.30 Motor/generator set load system power flows

The red line path in the figure indicates the power flow when the load motor is working as a generator for a negative torque on the shaft. The blue line path indicates the power flow when the motor is operating in motor mode to apply a positive torque. A negative/positive torque applied on the load motor has been used to simulate the forces applied on the bus depending on the bus speed and conditions. This force can be simulated by controlling the amount of power flow from/to the motor. The method to control the power flow has been proposed to use contactors controlled by a logic controller. The logic controller controls resistors on and off based on how much power it needs to dissipate.

Simulating bus operations by logic controller

The force applied on the bus determines how much power has been applied on the drive motor of the bus based on the equation:

$$power = force \times bus\ velocity \tag{4-2}$$

The bus velocity is determined by the drive motor throttle (throttle potentiometer) and the power is determined by the brake command (brake potentiometer). The motor loading system has two main control functions: to dissipate the required amount of power through resistors and to feed power back to the motor through batteries. The

load system configuration consists of a set of logic controlled contactors as Figure 4. 31 shows.

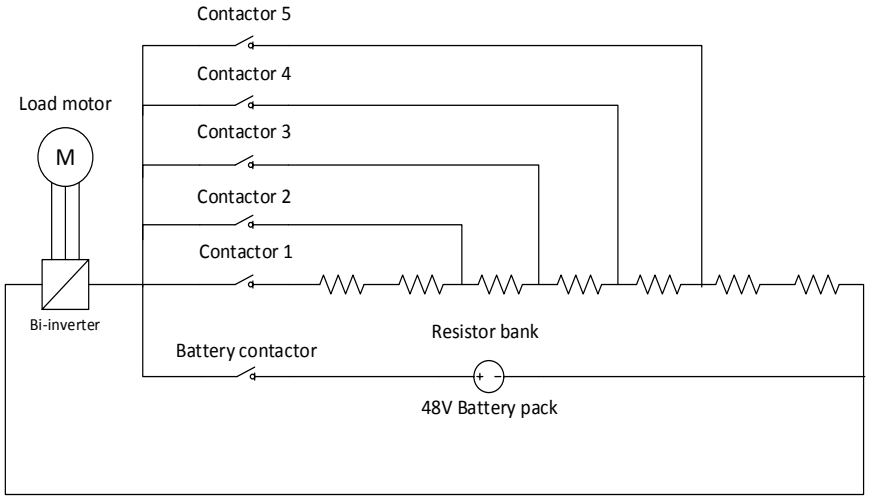

Figure 4.31 Logic controller and contactor configurations for the load system

The switching control of the contactors has been carried out with a logic controller. The voltage and current applied to the load motor has been used to calculate the power in real time. This real time power is used to control the contactors depending on a pre-defined minimum and maximum power range. The minimum power and maximum power on the resistors have been determined by the minimum and maximum operating voltage of the load motor which are 42 V and 58 V respectively (40 V will trigger motor low voltage protection while 60 V will trigger over voltage protection). The operation strategy of the logic controller has been summarised in Table 4.6.

Table 4.6 Logic controller control strategy for motor load system

Operation mode	R (Ω)	V_{min} (V)	V_{max} (V)	P_{min} (W)	P_{max} (W)	Contactor closed
Motor	7	42	58	252	480	1
Motor	6	42	58	294	560	not used
Motor	5	42	58	353	672	2
Motor	4	42	58	441	841	3
Motor	3	42	58	588	1121	4
Motor	2	42	58	882	1682	5
Generator	n/a	n/a	n/a	n/a	n/a	Battery contactor

The load system can automatically adjust the contactors for the resistor bank or battery pack to meet the load motor power demands. The number of resistors and contactors can be adjusted to extend the power range if required. To test the motor load response, the same configuration as Figure 4.32 has been installed in the laboratory as Figure 4.32 shows.

Figure 4.32 Motor load and contactor set up on a rack

After the logic controller system has been integrated with the motor generator set, the load system has been tested with the FC system. The test has been carried out by slowly increasing both the drive motor throttle (hence speed up) and load motor brake (hence increase power dissipated on the load side). The results have been plotted in Figure 4.33.

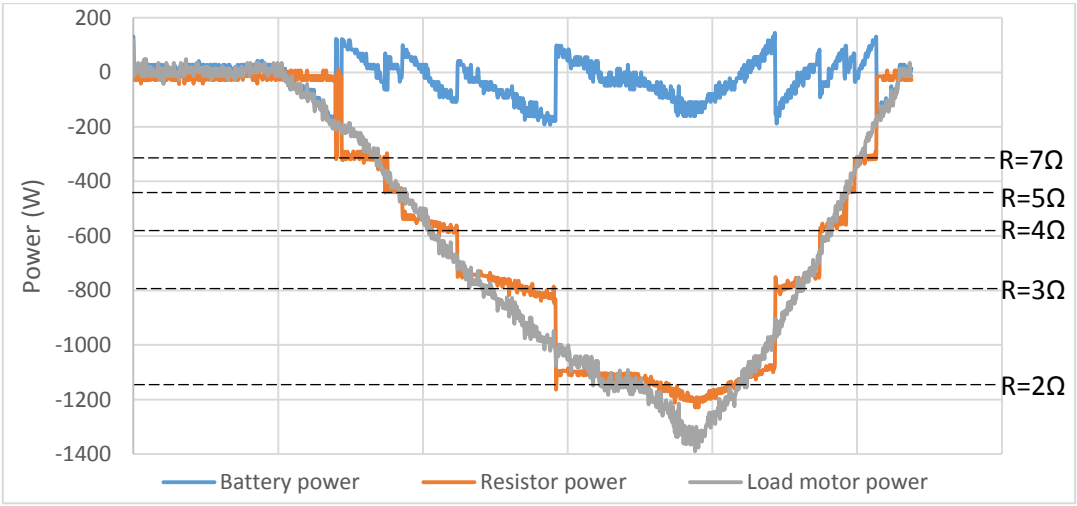

Figure 4.33 Contactor controlled load system responding to varying power

As the brake command increases, more regenerative power has been generated and required to be dissipated through the resistor bank. Hence the resistor contactors will be closed depending on the real time power. As the results showed, most of the power generated by the load motor has been dissipated through the resistors automatically (step changes in orange line). The battery power (blue line) will cover any difference caused by the step change to ensure the right amount of power being dissipated by the resistors. The results showed the loading system automatically adjusting the resistance to meet the power dissipation requirement.

The generator mode (external battery powering load motor) was not tested at this stage because the SC was not integrated, but the battery should simply supply the required power depending on the load motor commands.

4.8 Energy storage system

4.8.1 Energy storage selection

As discussed in the literature review (section 2.5.2), li-ion based batteries and supercapacitors (SC) are two of the more promising energy storage options for transportation applications. A detailed comparison between SCs and li-based batteries can be found in [4.8.1, 4.8.2] whereas the authors concluded the preference of those technologies would be highly dependent on the application types.

From the Ragone plot shown previously (Figure 2.28), it can be seen that Li-based batteries generally have a higher energy density but lower power density than the SCs. Comparing these two technologies, batteries are still much more commonly used, particularly dominating the energy storage for hybrid vehicle industry. The Li-based batteries can provide a better compromise between specific energy and power density than other batteries [4.8.3]. On the other hand, SCs have very high power density, but very poor energy density. The low energy density of SCs means the amount of energy SCs can store per unit weight is relatively small. This is the reason why Li-based batteries were believed to be a more appropriate option in a number of literature studies when comparing both li-on and SCs for diesel electric hybrid vehicle applications [4.8.4-4.8.6]. However, none of the literature considered hybridised energy storage with a FC unit. As discussed before, one of the most important advantages of FCs is their superior energy density but one of their main weaknesses is their slow response because of low power density. It can be seen that SCs are the opposite of FCs in terms of power/energy density performance which actually makes them complement each other when they work together.

The high energy density of FCs makes them more suitable to work as a near constant energy supplier while the high power density of SCs makes them suitable for fast charge/discharge operations. Considering the characteristics identified for the FC in this laboratory drivetrain, the determining factor to select the energy storage option for the FC is the power density, which makes SCs more suitable in this case. Similar conclusions were also addressed by other literature that concentrated on FC hybrid systems specifically [4.8.7-4.8.9] and in hybridisation degree studies from the critical

reviews (section 2.6.3).

Some recent research has concentrated on the potential of SCs in transportation applications and showed that SCs had a much better ability to absorb and release energy during regenerative braking and acceleration [4.8.10] which provides the potential for higher fuel economy in city driving conditions [4.8.11]. Additionally, unlike batteries, the SC does not involve chemical reactions which makes them able to sustain millions of charge/discharge cycles without degrading their energy storage capability [4.8.12, 4.8.13]. This is not possible for most types of batteries because of their slow reaction process and peak charge/discharge which can degrade the chemical compounds in the battery over thousands of cycles [4.8.14, 4.8.15].

Additionally, the London RV1, (as discussed in section 2.3.3) which is the only operational FC/SC hybrid bus fleet, offers a comparison case study for this drivetrain development. Therefore, for the above reasons, SCs have been selected as the energy storage technology for this FC hybrid drivetrain development research.

4.8.2 Supercapacitor design

Supercapacitor theory

A SC normally consists of two electrodes that are isolated by a separator in an electrolyte [4.8.16]. The SC works by the absorption of the ions from the electrolyte to the interfaces between the activated carbon and the electrolyte. This direct electrical process does not involve a redox reaction which consequently means the process is quick, reversible and offers very high mass power densities and lifetime [4.8.17, 4.8.18]. This research will not look into the detailed reaction processes within the SC, but focus more on the electrical performance of the SC.

The SC has the ability to store charge (q) and this charge is proportional to the applied voltage (V). This relationship has been formulated as:

$$q = C \times V \tag{4-3}$$

The “C” in the equation represents the capacitance of this SC which is defined as the ability to store an electrical charge. The capacitance of a SC is affected by the plate area, plate spacing and dielectric material which means the capacitance is independent of charge and potential while the SC is operating. If the voltage applied on the SC is increased, then the charge will also increase consequently to keep the charge/voltage ratio constant. Hence the amount of charge in the SC can be calculated

by measuring the voltage applied.

After calculating the charge in the SC, the work done to carry charge q from the negative to the positive plate is simply:

$$dW = V \times dq \tag{4-4}$$

Substituting the equation 4-3 into 4-4 gives:

$$dW = \frac{qdq}{C} \tag{4-5}$$

Then through integration this and rearranging this yield:

$$W(q) = \int_0^q \frac{qdq}{C} = \frac{q^2}{2C} \tag{4-6}$$

The work done W in charge/discharge is basically the energy stored/released from the SC. Therefore, by substituting equation 4-3 into 4-6, the equation to calculate energy stored in a SC can be formulated as:

$$W = \frac{q^2}{2C} = \frac{C^2 \times V^2}{2C} = \frac{1}{2}CV^2 \tag{4-7}$$

Since capacitance can be considered as a constant value, the energy stored can also be calculated by measuring the voltage. Since the state of charge (SoC) represents how much energy is left (equivalent to a fuel gauge), so the SoC can also be calculated as:

$$SOC = \frac{W_{current}}{W_{full}} = \frac{\frac{1}{2}CV_{current}{}^2}{\frac{1}{2}CV_{full}{}^2} = \frac{V_{current}{}^2}{V_{full}{}^2} \tag{4-8}$$

Since the full voltage (rated voltage) is usually provided as part of the SC datasheet, therefore the SoC of the SC can be calculated as a square function of the applied voltage. By measuring the voltage, the charge, energy stored and SoC can all be calculated [4.8.20]. The other important parameter that needs to be identified is the charge/discharge current, which is given by the change of charge in a certain time and is formulated as:

$$I = \frac{dq}{dt} \tag{4-9}$$

Substituting equation 4-3 into 4-9 gives:

$$I = C\frac{dV}{dt} \tag{4-10}$$

This equation shows that the SC charge/discharge current would be dependent on how fast the voltage change occurs.

Supercapacitor sizing

Based on the SC fundamental equations identified, the two most important parameters to size the SC are the rated voltage and capacitance. In the FC hybrid system, a parallel connection with the FC (after boost converter) meaning the voltage from the SC and buck/boost converter will also be the same. The first step to size the SC for this FC hybrid system is to select one that can work with the 48 Vdc bus bar voltage. After product and company evaluations, a SC option has been selected from Maxwell which is not only one of the largest SC manufacturers worldwide but also the SC supplier for the energy storage system on the London FC bus RV1. This Maxwell SC option is an off shelf unit rated at 48 V and Table 4.7 summarised some of the key specifications from the product datasheet.

Table 4.7 Key specifications of the proposed SC for the FC hybrid system

Model	P48 B01
Rated voltage	48 V
Rated capacitance	83 F
Maximum ESR_{dc}	10 mΩ
Absolute maximum current	1,150 A
Absolute maximum voltage	51 V
Stored energy, individual cell	1.5 Wh
Number of cells	18
Stored energy, total	27 Wh
Cooling	Natural convection
Projected cycle life at 25 ℃	1,000,000 cycles

Since the London RV1 used a 75 kW FC as primary power source and a 0.5 kWh Maxwell SC as energy storage, selecting the 0.027 kWh SC for this 8.5 kW FC system would also be a similar and appropriate selection for the FC hybrid bus system based on this scaling. The stored energy, which was identified before, can be calculated with equation 4-7 based on voltage and capacitance. The 27 Wh means that the SC is capable of releasing 27 W of output power for one hour from full SoC and vice versa for storing energy. A power against time plot has been plotted in Figure 4.34 showing how long this SC can last supplying different power outputs.

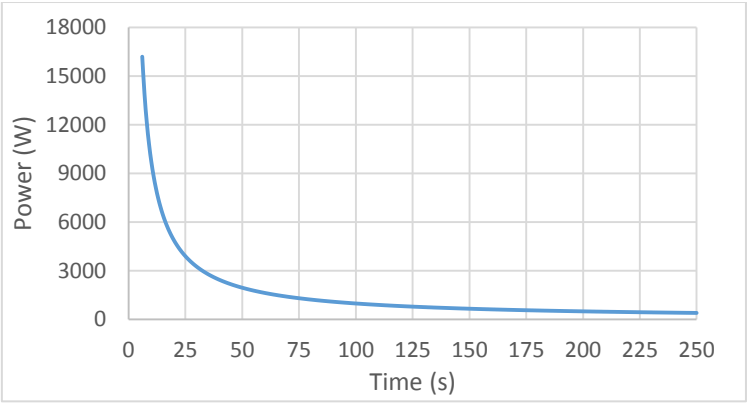

Figure 4.34 SC discharge power capability against time

As Figure 4.34 shows, the more output power the SC releases, the shorter the discharge time becomes. Since the energy storage in this FC hybrid system will be used to supplement power peaks and absorb regenerative energy, the amount of energy required from the SC would depend on the driving cycle, hybrid control strategy and scaled power profile which will be analysed in Chapter 6.

SC evaluation test

The 48 V Maxwell SC was ordered and delivered to the laboratory as Figure 4.35 shows. The installation of the SC unit is also very simple because it is one-unit-module. Since the monitor cable (in the middle) is only used to monitor the real time status of the SC, the only electrical connections for this SC are the main positive/negative connections.

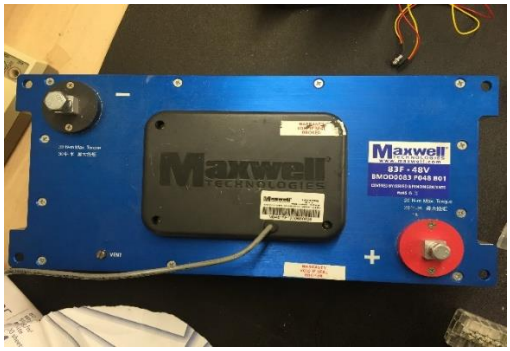

Figure 4.35 Photo of the selected 48 V Maxwell SC

In order to evaluate the performance of the SC unit, a discharge test has been carried out with this SC. The SC was connected to a 2 Ohm resistor and the discharge curves have been plotted in Figure 4.36.

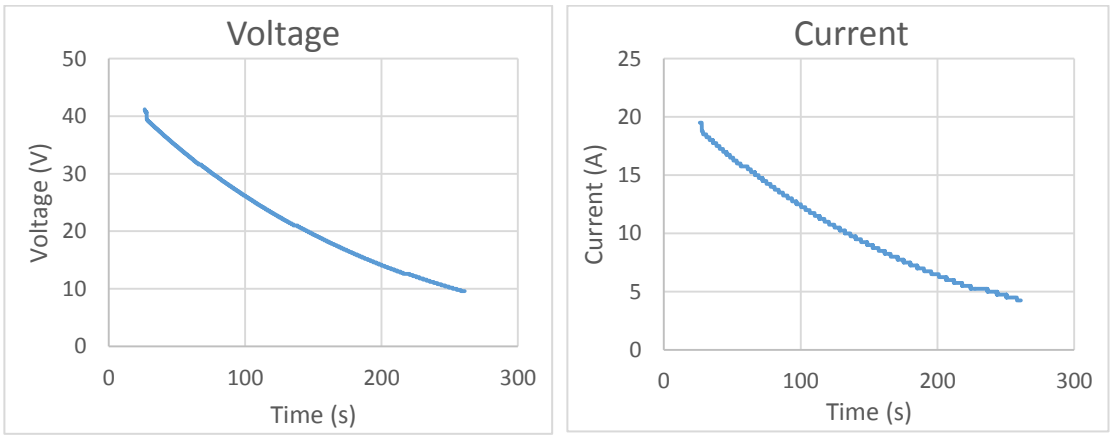

Figure 4.36 48 V Maxwell SC discharge curve under 2 Ohm load

As Figure 4.36 shows, the discharge voltage reduces in an exponential function curve which reflects equation 4-7. The voltage started from 41 V and takes 240 s to drop to 10 V. The current also has a similar curve because the resistance remains unchanged so it is proportional to the voltage because of the Ohm's Law [4.8.21] and [4.8.22].

Based on the logged data, the SoC change can be calculated based on equation 4-8 identified before:

$$SOC_{change} = SOC_{initial} - SOC_{final} = \frac{{V_{initial}}^2}{{V_{full}}^2} - \frac{{V_{final}}^2}{{V_{full}}^2} = \frac{41^2}{48^2} - \frac{10^2}{48^2}$$
$$= 0.7296 - 0.0434 = 0.686$$

It can be found that the SC discharged 68.6% of its energy in 240 s on a 2 ohm resistor. The change in energy stored by the SC can also be calculated according to equation 4-7:

$$E_{change} = E_{initial} - E_{final} = \frac{1}{2}C({V_{initial}}^2 - {V_{final}}^2) = \frac{1}{2} \times 83 \times (41^2 - 10^2)$$
$$= 65611.5\ joules$$

The discharge power, however, is not been equally distributed because the current changes due to the constant resistance on the SC load. With the current and voltage both decreasing, the power delivered during discharge reduces as the SoC drops. The real time power of the SC discharge through a 2 ohm resistor has been calculated and plotted in Figure 4.37. As the plot shows, the power dissipated by the resistors started at around 800 W and then reduced as a square function curve.

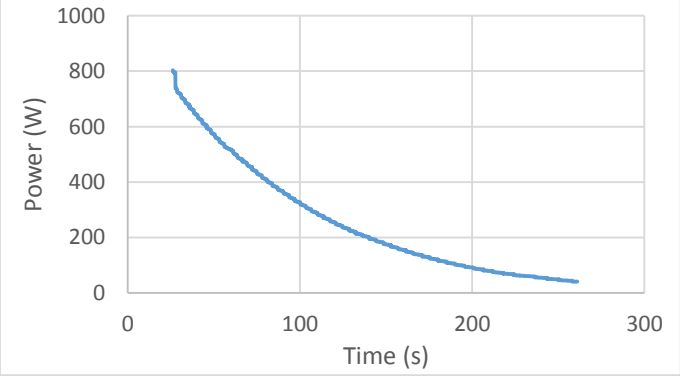

Figure 4.37 48 V Maxwell SC discharge power curve

From the discharge test, it can be seen that the SC would directly react to the load demand (resistance in this case). Therefore it is important to control the discharge and charge of the SC to avoid releasing or drawing too much power. A charge test was not carried out at this stage because it was recommended that a SC controller should be integrated with the SC to control the charge current to avoid in-rush current to the SC.

4.8.3 Buck/boost converter for Supercapacitor

A DC/DC converter has been proposed to control the SC. As the SC evaluation test result shows, the SC voltage is proportional to the SoC which means the SC voltage will vary as the SC is charging or discharging. Therefore the converter to control the

SC will not only control the power flow to the SC depending on the power demand, but also regulate the output voltage to the motor controller. The converter for this SC has been manufactured by an external supplier. After consulting with the Maxwell Company, a SC controller from AEP Hybrid Power has been recommended for this 48 V SC. The proposed product is a 48 V Bidirectional DC/DC converter specifically designed for SC control. The converter is capable of controlling the bidirectional charge/discharge of the SC and regulating constant supply voltage from variable sources (step up or step down). The key specifications have been summarised in Table 4.8.

Table 4.8 Key specifications of the proposed DC/DC converter for the SC

Technical information	
Model	USCDCDCca-6-80-24-IP20
Rated power	6 kW @ 48 V
Switching frequency	24 kHz
Voltage range	0-80 V
Maximum current	150 A
Control voltage	24 V
Operation modes	
1. Input power control	5. Output voltage PI control
2. Input current control	6. Input voltage static
3. Output current control	7. Output voltage static
4. Input voltage PI control	

The converter is capable of operating in various control modes to control different parameters (control mode 1 to 7). However, only one operation mode can be selected at any time.

Buck/boost converter theory

A buck/boost converter can function as a boost converter or a buck converter. The buck converter has similar working theory as a boost converter but uses a slightly different configuration as Figure 4.38 shows.

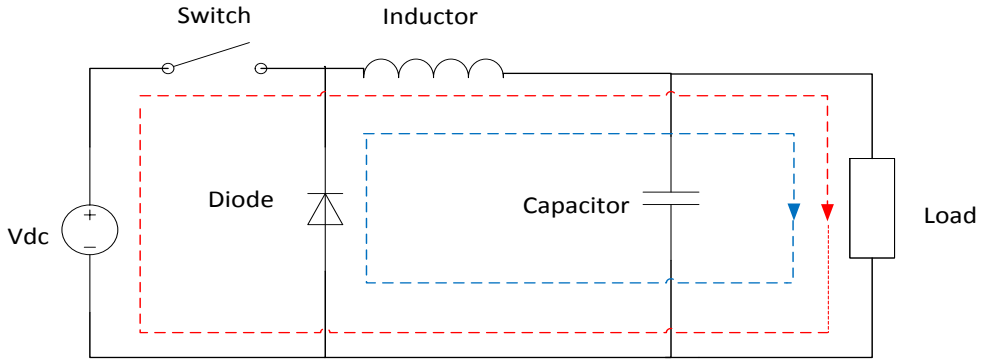

Figure 4.38 Typical buck converter configuration and operation

The operation concept of the buck converter is similar to that of the boost converter where the voltage is controlled by electronic switching.

a) When the switch is closed, the current flows via the red loop. The inductor will be charged with the voltage source, thus reducing the voltage applied on the load.
b) When the switch is opened, the current flows via the blue loop. The inductor opposes any drop in current with the current produced through the collapses of the magnetic field and keeps the current flow to the load [4.8.23]. The inductor in the buck converter configuration worked as a secondary transient source being constantly charged and discharged, therefore reducing the voltage applied on the load. The amount of voltage to be stepped down can also be controlled by the switching duty cycle [4.8.24]. Generally, the buck converter configuration is used for voltage step down operations while the boost converter is for step up operations [4.8.24].

AEP converter control structure

The proposed converter from AEP developed for this FC hybrid system application utilises an adapted H bridge configuration based on the described theory. The detailed operation of the H bridge converter can be found in Appendix K. The block diagram of the proposed converter has been shown in Figure 4.39.

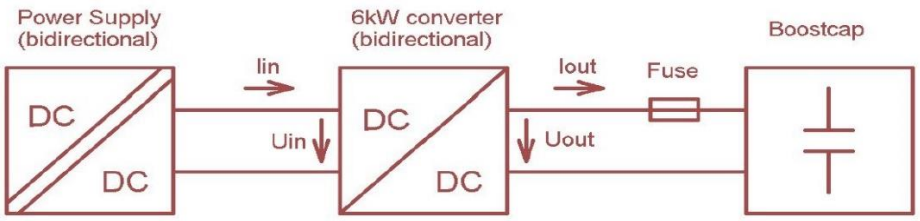

Figure 4.39 Block diagram of the SC and AEP buck/boost converter structure

The four parameters indicated in the diagram are the input current, output current, input voltage and output voltage which are the parameters that can be controlled depending on the control mode selection. The reference value of the selected parameter will be subtracted by the actual measured value to generate an error signal. This signal will be the input to a PID controller and a PWM system to calculate the required duty cycle for the electronic switch. Further description of this AEP converter on the control method and converter operation can be found in Appendix L.

The reference value can either be determined via user controlled software (PowerPanel) or controlled by the CAN RS232 connection. The PowerPanel software provided for this converter can be used to select the control mode and input the reference values. However, this software requires the user to input the reference

values manually. The initial test for the converter will be carried out with this software and it will be replaced with CAN communication later. A CAN communication is capable of sending reference value based on real time information which enables the simulation of more complex driving cycles.

Buck/boost converter test result

An initial test for the buck/boost converter has been carried out to evaluate the performance before integrating it with the FC drivetrain. The test has been built as the configuration shown in Figure 4.40.

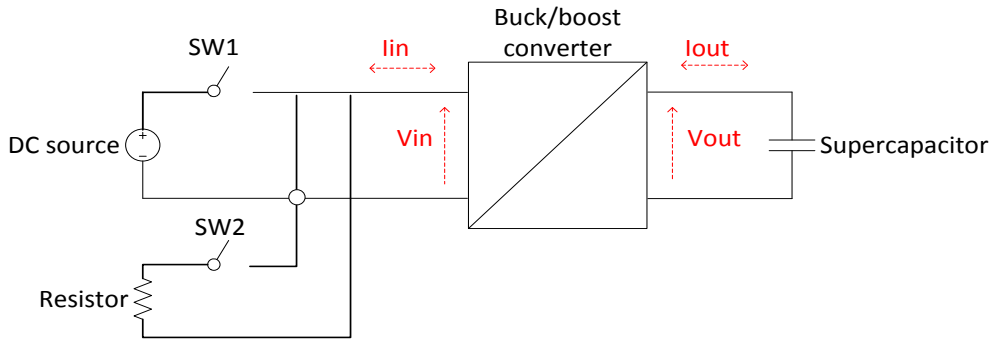

Figure 4.40 Buck/boost converter initial evaluation test configuration

In this initial test configuration, two switches have been used to connect the SC and converter with a DC source for charge or a resistor bank for discharge. The objective is to use the converter to control the four parameters to test the four main control modes. The result of input current control mode has been logged and plotted in Figure 4.41.

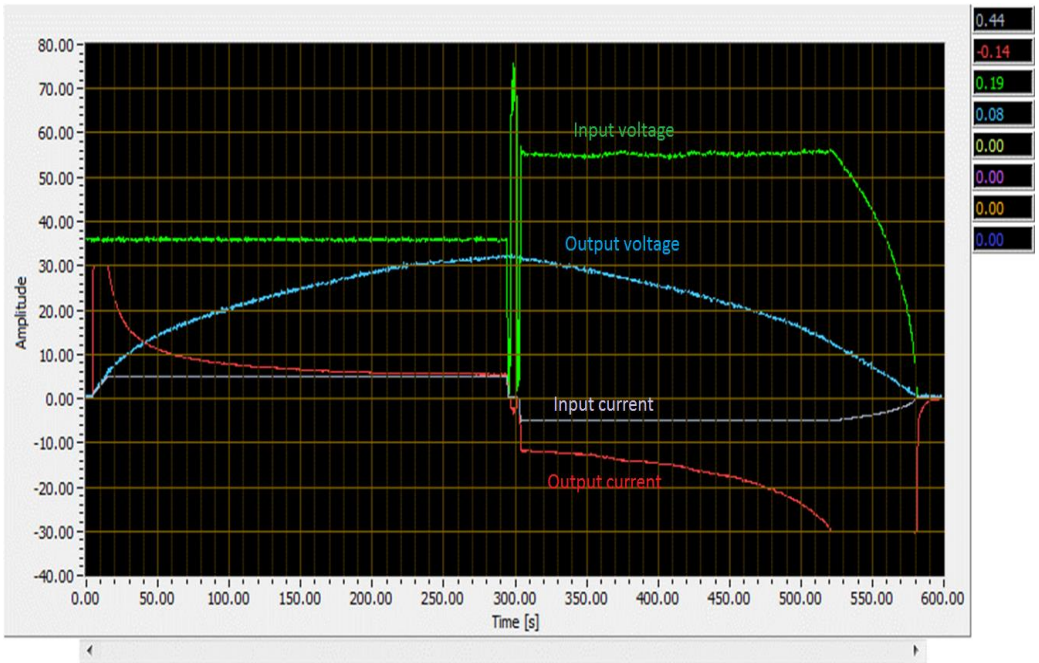

Figure 4.41 Input current control mode under low power test

The left half of the plot (before 300 s) represents results of the SC being charged while the right half (after 300 s) represents the results of SC being discharged. The following bullet points explain the curves of the four parameters for the input current control mode test.

Charge test (0-300 s)

1. Input current (purple): The input current has been kept at a stable 5A from the DC voltage source as expected (5A defined in the PowerPanel software by user).
2. Input voltage (green): The input voltage is the same as the DC voltage source which is a constant 36 V.
3. Output current (red): A large initial current (which is known as the inrush current of SCs) has been drawn from the SC due to the large potential difference between the DC voltage source and SC voltage. The reason it only reaches 30 A is because the maximum current has been limited to 30 A by the software. The output current then started to drop as the SC voltage increases.
4. Output voltage (blue): The output voltage directly reflects the voltage of the SC which also indicates the SoC of the SC as a square function.

Discharge test (300-600 s)

1. Input current: The input current has been kept at the requested 5 A until approximately 525 s where it started to reduce afterwards.
2. Input voltage: A spike on the input voltage has been observed when switching between charge test and discharge test. This is caused by internal capacitance within the converter after the DC source has been switched off. After the spike, the input voltage was kept around 56 V until approximately 525 s again. This voltage is because the 5 A input current was applied on a 10 Ω resistor bank which gives around 50 V (56 V is because of the variation in the resistance and connector resistances).
3. Output current: The output current started with a smaller current and then increased as the SC SoC decreased. The larger the potential difference there is, the more current would be required to boost the voltage. After the current reaches 30 A (due to current limit) at 525 s, then the remaining charge was unable to cover the continually dropping voltage so that caused all four parameters to start to drop.
4. Output voltage: The output voltage reflects the SC voltage and has nearly the same reducing curve as the charge test (except after 525 s).

As the results showed, the converter controlled the input current to a requested 5A. The other three modes have also being tested with the same configuration and all proven to work as expected. The buck/boost converter conversion efficiency has also been calculated and showed a 93 to 98% efficiency.

There are three main parts of the FC hybrid system: FC (and boost converter) as the main power source, SC (and buck/boost converter) as the energy storage and AC motor as the load. The drive motor will send a power demand signal depending on the load and this power demand will be met by the FC system and SC system. Since the FC is a passive power source while the motor will be the traction force which meets the throttle and brake commands, controlling the SC will be the most important part in the FC hybrid system.

As identified before, the buck/boost converter has four main control modes. First, instead of controlling the voltage and current from the SC, controlling the input to the SC and converter will be easier to balance the power demand between motor and FC system. This can not only eliminate the calculation of buck/boost conversion processes but also make the best use of the high power density of SC to meet any demands the buck/boost converter requests (as long as the SoC allows). Then the control mode option would be a choice between input voltage control and input current control. Since the SC system will be connected in parallel with the FC unit, which is going to be kept at a constant 48 V by the FC boost converter, the same voltage level can also be expected due to the parallel connections. Therefore the input current control mode has been selected to control the power in and out of the SC and buck/boost converter system.

4.9 Discussion on FC hybrid drivetrain justification

As identified in section 3.3.3, the justification purpose of the load system was:

1. Analyse the FC performance when it is directly driving a motor to simulate more realistic FC bus performance.
2. Enable load control (power, speed and torque) of the motor so that different realistic driving conditions (acceleration, braking, uphill, overloaded etc.) can be applied on the driving motor.

The performance of the FC can be analysed by controlling the two potentiometers (motor throttle and brake) to control the power and torque applied on the motor. Although only simple tests have been carried out at this stage, more complex and actual driving cycles can be simulated once the potentiometers have been replaced with software controlled digital potentiometers. The two potentiometers also enable load control on the FC hybrid system. Additionally, an electrical load system that can take or supply the power generated or required by the motor has also been developed that is capable of simulating different driving cycles.

As identified in section 3.3.3, the justification purpose of the ES system was:

1. Identify the appropriate ES system for this FC hybrid drivetrain application and explain why it is more appropriate than other ES options.
2. Design the control system and conditioning system for the ES for better integration with the FC hybrid drivetrain.
3. Investigate the performance of the FC hybridised with the energy storage under different load conditions.

The more appropriate ES option has been selected as a SC module based on literature reviews and the FC characteristic tests carried out previously. The SC has been sized and evaluated to work as expected. The control system for the SC, which is a buck/boost converter, has been manufactured by an external supplier. The converter has shown that it is capable of controlling charge and discharge of the SC and the control strategy has been selected to be the input current control mode for this FC hybrid system. The results showed the converter is capable of controlling the current going in and out of the SC system (both SC and converter) which enables the power balancing between the FC and the SC. The third point focused on investigating the performance of the FC in a hybridised system. Since this point investigates the completed FC hybrid system, both the computer model and system optimisation, along with the control system, are also required to investigate the hybrid system performance. Therefore this point will be investigated together with the other justification points identified in section 3.3.4.

4.10 Summary

In this chapter, a FC basic drivetrain and a FC hybrid drivetrain have been developed and installed in the laboratory. A FC along with its conditioning systems and electrical load system have been specified, designed and constructed. The FC system has been evaluated with initial experiments and the results showed the characteristics of the FC. A boost converter has also been designed and built for this FC as a power conditioning system. The developed drivetrain has been subjected to a set of experiments to gain a better understanding of the FC system.

The second section of this chapter described the development of the FC hybrid drivetrain constructed on top of the developed FC basic drivetrain. Four design steps have been identified and completed to upgrade the basic FC drivetrain into the FC hybrid drivetrain. The motor and its loading system has been installed and tested. The energy storage has been selected as a SC module and a control system has been designed specifically for this SC. The motor load and SC system both showed good performance and functioned as expected.

Chapter 5 Computer system modelling

5.1 Introduction

This chapter describes the simulation of the laboratory FC systems by computer modelling. The chapter presents descriptions for the simulations of each individual systems and the integrated FC hybrid system. The FC laboratory evaluation test results were used to provide the information for the FC simulation. From this point onwards, the laboratory and simulation models were developed in parallel and validated against each other. The validation tests have been used to ensure the simulation is suitably representative of the laboratory FC system. The simulation procedure is as follows; theoretical analysis – mathematical build – computer simulation – validation against laboratory results. This chapter presents descriptions for each of the constituent sub-system models that comprise the integrated FC hybrid system model.

5.2 Modelling purpose

The purposes of modelling the FC hybrid system are:

1. To provide a validated computer simulation of the test bench model that can be used for a wider range of load condition experiments than could not be carried out practicably with the test bench model.
2. To enable the optimisation of the system which investigates the effect of degree of hybridisation and control strategy between the FC and the energy storage.

5.3 Software selection

The software package selected to build the FC hybrid model is MATLAB/Simulink. MATLAB/Simulink is a graphical programming environment for modelling, simulating and analysing multi-domain dynamic systems. Another option, PSCAD (Power Systems Computer Aided Design), was also considered and tested with a number of models. Although both software packages provide good graphical electrical simulation platforms and have been tested with some models for comparison and selection. Simulink was selected for the following reasons.

1. To align with the HyFCaP project. Other members of the HyFCap project in the FC bus group was also using MATLAB/Simulink to enable easier collaboration.
2. To facilitate the integration of existing models. Simulink has many existing models which can be used directly for simulations such as the FC and the SC. These would have to be built by individual components in PSCAD.

3. To match previous works in the research field. Significant amount of FC bus simulation research was carried out using the MATLAB/Simulink software package while only a very small amount of work used PSCAD.

5.4 FC simulation

5.4.1 FC model

FC mathematical model

This research is more interested in the output characteristics and performance rather than chemical reactions within the stack. Hence the FC simulation will be focusing on the electrical characteristics of the proposed 8.5 kW FC described in the laboratory system. As discussed section 2.4.3 of the literature review, the PEMFC output voltage can be calculated as:

$$V_{output} = E_{theoretical} - V_{activation} - V_{concentration} - V_{ohmic} \quad (5\text{-}1)$$

The four voltage parameters need to be mathematically represented in the computer simulation in order to calculate the output voltage of the FC. The cell thermodynamic potential difference (emf), which was described as the theoretical voltage of a FC (Figure 2.26), is also known as the Nernst voltage. The Nernst voltage of the FC can be calculated by a modified version of the Nernst equation with an additional term to take account of changes in temperature with respect to the standard reference temperature (25 °C) [5.4.1]. The Nernst voltage calculation for a FC is formulated as:

$$E_{Nernst} = 1.229 - 0.85 \times 10^{-3}(T - 298.15) + 4.3085 \times 10^{-3}T(lnP_{H_2} + 0.5lnP_{O_2}) \quad (5\text{-}2)$$

where T is the cell temperature in Kelvin, P_{H2} and P_{O2} are respectively the hydrogen and oxygen partial pressures in atm. The temperature can be monitored and the pressure is controlled by regulators, hence the Nernst voltage of the FC can be calculated in real time.

The three voltage losses are the activation loss, concentration loss and ohmic loss. The activation loss is defined as the energy required to initiate the maintain the chemical reaction and is formulated:

$$V_{act} = -[\xi_1 + \xi_2 T + \xi_3 T ln(C_{O_2}) + \xi_4 \ln(I_{stack})] \quad (5\text{-}3)$$

where T is still the cell temperature in Kelvin, I_{stack} is the cell operating current in A, while the ξ1, ξ2, ξ3 and ξ4 are the parametric coefficients for each cell model. The parametric coefficients are determined based on theoretical equations with kinetic, thermodynamic and electrochemical foundations [5.4.2]. C_{o2} is the concentration of oxygen in the catalytic interface of the cathode which is determined by another

equation:

$$C_{O_2} = \frac{P_{O_2}}{508 \times 10^6 \times exp^{\frac{-498}{T}}} \quad (5\text{-}4)$$

The concentration loss is defined as the energy loss when reactant cannot be supplied in response to a significant rate of change in demand which is formulated as:

$$V_{conc} = -B \times \ln(1 - \frac{J}{J_{max}}) \quad (5\text{-}5)$$

where B is a parametric constant depending on the cell type, J represents the current density and J_{max} represents the absolute maximum current density input rate passing through the cell at each moment in A/cm^2.

The ohmic loss is due to the membrane resistance and fuel cell component resistance which is formulated as:

$$V_{ohm} = I_{stack}(R_m + R_C) \quad (5\text{-}6)$$

where R_c represents the resistivity to the transfer of electrons through the electrodes, which is generally considered as a constant value in FCs. R_m represents the equivalent resistance of the membrane which is calculated as

$$R_m = \frac{\rho_m \times l}{A} \quad (5\text{-}7)$$

where ρ_m is the membrane-specific resistivity to the flow of protons in Ωcm, l is the membrane thickness of the membrane in cm and A is the cell active area in cm^2.

As can be seen from the equations, the three voltage losses can be calculated from the FC data and real time operating conditions. The voltage output of the FC can be calculated by applying these mathematical equations to the computer software. More details on the derivations of the Nernst voltage and the three FC voltage loss equations can be found in [5.4.1-5.4.6].

FC computer model

The FC model can be represented by an equivalent circuit. Figure 5.1 shows the simplified equivalent circuit of a FC power source based on the mathematical equations. The FC output voltage can be calculated in real time. However, some of the information required by the equations such as membrane thickness, FC parametric coefficients (ξ) and parametric constant (B) are not provided in the datasheet nor allowed to be released for reasons of commercial confidentiality. As a consequence, certain parameters and values would have to be derived from the FC laboratory evaluation test results.

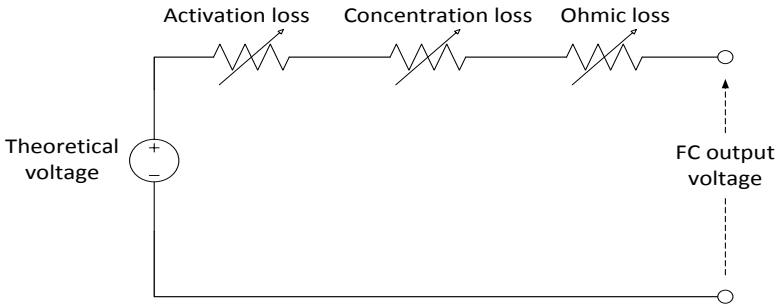

Figure 5.1 Equivalent circuit of a typical FC model

In MATLAB Simulink, a generic hydrogen fuel cell stack model can be modified to represent some of the more popular types of fuel cell stacks. The model uses the equivalent circuit as shown in Figure 5.2. The Simulink model calculates the three voltage losses based on the current output and assigns a calculated voltage by mathematical method. A diode has been added to the equivalent circuit model to prevent reverse current. An internal resistance has been added to simulate the resistance across the power transmission elements i.e. cable and contacts.

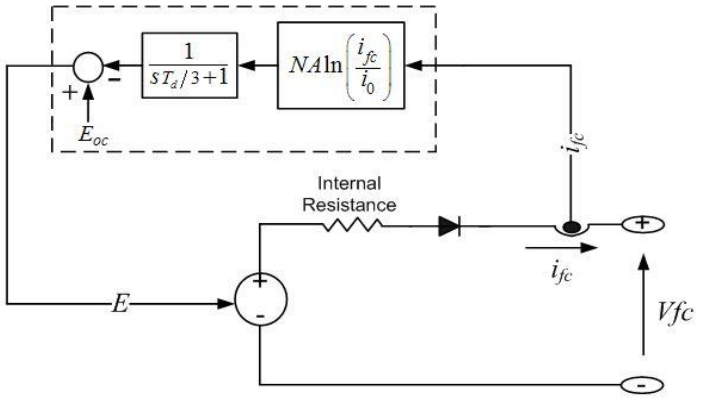

Figure 5.2 Equivalent circuit of the Simulink generic FC model

Simulink was used to produce a polarisation curve through calculation using the parameters loaded from the data sheet. The missing information mentioned before has been derived based on the laboratory FC evaluation test. Details on the Nernst voltage and voltage losses calculation in the model and extra FC model schematics in Simulink can be found in Appendix M. The Simulink FC model block parameter set up interface and the model produced polarisation curve are shown in the Figure 5.3.

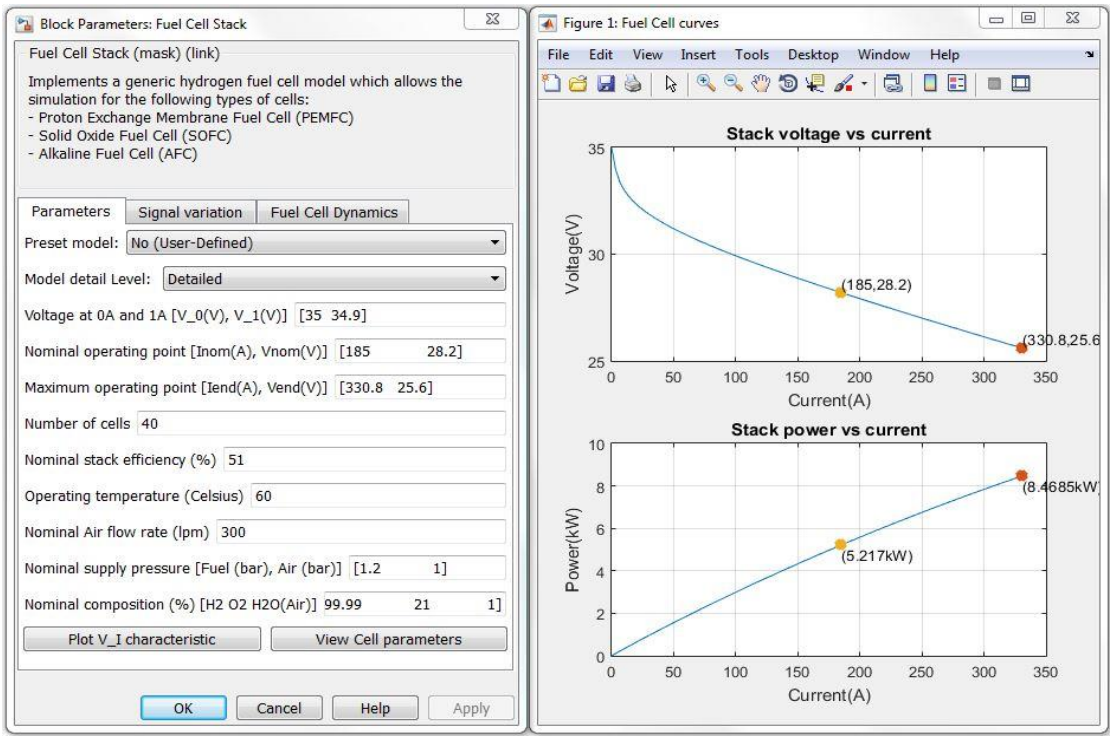

Figure 5.3 Simulink FC model block parameter set up and polarisation curve

5.4.2 FC model validation

In the laboratory FC evaluation test carried out in section 4.2.3, the FC was connected with up to ten parallel connected resistors to evaluate the FC performance. A series of simulation tests using corresponding loads was carried out using the Simulink FC model to evaluate the accuracy of the simulation model. The resistive load was modelled in Simulink. The FC under load model evaluation circuit is shown at Figure 5.4.

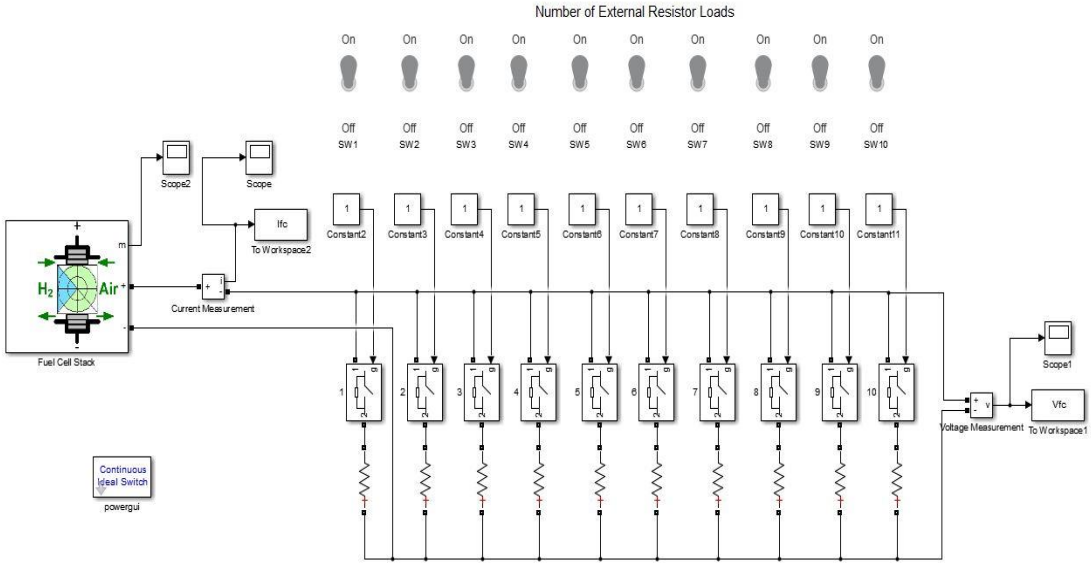

Figure 5.4 Simulink model of the FC with resistive loads

The resistance values of the resistors were set to match those of the laboratory system and the same experimental sequence for loading the FC was followed. The simulation model results have been compared with the earlier FC test results and are shown at Figures 5.5 and 5.6.

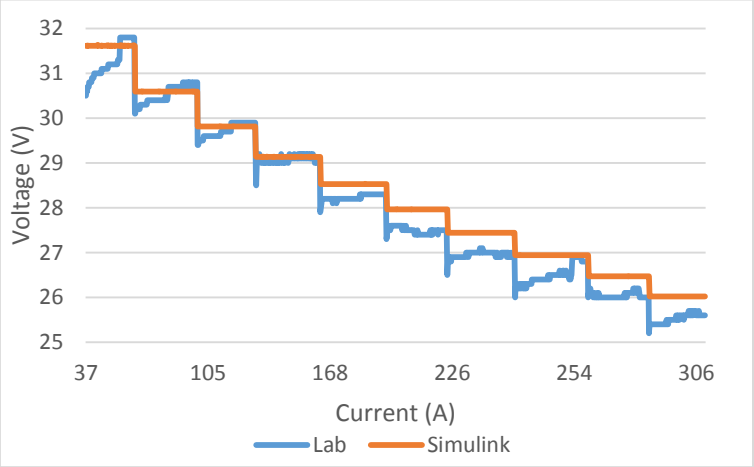

Figure 5.5 FC simulation and lab result of output voltage against current

As the voltage against current curve shows, the FC output step responses are generally the same as the laboratory result. However, the voltage outputs from the Simulink FC model is slightly higher than the results from the laboratory system. It has been found that the difference is approximately 1-2 % depending on the power level. This is caused by the temperature stabilisation identified in the laboratory FC evaluation test (Figure 4.13). The FC temperature takes time to stabilise in the laboratory system while this is not a factor for the computer simulation. This will have less impact on the difference between laboratory system and Simulink model if the load change is not stepped.

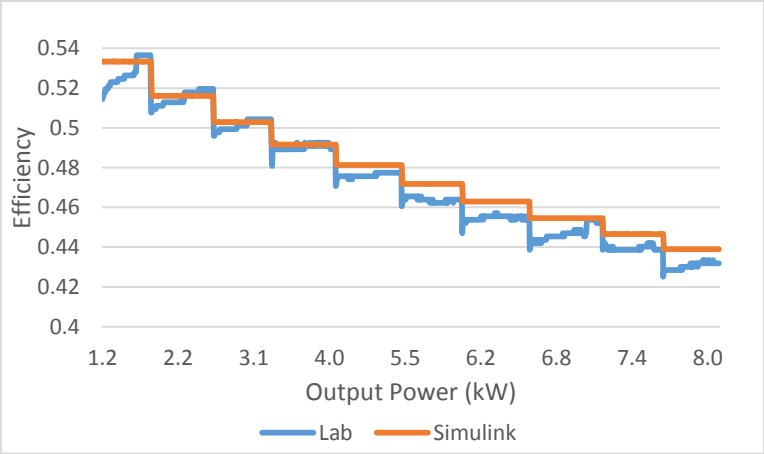

Figure 5.6 FC simulation and lab result of efficiency against output power

Figure 5.6 shows the efficiency against power curve of the simulated and laboratory FC. The difference has also been found to be 1-2 % when comparing the results obtained from laboratory test and computer simulation. The efficiency curve is

generally proportional to the voltage curve. As the FC warms up, the efficiency and output voltage both approach those of the Simulink model curves. Although the results do not exactly correlate, the Simulink model can still reasonably simulate the laboratory FC in the computer model.

5.5 Boost converter simulation

5.5.1 Boost converter model

The boost converter consists of an inductor, a capacitor, a diode and a switch along with its switching modulation controls. The boost converter model was built in Simulink. The control algorithm is programmed to maintain the output voltage at 48 V. The boost converter sub-system model in Simulink is shown in Figure 5.7. The actual output voltage will be subtracted by the reference 48 V to generate an error signal. The error will be passed to a tuned PID controller and fed to a PWM generator to determine the switching frequency.

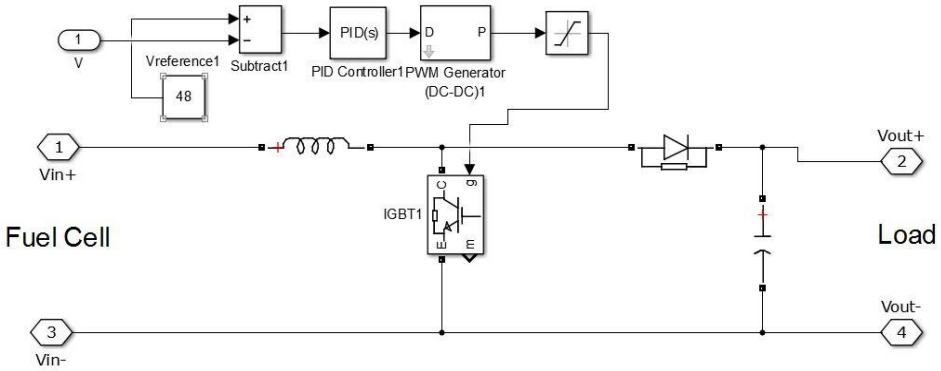

Figure 5.7 Boost converter schematics for FC Simulink model

5.5.2 Boost converter model validation

To effectively validate the model, the same laboratory resistive load system (Figure 4.18) has been used in the model. The identical laboratory FC basic drivetrain has been built in the Simulink model as Figure 5.8 shows.

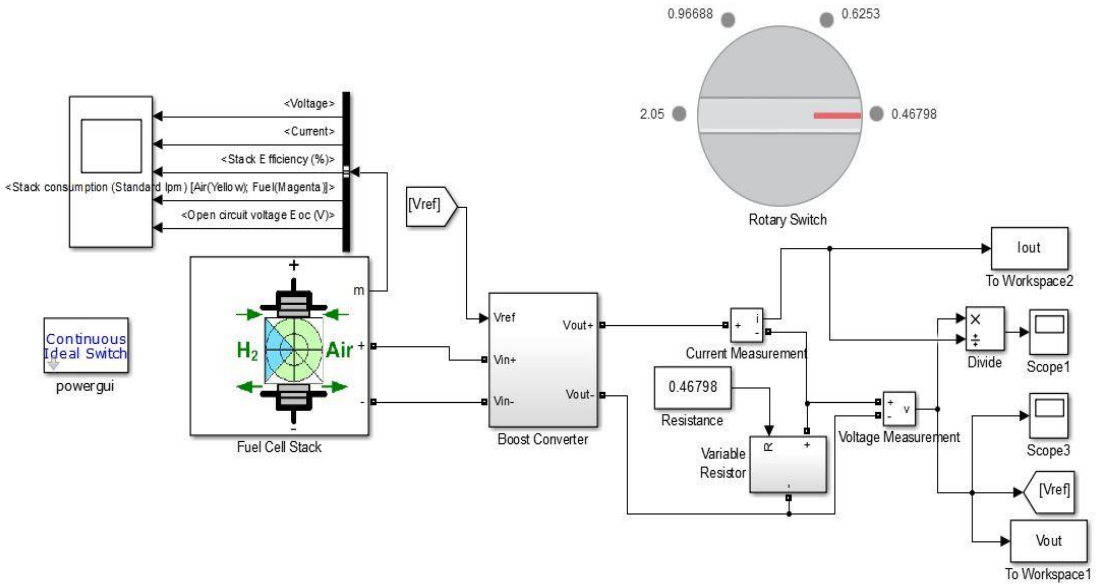

Figure 5.8 FC basic drivetrain Simulink model with user controls

The same experiment (load 1-4 with different resistance as discussed in section 4.3.3) has been carried out for validation purpose. The output of the boost converter has been plotted in Figure 5.9.

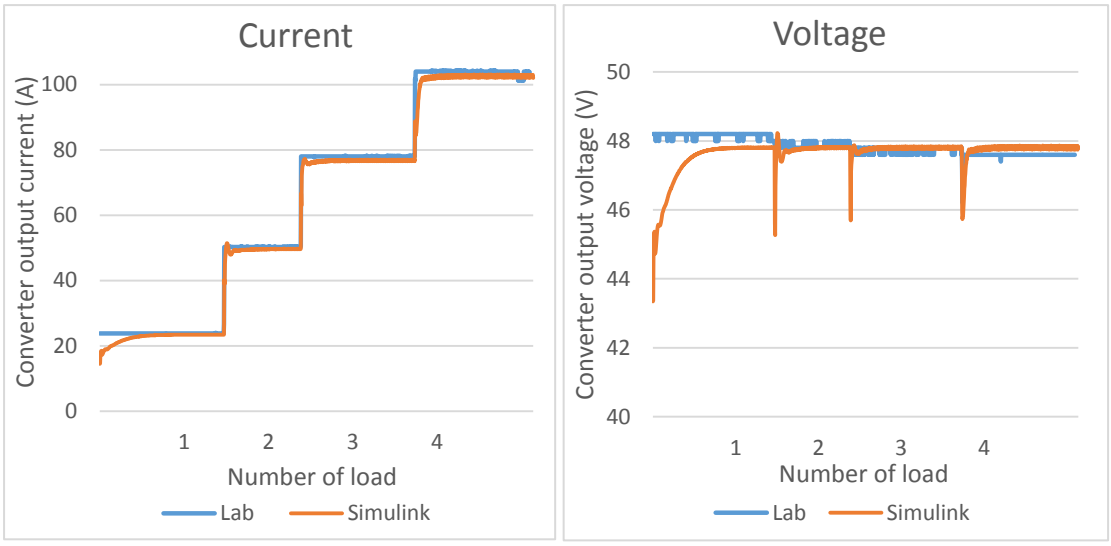

Figure 5.9 Lab/Simulink comparisons of boost converter output

The boost converter output current characteristic of the Simulink model is nearly identical (<1 % difference) to the laboratory result. The boost converter output voltage of the Simulink model was maintained at 48 V, however, voltage drops have been observed whenever the resistor bank switched to the next level. This is caused by the PID controller taking a short time (~5 s) to reset the new switching frequency to match the voltage change. Another reason is the logger sampling frequency of the laboratory system is lower than the Simulink model which means not all transient responses have been logged. The conversion efficiency of the boost converter has been calculated and plotted in Figure 5.10.

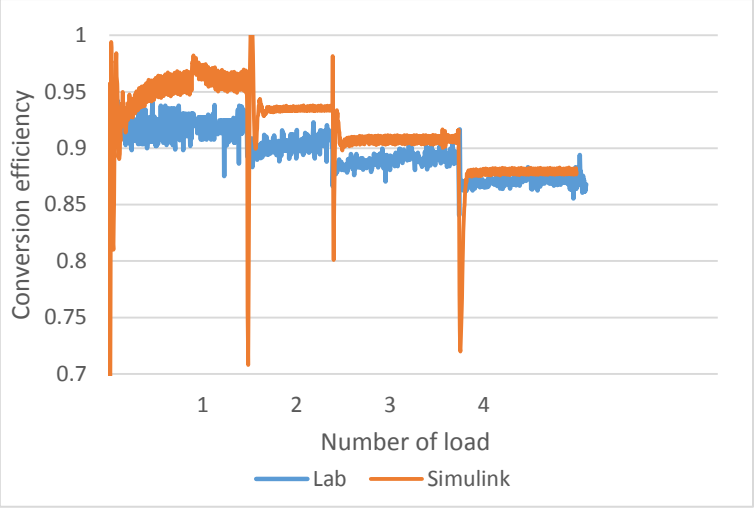

Figure 5.10 Lab/Simulink comparisons of boost converter conversion efficiency

The Simulink model converter showed approximately 4% higher efficiency than the laboratory system and the difference become smaller as power increases. The slight difference in efficiency is caused by the difference in FC output power being affected by the FC temperature. There is a trend showing the Simulink efficiency approaches to the laboratory converter efficiency as the power increases. Although there is some offset in the boost converter input power, the Simulink model was able to simulate the boost converter output reasonably accurately.

5.6 SC simulation

5.6.1 SC model

The SC unit selected for this FC hybrid model was the Maxwell 48 V Supercapacitor as discussed in the laboratory design section. To simulate a SC in Simulink, a generic SC equivalent circuit has been used as Figure 5.11 shows.

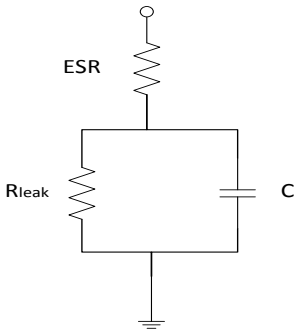

Figure 5.11 SC generic equivalent circuit

In the generic SC equivalent circuit, a capacitor (C) has been used to represent the capacitance of the SC, R_{leak} and ESR represents the losses due to leakage current and equivalent series resistance correspondingly. There are a number of methods to

simulate this capacitance C in the equivalent circuit and two of the more commonly used methods are to use a controlled voltage source or a controlled current source [5.4.7] [5.4.8]. The control algorithm for both methods are similar. Both methods use a current or voltage as reference to mathematically determine the voltage source or current source to simulate the SC output voltage as Figure 5.12 shows.

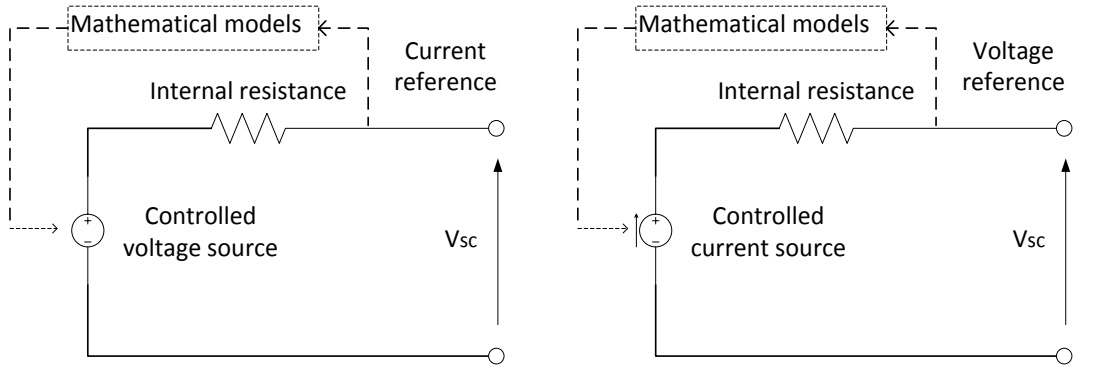

Figure 5.12 SC equivalent circuit control method using voltage/current source

In Simulink, a generic SC block can be parametrised to simulate a SC model. The generic SC model in Simulink utilises the controlled voltage source method discussed above. The equivalent circuit of the Simulink SC model has been shown in Figure 5.13.

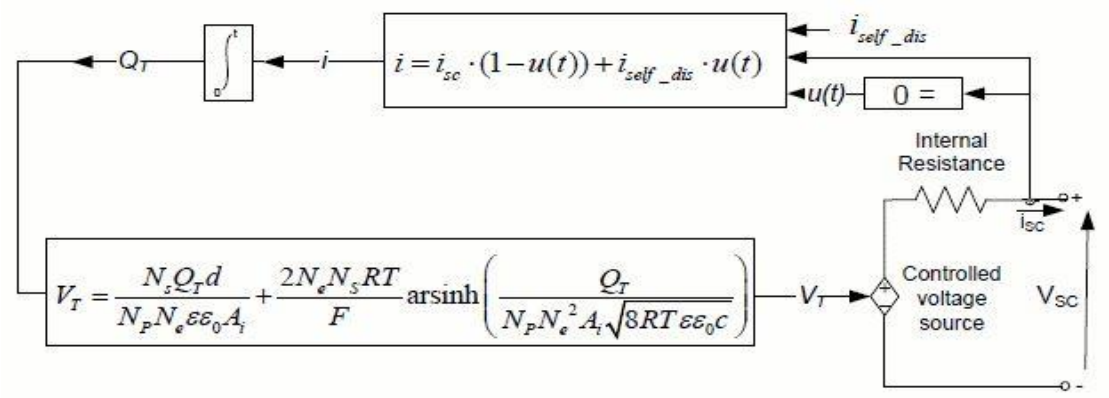

Figure 5.13 Equivalent circuit of the Simulink generic SC block

In this Simulink SC model, the SC output voltage is expressed using a Stern equation based on SC specifications and formulated as:

$$V_{SC} = \frac{N_S Q_T d}{N_p N_\varepsilon \varepsilon \varepsilon_0 A_i} + \frac{2N_\varepsilon N_s RT}{F} sinh^{-1}\left(\frac{Q_T}{N_p {N_\varepsilon}^2 A_i \sqrt{8RT\varepsilon\varepsilon_0 c}}\right) - R_{SC} i_{SC} \quad (5\text{-}8)$$

The derivation of this equation is beyond the scope of this research and hence will not be discussed further. More details of the derivation of the Stern equation for the Simulink model can be found in literature sources [5.4.9-5.4.11].

The SC model calculates the real time voltage from the source to simulate the SC performance. The SC model carries out the calculations within the block based on the parameters entered by the user and simulates the SC performance in Simulink. After

the datasheet parameters of the laboratory Maxwell SC module have been imported to this Simulink model, the SC block is capable of generating the same output as the laboratory system. The equivalent circuit of the SC has been shown in Figure 5.14.

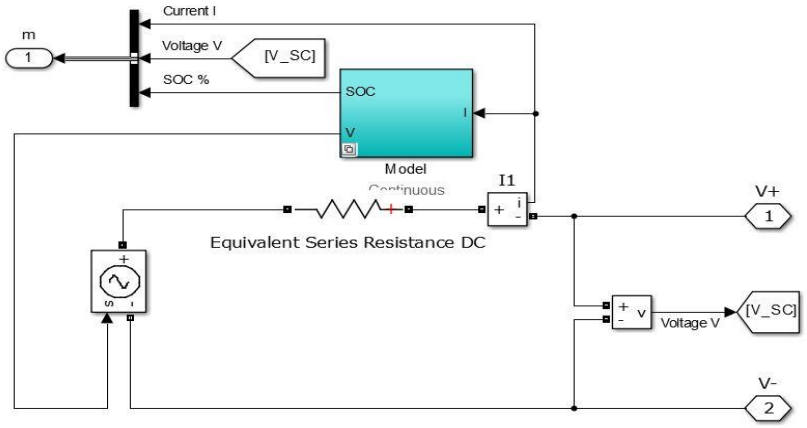

Figure 5.14 SC equivalent circuit built in Simulink

5.6.2 SC model validation

To test the Simulink SC block against the laboratory SC module, the same evaluation test was carried out. The discharge test circuit is shown in Figure 5.15.

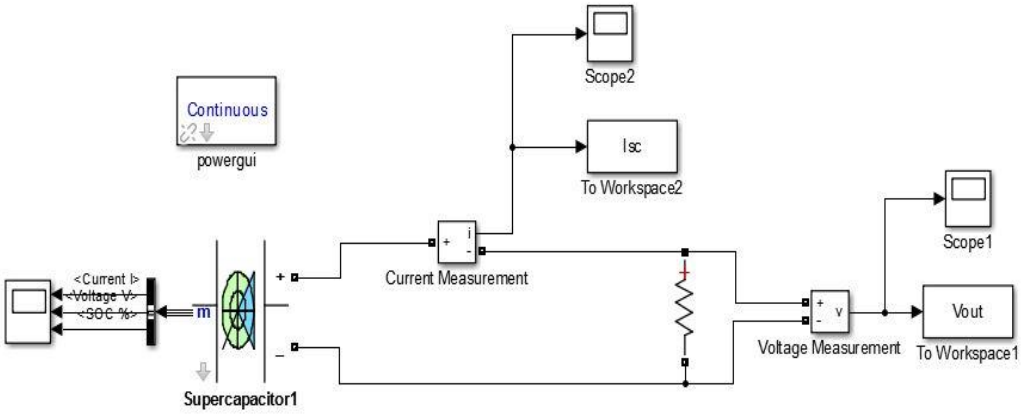

Figure 5.15 Simulink SC discharge test with resistor schematics

In the laboratory SC discharge test, the SC was discharged through a 2Ω resistor from 41 V to 6.74 V in 234 s which is approximately 73% initial SoC to 2% final SoC as discussed in section 4.8.2. After setting the Simulink SC to the same initial voltage, the same test was carried out in the Simulink model for validation. The SC voltage and current comparisons have been plotted in Figure 5.16.

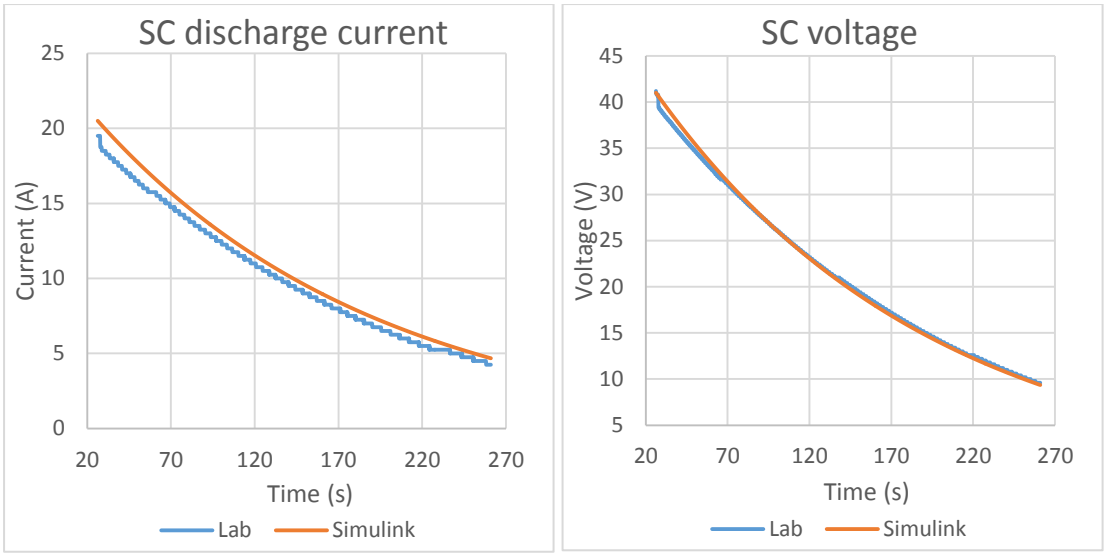

Figure 5.16 Lab/Simulink SC comparison for discharge current and voltage

As Figure 5.16 shows, the discharge voltage and current curves of the laboratory and Simulink SC are nearly identical (<2 % difference). There is some slight difference which was caused by the small difference in total resistance of the laboratory resistor, cable and contacts.

Although the SC charge test was not carried out for the laboratory systems due to lack of appropriate controlled sources, this can be carried out in Simulink. The SC can be charged with either a voltage source or a current source. The resistor bank in the discharge test has been replaced with a voltage and a current source and the initial voltage of SC has been set to 1 V. The charge characteristics have been plotted in Figure 5.17.

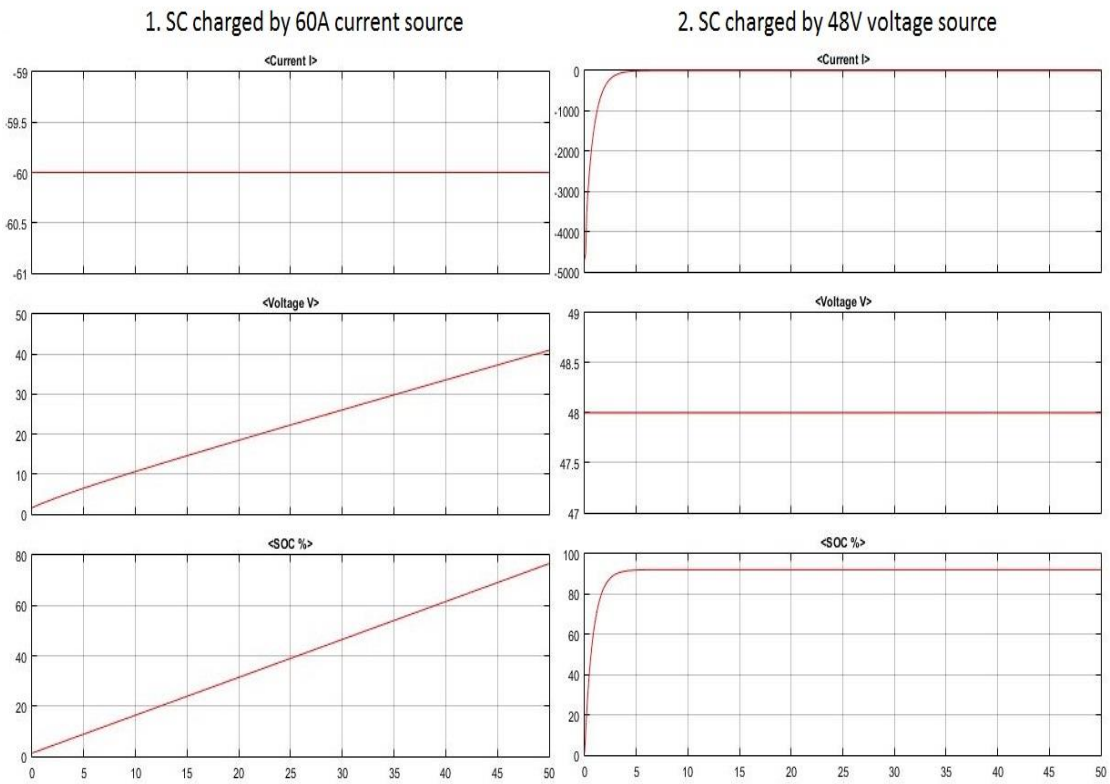

Figure 5.17 Simulink SC model charged by voltage source or current source

When the SC was charged by a 60 A current source, the current was delivered to the SC at a constant level. As a result of the constant current, the SC voltage and SoC also increased at a constant rate. When the SC was charged by a 48 V voltage source, a massive current was drawn from the source because of the large potential difference between the voltage source and the SC initial voltage. The SoC was rapidly charged and stayed at around 95% SoC (because of the SC safety setting). Although this would only occur with an unlimited source in Simulink, the SC would still try to draw the maximum current the source can provide instantly. The 48 V voltage in the figure represents the voltage applied on the SC which is why it remains constant. The actual voltage of the SC should still be proportional to the SoC. This massive current is the reason why the charge test was not carried out for the laboratory SC system.

5.7 Buck/boost converter simulation

As the SC charge test showed, it is very important to integrate a charge and discharge controller for the SC. The selected buck/boost converter for the 48 V Maxwell SC utilised an adapted H-bridge converter configuration as discussed in the laboratory system. Figure 5.18 showed a block diagram of the controlling parameter in the FC/SC hybrid system.

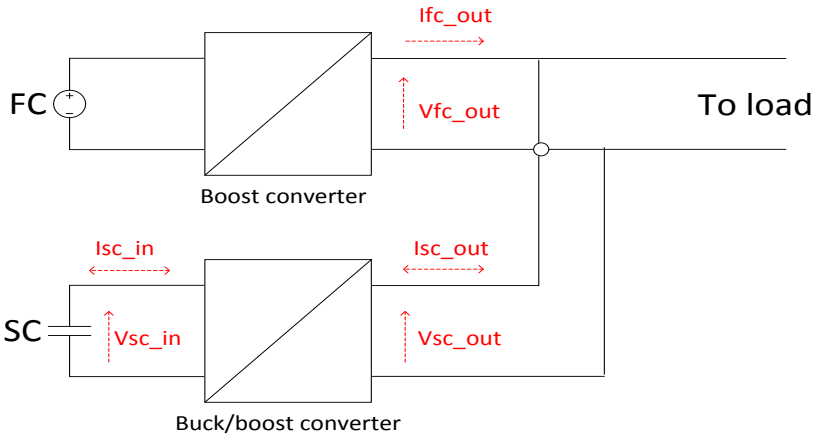

Figure 5.18 Buck/boost converter control parameter block diagram for the SC

The boost converter for the FC has been designed to provide a 48 V output (which is Vfc_out). The buck/boost converter output (Vsc_out) will also have to deliver 48 V output because of the parallel connection. Therefore the output power of the SC and buck/boost converter can be controlled by controlling the output current (Isc_out). This control mode is defined as input current control in the laboratory AEP converter datasheet, however, it will be defined as the buck/boost converter output current control hereafter on to avoid confusion.

The SC and converter have been designed to work as a dynamic energy storage system to meet the power demands of the loads. Therefore it has to be able to not only work bidirectionally but also be capable of operating in both voltage step up and step down modes. The converter for the SC has to be able to operate in four quadrants which are discharge boost, discharge buck, charge boost and charge buck.

5.7.1 Buck/boost converter discharge model

In the discharge mode, two IGBTs (S1 and S4) in the H bridge converter will be utilised to control the output as a boost converter or buck converter. The Simulink model of the discharge configurations is shown in Figure 5.19.

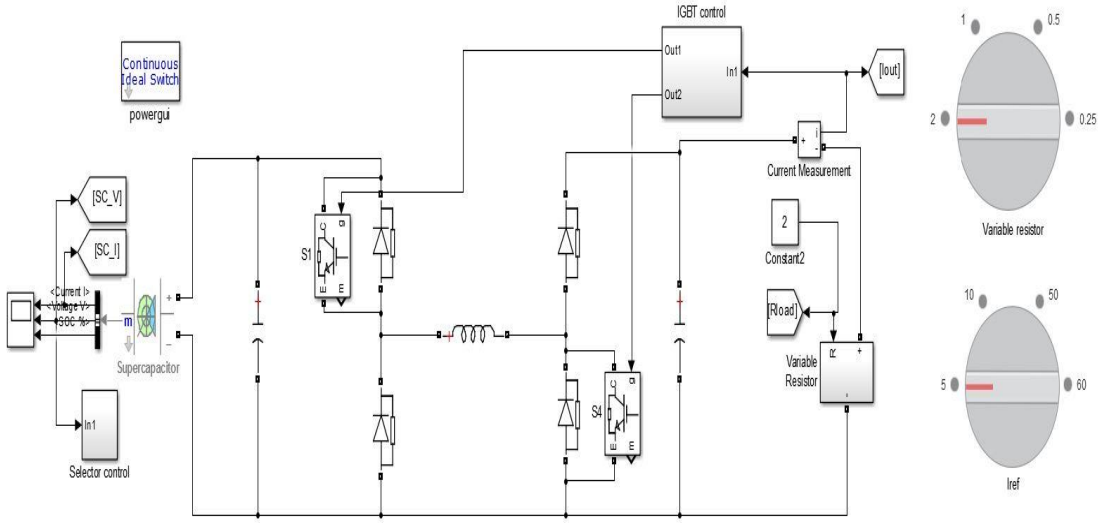

Figure 5.19 H bridge converter discharge configuration Simulink model

To test the simulation model against the laboratory converter, a variable resistor has been connected as the load for the converter controlled by a rotary switch. A selector signal has been used to choose between boost mode and buck mode depending on the voltage and resistance. The IGBT signal control has been integrated as a sub-system block and shown in Figure 5.20.

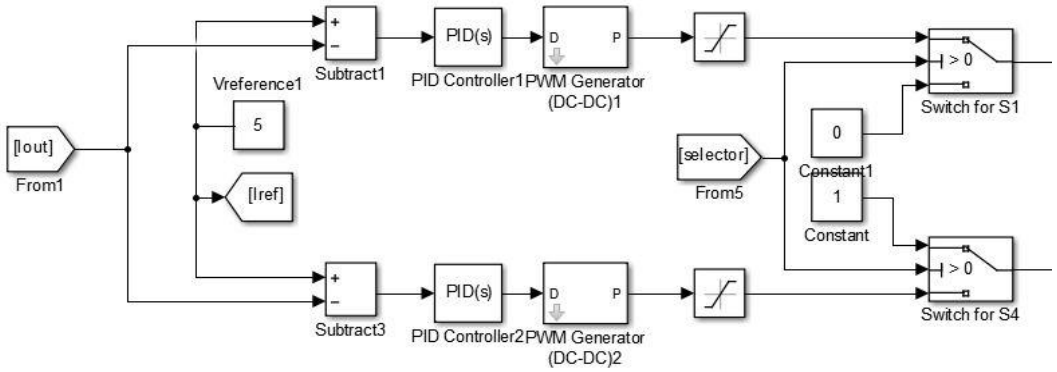

Figure 5.20 Simulink IGBT block for H bridge converter discharge configuration

In the IGBT control block, the output current (from the buck/boost converter) will be fed to a feedback loop to calculate the error between the actual current and the reference value. The error will be the input to a PID controller and a PWM generator to generate the duty cycle for the switches.

5.7.2 Buck/boost converter discharge model validation

The laboratory discharge validation test for the SC converter was carried out by supplying a controlled 5 A discharge current to a 10 ohm resistor as discussed in section 4.8.3. In the test, the SC started at 32 V initial voltage which means the output current would be 3.2 A at this resistive load. Hence the output current from the buck/boost converter has to be boosted to attain a 5 A discharge current. After setting the Simulink model to the same experiment environment as the laboratory system, the discharge test results have been plotted and compared in Figure 5.21.

Laboratory test bench **Simulink model**

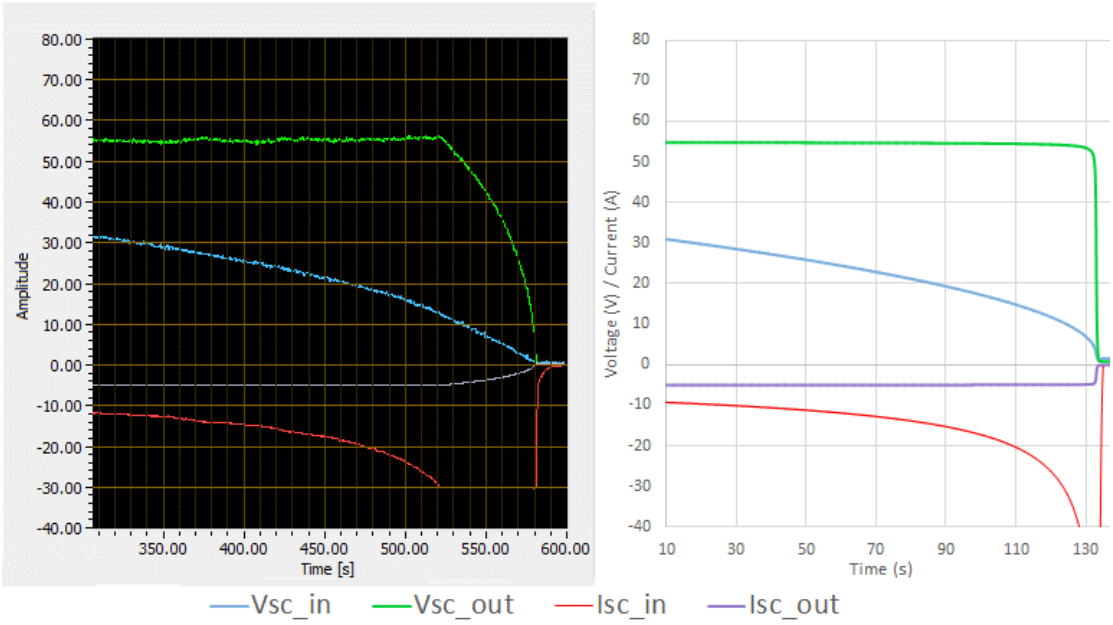

Figure 5.21 Buck/boost converter discharge validation test

The plot from the AEP converter software does not allow export of the plotting data, so it can only be displayed in separate graphs. The Simulink converter plots show reasonably the same curves with two exceptions. The first is the SC current (Isc_in) difference (red line). In the laboratory experiment, the current has been limited to 30 A for safety reasons. There is no need for a current limit for the Simulink buck/boost converter. Therefore the laboratory converter current stopped increasing at 30 A while the Simulink converter increased to 120 A (not shown in Figure 5.21 to keep the scale the same). The second difference is the Simulink SC completely dissipated in approximately 130 s while the laboratory SC dissipated in around 250 s with the same experimental settings. The reason for this is because the SC was discharged at a 30 A current in the laboratory system while the Simulink SC was discharged with a much higher current, hence dissipated quicker.

Additional simulations have also been carried out to test the performance of the model under higher power and also test the converter under buck operation. This was not an option due to lack of appropriate laboratory equipment for the laboratory system. In the simulation, the output current reference has been selected to be 60 A and the SC (and buck/boost converter) has been connected to four different levels of resistance. These are 0.25 ohm, 0.5 ohm, 1 ohm and 2 ohm. Since the initial SC voltage has been selected to be 48 V, so the output current without the converter would be 192 A (buck), 96 A (buck), 48 A (boost) and 24 A (boost). Hence, this experiment can test both the boost mode and buck mode and check if the converter is capable of automatically switching modes. The current and voltage results have been plotted on Figure 5.22 and 5.23.

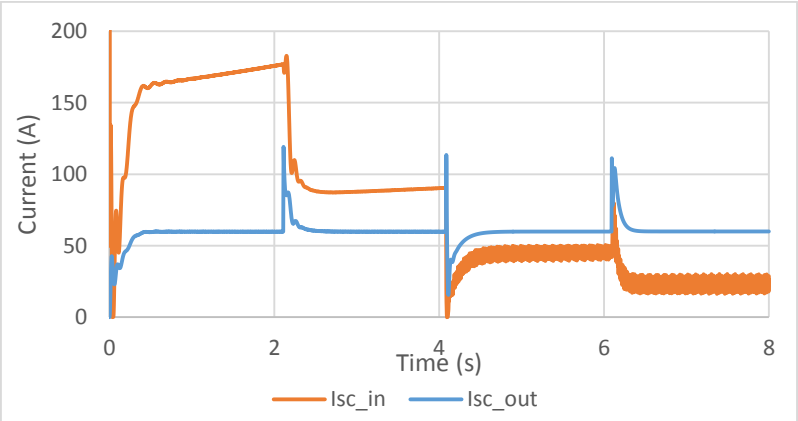

Figure 5.22 Input and output current of buck/boost converter discharge test

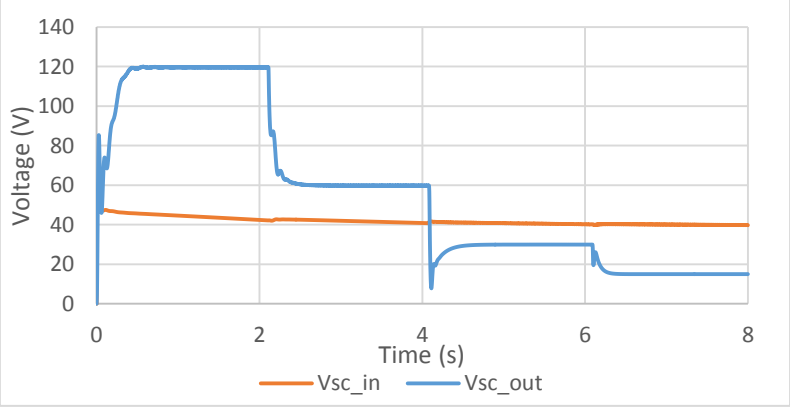

Figure 5.23 Input and output voltage of buck/boost converter discharge test

As Figure 5.22 shows, the output current has been kept at 60 A while the output load is changing. The Simulink converter worked in buck mode for the first two step changes and then switched to boost mode for the final two step changes.

5.7.3 Buck/boost converter charge model

The charge configuration for an H bridge converter is similar to the discharge configuration except it uses two different IGBTs (S2 and S3). The charge configuration for Simulink has been shown in Figure 5.24.

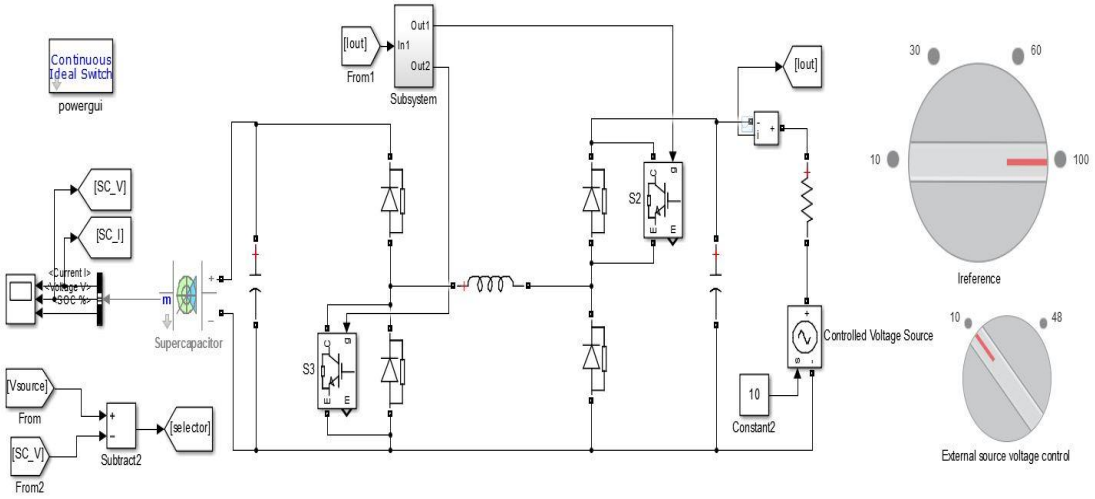

Figure 5.24 H bridge converter charge configuration Simulink model

To test the SC and buck/boost converter under charge operation, an external DC voltage source has been integrated to replace the variable resistor. A selector has been used to determine the operation mode (boost or buck) by comparing the input and output voltage. The IGBTs are also controlled in a separate sub-system and shown in Figure 5.25.

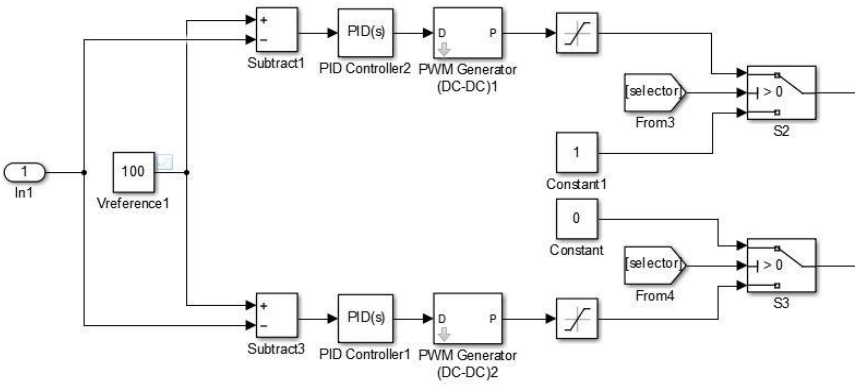

Figure 5.25 Simulink IGBT block for H bridge converter charge configuration

The IGBT controls use the same concept as the discharge IGBT controls where an error signal has been sent to the PID controller and PWM generator for a real time controlled duty cycle.

5.7.4 Buck/boost converter charge mode validation

In the laboratory charge validation test, a constant 5 A current from an external 36 V source has been used to charge the SC. The aim is to use the controlled 5 A current to charge the SC from 0 V initial voltage to approximately 32 V. After setting the Simulink converter to the same experimental environment, the results have been compared and plotted in Figure 5.26.

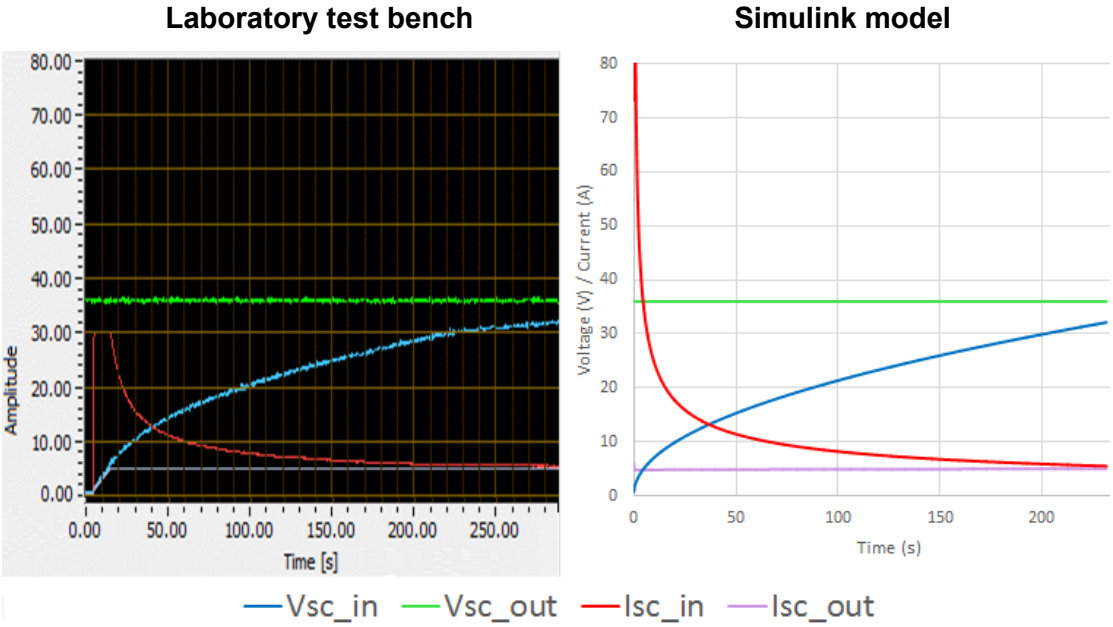

Figure 5.26 Buck/boost converter charge validation test

As the comparison results show, the Simulink converter model provides the same curves as the laboratory converter. The current from SC (Isc_in) also was much higher at the beginning because there is no current limit in the computer model. The charge test in the laboratory system takes around 290 s to charge from 0-32 V while it takes 240 s in the Simulink model. This is caused by the initial larger charging current and converter efficiency difference.

Additional higher power simulations have also been carried out for the charge configuration to test the converter in both boost and buck operations. The simulation procedure has been summarised in two steps.

1. Apply a 10 V source to charge the SC (20 V initial voltage) to test the boost mode. Once boost mode is activated, change the output current reference to four different levels: 10 A, 30 A, 60 A and 100 A.
2. Replace the 10 V source with a 48 V source to charge the SC to test the buck mode. Once the converter switches to buck mode, change the output current

reference to the same four steps in reverse order: 100 A, 60 A, 30 A and 10 A. Results from the two steps have been plotted in Figures 5.27 and 5.28.

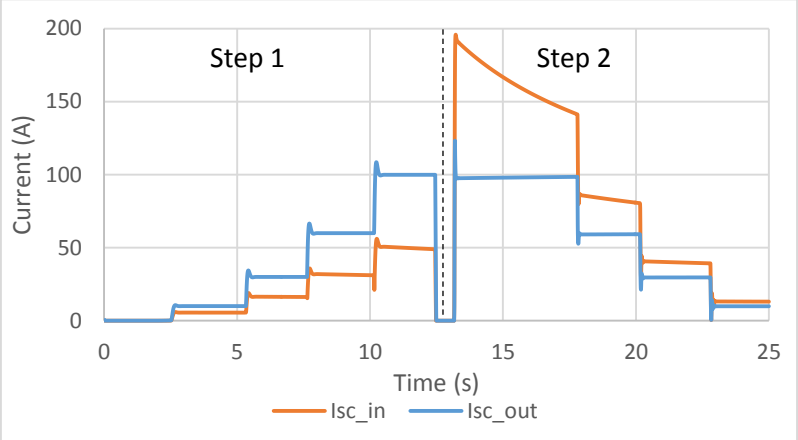

Figure 5.27 Input and output current of buck/boost converter charge test

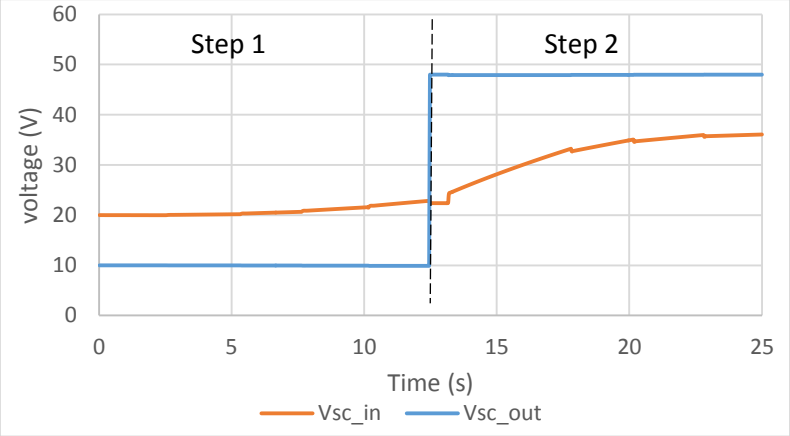

Figure 5.28 Input and output voltage of buck/boost converter charge test

As the current plot shows, the current from the source has been controlled to the four steps as expected. The model also showed it is capable of automatically switching from boost mode to buck mode. The voltage plot showed the SC has been charged much faster when the charging current is 100 A.

5.7.5 Buck/boost converter full bridge model

So far the Simulink H bridge converter has been tested in discharge and charge configurations. In the full H bridge converter, all four IGBTs will be integrated in the circuit and the Simulink full bridge converter has been shown in Figure 5.29.

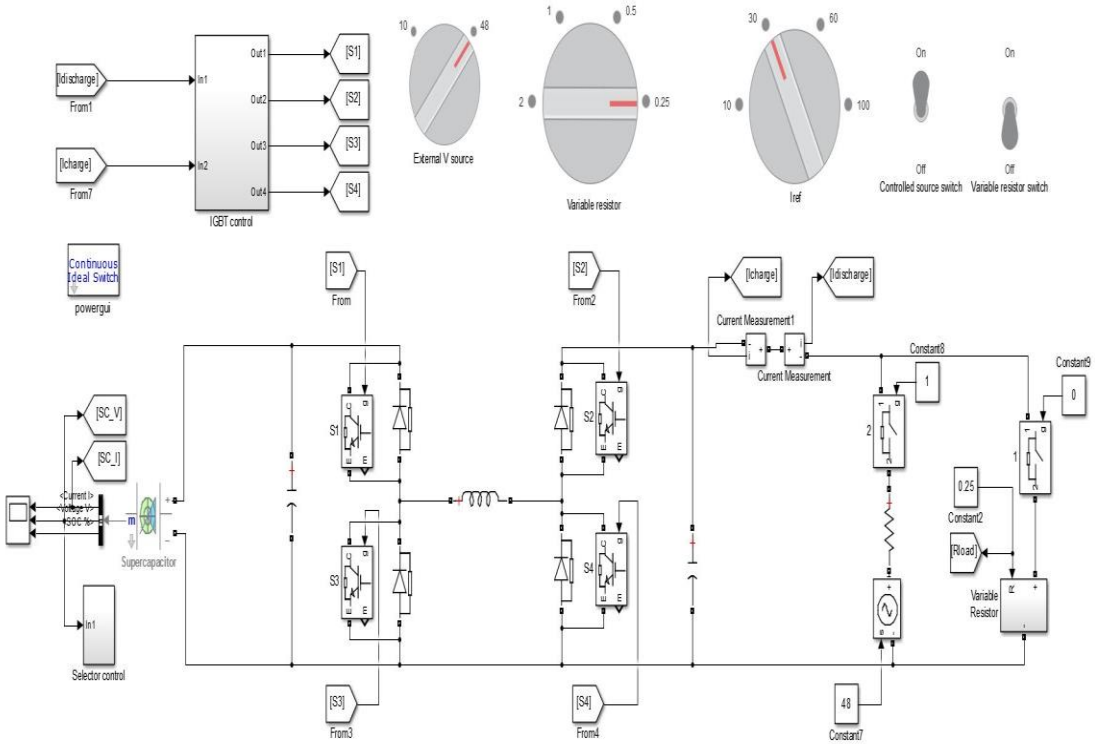

Figure 5.29 Simulink model of the H full bridge converter configuration

In the full bridge configuration, apart from the boost/buck selectors, another charge/discharge selector has also been used to determine whether the converter is to be operated in charge configurations or discharge configuration. This charge/discharge selector has been achieved by measuring the charging current and discharging current in real time. When the charging current is positive, the selector will choose the charge configuration and then go through another selector to determine if it is either boost or buck operation and vice versa for the discharge mode.

In the Simulink full bridge converter test, the output current (Isc_out) has been set to be a constant 60 A reference current while engaging all four quadrant operations (discharge buck, discharge boost, charge buck and charge boost). In the test, the resistor bank would have to be replaced with an external source in the middle of the simulation and the SC SoC also needs to be changed. The resistor bank, source and SoC have been set up to match all four modes in the full bridge configuration. The current and voltage results have been plotted in Figures 5.30 and 5.31.

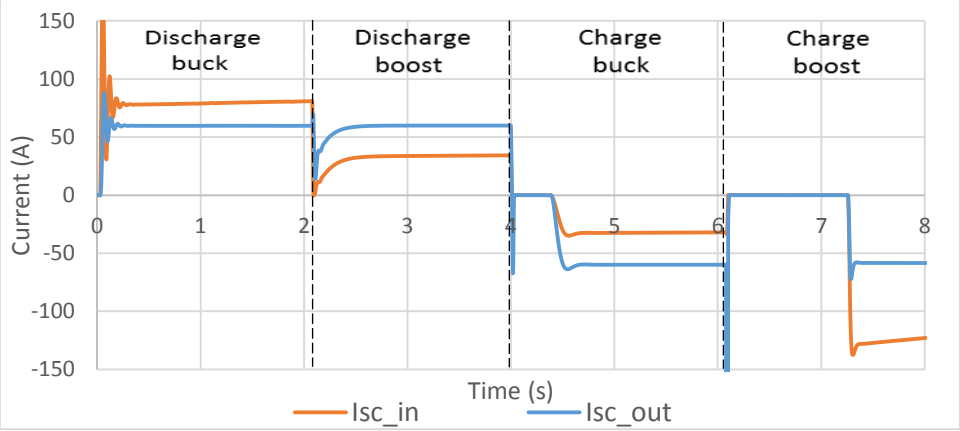

Figure 5.30 Input and output current for four quadrant operations

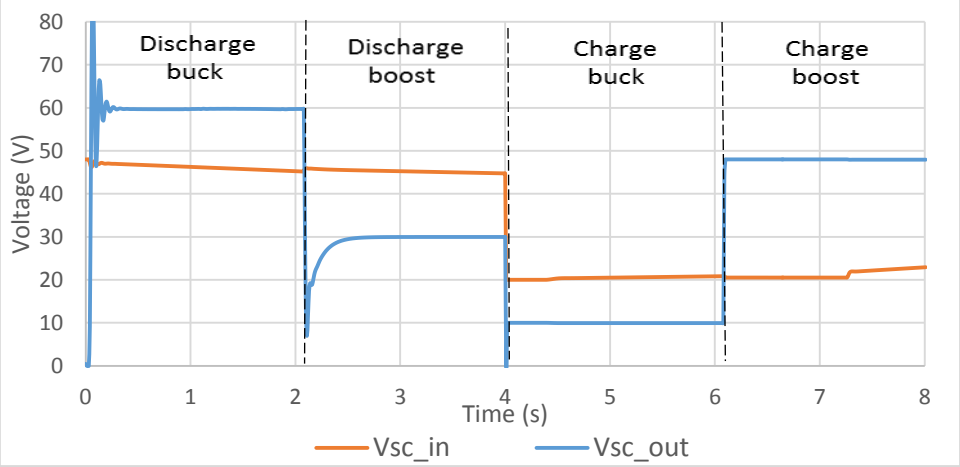

Figure 5.31 Input and output voltage for four quadrant operations

As the current and voltage results show, the discharge and charge currents have been kept at the required 60 A as expected. The converter is capable of operating in four quadrants. One point that has been observed is the charge boost operation takes slightly longer to adjust to the requested current than the other three modes. This is caused by the PID controller taking longer to tune when switching operation modes.

5.8 FC hybrid model integration

5.8.1 FC/SC hybrid model

Following the simulation of the sub systems, the next task is to integrate the systems to the FC hybrid model representing a scaled FC hybrid bus system.

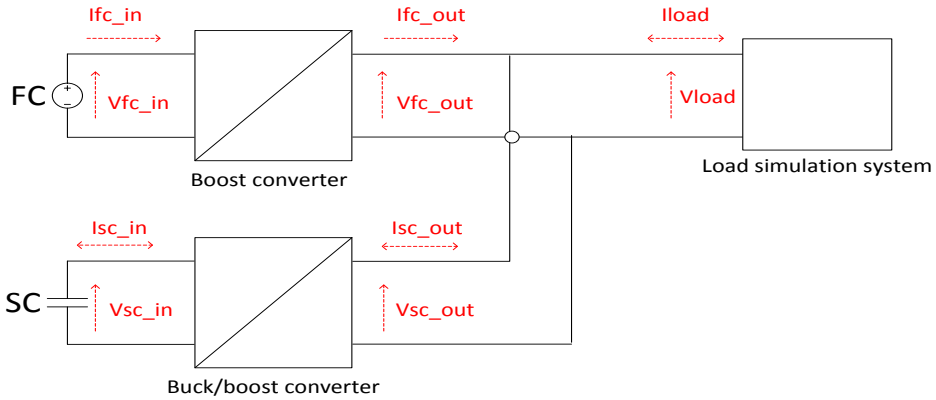

Figure 5.32 FC hybrid model controlling parameters

As Figure 5.32 shows, the boost converter for the FC will maintain a constant 48 V output (Vfc_out) as the overall bus bar voltage for the hybrid system. The buck/boost converter for the SC has been designed to control the output current (Isc_out) based on user commands. Therefore, because of the parallel structure, a relationship between the three currents can be formulated as:

$$Ifc_{out} + Isc_{out} = Iload \tag{5-8}$$

Based on this relationship, a hybrid control system focusing on current balancing can be determined for bus operations. Three main kinds of operation modes are expected to occur during bus operations. The three operation modes and their current flows have been shown in Figure 5.33.

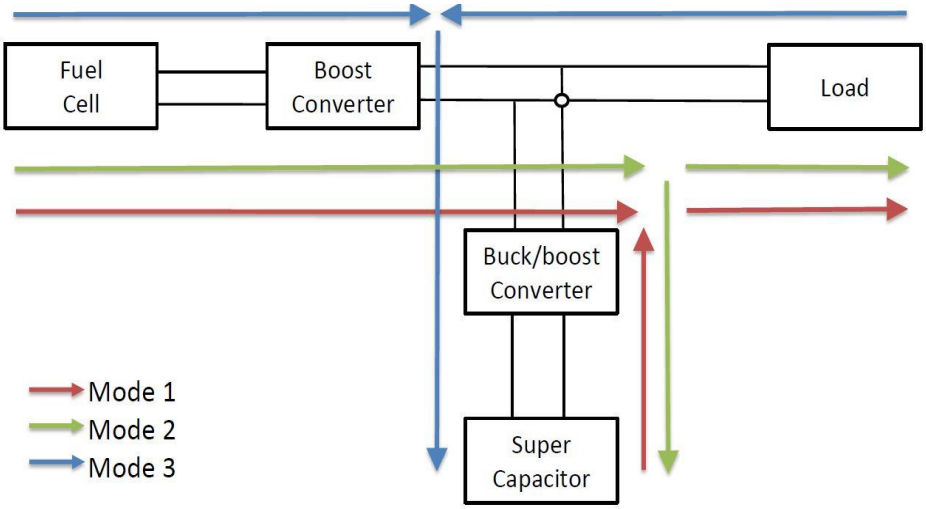

Figure 5.33 FC hybrid bus model operation modes and power flows

- Mode 1 (red): The SC will discharge to supplement the FC for a transient higher output. This type of operation is expected to occur during accelerating, climbing hills or under heavy load.
- Mode 2 (green): The FC will power the load and use excess power to charge the SC. This is expected to occur when the FC is providing more power than the load required.
- Mode 3 (blue): The power from the FC and generated power from regenerative braking will both be used to charge the SC. This is only expected to occur when the bus is in regenerative brake mode.

5.8.2 FC/SC hybrid model validation

Static test validation

Experiments have been carried out to test the proposed current control strategy for the three operation modes and provide validation for the integrated hybrid system. As stated in section 4.8.3, the control of the buck/boost converter has been carried out by the PowerPanel software which requires the user to manually input the user requested output current. Hence a static test has been carried out first. The experiment parameters are shown in table 5.1.

Table 5.1 FC hybrid system validation test parameters

Operation mode	1	2	3
FC and boost converter output current (Ifc_out)	44.5 A	24.4 A	7 A
SC and buck/boost converter output current (Isc_out)	14.5 A (charge)	-5.6 A (discharge)	13.86 A (charge)
Load current (Iload)	30 A	30 A	-6.86 A

The amount of current in the table was selected with consideration to the laboratory equipment capability. The current balancing between FC, SC and load is also expected to satisfy equation 5-8. The positive load current indicates the load is drawing a current from the FC/SC hybrid model. This was achieved by using a controlled resistor bank. The negative load current indicates the load is supplying a current to the FC/SC hybrid model. This was achieved by using external battery. Three experiments have been carried to test the operation modes.

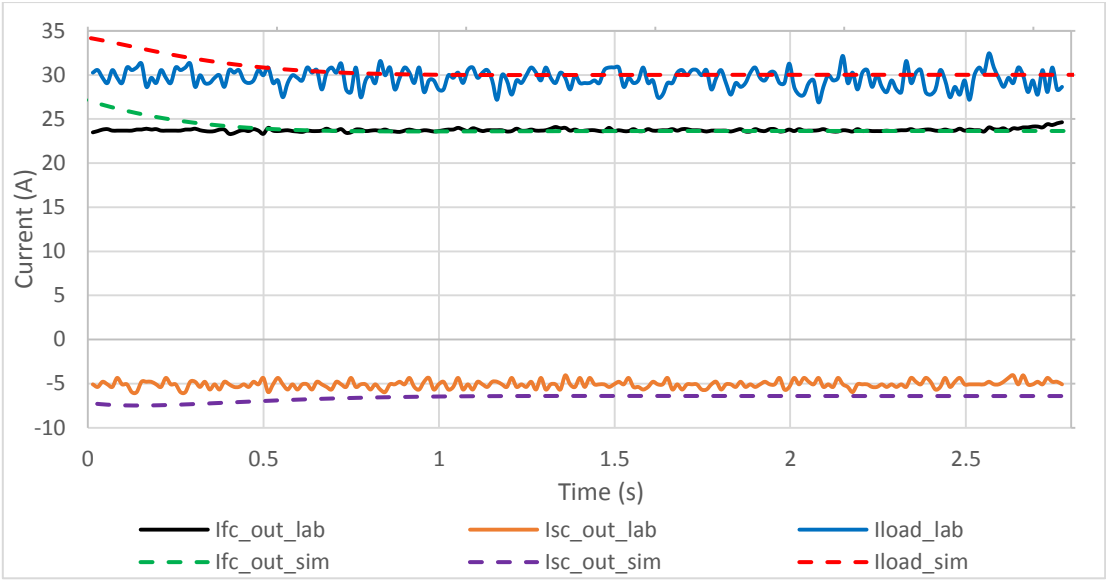

Figure 5.34 FC hybrid lab and computer model validation for mode 1

In the mode 1 operation, the load current 30 A was delivered by the combined current of 24.4 A FC (and boost converter) output and 5.6 A SC (and buck/boost converter) discharge current. In the Figure 5.34, the solid line indicates the results obtained from laboratory system while the dashed ones indicate the computer simulated results. The plot shows the buck/boost converter managed to maintain the load current at the requested 30 A in both laboratory and computer system. The SC discharges the expected current to meet the higher current load demand with the FC. The results from the laboratory and computer showed reasonably close performance in terms of the current balancing. The noise in the laboratory system and slight offsets are caused by the quality of the current transducer in laboratory system.

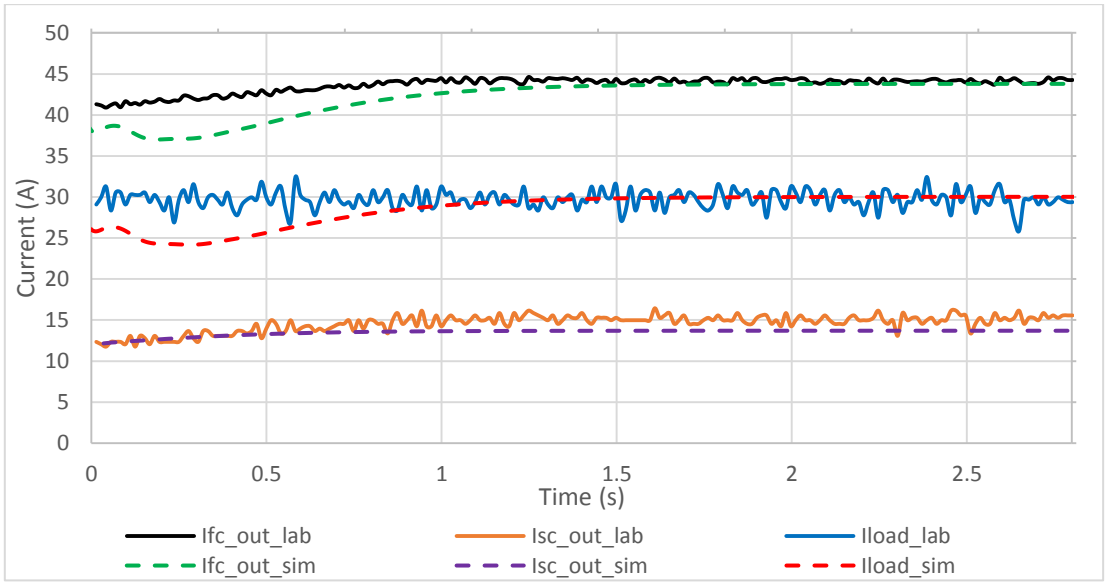

Figure 5.35 FC hybrid lab and computer model validation for mode 2

In the mode 2 operation, the FC (and boost converter) provides a 44.5 A current to both power the 30 A load and charge the SC (and buck/boost converter) with 14.5 A. The results have been plotted in Figure 5.35. As the results showed, the laboratory obtained results also reasonably match the computer simulated results. Additionally, the mode 2 test was carried out right after mode 1. The controller also showed it is capable of switching between different operation modes. The FC simply adjusts its output to meet the balance between load demand and user defined SC output because FC is a passive reactive power source.

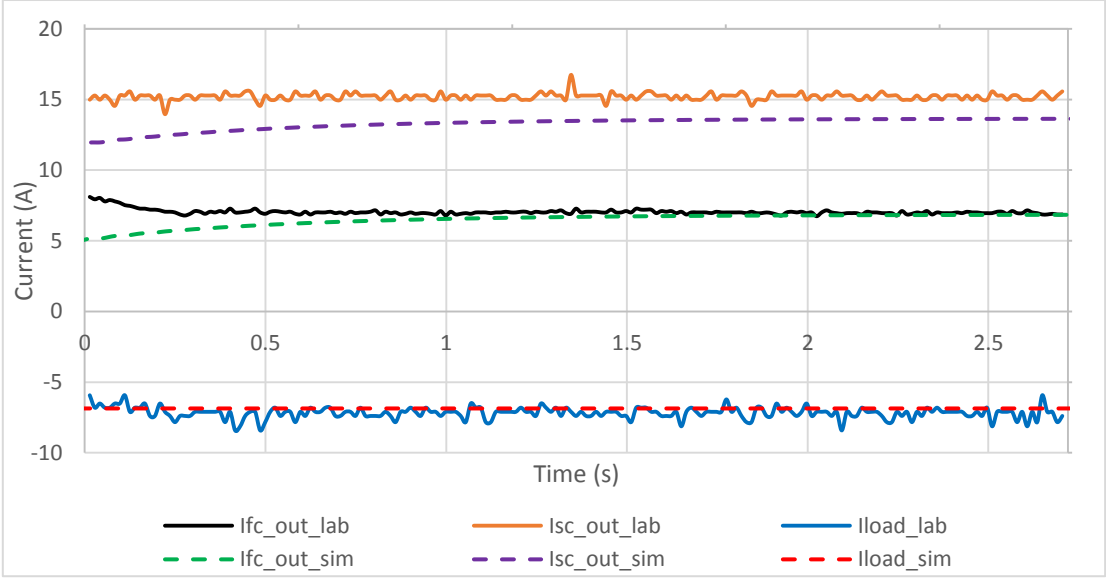

Figure 5.36 FC hybrid lab and computer model validation for mode 3

In the mode 3 operation, the SC (and buck/boost converter) has been charged by a total current of 13.86 A jointly supplied by the 7 A output from FC (and boost converter) and the generated current of 6.86 A simulated from regenerative brake. As Figure 5.36 shows, the laboratory and computer results match and functioned as expected. It can be seen the current controller functioned as expected for all three operation modes.

Hybrid control strategy

The static tests validated the integrated hybrid computer model against the laboratory system. Additionally, the tests showed that the proposed current control strategy is capable of manging the power between FC, SC and the load. In the static test, the FC has been used to balance the power gaps between the load power and the SC output power. As discussed before, the current relationship has been identified as:

$$Ifc_{out} + Isc_{out} = I_{load} \tag{5-9}$$

In the current relationship, the load current is been defined by the power profile. The SC output current is been defined by the user via the software. If a power profile has been applied on the FC hybrid control system, the FC would react to the calculated

load current demand minus/plus the SC output current. However, this is the opposite of the design concept of the FC hybrid system. The original idea is to control and keep the FC output as stable as possible to avoid too many transient power variations which could potentially damage the FC and reduce the overall FC efficiency. The FC hybrid control system would have to be modified to meet this controlled FC output requirement.

The proposed strategy is to assign a user defined reference value Ifc_{ref} representing the required FC and boost converter output current. Then use the buck/boost converter to meet the demand calculated as:

$$Isc_{out} = I_{load} - Ifc_{ref} \tag{5-10}$$

In the equation, the SC output current is reduced by the reference value. In this case, the current from the SC and buck/boost converter always have a gap in meeting the load demand. This power demand gap can only be meet by the FC and boost converter output. The SC output current can meet the load profile only if the FC output current is the same as the reference value. The equation (5-10) can be substituted into (5-9) as:

$$Ifc_{out} + I_{load} - Ifc_{ref} = I_{load}$$

$$Ifc_{out} = Ifc_{ref} \tag{5-11}$$

As a result, the SC and buck/boost converter output would be constantly adjusting to match the load demands ensuring the FC and boost converter output is controlled as the reference value. This hybrid control system not only keeps the FC output controlled but also takes the advantage of the high power density of the SC systems.

Dynamic test validation

To test the modified current control strategy, a simple dynamic test has been carried out to validate the model and evaluate the controller. In the laboratory test bench, a CAN RS232 connection has been integrated to control the output current from the buck/boost converter for the SC. LabVIEW software, which is an integrated development environment for building measurement and control systems, has been used to assign a current signal to the buck/boost converter. The current signal will be defined by the difference between the user defined FC output current and the load current.

To test the control strategy, a dynamic load needs to be applied to the hybrid model. However, due to lack of laboratory equipment, only a low power dynamic test can be carried out for validation. In the test, the FC output current has been set at a constant

10 A while applying dynamic load to the FC hybrid model. The current balancing between the sources of laboratory system and computer model are plotted in Figures 5.37 and 5.38.

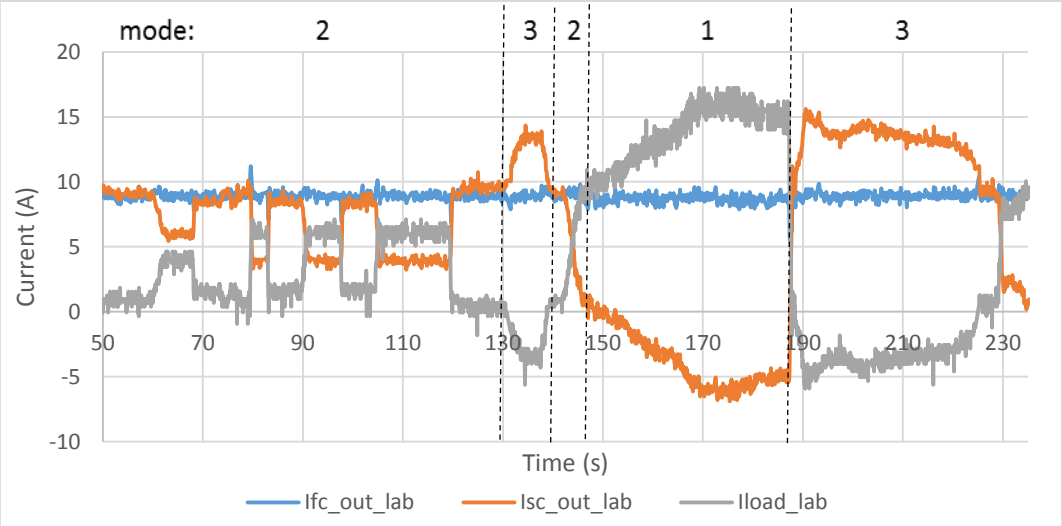

Figure 5.37 Current balancing under dynamic load for lab system

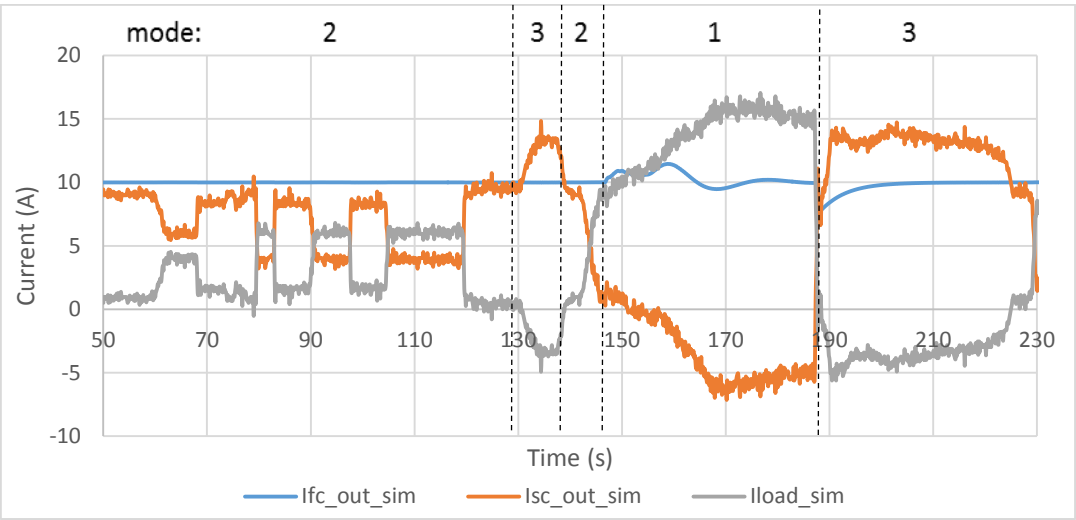

Figure 5.38 Current balancing under dynamic load for computer model

As Figure 5.37 and 5.38 show, both laboratory system and computer model managed to keep the FC output constant at 10 A while using the SC to meet the variation in load demand. The 10 A FC output was used to both power the load and charge the SC from 50 to 130 s and 140 to 148 s which is mode 2 operation in the static test. The SC was discharged to supplement the 10 A FC output to provide a higher load output between 148 s and 188 s which is mode 1 operation. The 10 A FC output and negative load current were both used to charge the SC from 130 to 140 s and 188 to 224 s which is mode 3 operation. The modified control strategy showed it is capable of operating in all three modes as well as with dynamic load. The current change of each parameter has also been separately plotted for clearer presentation of the validations as shown

in Figures 5.39-5.41.

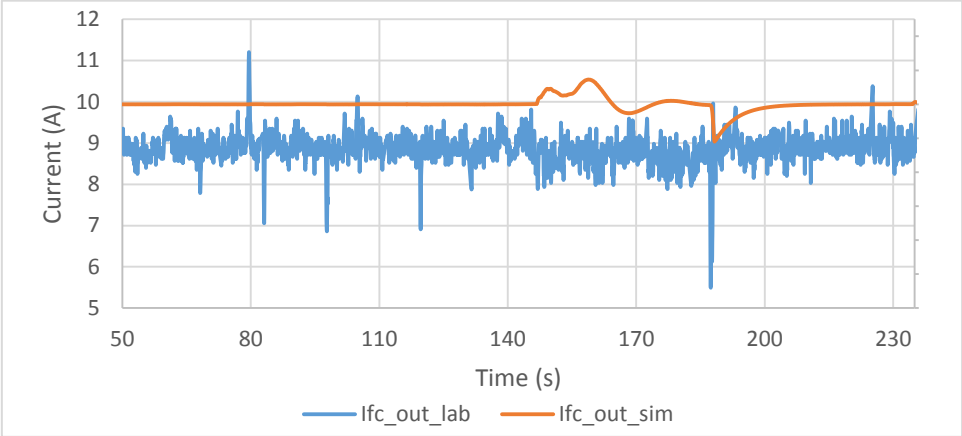

Figure 5.39 Validation of FC output current under dynamic load

The FC output current of the laboratory system showed more noise because of the current transducer quality. The current of the laboratory system is generally 1 A lower than the requested 10 A current. This is caused by the discrepancy in the current transducer. There are also some transient changes on the FC output current for both laboratory system and computer model. These are caused by the PID controller re-tuning the output current to the requested 10 A under large load changes.

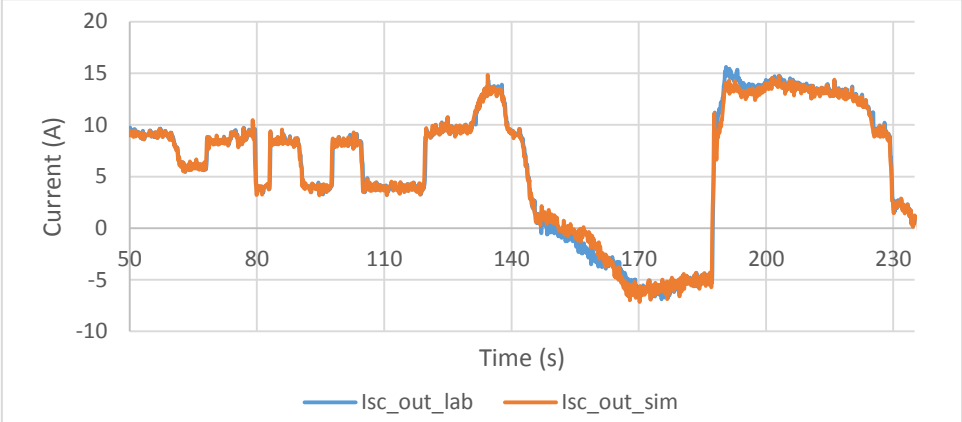

Figure 5.40 Validation of SC output current under dynamic load

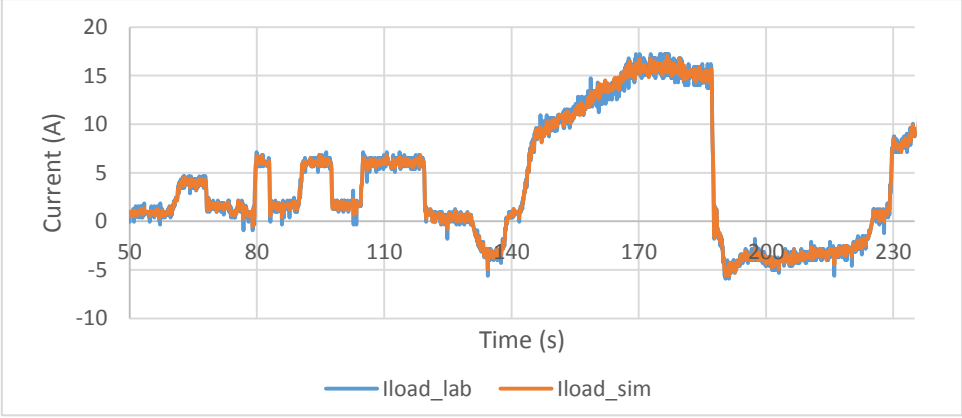

Figure 5.41 Validation of load current under dynamic load

The buck/boost converter output current and load current showed nearly identical results for laboratory system and computer model. Therefore it can be concluded the computer model can effectively represent the laboratory system in both static load and dynamic load simulation. The modified current control strategy also managed to keep the FC output constant under dynamic load as requested.

5.9 Discussion on modelling justification

This chapter concluded the development of the main components in the scaled FC hybrid system for both laboratory and computer model. A current control strategy has been proposed and tested with static and dynamic experiments. The control strategy has been designed to keep the FC output constant while using the SC to supplement the additional power demand. The control strategy has been shown to work as expected in both laboratory system and computer model. The computer model has been validated to be able to effectively represent the actual laboratory system.

The model validated in this chapter can be used to investigate the following points:

1. Scale up the computer model to represent a full scale bus.
2. Evaluate the hybrid control system by using actual driving cycles.
3. Investigate the effect of degree of hybridisation between FC and SC in the hybrid system.
4. Test the hybrid model with a downsized FC design and evaluate the feasibility of this design under actual driving cycles.
5. Identify the optimisation strategy of the FC hybrid system for bus applications.

5.10 Summary

This chapter describes the performance tool constructed to conduct simulation based on the laboratory system design. The simulation models have been developed based on mathematical models within Simulink. To ensure the computer model can sufficiently represent the installed laboratory model, both systems from laboratory and computer have been validated against each other using the same experiment configurations. It was concluded that each model is suitable for use in this research and capable of accurately representing the practical FC and SC systems. Additional simulation in the computer model have also been carried out to extend the understanding which was limited in the laboratory environment due to lack of higher power equipment. The simulated individual systems have been integrated and tested in both laboratory and computer model. A hybrid controller for controlling the power flows has also been proposed and tested and showed good capability of managing the power balance between the FC and the SC sources. Further research methods have been identified to investigate the research question which leads to hybrid system optimisation in the Chapter 6.

Chapter 6 System optimisation

6.1 Introduction

Following the construction, simulation and validation of the FC hybrid model, this chapter will analyse the developed system and investigate the research question as formulated in Chapter 3. The chapter is divided into the following five sections.

1. Section one scales up the computer model and uses it to represent a full scale bus and evaluates the proposed control strategy against data recorded from actual driving cycles.
2. Section two presents a series of simulations using different degrees of hybridisation to investigate how the degree of hybridisation would affect system performance.
3. Section three investigates the methods to identify the appropriate degree of hybridisation between FC and SC for a certain driving cycle.
4. Section four explores the methods to optimise the identified degree of hybridisation for a certain driving cycle.
5. Section five presents the key arguments for identifying and optimising the FC/SC degree of hybridisation for bus use based on the results of the previous investigations.

6.2 Full scale FC/SC hybrid model

The previous chapters developed a software model of a scaled FC/SC hybrid propulsion chain using the laboratory power train to validate the software model. The proposed current control strategy showed how the FC interacts together with the SC to satisfy the total power demand. The FC hybrid model was tested with static tests and simple dynamic tests. The model and control strategy will be tested with more complex dynamic driving cycles. To evaluate the FC/SC hybrid system performance in a realistic dynamic environment, actual driving cycles will need to be applied on the model. Since it is beyond the scope of the HyFCap project to develop a full scale laboratory system, the research hereafter will be carried out utilising computer modelling.

6.2.1 FC/SC hybrid model scaling

Since the power level of the actual power profile recorded from the bus are full scale power, the components in the scaled model developed could not be representative of the full power profile. The FC/SC hybrid model would need to be scaled up to the power level of a full sized system. The computer model has been scaled up for use in analysing the performance of the power system against actual bus data. There are three main components that require scaling up to meet the power requirement: the FC as primary power source, the SC as energy storage and the busbar voltage for bus application.

The FC used in the scaled computer model was an 8.5 kW PEMFC. The full scale FC was selected to be an existing FC, Ballard FCvelocity 85 kW PEMFC. The 85 kW FC can be simulated in Simulink based on the manufacture's specifications. The 85 kW FC has an operating voltage of 280-420 V which will consequently affect the output current as well. It has been noted that scaling the FC system will affect the fuel consumption, efficiency and losses since the performance curves of this FC system were not provided. The accurate fuel consumption, efficiency and losses can be worked out by using the energy delivered from the FC throughout the driving cycle. This would require the full scale model to be validated which can be carried out as future work. However, this is expected to have small impact on the research as this research is more focused on the performance in terms of the balance of power. The power demanded from the FC will not be impacted by the scaling of the FC. As a result, the scaling of the FC was made based on the rated power. Additionally, the Ballard FCvelocity is one of the most widely used the off shelf FC for transportation applications. The design Specifications of the Ballard FCvelocity 85 kW PEMFC can be found in Appendix N.

The SC used in the scaled computer model was a 48 V, 83 F Maxwell SC. The SC was selected due to laboratory equipment availability and to meet the 48 V busbar voltage of the FC/SC hybrid propulsion chain. The scaling of the SC for the full scale bus model requires the SC energy capacity to be properly sized as well. However, it is unclear what the energy capacity requirements will be for the bus application. As a result, the SC will be initially scaled up using multiple units of the same 48 V Maxwell SC unit. Considering the high voltage of the FC, ten SCs were first connected in series to provide the 480V output voltage. As a result of series connection, the total capacitance would be 8.3F which has a stored energy of:

$$Stored\ energy = 0.5 \times 8.3F \times 480^2 \div 3600s = 0.2656\ kWh$$

The calculated stored energy indicates the SC is capable of releasing 0.2656 kW for 3600 s or releasing 100 kW for 9.56 s. It can be seen the initial SC energy capacity is not sufficient for a double decker London bus which can require a peak power of 200 kW. As a result, the SC size has been increased further (by series connecting more SC units) to maintain the capacitance of 83 F but with an output of 480 V. The maximum stored energy of the full scale sized SC can be calculated as:

$$Stored\ energy = 0.5 \times 83F \times 480^2 \div 3600s = 2.656\ kWh$$

The scaled model utilised 48 V as the busbar voltage of the hybrid system as a safety requirement. Such a voltage level is too low to power a practical bus system. Since the bus UCL used for data logging operates with a busbar voltage of 630 V, the same busbar voltage will be used for the full scale bus model. The boost converter for the full scale 85 kW FC has therefore been scaled to produce a 630 V.

Table 6.1 Scale and full scale FC/SC hybrid model specification

	Scale	**Full scale**
PEMFC		
Model	Hydrogenics HD8	Ballard FCvelocity
Rated power	8.5 kW	85 kW
Operating current	0-380 A	0-288 A
Operating voltage	20-40 V	280-420 V
SC		
Model	Maxwell P048 B01	Maxwell P048 B01
Number of SC unit	1	100
Total capacitance	83 F	83 F
Rated voltage	48 V	480 V
Stored energy	0.0265 kWh	2.65 kWh
Hybrid system		
Bus bar voltage	48 V	630 V

A summary of scaling information of the laboratory and scaled up computer model has been provided in Table 6.1. The full scale bus model was not scaled with a straight scale, the scaling was only made as an initial estimation. The purpose of scaling up the computer model is to analyse the performance of the power system against actual bus profile data. The models discussed hereafter will be the full scale computer model.

6.2.2 Practical bus profile simulation

Driving cycle collection

A bus in normal service was used to collect the driving cycles for this research as part of the HyFCap project. The bus driving cycle data was collected from a bus operating in Central London on Route 388. The bus is an Enviro 400H double decker diesel engine / lithium battery series hybrid bus that is part of the London hybrid bus fleet. Although RV1 was selected as the template to develop the models for this research, the driving cycle data of RV1 was not available due to commercial confidentiality. Additionally, RV1 is a specialised route with less gradient changes for the single decker RV1 FC bus. The use of driving cycle data from a typical London double decker bus can further test the performance of the FC/SC hybrid system and explore the practicality of diesel hybrid double decker bus replacement.

The bus data was recorded by BAE loggers as part of the HyFCap project. The data was logged under various scenarios (daily service, no passenger operation, heavy/light traffic operation, high gradient route etc.). The logged data includes parameters such as vehicle speed, battery power, traction motor power, fuel flow rate, throttle/brake command etc. Although the hybrid configuration is different from that of the FC/SC model proposed in this research, the purpose of the driving cycle evaluation is to test the performance of the computer model against actual driving cycles. As a result the most important parameter for this research is the traction motor power. The traction motor power parameter provides all motoring power to the vehicle and is also used as a generator to recover regenerative braking energy. A positive value for the traction motor power parameter indicates all the power demands is being used to propel the vehicle. A negative value indicates power is being recovered through regeneration. This usually occurs when the operator is trying to slow the vehicle or limit acceleration on a downhill section. Hence the power requirement throughout the bus operation can be simulated by applying the traction motor power on the hybrid model.

It must be noted that the negative power of the profile trace accounts for the regenerated energy sent to the energy storage of the diesel hybrid bus. It does not include the mechanical braking that is also required to decelerate and stop the bus. The impact of mechanical braking will depend upon the bus braking characteristics which were not provided. As a result, the power losses associated with the mechanical braking are not included in this research.

The auxiliary power consumption was not provided as part of the bus logged data. The power demand from the auxiliaries including lighting, door control, windscreen wipers, driver controls, CCTV etc. can be considered negligible when compared with the traction motor power. The auxiliary power from the heating can be a significant contributor to the total power required for the bus. The heating requirement would be dependent on weather conditions and the bus operator. Owing to this uncertainty, the heating auxiliary power was not taken into consideration in this research. However, the auxiliary power can be simulated by putting a controlled load on the energy storage of the bus given if the auxiliary power data can be provided. Additionally, unlike battery electric buses, the high energy density of FCs make them outstanding in meeting auxiliary power demands. It has been noted that battery electric buses generally have a hard time maintaining the same performance in winter time due to heating requirement, however, this is not a significant issue for the FC bus as the bus can easily store more hydrogen on-board by adding more cylinders or fuelling more hydrogen.

Details of the driving cycle data including data collection method, route information and data analysis can be found in Appendix O.

Driving cycle simulation

A load simulation system has been designed with the purpose of simulating the traction motor power profile for the FC/SC hybrid model. The load simulation system consists of a controlled variable resistor and a current source. The load simulation system has been shown in Figure 6.1 below.

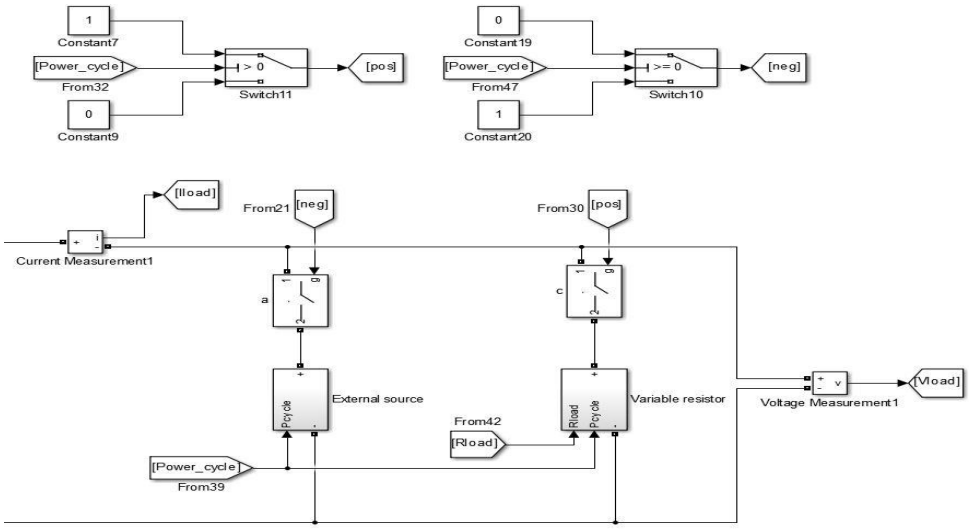

Figure 6.1 Simulink load simulation system for the computer model

Since the dc voltage in the hybrid system (after converters) is 630 V (regulated by the boost converter), the power profile can be simulated by matching the current to and from the load. When the power is positive (propelling the bus), the variable resistor will be switched on to dissipate the required amount of power calculated by:

$$R_{variable} = \frac{630^2}{P_{positive}} \quad (6\text{-}1)$$

When the power is negative (slowing the bus), the current source will be switched on to provide a controlled current. The current will be determined by:

$$I_{source} = \frac{P_{negative}}{630} \quad (6\text{-}2)$$

The system can determine the required resistance and current depending on the power requirement and simulate the power profile as the load of the FC/SC hybrid model. To test the simulated power profile against the actual power cycle, a 5 min segment of the driving cycle has been selected for comparison. The comparison between the actual power profile and simulated power profile has been plotted in Figure 6.2.

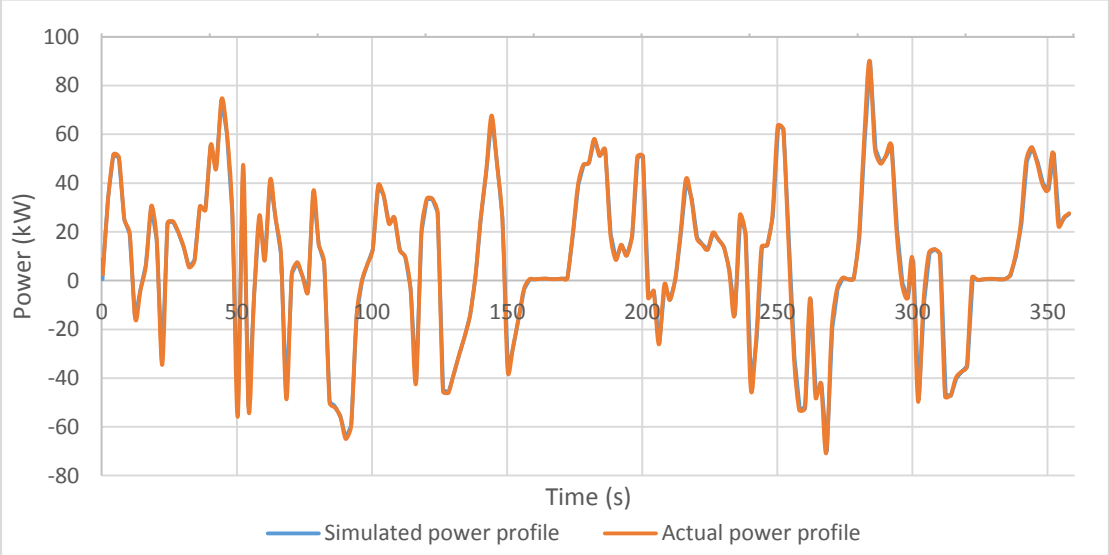

Figure 6.2 Comparison between actual bus power profile and Simulink simulated power profile

As Figure 6.2 shows, that the actual power profile is nearly identical to the simulated profile. The difference between simulated power profile and actual power profile has been calculated to be less than 0.01% which is the reason they overlap with each other. It shows the load simulation system in the computer model is capable of simulating the same power demands as the actual power profile.

6.3 Degree of hybridisation identification

With the integration of a load simulation system and scaling of the main power sources, the FC/SC hybrid model can be tested with the recorded power profiles. The output current control strategy proposed in section 5.8.2 showed the FC and boost converter output current can be kept constant while using the SC to supplement the power demand. However, only simple dynamic tests have been carried out to test the controller due to lack of appropriate laboratory equipment. The FC/SC hybrid model will be tested with a realistic dynamic load. The purpose is to investigate the required degree of hybridisation between the FC and the SC with the load of a practical London double decker bus. The complete computer model is shown in Figure 6.3.

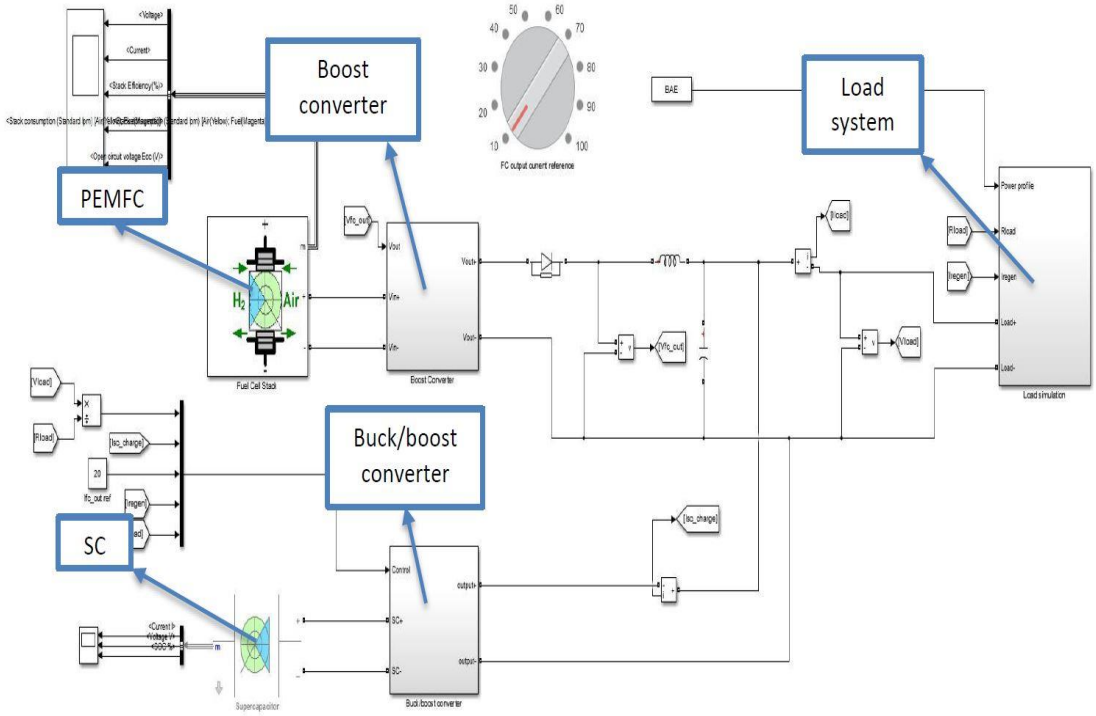

Figure 6.3 Simulink complete FC hybrid model for driving cycle test

The model consists of a FC, boost converter, SC, buck/boost converter and load simulation system. The three parameters that the user is required to define are as follows.

1. FC and boost converter current output reference (rotary switch).
2. Driving cycle power profile (BAE workspace block next to the rotary switch).
3. SC initial SoC (defined within the SC block).

6.3.1 Driving cycle selection

An extensive amount of data was collected from an actual bus. Bus driving cycle data from a 24 hour operation route (approximately 19 hour of bus operation and 5 hour of bus powered down) has been selected for this research. The 24 hour bus data was collected from a bus selected by UCL that is in daily service. Information regarding the 24 hour bus data is summarised in Table 6.2 and the complete power profile has been plotted in Figure 6.4.

Table 6.2 Route 388 bus data logging information

Route statistics	
Bus route	388
Length	12.83 km
Stops	37
First stop	Elephant & Castle
Last stop	Stratford City Bus Station
Bus data logging	
Date	04/08/2014 (Monday)
Time of first bus	05:40:00
Time of last bus	23:50:00
Completed journey (inbound and outbound)	20
Speed profile information	
Highest speed of the day	35.7 miles/hour (57.5 km/h)
Average speed of entire day	7.68 miles/hour (12.4 km/h)
Average speed of entire day (exclusive of bus long stops due to driver break)	8.57 miles/hour (13.8 km/h)
Power profile information	
Peak power (positive)	202 kW
Peak regenerative power (negative)	-169 kW
Average power of entire day	8.31 kW
Average power of entire day (exclusive of bus long stops due to driver break)	9.45 kW

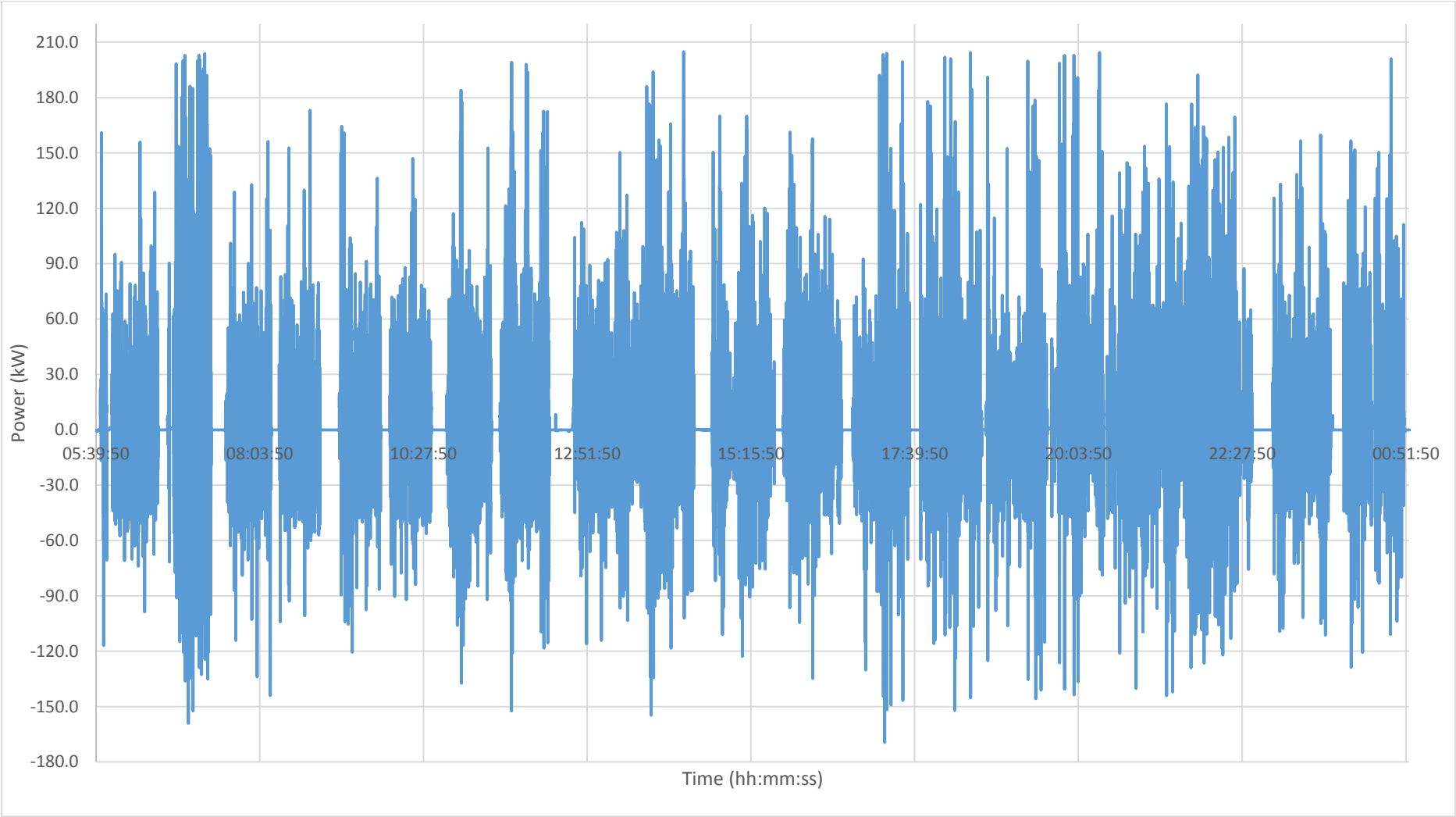

Figure 6.4 Route 388 full operation day traction motor power profile

As the power profile shows, the power demand varies significantly during each journey and also varies depending upon the time of operation. The power profile represents the power required to power the bus on the selected driving cycle. This power profile will be applied to the FC/SC hybrid model. However, due to restrictions resulting from limitations of the processing power of the computer used for the Simulink model, the computer processing power was not enough to run the entire data set. It would require an inordinate and impractical length of time and a powerful computer power to run the entire data set. As a result, the performance of the FC/SC hybrid model will be investigated with selective segments of the power profile selected from the 24 hour data set. The samples were selected with consideration of power level, vehicle speed and traffic conditions as some of the more representative power cycles.

6.3.2 FC/SC hybrid model operation

One of the selected samples was a 360 s segment of the power profile selected from the 24 hour route 388 bus data. The sample was selected from within the period 06:40 to 07:28 when the highest peak power occurs. Within this 360 s power profile sample segment both the highest peak power (202 kW) and highest average power (26.1 kW) were recorded. This 360 s power profile sample segment will be denoted as the **peak power profile** throughout the following analysis. The power and speed profile of the peak power profile is shown in Figure 6.5.

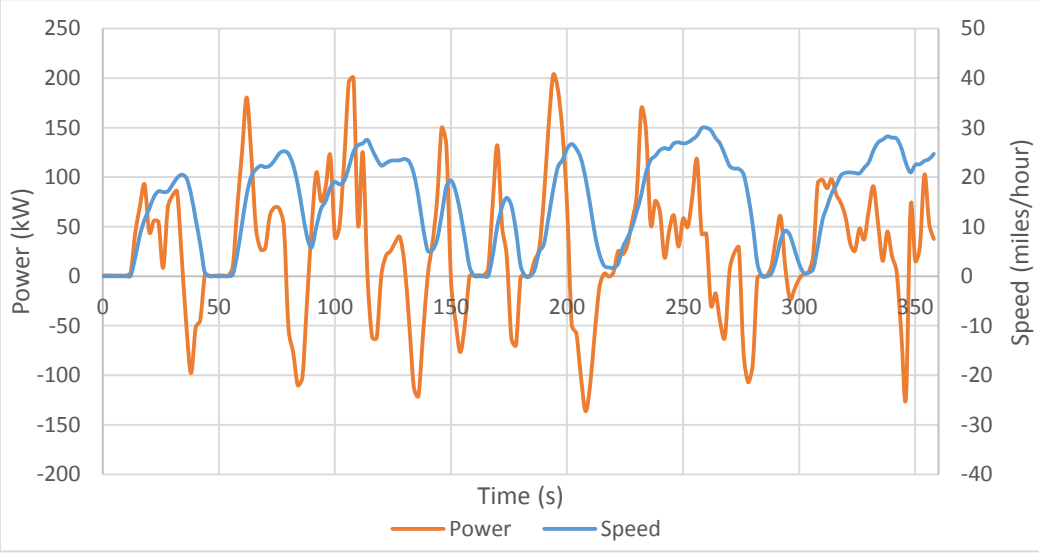

Figure 6.5 Power and speed traces of the peak power profile

As the power and speed traces of the peak power profile show, the bus undergoes frequent acceleration and deceleration due to traffic conditions. Positive power has been observed when the bus is accelerating and negative power has been observed when the bus is braking. It can be seen that the power demand varied significantly in

terms of both magnitude and frequency in this dynamic driving environment. The FC/SC hybrid model needs to be able to satisfy complex dynamic power demands in order to realise any practical value from the design.

Analysis of the performance of the FC/SC hybrid model will now be carried out using the power trace from Figure 6.5. First parameter values for the FC and boost converter output current and the SC initial SoC will be determined. As an initial estimation, the FC and boost converter output current has been set to be 40 A which equates to a 25.2 kW output after the boost converter. The SC initial voltage has been set to be 400 V which equates to initial SoC of 82%. After all three parameters have been imported and set up, the first driving cycle test was carried out in the computer model.

The same parameter names have been used for plotting (Figure 5.32). The plotting parameters are described in the following points.

- I_{fc_in} / V_{fc_in} – FC output current / FC output voltage
- I_{fc_out} / V_{fc_out} – Boost converter output current / Boost converter output voltage
- I_{sc_in} / V_{sc_in} – SC output current / SC output voltage
- I_{sc_out} / V_{sc_out} – Buck/boost converter output current / Buck/boost converter output voltage
- I_{load} / V_{load} – Current delivered to/from the load / Voltage applied on the load

The first parameter to look at is the performance of the FC and boost converter. The results have been plotted in Figure 6.6.

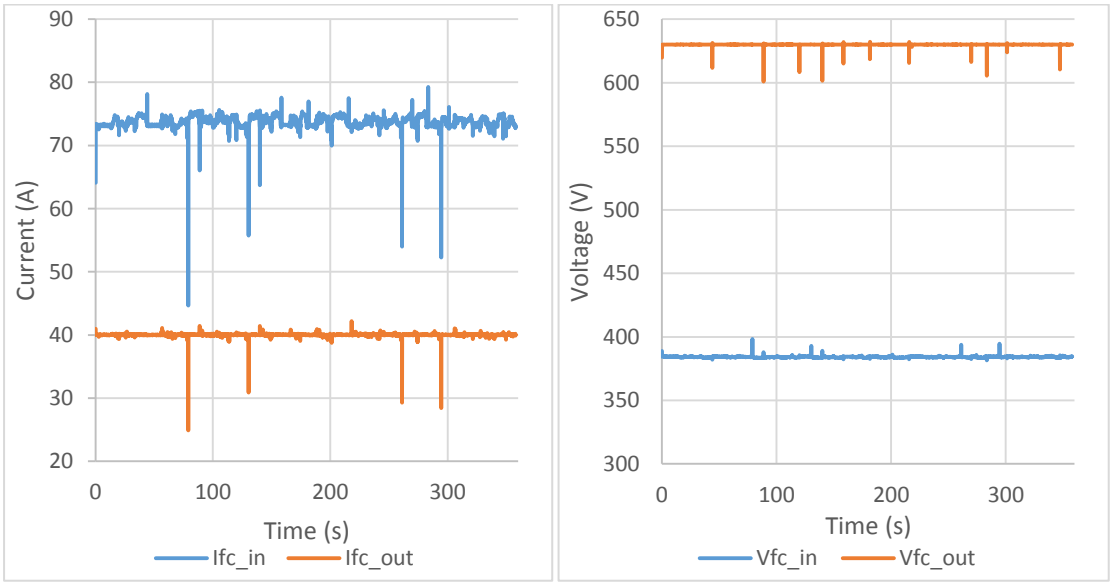

(a) **(b)**

Figure 6.6 FC and boost converter traces of the peak power profile (a) current (b) voltage

As the results show, the FC and boost converter output current (Ifc_out) has been kept nearly constant at 40 A as the reference requested. The boost converter managed to boost the output voltage to 630 V independent of the varying power traces. Transient voltage and current changes have been observed on the FC and boost converter output. This has been caused by the delay caused by PID tuning of the boost converter. The transient under and over-shooting can be mitigated by increasing the sampling frequency of the PID controller. Justification of this argument and more information on the sampling frequency of the model can be found in Appendix P.

The voltage and current performance indicate the FC and boost converter output power can be kept near constant throughout the peak power profile. The boost converter efficiency has been plotted in Figure 6.7. As Figure 6.7 shows, the boost converter efficiency averaged at around 89% conversion efficiency. The slight variations of the FC and boost converter output current and voltage also caused the efficiency to vary by ±2% which is deemed to be acceptable.

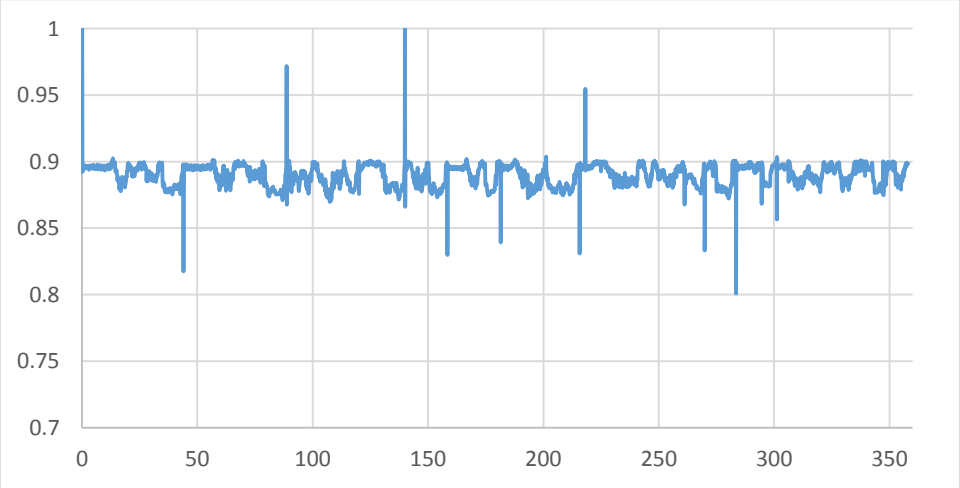

Figure 6.7 Boost converter efficiency trace of the peak power profile

The second parameter to analyse at is the performance of the SC and buck/boost converter. The results have been plotted in Figure 6.8.

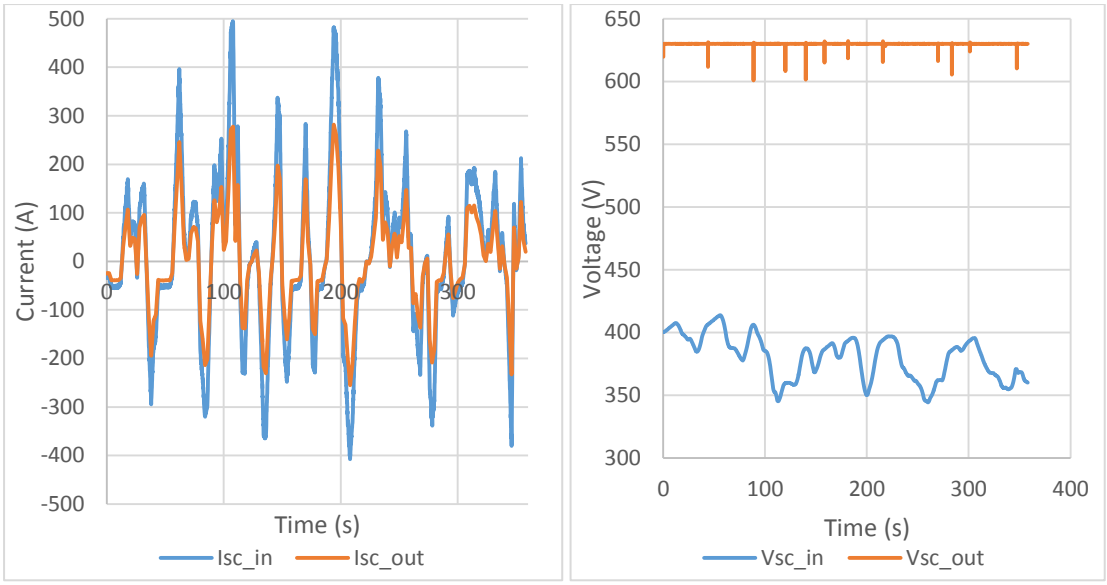

(a) **(b)**

Figure 6.8 SC and buck/boost converter traces of the peak power profile (a) current (b) voltage

Unlike the constant output of the FC, the SC was frequently charged or discharged at much higher current levels. The SC was used to supplement all the power that is higher than the FC output, absorb all the regenerative energy and excessive energy when the FC output is greater than the load demand. The voltage at the SC side of the buck/boost converter is directly dependant upon the SC SoC while the voltage at the buck/boost converter output is the same as the busbar voltage (630 V). Isc_in is always higher than the Isc_out as Figure 6.8 shows. This is because the different voltages at the input and output sides and the regenerative energy can never be recovered at 100% efficiency. The buck/boost converter efficiency has been plotted in Figure 6.9.

Figure 6.9 Buck/boost converter efficiency traces of the peak power profile

A positive Isc_out current indicates the SC is discharging while a negative Isc_out current means the SC is being charged. The buck/boost converter efficiencies are directionally dependent i.e. the efficiency during discharge of the SC differs from the efficiency during charge of the SC. There are also efficiency drops at the cross over points between discharge and charge. The moving average every ten samples has been plotted as red dots in Figure 6.9 for better observation. It can also be observed that the efficiency varies with the magnitude of power. This is more significant for the charge efficiency. It can be seen the efficiency is lower (around 85%) when the charging current is low (<100 A) and the efficiency is higher (around 92%) when the charging current is high (>100 A). The average efficiency of discharge for this peak power profile has been calculated to be 94.1% while the average efficiency of charge is 91.2%. To verify the validity of discharge and charge efficiency, the battery discharge and charge efficiencies of the test bus have been calculated. The method to work out the discharge/charge efficiency is to divide the battery input/output power by the algebraic sum of generator output and traction motor output. It was found the average discharge efficiency of the entire 24 hour route data is 85.04% and the average charge efficiency is 83.94%. Although the system configuration of the test bus is different to the computer model, the regenerative braking efficiency and battery discharge efficiency can be used as a reference. Hence it can be seen the discharge/charge efficiencies calculated for the computer model are reasonable compared with those from the test bus.

The output power of the hybrid system can be calculated by the voltage and current data. The power balancing of the hybrid system has been plotted in Figure 6.10.

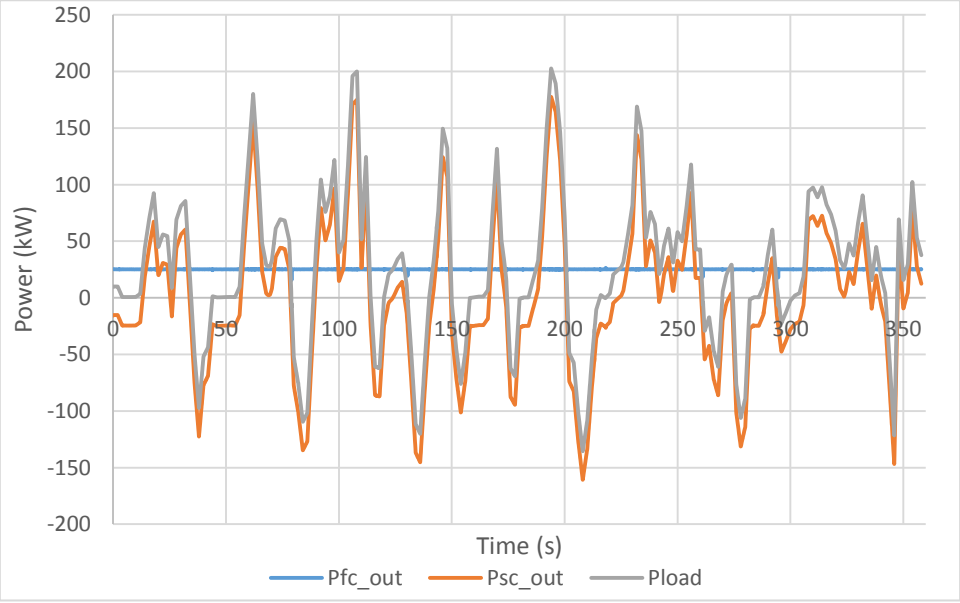

Figure 6.10 Power balancing of the hybrid system of the peak power profile

The Pfc_out is always constant at around 25.2 kW (40 A*630 V=25200 W) as expected. The Psc_out is used to supplement the varying power demands that differs from the FC and boost converter output power. The load power is always the algebraic sum of Pfc_out and Psc_out. It can be seen that the SC and buck/boost converter have allowed the FC and boost converter output to remain constant while meeting the dynamic load demands. The power delivered to the load simulation system in the computer model has been compared against the actual bus peak power profile. The comparison has been plotted in Figure 6.11. The comparison shows the simulated power profile is nearly identical (<0.1 % difference) to bus power profile.

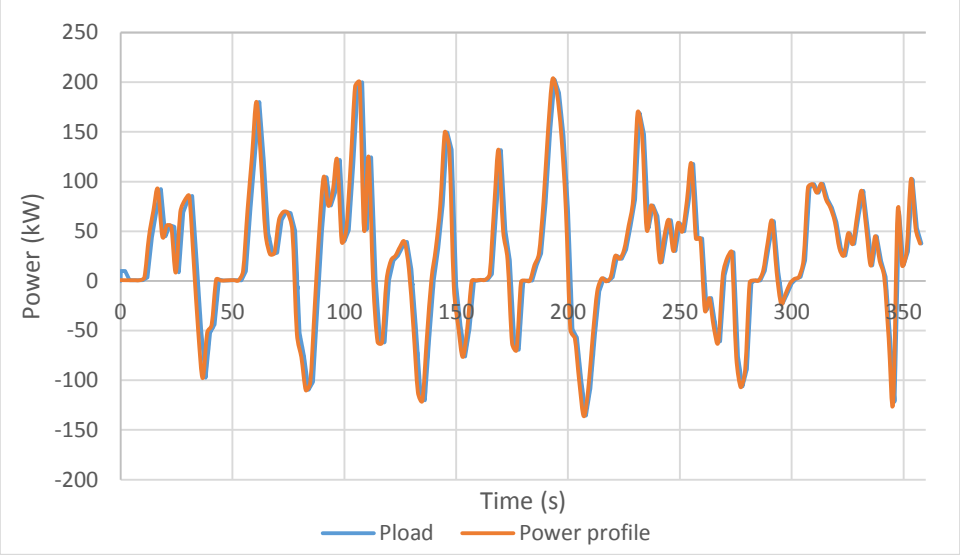

Figure 6.11 Comparison between simulated and actual peak power profile

The last main parameter is the SoC of the SC change throughout the power profile. The SoC change has been plotted in Figure 6.12.

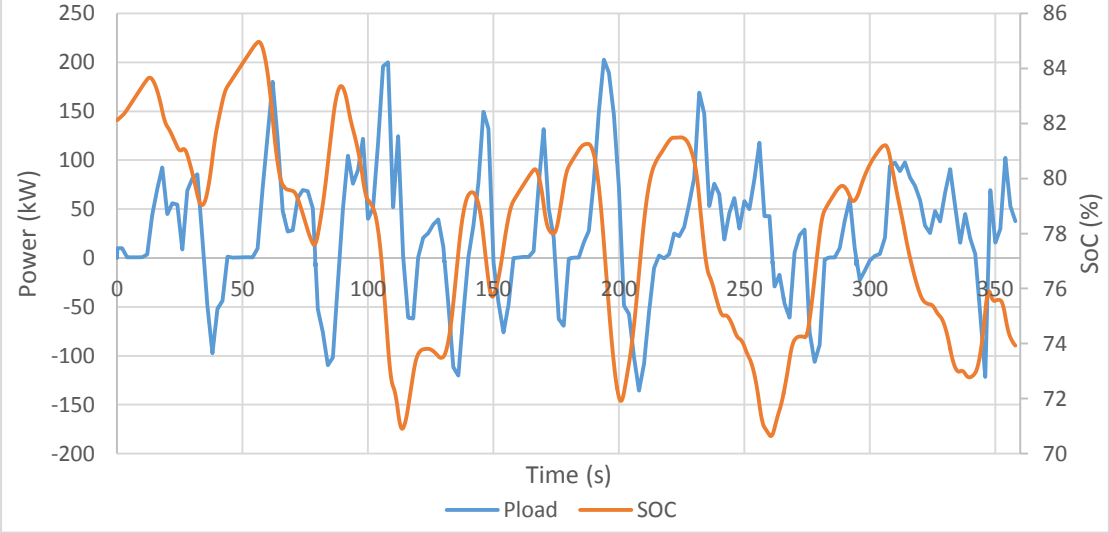

Figure 6.12 SoC change against load power of the peak power profile

It can be seen the SoC decreased when the power profile is positive (discharging) and increased when the power profile is negative (charging). When the bus is stopped (45-53s), all the FC and boost converter output power has been used to charge the SC because there is no traction load. It can be concluded the SC discharged from 82% (initial SoC) to 74% (final SoC) in the peak power profile with the FC and boost converter providing a constant 25 kW output. It has been shown the FC/SC hybrid system functioned as expected in terms of controlling the FC output and meeting the dynamic load.

6.3.3 FC and boost converter output identification

In the tests carried out with the peak power profile, the boost converter output reference current was set at 40 A. The buck/boost converter has managed to adjust its output to allow the boost converter output current to remain at the user requested reference value. The boost converter output determines the output power from the FC. This section investigates how modifying the boost converter reference would affect the system performance and how to determine the required optimum reference value.

Response to reference variation

The same peak power profile has been used to allow clear comparison when the boost converter reference values are varied. The SC energy capacity (83 F) and initial SoC (82%) have also both been kept the same. The same peak power profile has been tested with FC and boost converter reference currents at 20 A, 30 A, 40 A and 50 A which are approximately 12.6 kW, 18.9 kW, 25.2 kW and 31.5 kW. The results have been plotted in Figure 6.13.

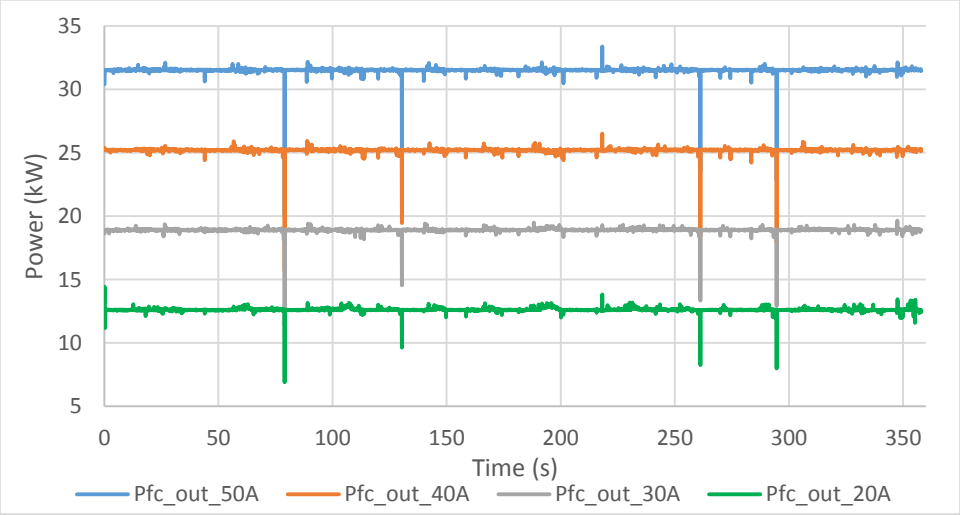

Figure 6.13 FC and boost converter power reference variation of the peak power profile

As Figure 6.13 shows, the boost converter output has been regulated to the user requested reference values. Since the power profile of these tests are the same, the Psc_out parameter would have the same curve with different magnitudes due to the different levels of Pfc_out as Figure 6.14 shows.

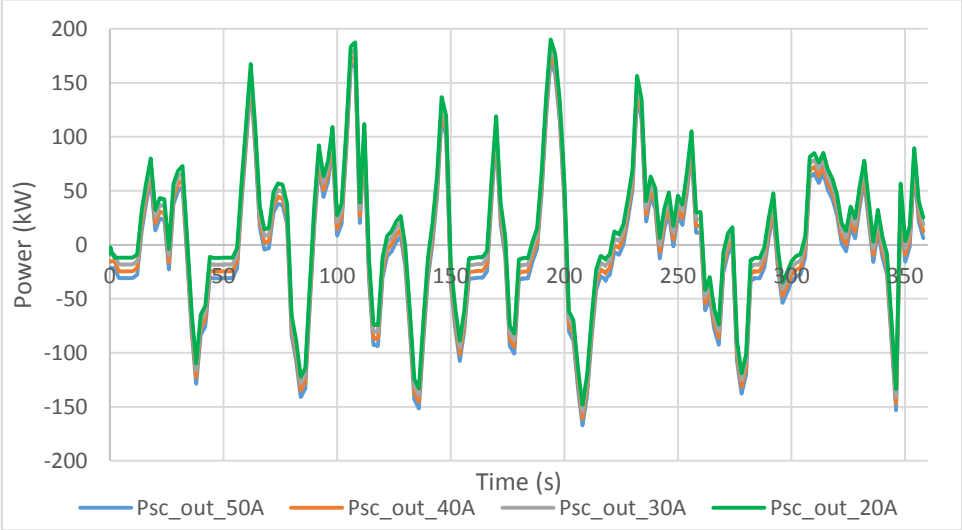

Figure 6.14 SC and buck/boost converter power variation of the peak power profile

It has been shown that the FC and boost converter output reference power can be controlled to be held constant at the user defined reference value. The SC output power would need to adjust its magnitude to supplement the FC output power to satisfy the total load power demand. The different SC output powers would also result in different SoC change. The SoC of the SC throughout the peak power profile with different FC and boost converter output reference has been plotted in Figure 6.15.

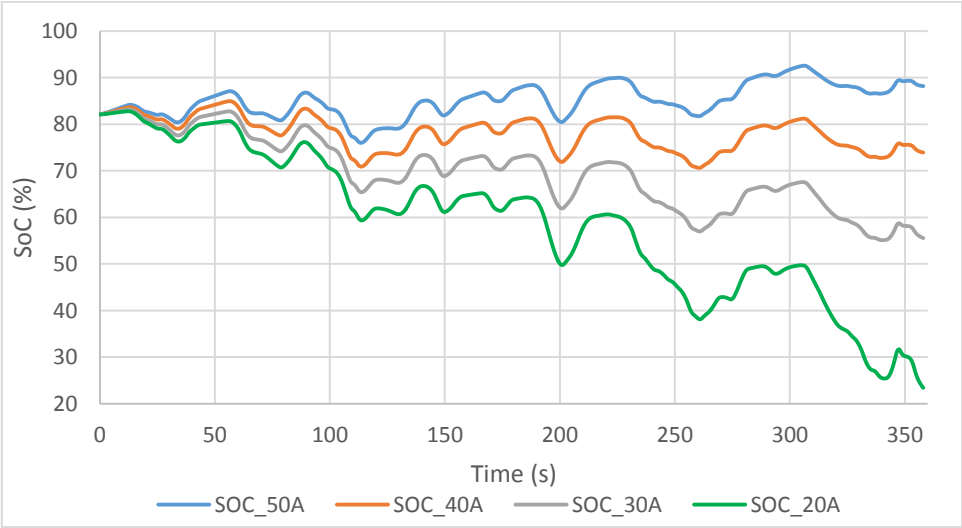

Figure 6.15 SoC change with reference variation of the peak power profile

As Figure 6.15 shows, the smaller the FC output is, the more energy the SC would have to discharge to supplement the power profile. The SC was discharged to different levels when the reference is 20 A, 30 A, 40 A with the SC maintaining a higher final SoC when the reference is 50 A. The average total algebraic power of the peak power profile is 26.1 kW which provides a 41.5 A reference current. It can be seen there is a link between the average power and the final SoC of the SC for a certain driving cycle.

Discussion on reference identification

It has been concluded that the FC and boost converter output reference power value would only affect the amount of energy delivered or absorbed by the SC in the same power profile. The SC will be discharged if subjected to certain driving cycles with driving cycle average power higher than the FC and boost converter output. On the other hand, the SC will be charged in this driving cycle if the average power of the power profile is lower than the FC and boost power. If the average total algebraic power of the driving cycle is close to the FC and boost converter power, the SC would end up with nearly the same final SoC as the initial SoC. Depending upon the FC and the boost converter output reference, SC overall capacity, SoC and load imposed by the driving cycle, the SC can end up in overall deficit, near parity or with a higher final SoC. This would depend upon how close the set FC and boost converter power was to the journey overall average power requirement. As a result the boost converter reference output can be determined by using the average power of the power profile in the selected driving cycle.

The peak power profile has been tested again with a 41.5 A current as the reference current. The SoC change of the profile has been plotted in Figure 6.16.

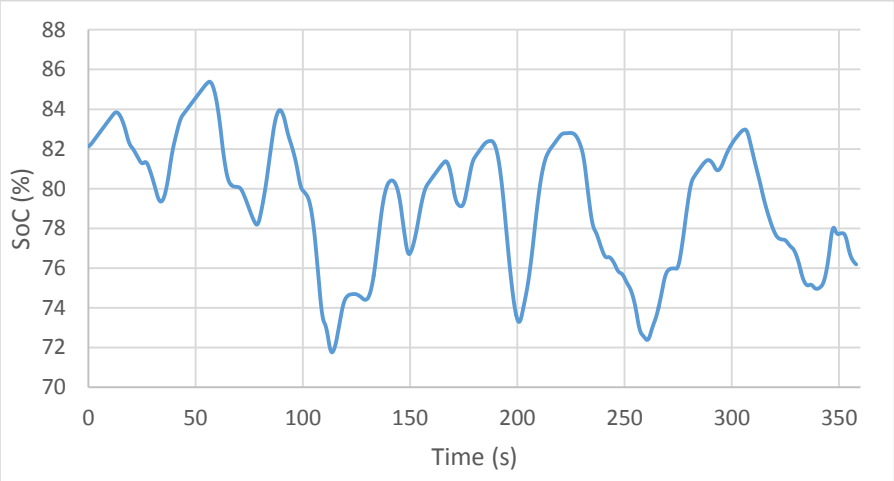

Figure 6.16 SoC change of the peak power profile with profile average power as reference

As the plot shows, the final SoC (76.2%) is still lower than the initial SoC (82.2%) meaning the SC still discharged even when the FC and boost converter output power equal the average power of the driving cycle. The reason for this is the buck/boost converter efficiency is different for charge and discharge operation. The conversion efficiency has been calculated using the same method showed in Figure 6.9. It was found the average discharge efficiency is 94.3% and the average charge efficiency is 91.2%. This indicates the SC needs to provide 5.7% more energy to the converter during discharge operations to provide the net output from the converter to the load. While the SC received 8.8% less energy from the gross regeneration output during charge operations. As a result, the final SoC will be lower than the initial SoC because of these losses. The final SoC can only be exactly the same as the initial SoC if the buck/boost converter has no losses, which is scientifically impossible. As a result, the FC and boost converter output power would have to be increased in order to keep final SoC reasonably close to the initial SoC. The increased FC and boost converter output power would be used to compensate for the losses during charge and discharge. Since the conversion losses can be subject to change dependent on the load profile, it would be difficult to determine exactly how much of a power increase is required. As a result, a constant 10% increase in FC and boost converter reference output power has been added to the average power calculated from the driving cycle to keep the final SoC reasonably close to the initial SoC.

The peak power profile has been tested again with a 10% increase in the FC and boost converter reference output power above the average power. Since the route average power required a 41.5 A FC and boost converter output reference current for an ideal converter, the new reference with a 10% increase would be 45.65 A reference. The SoC change of the new reference current has been plotted in Figure 6.17. As Figure 6.17 shows, the final SoC is now 82.3% which is reasonably close to the 82.2% initial SoC. The required FC and boost converter output reference has been identified by using 1.1 times of the selected driving cycle average power.

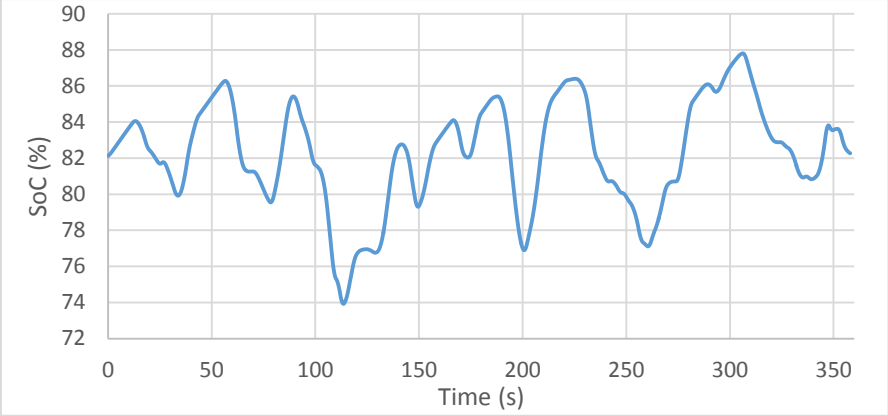

Figure 6.17 SoC change of the peak power profile with 10% increase of profile average power as reference

6.3.4 SC size identification

Keeping the FC and boost converter output to 1.1 times of the driving cycle average power can not only maintain the FC output at a near constant output but also ensure sufficient SoC is being maintained to complete the selected driving cycle. In theory, continually matching the reference output to the real time driving cycle power can provide better performance in terms of vehicle operation and fuel economy, but this would be counter to the concept of maintaining a constant FC output. One consideration would be to use the overall journey average power to determine the boost converter reference setting. As a result the SC would need to be sized to be able to satisfy any other power demands higher than the FC output power.

To determine the required SC size, the SC would need to be sized from two perspectives: power density and energy density. The power density determines the peak power that can be provided by the SC while the energy density determines the energy capacity of the SC. As discussed before, one of the most important advantages of the SC is its high power density. The Maxwell 48 V SC used in the laboratory test bench only has an energy storage capacity of 26.56 Wh but can achieve the peak power of 56 kW according to the data sheet. Since the peak power required from the bus is 200 kW, it is reasonable to make the assumption that a suitably sized SC can satisfy the peak power requirement for bus operation. The system has been assumed to be capable of covering charge and discharge rate limitations in the bus operation. Hence this research will focus on the energy capacity sizing of the SC for the hybrid system. This section will investigate how the SC size would affect the system performance and the strategy to identify the required SC size. Please note all the SC sizes are referred to energy capacity and not the physical dimensions of the SC in this

research.

Response to SC size variation

In the previous tests, the SC capacitance has been set to be 83 F which has an energy capacity of 2.656 kWh. As Figure 6.17 showed before, the final SoC is nearly the same when the FC and boost converter output power is 1.1 times of the driving cycle average power. The same peak power profile with the same boost converter output reference (45.65 A) has been tested with a number of different sized SCs. Five tests at SC capacitance values of 83 F, 60 F, 40 F, 20 F and 10 F were performed. The SC and buck/boost converter output power and SoC change throughout the peak power profile have been plotted in Figure 6.18 and 6.19.

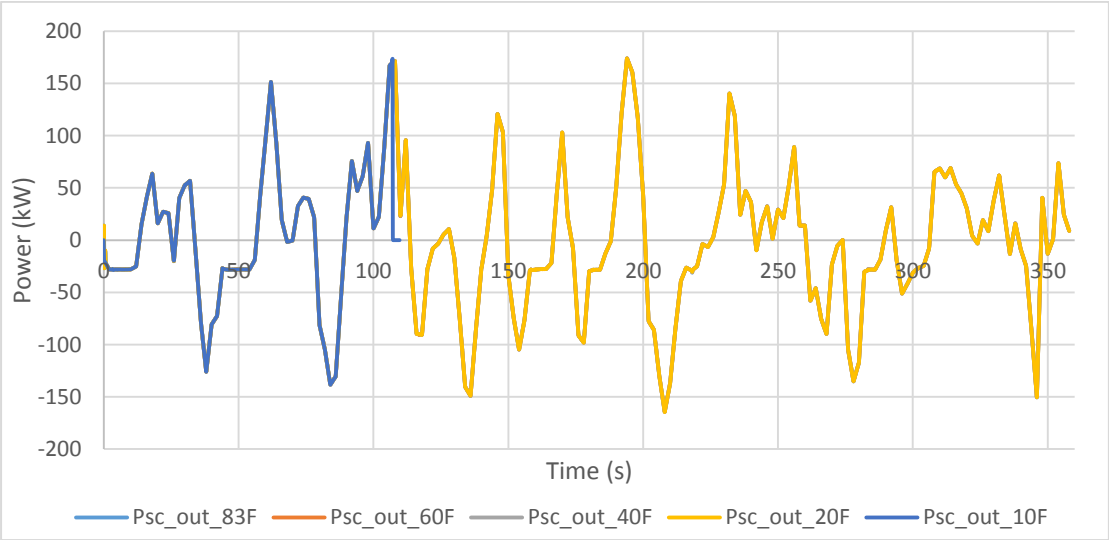

Figure 6.18 SC and buck/boost converter output power with different SC size of the peak power profile

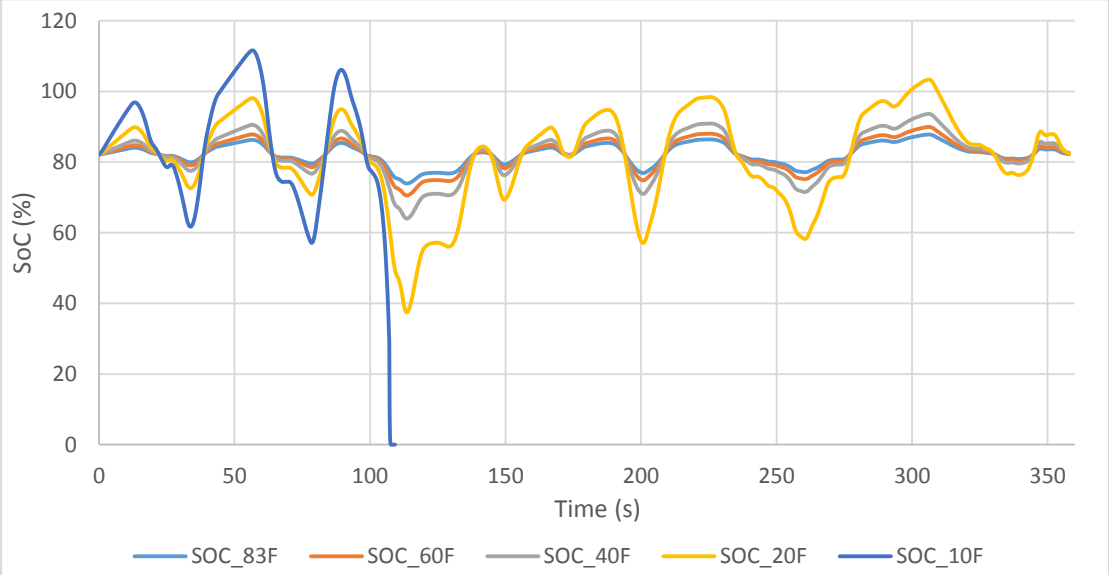

Figure 6.19 SoC change with different SC size of the peak power profile

The power plot showed the SC and buck/boost converter provides exactly the same output power with different sized SCs with the exception of when the SC capacitance is 10 F. From the SoC plot, it can be seen that different sized SC end up with the same final SoC when 1.1 times the driving cycle average power has been used as the FC and boost converter reference output. The simulation with the 10 F SC was terminated when the SoC dropped to zero around 109 s where a peak power demand occurs. A 10 F capacitance can store a total energy of 0.32 kWh. The 0.32 kWh energy means the SC can only supply a constant 15 kW output for 8 s even at full SoC. This indicates the SC size is simply too small to provide the peak power demand requested by the driving cycle. Apart from the 10 F SC, the other SCs managed to supplement the FC to provide the required power profile. Since the total energy the SC has to provide or absorb are the same throughout the operation, the main difference is the magnitude of the SoC change. For the 20 F SC, the SoC dropped to 37.8% at 109 s and reached 102.6% at 307 s indicating the SC was overcharged. However, the overcharge problem has also been partially caused by the initial SoC (82%). The sizing of the SC also is dependent on the initial SoC. It is noted a lower initial SoC or higher initial SoC will also affect the curves presented in Figure 6.19.

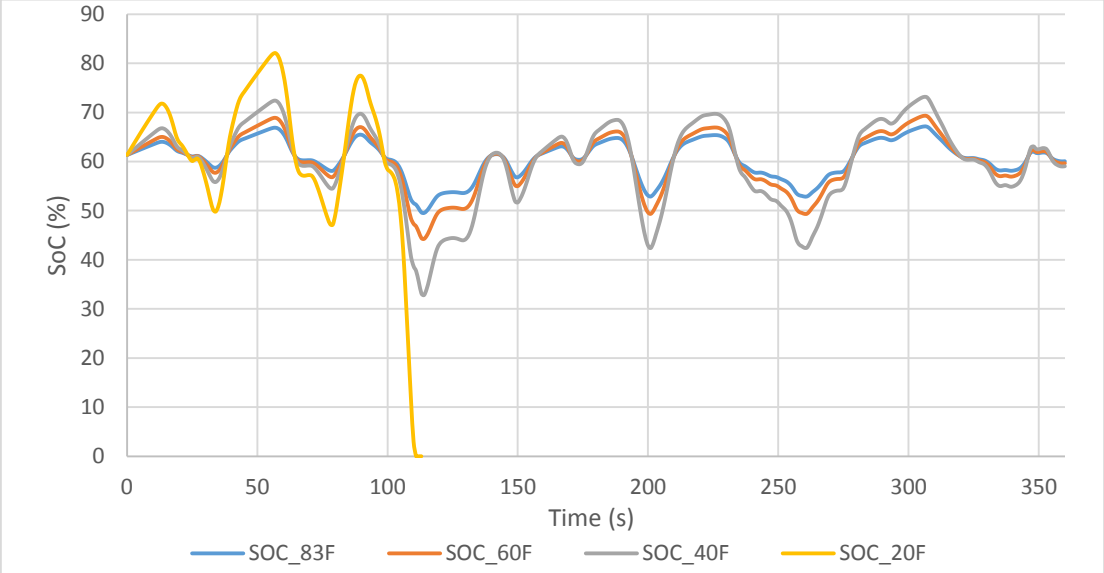

Figure 6.20 SoC change with different SC size of the peak power profile at different initial SoC

The same tests as Figure 6.19 have been carried out with the SC at a lower initial SoC (62 %). The SoC change has been plotted in Figure 6.20. As expected, it can be seen the SoC of each SC generally shifted towards a lower SoC level compared with the tests carried out with 82% initial SoC. The overcharge problem was not observed because of the lower initial SoC. However, the 20 F SC, which worked with the 82% initial SoC, was unable to satisfy this particular driving cycle with a 62% initial SoC. It

can be noted the initial SoC also needs to be considered when sizing the SC.

The results suggested the SC size will not affect the power delivered or absorbed by the SC as long as the SC is within its operating range. Although the tests showed a bigger SC is generally better in the computer model, an over-sized SC would also result in significantly more cost and space-demands. From the energy capacity perspective, the following criteria to size the SC can be addressed.

1. The SC SoC cannot reach its lower limit (must be greater than 0%) to prevent undercharge.
2. The SC SoC cannot reach upper limit (must be smaller than 100%) to prevent overcharge.
3. The SC can sufficiently satisfy the varying power demands throughout the selected driving cycle.
4. Preferably, the SC needs to be as small as possible in terms of both physical size and energy capacity as long as the first three criteria can be met to reduce system cost.

For the SC size tests carried out using the peak power profile, the SC size that best met all the criteria is the 40 F SC. Although the criteria to size the SC has been addressed, this is not an efficient method to size the SC for a certain driving cycle. Additionally, it is not efficient to repeatedly run the simulation with different SC sizes until the required SC size has been determined. Considering the criteria, the main parameter used to size the SC is to ensure there is sufficient remaining energy to satisfy peak power demand and to ensure there is sufficient capacity left to store additional energy. As a result, the SC can be sized if the energy going in and out of the SC can be predetermined.

Discussion on SC size identification

The main requirement is to determine the capacity of the SC that, in conjunction with the FC will enable the requisite amount of energy and power to be delivered to satisfy the load profile for the entire bus route. The challenge to size the SC in the computer model has been identified to be the requirement for simulation of the selected driving cycle with different SC sizes which would be a time consuming process. Since the power profile of a route varies significantly depending on the time, traffic, weather and operational profile, it is not practicable to simulate every route profile. A method is required to optimise the model to practically use the computer model to properly size the SC.

A power relationship for the FC hybrid system based on current balancing and voltage regulation can be formulated as:

$$P_{fc\_out} + P_{sc\_out} = P_{load} \quad (6\text{-}3)$$

The equation indicates the FC (and boost converter) and SC (and buck/boost converter) will always work together to meet the power demand from the driving cycle. The control strategy is to have the FC and boost converter output user-controlled which means the P_{fc_out} is user defined and maintained constant. The load power is obtained from the power profile of the driving cycle which is supplied by the test bus data. The required SC power can be calculated by subtracting the FC power from the power trace of the driving profile. As a result, the energy going in/out of the SC each sample can be calculated by multiplying the Psc_out by the duration of each sample which is one sample every 1^-5 s. The energy calculated using this method has been plotted in Figure 6.21.

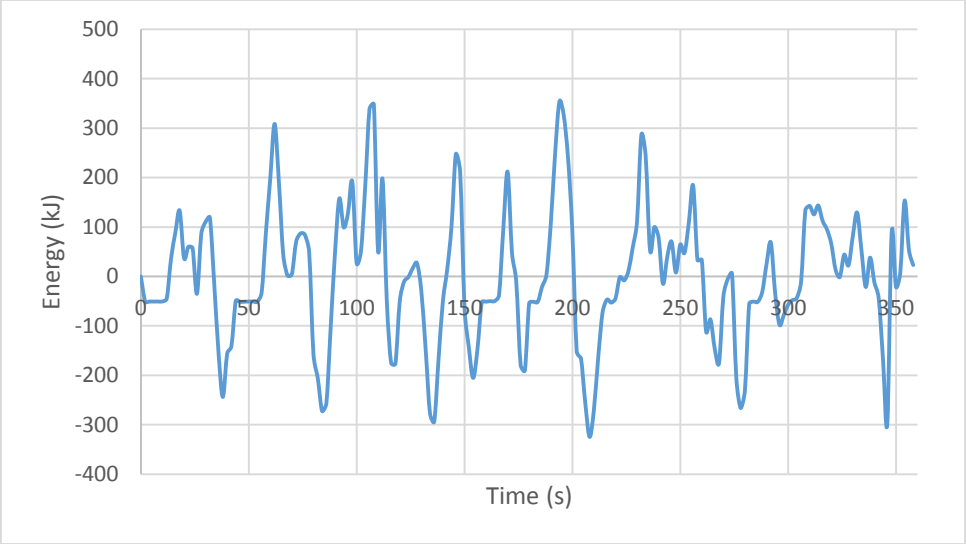

Figure 6.21 Energy required from the SC each sample of the peak power profile

The cumulative energy required from the SC can be calculated by adding the required energy of each sample. The total cumulative energy in kilojoules can be divided by 3600 s to give the total cumulative energy in kWh. The total required energy of the SC has been plotted in Figure 6.22.

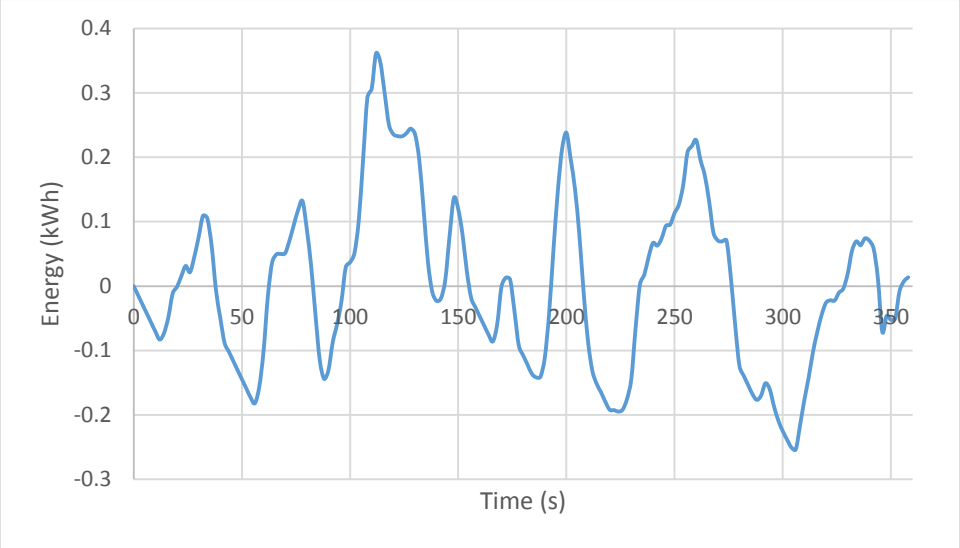

Figure 6.22 Cumulative energy required from the SC throughout the peak power profile

Figure 6.22 shows the cumulative energy required from the SC throughout the peak power profile. The positive area indicates the energy required to be drawn from the SC while the negative area indicates the energy that is harvested through regeneration to charge the SC. The highest energy of positive area would determine the most energy required from the SC which is 0.371 kWh at 112 s. The lowest energy of negative area would determine the most energy required to go to the SC which is -0.263 kWh at 306 s. As a result the SC size needs to be at least 0.634 kWh to deliver or absorb required energy throughout the peak power profile. Then the required capacitance can be calculated by:

$$0.634\ kWh \times 1000 \times 3600s = 0.5 \times C \times 480^2$$

$$C = 19.81F$$

Although the calculation based on power profile showed the required SC size is 19.81 F, the simulation carried out before showed that the SC was overcharged even with a 20F SC. This indicates the SC size calculated by the power profile is smaller than it needs to be. The reason for this is because the calculation carried out with the power profile does not take the initial SoC and the charge/discharge efficiency into consideration. This suggests the cumulative energy plotted in Figure 6.22 needs to be increased further to account for the charge/discharge efficiency. Since the exact efficiency would be dependent on the power profile of the selected driving cycle, the SC size can only be increased as an estimated value based on empirical calculation. Since the charge and discharge efficiency averaged at around 90% as showed before, the total SC size has been increased by 10% for efficiency compensation and an additional 10% for a buffer. It also must be noted the calculated energy is the total

stored energy in the SC. The actual available energy will be dependent on the SoC conditions.

A total 20% compensation increase has been applied on the calculated SC capacitance which gives a 23.772 F for the peak power profile case. The same peak power profile test has been carried out with the new SC size and the SoC change has been plotted in Figure 6.23.

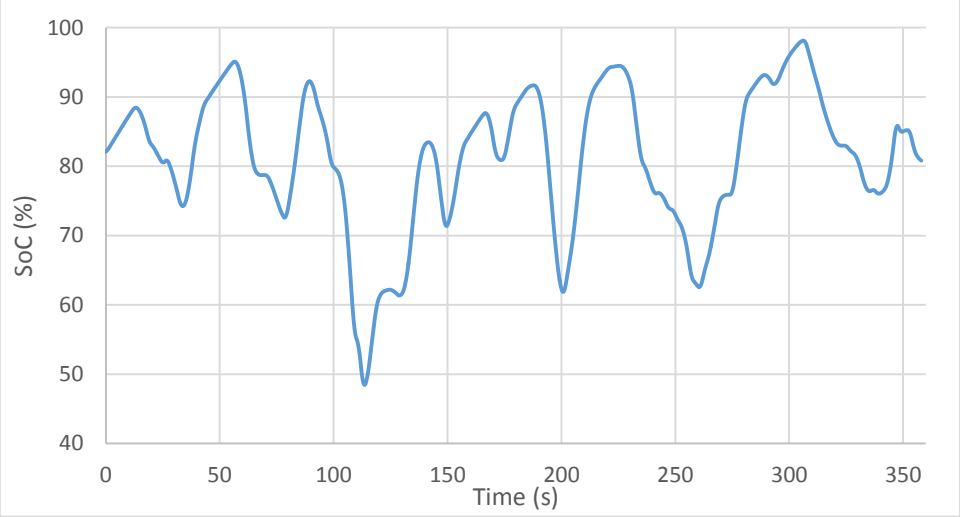

Figure 6.23 SoC change with determined SC size of the peak power profile

As Figure 6.23 shows, the SC has not been overcharged throughout the driving cycle with the increased SC size. It can be seen that the SC size can be calculated by using the power profile. This can be carried out much more easily because only the power profile is required. However, this method can only provide an initial estimation of the required SC size. The SC and buck/boost converter charge and discharge efficiency needs to be calculated to properly size the SC. Although the model needs to be simulated with the calculated SC size for validation, the calculation method can still significantly facilitate the sizing of the SC.

6.3.5 Performance with identified degree of hybridisation

Degree of hybridisation identification strategy

The previous sections have carried out tests to show how the system performs for various FC output as well as varying SC size. Methods to determine the required FC and boost converter output and required SC size have been identified with the 360 s peak power profile. Based on the discussions of previous sections, the strategy to identify the FC and boost converter output and the SC size for the FC/SC hybrid model can be summarised into the following steps.

1. Collect the power profile of the driving cycle.
2. Use the average power of the profile as FC and boost converter output reference.
3. Subtract the power profile of the FC and boost converter output power to determine the power required from and to the SC.
4. Calculate the cumulative energy required from and to the SC to determine the required capacitance.
5. Increase the determined capacitance by 20% for efficiency compensation and extra buffer.
6. Run the simulation with 1.1 times of route average power as FC and boost converter output reference and increased capacitance as SC size.
7. Verify and validate the calculated degree of hybridisation.

To further verify the degree of hybridisation identification strategy, more driving cycle tests have been carried out. As discussed in Table 6.2, the 24 hour route 388 bus profile includes 20 completed bus journeys either from depot to final stop or from final stop back to the depot. The bus journey with the highest average power and the lowest average power has been selected to test the degree of hybridisation identification strategy.

Bus journey with the highest and lowest average power

The completed bus route with the highest average power has been found to be the bus journey within the period 06:38 to 07:10 in the morning. The bus journey lasts approximately 32 minutes. The journey has an average power of 16.03 kW and an average speed of 13.05 miles/hour (21.0 km/h). The completed bus route with the lowest average power has been found to be the bus journey within the period 19:00 to 19:50 in the evening. This bus journey lasts around 50 minutes. The journey has an average power of 5.65 kW and an average speed of 7.39 miles/hour (11.9 km/h). The power and speed traces for the journeys with highest average power and lowest average power have been plotted in Figures 6.24 and 6.25 respectively.

The bus journey with the highest average power occurred right before the morning rush. The bus at that period of time is expected to encounter less traffic but with significant passenger loading. It can be seen the power magnitude of the highest average power journey is significantly higher than the one with lowest average power. The bus journey with the lowest average power occurred at the evening rush hour. It can be noted that the power magnitude is lower and the bus frequently stops due to traffic density. This is the reason the journey with the lowest average power takes longer to complete the route than the one with highest average power.

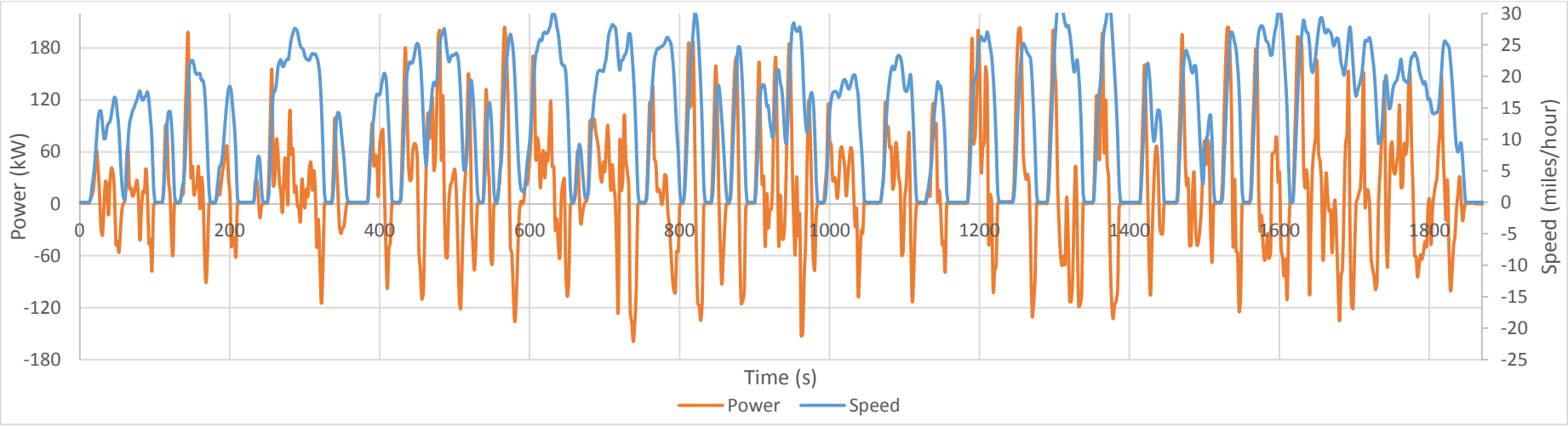

Figure 6.24 Bus journey with the highest average power from the 24 hour route 388 bus profile

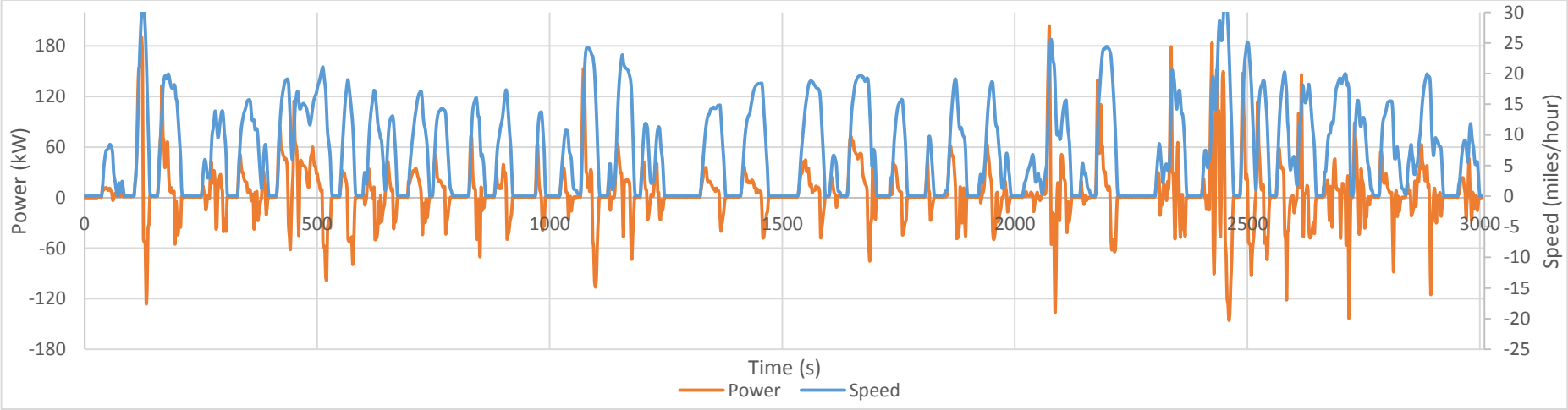

Figure 6.25 Bus journey with the lowest average power from the 24 hour route 388 bus profile

These power profiles represent two very different bus operations. The degree of hybridisation of each power profile has been identified based on the degree of hybridisation identification strategy developed earlier. For the bus journey with highest average power, the FC and boost converter output current reference has been calculated to be 25.44 A based on the 16.03 kW average power. The FC and boost converter output current reference in the model has been identified to be 27.99 A (17.63 kW) with the 10% increase for buck/boost converter efficiency compensation. The required SC size has been calculated based on the cumulative energy calculation method discussed before. The required SC capacitance has been calculated to be 65F (with the 20% compensation increase) which equates to a 2.08 kWh total stored energy. Hence the proposed operating degree of hybridisation for this journey with highest average power is an FC and boost converter output of 17.63 kW and a 2.08 kWh SC. The FC/SC hybrid model has been tested with the proposed parameters. The power balancing and SoC change have been plotted in Figure 6.26.

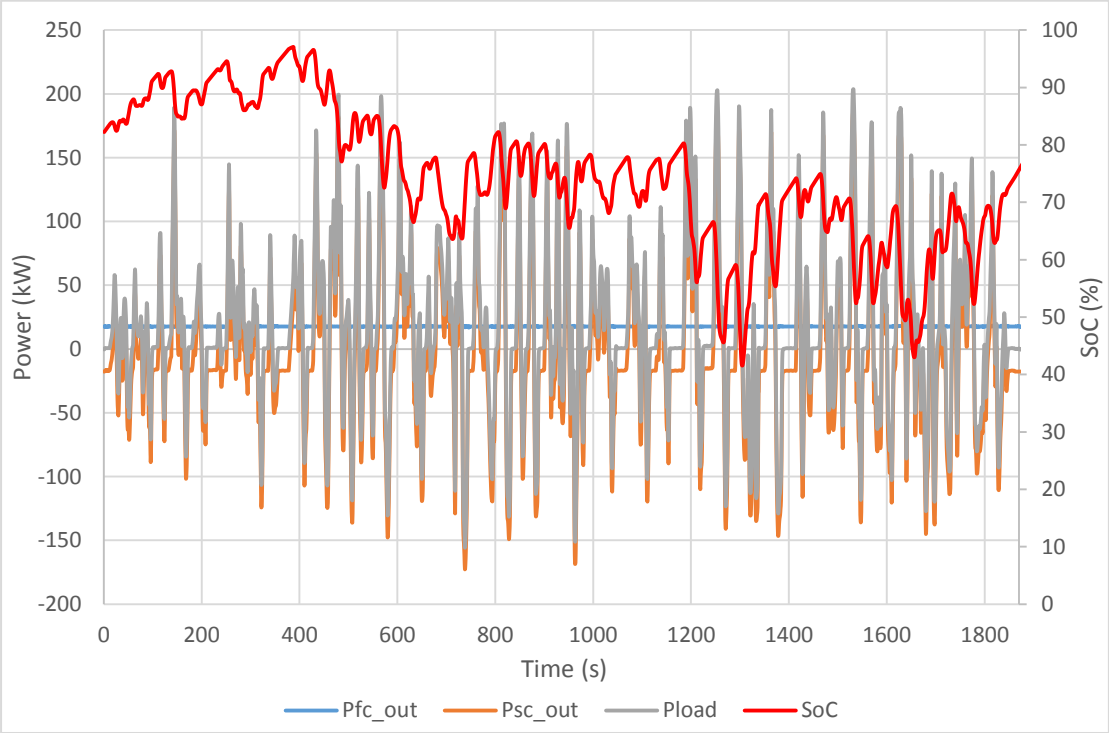

Figure 6.26 Power balancing and SoC change of the bus journey with the highest average power

The FC and boost converter output power has been kept at 17.6 kW constant output with ±0.5% variation. It can be seen the SC and buck/boost converter output power have the same shape as the load demand power profile with an offset equal in magnitude. This offset is of course the FC and boost converter output power. The FC/SC hybrid model functioned as expected in terms of meeting the dynamic power profile with the FC and boost converter output remaining near constant. The SC

attained a maximum SoC of 95.6% and a minimum SoC of 41.1%, neither of which exceeds the limits defined earlier. The SC was frequently charged and discharged to meet the dynamic load demand. It has been observed the final SoC is 74.8% which is 7.4% lower than the initial SoC. The SC discharged overall during this driving cycle even with the 10% increased FC and boost converter reference power output. This indicates the efficiency of buck/boost converter operation during this bus journey is lower than during the peak power profile tests. The 10% increase of the FC and boost converter output reference cannot fully compensate the efficiency loss. Calculation showed the efficiency during discharge averaged 93.3% while the efficiency during SC charge averaged 87.6% throughout the bus journey with highest average power. It can be seen the charge efficiency is lower than expected meaning less power will be absorbed by the SC during regeneration.

For the bus journey with lowest average power, the FC and boost converter output current has been calculated to be 8.97 A based on the 5.65 kW average power. The FC and boost converter output current reference in the model has been calculated to be 9.87 A (6.22 kW) with the 10% increase for efficiency compensation. The required SC capacitance has been calculated to be 44 F (with the 20% compensation increase) which equates to a 1.41 kWh total stored energy with full SoC. Hence the proposed operating degree of hybridisation for this journey with lowest average power is 6.22 kW FC and boost converter output and a 1.41 kWh SC. The FC/SC hybrid model has been tested with the proposed parameters. The power balancing and SoC change have been plotted in Figure 6.27.

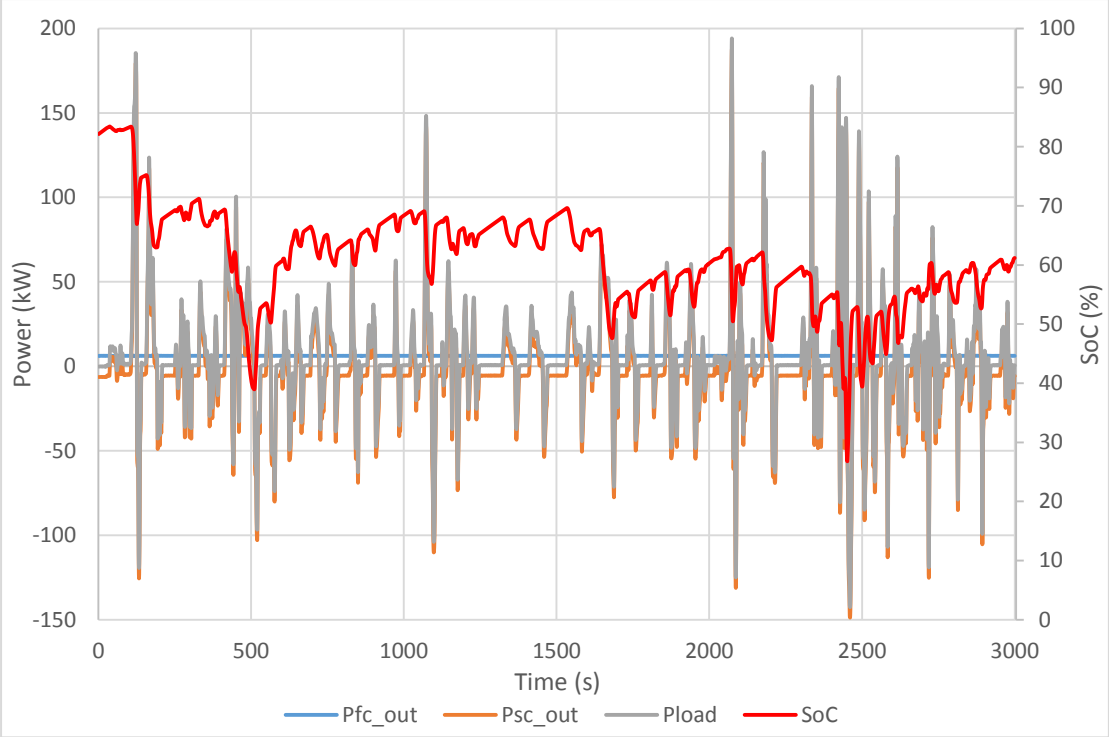

Figure 6.27 Power balancing and SoC change of the bus journey with the lowest average power

The simulation showed similar results in terms of power balancing with the bus journey with the lowest average power. By aligning the SoC change and power change, it can be seen the SoC increases at the same rate whenever the bus is stationary. This is because the output from the FC and boost converter being used to charge the SC when the bus is stationary. The SC attained a maximum SoC of 82.7% and a minimum SoC of 26.8%. It was also found that the final SoC is 61.2% indicating the SC discharged by 21% throughout this driving cycle. The average discharge efficiency has been calculated to be 90.3%. The average charge efficiency has been found to be 78.2%. It can be seen that the bus journey with the lowest average power has overall lower charge and discharge efficiency, particularly for charging operations. This reflects the discussion carried out previously (Figure 6.9) where it was found the charge efficiency is lower with lower power and higher with higher power. Additionally, the effectiveness of regenerative braking is reduced under low speed operations due to the more frequent requirement of mechanical braking.

Simulation with longer bus journey

The degrees of hybridisation for the bus journey having highest average power and lowest average power have been identified and showed to work as expected. The method to calculate the degree of hybridisation based on power profile has been verified by the computer model. The proposed operating degrees of hybridisation for the journey with highest average power and lowest average power showed very different results. It was found the power profile played an important role in determining the required degree of hybridisation of a selected driving cycle. The identified degree of hybridisation can only be considered as an appropriate degree for the specific driving cycle. Taking the 24 hour driving cycle data of route 388 as example, the different route power profile will result in different required FC and boost converter output power and SC size for every individual bus journey. One consideration would be to use the entire power profile to determine the required degree of hybridisation following the same procedure. However, the computer used for simulation was unable to perform the processing of the entire day's power profile due to processor limitation. Instead, the simulation was carried out using the power profile of the first 135 minutes (within the period 05:40-07:55) of the 24 hour bus data. The reason for selecting the first 135 minutes of the profile is because it includes three completed bus journeys with various power ranges. The parameters of the selected profiles have been summarised in Table 6.3.

Table 6.3 First 135 minutes of route 388 24 hour bus profile parameters

Bus journey	Frist journey	Second journey	Third journey	All three journey
Time	05:40-06:20	06:38-07:10	07:13-07:55	05:40-07:55
Duration	40 minutes	32 minutes	42 minutes	135 minutes
Driving condition	Minimum traffic and light load	Light traffic and heavy load	Heavy traffic and heavy load	Overall
Average power	9.23 kW	16.03 kW	7.94 kW	10.70 kW
Required FC an boost converter output power	10.15 kW	17.63 kW	8.73 kW	11.77 kW
Required SC size	52 F (1.66 kWh)	65 F (2.08 kWh)	50 F (1.6 kWh)	124 F (3.97 kWh)
Proposed operating degree of hybridisation	10.15 kW FC and boost converter / 1.66 kWh SC	17.63 kW FC and boost converter / 2.08 kWh SC	8.73 kW FC and boost converter / 1.6 kWh SC	11.77 kW FC and boost converter / 3.97 kWh

As the table shows, the proposed degree of hybridisation can also be worked out using the power profile. It can be seen the SC size has been significantly increased in order to run all three bus journeys. The 135 minute power profile has been tested with the proposed overall degree of hybridisation. Please note the driver break time between each completed bus journey was excluded from the power profile used for simulation because the bus is normally powered down in those periods. This is the reason the simulation duration was 6500 s instead of the 8100 s (135 minutes). The recorded power profile and the FC/SC hybrid model simulation results in terms of power balancing have been plotted in Figure 6.28 and 6.29.

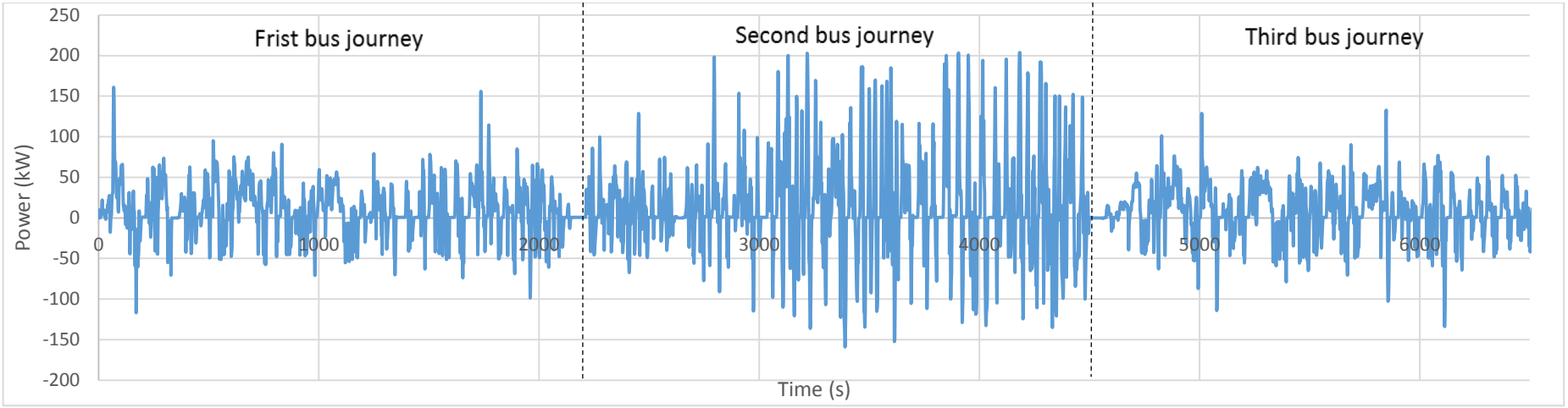

Figure 6.28 135 minutes bus power profile from the route 388 24 hour power profile

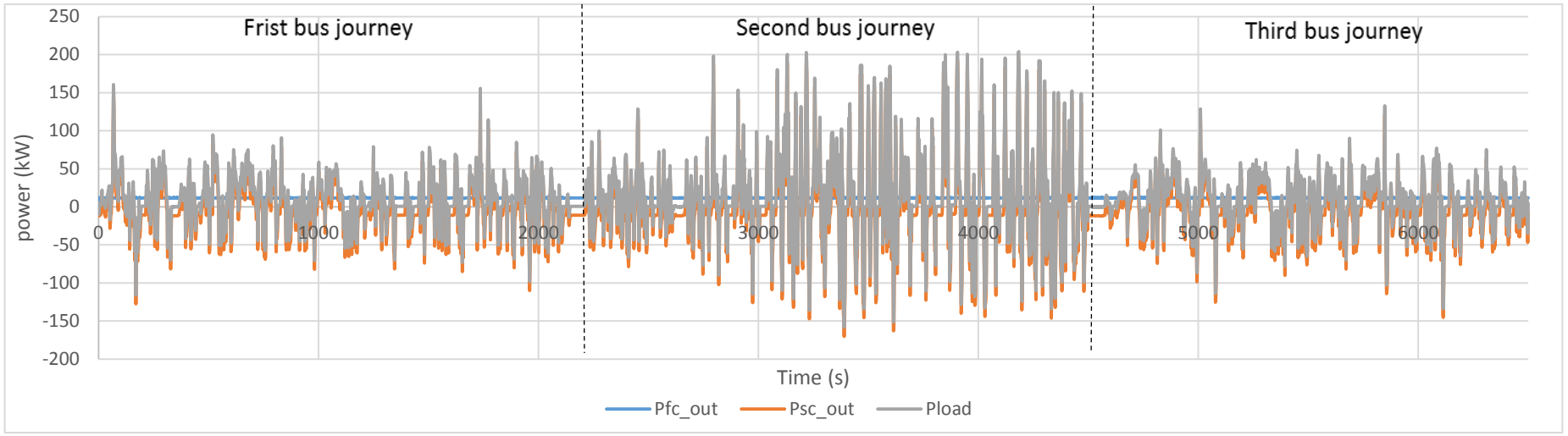

Figure 6.29 Simulated power balancing of 135 minutes bus profile from the route 388 24 hour power profile

As Figure 6.29 shows, the FC/SC hybrid mode managed to meet the 135 minutes bus power profile while keeping the FC output constant. The power balancing functioned as expected. The SoC change throughout the driving cycle has been plotted in Figure 6.30.

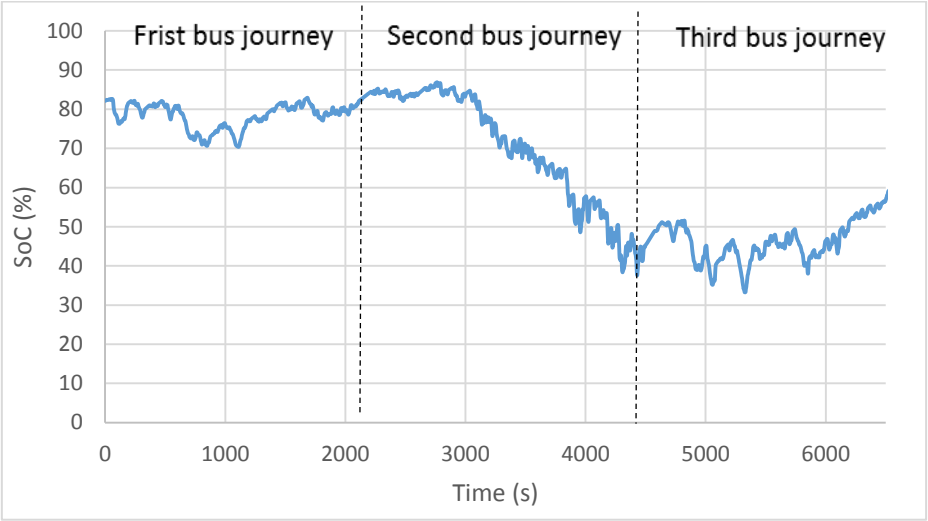

Figure 6.30 SoC change of 135 minutes bus profile from the route 388 24 hour power profile

The SC SoC discharged from 82.2% to 55.6% after the 135 minutes driving cycle. The average power of the 135 minutes is 10.7 kW which equates to an 11.77 kW FC and boost converter output reference for the model. The discharged SC suggested the 10% increase of the FC and boost converter output reference was still unable to compensate for the charge and discharge loss. To investigate the relationship between SoC change and efficiency, the results obtained from previously tested driving cycles have been summarised in Table 6.4.

Table 6.4 Parameter summary of previous tests

Driving cycle	Highest average power journey	Lowest average power journey	Three completed combined journey
Duration	31 minutes	50 minutes	135 minutes
Route average power	16.03 kW	5.65 kW	10.7 kW
Initial SoC	82.2 %	82.2 %	82.2 %
Final SoC	74.8%	61.2 %	55.6 %
Discharged	7.4 %	21 %	26.6%
Average charge efficiency	87.6%	78.2 %	86.6 %
Average discharge efficiency	93.3%	90.3 %	90.8 %
Total energy provided by FC	37,907,368 J	22,168,597 J	78,254,199 J
Total energy provided by SC	502,410 J (discharge)	2,251,418 J (discharge)	7,754,859 J (discharge)
Extra reference increase (in addition to the 10% increase)	1.32 %	10.2 %	9.91 %

In the constant FC output control strategy, the FC output has been kept constant throughout all the tested journeys while using the SC to meet the variable power demands. As the table shows, the longer the driving cycle is, the lower the final SoC has become. This indicates the 10% increased FC and boost converter output was not sufficient to compensate for the efficiency loss. The SoC kept decreasing throughout the driving cycle which is why it becomes more significant in longer runs. The total energy provided by the FC and the SC have also been calculated in the table. In order to keep the final SoC the same as the initial SoC, the net energy delivered by the SC should be zero because of the charge and discharge. As a result, the energy provided by the SC showed in the table is the amount of energy that needs to be provided by the FC as well. This suggests a further increase to the FC and boost converter output reference is required. The extra reference increase shown in the table indicates the magnitude of the additional increase required from the reference. As can be seen they differ depending on the driving cycle. A further increase in the FC output by 1% will not be able to keep the SoC the same for the lowest average power journey and the three completed journeys. A further increase in the FC output by 10% will approximately keep the SoC the same for the lowest average power journey and the three completed journeys, but consequently will overcharge the SC for the highest average power journey. Therefore, it can be seen the exact amount of energy increase required on the FC and boost converter output reference varies depending on the driving cycle.

6.3.6 Discussion on degree of hybridisation identification

The previous sections showed the operation of a FC/SC hybrid propulsion system against actual driving cycles using the computer model. The operational strategy showed the FC output can be kept at near constant while using the SC to satisfy the dynamic load. A strategy to identify the FC and boost converter output power and required SC size has been proposed and has been shown to perform as expected. In principle, the FC and boost converter output only needs to provide constant output power equal to the average power of the driving cycle. It was found this can only be true if the SC charge and discharge efficiency was 100%, which is scientifically impossible. As a result, an estimated 10% increase to the FC and boost converter output has been applied to compensate for the charge and discharge losses. The 10% increase in FC and boost converter output reference could only partially compensate for the efficiency losses. The exact percentage increase to the FC and boost converter output reference is dependent on the power profile of the driving cycle. This is because the charge and discharge efficiency varies with the power magnitude as well. This highlights a limitation of the proposed FC/SC operation strategy. The exact magnitude required of the FC and boost converter output reference cannot be accurately determined because of the variation in charge and discharge efficiency. A number of points have been addressed regarding this limitation.

First, to overcome this limitation, the entire driving cycle needs to be simulated to calculate the required FC and boost converter output. The calculated FC and boost converter output reference needs to be capable of both meeting the load demand and compensating for the charge and discharge efficiency loss. To determine the reference output, a large amount of driving cycle data needs to be tested in the model and the power requirement for the route also needs to be known in advance. This requires more time and resources to process and collect driving cycle data.

Second, it can be seen the SoC keeps reducing with the proposed FC and boost converter output in the 135 minutes driving cycle tests. The FC and boost converter output reference needs to be increased by a certain percentage to prevent the SC being depleted. However, the increased FC and boost converter output reference will probably overcharge the SC during lower power driving cycles (such as the lowest average power journey). As a result, in order to prevent overcharge during lower power driving cycles and undercharge during higher power driving cycles, the SC size also needs to be significantly increased.

Third, even if the exact FC and boost converter output reference can be identified after simulating the entire driving cycle and the SC size has been increased to keep the SoC within operational range, the model has only been shown to be operational with the tested driving cycle. The route condition could vary dependent on many factors such as traffic, weather, driver characteristic, passenger loading etc. The degree of hybridisation sized by this method would reduce the flexibility of the bus as it has only been tested on particular driving cycles. In order to be able to deal with possible worst case scenarios, the SC would have to be significantly increased to be able to deal with what may be a rarely occurring situation.

These three points lead to another question: Is it best practice to maintain the FC and boost converter power output predefined and constant throughout the entire journey? This question will be further explored in the next section.

6.4 FC/SC operation strategy optimisation

6.4.1 Optimisation strategy

To investigate the FC/SC operation strategy, a driving cycle including both high and low power operations has been selected. The driving cycle was on a specific bus operation. The bus was taken to a UCL assigned route on 20th March 2015 for research purposes. The UCL assigned route was a 30 minutes route with appreciable gradients (London Highgate hill). The bus was not in service during the assigned route, hence there were no bus stops or variation in passenger load. The power profile of the UCL assigned route will be denoted as the **high gradient profile** throughout the following analysis. The power profile of the high gradient profile has been plotted in Figure 6.31. It must be noted that the variation in passenger load will have an impact on the power demands. A fully loaded bus will have significantly larger power demands than a lightly loaded bus in the high gradient profile. The effect of passenger load also need to be investigated as a possible worst case scenario study as part of future work.

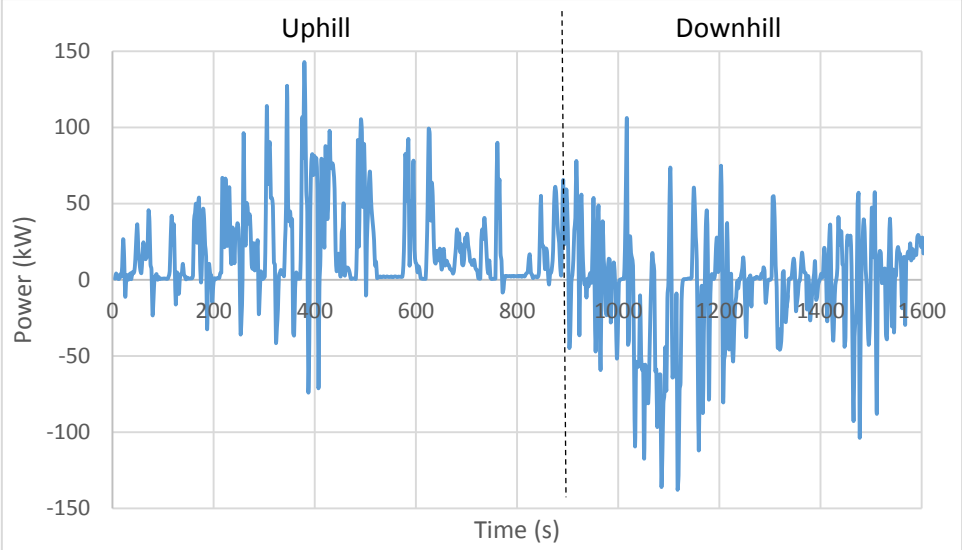

Figure 6.31 Power profile of the high gradient profile

As the power profile shows, there was a clear uphill section and a downhill section. The logger was turned on after the start of the uphill section and turned off after the downhill run had been completed. The average power of the uphill section (0-900 s) was 20.6 kW and the average power of the downhill section (900-1603 s) was -3.38 kW and the overall average power of the high gradient profile is 8.53 kW. As it can be seen, the high gradient profile includes two very different bus power profiles where one is mainly uphill and the other is mainly downhill.

The same degree of hybridisation identification strategy was carried out for the high gradient profile. The same 10% increase on the FC and boost converter output reference has been used. Since the high gradient profile average is 8.53 kW, the FC and boost converter output reference would be 9.38 kW. The required SC size has been calculated to be 3.58 kWh which gives a 134 F with a 20% compensation increase. The simulation has been carried out with the proposed degree of hybridisation. However, it was found the SoC of the SC reached zero before it entered the start of the downhill section. After a series of tests with the same FC and boost converter reference while increasing the SC size, it was found the SC would need to be 165 F to achieve this driving cycle. The power balancing and SoC change of the high gradient profile have been plotted in Figure 6.32 and 6.33. The same parameter name was used as previous simulations.

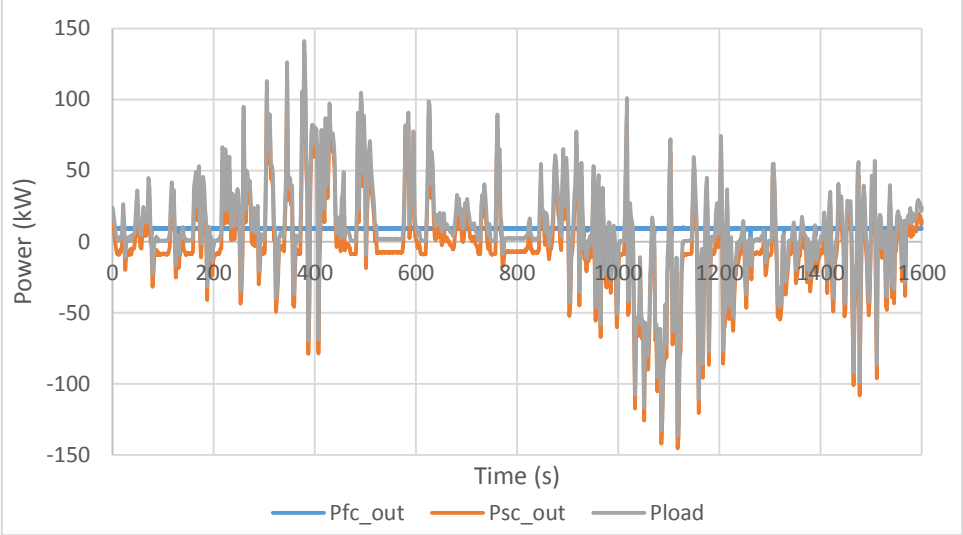

Figure 6.32 Power balancing of the high gradient profile

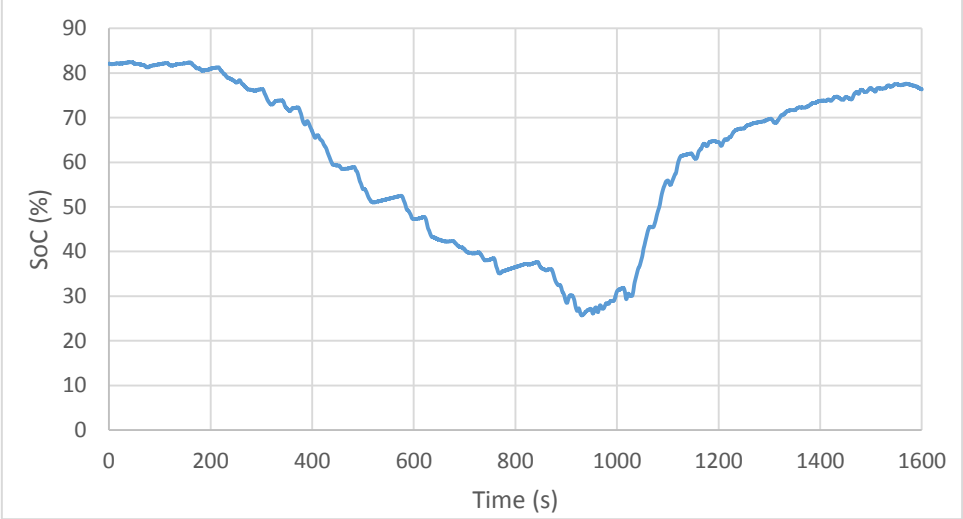

Figure 6.33 SoC change of the high gradient profile

As the SoC figure shows, the SoC clearly decreased during the uphill section and increased during the downhill section. The SoC decreased to 25.8% at 933s even with the 165 F SC. The theoretical calculation (cumulative energy calculation method) showed the bus can operate with a 134 F SC. There are two reasons for the requirement of the larger SC (165 F). One is because the charge and discharge efficiency will cause the SoC to reduce even lower with the 134 F SC. The other is the theoretical calculation assumes the SoC can deliver the desired output at any SoC. However, practically, the buck/boost converter will struggle to maintain the output if the SC voltage is too low. The SoC with the 165 F SC dropped to less than 30% from 902s to 1017s. The previous tests showed the buck/boost converter was unable to operate if the SC SoC was less than 20 to 25%. As a result the SC storage capacity would need to be increased even further than the calculated result to perform as required over the high gradient profile.

The FC and boost converter output reference has been kept constant at the 1.1 times the high gradient profile average power, as Figure 6.32 shows. The SC size has been increased to prevent undercharge during the uphill section and overcharge during the downhill section. As discussed before, the average power of the uphill section is 20.6 kW and the downhill section is -3.38 kW. In the uphill and downhill sections, the SoC would not easily recover to be within the operational range because the FC output is set to be constant. One consideration is to increase the FC and boost converter output reference when the bus is going uphill and decrease it when the bus is going downhill. To achieve this a control system needs to be designed to adjust the FC and boost converter output reference. Since the main purpose of adjusting the FC and boost converter output reference is to keep the SC SoC within the operational range, the control system can be designed by developing a relationship between FC and boost converter output reference and the real time SoC. A number of criteria for the FC variation control system can be addressed based on the previous tests.

1. A 30% lower limit has been defined for the SC SoC to prevent undercharge.
2. A 90% upper limit has been defined for the SC SoC to prevent overcharge.
3. The FC and boost converter output should be adjusted by ramped change response. Small ramp change is preferred for FCs because FCs are not designed for fast transient changes.
4. A maximum FC and boost converter output limit should be defined. Since the FC used for the model is an 85 kW FC and the boost converter efficiency averages at 90%, the FC and boost converter output reference power must be less than 76 kW (Ifc_out=120 A).
5. A minimum FC and boost converter output limit should be defined because turning off the FC in the middle of bus operation is not preferable. A 0.63 kW minimum output power needs to be defined to always keep the 1 A output from the FC and boost converter output.

Based on the above criteria, two equations for overcharge protection and undercharge protection has been developed.

Overcharge protection design

The calculation for overcharge protection has been carried out using the equation:

$$Ifout\_out\_new = \frac{1}{1 - higher\ threshold} \times (1 - SOC) \times Ifc\_out \quad (6\text{-}4)$$

The idea is to calculate a new Ifc_out reference (and thus a new Pfc_out) based on the SoC of the SC. The higher threshold of the overcharge protection has been selected to be 90% SoC (fractional calculation in equation).

$$Ifout\_out\_new = \frac{1}{1 - 0.9} \times (1 - SOC) \times Ifc\_out$$

$$Ifout\_out\_new = 10 \times (1 - SOC) \times Ifc\_out$$

Since the Ifc_out is defined by the route average power, the new Ifc_out calculated will be a decreased value. The reduced Ifc_out will not only reduce the charging rate to the SC during charge operation, but also increase the discharging requirement from the SC during discharge operation. The higher the SoC becomes, the smaller the new Ifc_out will be to prevent overcharge. Table 6.5 shows some examples of Ifc_out and the adjusted value of the new Ifc_out based on SoC for overcharge protection.

Table 6.5 Overcharge protection of the FC variation strategy

SoC (%)	Ifc_out (A)	Ifc_out_new (A)	Ifc_out (A)	Ifc_out_new (A)	Ifc_out (A)	Ifc_out_new (A)
90	15	15	32	32	84	84
91	15	13.5	32	28.8	84	75.6
92	15	12	32	25.6	84	67.2
93	15	10.5	32	22.4	84	58.8
94	15	9	32	19.2	84	50.4
95	15	7.5	32	16	84	42
96	15	6	32	12.8	84	33.6
97	15	4.5	32	9.6	84	25.2
98	15	3	32	6.4	84	16.8
99	15	1.5	32	3.2	84	8.4
100	15	1 (saturation)	32	1 (saturation)	84	1 (saturation)

A saturation current has added to maintain the minimum FC and boost converter output reference current at 1A. Limiting large transient power changes on the FC has also been proven to be very important in Chapter 4. Since the new current reference values are calculated and changed in steps, a rate limiter has been added to control the severity of even the ramp changes. The rate limiter has been set up to have a limited rising and dropping slew rate. The slew rate limits the maximum rate of increase or decrease of FC output power. It takes at least 30s at a constant rate to increase from

no load power (0 kW) to full load power (85 kW) and vice versa for decreasing. This is used to limit any large step changes for the FC.

Undercharge protection design

The calculation for undercharge protection has been carried out using the equation:

$$Ifc\_out\_new = Ifc\_out + \frac{120 - Ifc\_out}{(lower\ threshold \times 100) - 30} \times 100 \times (lower\ threshold - SOC) \quad (6\text{-}5)$$

The 120 A in the equation is the maximum output current the FC and boost converter can provide which is 76 kW maximum power. Unlike the overcharge protection design, the lower threshold of the undercharge protection cannot be the same as the lower limit of the SoC (30%). The previous tests showed the buck/boost converter failed to operate when the SoC drops below 30%. As a result, the lower threshold needs to be higher than the lower limit 30%. The lower threshold has been defined to be 50%.

$$Ifc\_out\_new = Ifc\_out + \frac{120 - Ifc\_out}{(0.5 \times 100) - 30} \times 100 \times (0.5 - SOC)$$

$$Ifc\_out\_new = Ifc\_out + (120 - Ifc\_out) \times 5 \times (0.5 - SOC)$$

The new Ifc_out will be increased based on the SoC. An increased Ifc_out will charge the SC at a higher rate and also reduce the power demand placed on the SC during discharge to satisfy the bus propulsion load. Table 6.6 gives some examples of Ifc_out and the adjusted value of the new Ifc_out based on SoC for undercharge protection.

Table 6.6 Undercharge protection of the FC variation strategy

SoC (%)	Ifc_out (A)	Ifc_out_new (A)	Ifc_out (A)	Ifc_out_new (A)	Ifc_out (A)	Ifc_out_new (A)
50	15	15	32	32	84	84
49	15	20.25	32	36.4	84	85.8
48	15	25.5	32	40.8	84	87.6
47	15	30.75	32	45.2	84	89.4
46	15	36	32	49.6	84	91.2
45	15	41.25	32	54	84	93
44	15	46.5	32	58.4	84	94.8
43	15	51.75	32	62.8	84	96.6
42	15	57	32	67.2	84	98.4
41	15	62.25	32	71.6	84	100.2
40	15	67.5	32	76	84	102
39	15	72.75	32	80.4	84	103.8
38	15	78	32	84.8	84	105.6
37	15	83.25	32	89.2	84	107.4
36	15	88.5	32	93.6	84	109.2
35	15	93.75	32	98	84	111
34	15	99	32	102.4	84	112.8
33	15	104.25	32	106.8	84	114.6
32	15	109.5	32	111.2	84	116.4
31	15	114.75	32	115.6	84	118.2
30	15	120 (saturation)	32	120 (saturation)	84	120 (saturation)

As Table 6.6 shows, the new Ifc_out will be increased by an amount determined by the SoC until Ifc_out reaches the maximum value of 120 A. A rate limiter has also been added to ensure the FC output changes in a ramped fashion and not be step change.

Using this method of undercharge protection and overcharge protection provides a different method to operate the FC and SC so this will be denoted as the FC variation strategy hereafter. The FC/SC model with the FC variation strategy will be able to adjust the FC output power based on the SoC which varies with power profiles. The same high gradient profile (still with the 165 F SC) has been tested again with the model with the FC variation strategy. The power balancing has been plotted in Figure 34.

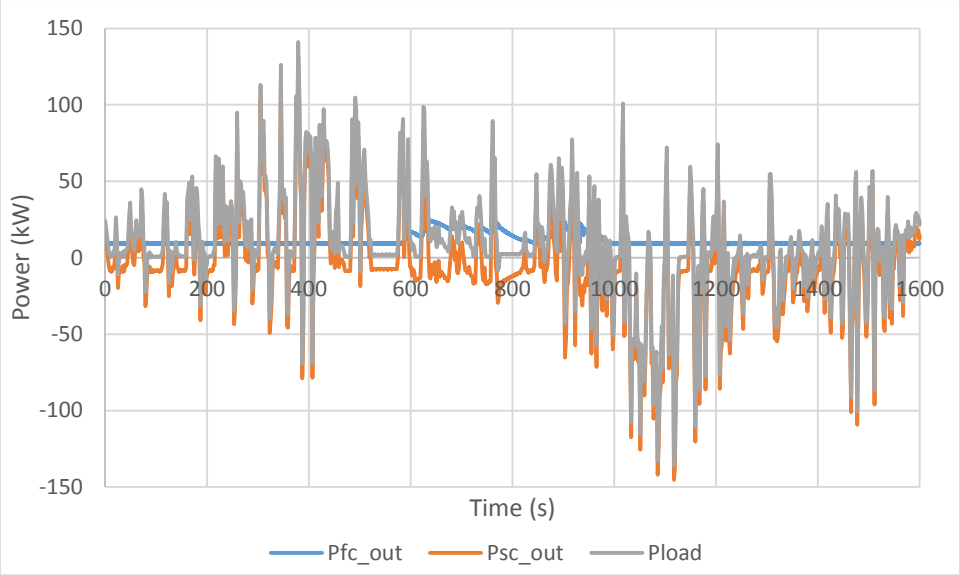

Figure 6.34 Power balancing of the high gradient profile with the FC variation strategy

The results show the FC and boost converter output increased from approximately 600 s to 1000 s. It can be seen the power difference between the Psc_out and Pload has increased because of the increased Pfc_out. To better observe how the variation of Pfc_out affect the SoC, these two parameters have been plotted in Figure 6.35.

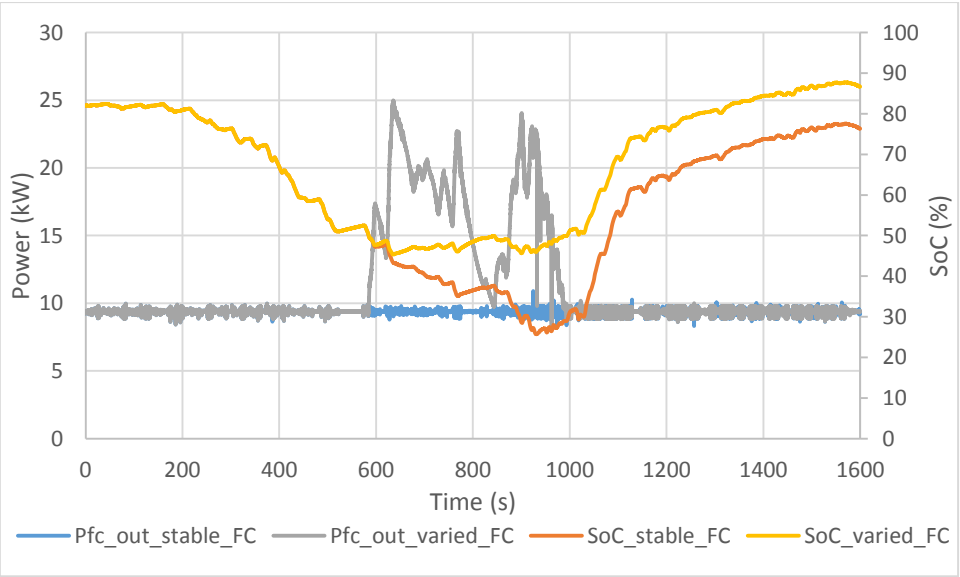

Figure 6.35 SoC change of the high gradient profile with the FC variation strategy

The SoC change in the system with and without the FC variation strategy is identical until the SC is depleted to a certain level. It can be seen the FC and boost converter power ramps up as soon as the SoC reaches the 50% lower threshold. The lower the SoC becomes, the higher the FC and boost converter reference. The system with the FC variation strategy prevents the SoC reaching the 30% lower limit during uphill

section. The final SoC after the high gradient profile of the model with the FC variation strategy is higher than the model without this strategy applied due to increase of the FC and boost converter output power. It can be seen the SC was discharged to below the lower desired limit after the high gradient profile for the model without the FC variation strategy while the SoC remained above the level of effective operation of the buck/boost converter for the model with the strategy applied. Energy delivered throughout the high gradient profile for the FC and the SC have been calculated to investigate the difference between the models with and without the FC variation strategy. Hydrogen consumption has also been calculated based on the energy delivered. However, as discussed before, the hydrogen flow of the full scale model was not validated. As a result, the hydrogen flow can only be estimated based on a scaling up of the validated scaled FC model. The results have been summarised in table 6.7.

Table 6.7 Difference between the model with and without the FC variation strategy

High gradient profile	Model without the FC variation strategy	Model with the FC variation strategy
Initial SoC	82.2%	82.2%
Final SoC	76.4%	86.7 %
SC size	165 F	165 F
Lowest SoC	25.9 %	45.3 %
Duration of constant FC output	1600 s	1200 s
Energy delivered by the FC	15,494,164 J	18,688,967 J
Hydrogen used	0.277 kg	0.321 kg
Energy delivered by the SC	1,636,963 J (Discharge)	-1,426,254 J (Charge)
Total energy delivered to meet the load demand	17,131,127 J	17,262,713 J
Percentage of total energy delivered	100%	100.77%

Based on the energy calculation, it can be found the difference of total energy delivered to meet the high gradient profile power profile between the model with and without the FC variation strategy is reasonably small (0.77%). It can be seen that the inclusion of the FC variation strategy prevented the SC SoC dropping below the lower limit (30%) with a corresponding variation in the FC power output for 25% of the journey time for the high gradient profile.

Discussion regarding the FC variation strategy

The FC variation strategy has been shown to be capable of adjusting the FC and boost converter output based on SoC control when applied to a particular driving cycle. The previous sections identified the limitations of the initial proposed strategy, which was to always keep the FC output constant throughout the driving cycle. The inclusion of the FC variation strategy can potentially eliminate or mitigate the impact caused by those limitations.

The first limitation identified was the requirement to test and examine through simulation of the entire driving cycle in advance to identify an optimised FC and boost converter output reference. The inclusion of the FC variation strategy can adjust the FC and boost converter output reference in real time. The need for the final SoC to be the same as, or nearly equal to, the initial SoC is no longer as critical. Hence the requirement to identify the exact FC and boost converter output reference that is capable of meeting the load and compensating for the charge and discharge efficiency is eliminated. Setting the FC and boost converter output at 1.1 times the route average power can be used as the initial FC and boost converter output power reference. The FC variation strategy will determine the required change to the reference based on the SoC in real time.

The second limitation that was identified is the need for the SC size to be significantly increased to prevent the SC being overcharged for lower power operations or undercharged during higher power operations. The ability to adjust FC and boost converter output power can effectively prevent overcharge and undercharge. Additionally, the calculated SC size can potentially even be reduced with the FC variation strategy.

The third limitation identified is the lack of ability to respond to worst case scenarios. The inclusion of the FC variation strategy can adjust the output reference in real time depending on the current driving cycle. This brings significantly more flexibility for the bus operation which is a very important practical requirement for buses. It can be seen the inclusion of the FC variation strategy adds more practical value to the FC/SC hybrid model compared with the initial operation strategy of keeping the FC output constant.

6.4.2 FC variation strategy optimisation

It has been found that integrating the FC variation strategy with the FC/SC hybrid model would make the operation strategy more viable. This section aims to investigate a number of parameters in order to optimise the strategy.

Effect of SC size on the FC variation strategy

All the high gradient profile tests were carried out using a 165 F SC. The SC size was initially selected to keep the model without the FC variation strategy performing as determined in the earlier tests with constant FC and boost converter output. As discussed previously, the inclusion of the FC variation system could reduce the size of the SC required. This section investigates the effect of the high gradient profile on SC capacity selection. The same high gradient power profile and initial FC and boost converter output reference will be applied while adjusting the SC size. Tests at SC capacitance values of 165 F, 145 F, 125 F and 105 F were performed. The FC and boost converter output power variation and SoC change have been plotted in Figure 6.36 and 6.37.

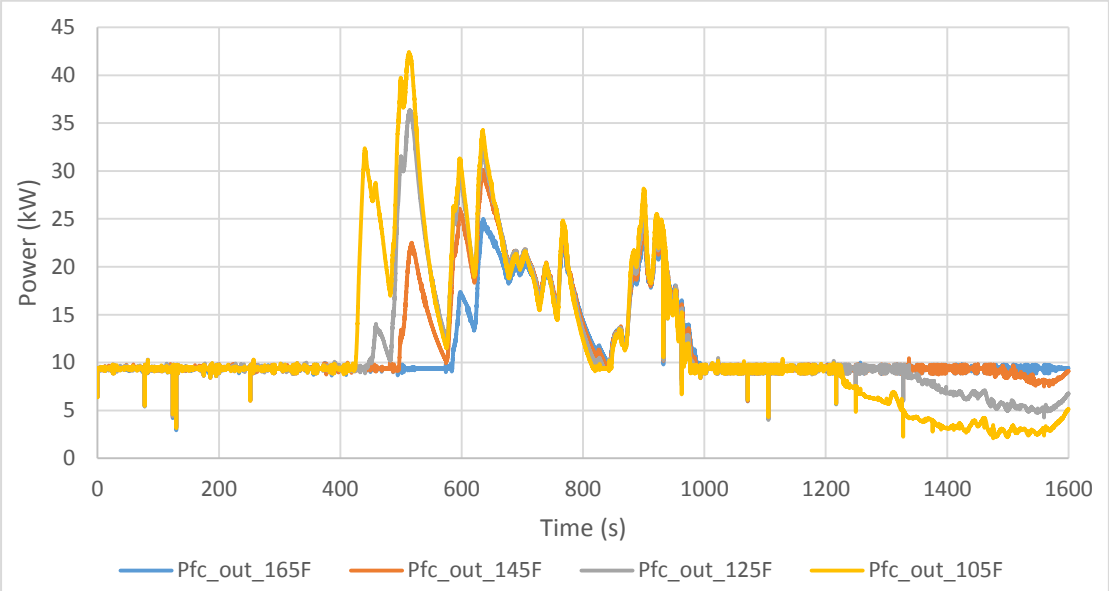

Figure 6.36 FC and boost converter output power with 165 F, 145 F, 125 F and 105 F SC of the high gradient profile

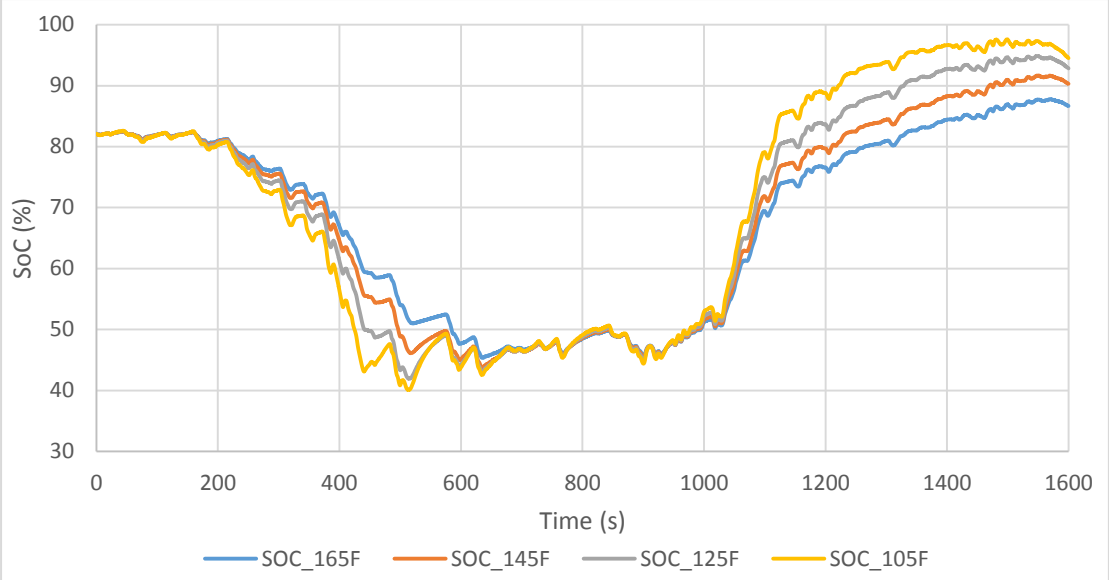

Figure 6.37 SoC change with 165 F, 145 F, 125 F and 105 F SC of the high gradient profile

As Figure 6.36 shows, the smaller the SC size becomes, the more pronounced the FC variation in terms of duration and magnitude. The increasing variation is because the SoC of a smaller SC will decrease at a faster rate which drives the requirement for modification of the new FC output from the initial base reference value. The FC and boost converter output power reduce after 1200 s to prevent overcharge. The 1200 s point coincides with the route changing from predominantly uphill to predominantly downhill. As expected, the SoC change plots showed the smaller the capacity of the SC, the quicker the SoC decreases or increases.

Tests with further SC size reduction have also been carried out. Tests at SC capacitance values of 85 F, 65 F, 45 F and 25 F were performed. The FC and boost converter output power reference and SoC change have been plotted in Figure 6.38 and 6.39.

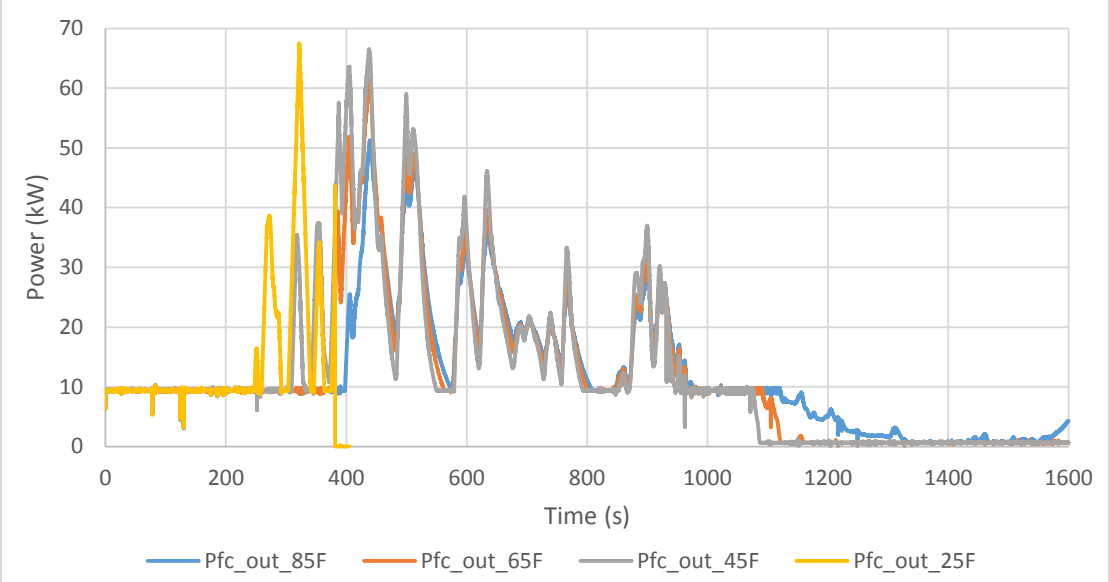

Figure 6.38 FC and boost converter output power with 85 F, 65 F, 45 F and 25 F SC of the high gradient profile

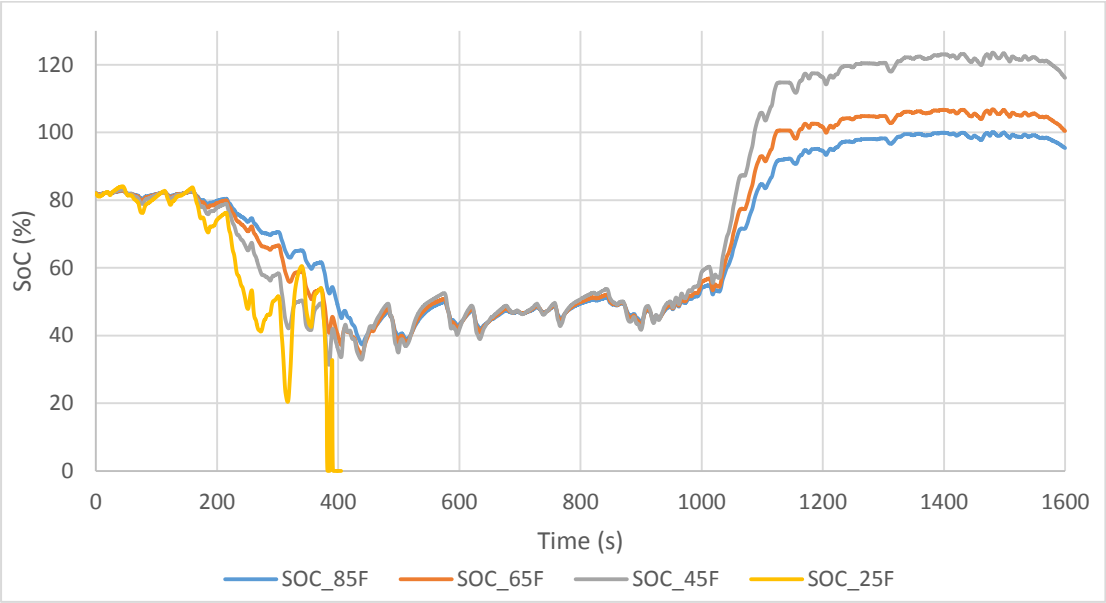

Figure 6.39 SoC change with 85 F, 65 F, 45 F and 25 F SC of the high gradient profile

As expected, the FC and boost converter output power vary more markedly as the SC size reduces. The simulation was terminated with the 25 F SC because the SC SoC dropped to zero which is below the lowest set limit. The inability of the FC to provide the power on its own once the SC is depleted emphasises the importance of including the FC variation strategy. When the SC capacitance is 25 F, the SC was unable to satisfy the discharge demand even with the FC at nearly full rated output at approximately 390s. The SC was unable to be charged back to operational range through with the FC and boost converter output reference increase quickly because the FC output was trying to satisfy the bus load and not resupply the SC. This indicates

the SC size can only be reduced up to a certain point. If the FC power rating is maintained at a constant value, the route requirement and dynamics govern the minimum capacity of the SC that can satisfy the load power demands. Also the SC was overcharged when the SC capacitance is 65 F, 45 F and 25 F. It can be seen the FC and boost converter has been reduced to the lower saturation value (0.63 kW). However, the SC was still charged during the downhill section of the bus even with the minimum FC output power because the charging is mainly from the regenerative braking in the downhill section.

It was found the SC size can be significantly reduced compared with the original 165 F SC with inclusion of the FC variation strategy. Reducing the SC size will consequently increase the rate and magnitude of the FC and boost converter output reference. It was also found there is a certain limit to which the SC size can be reduced. The total energy delivered by the FC and the SC have also been calculated with the SC sizes that were used in the tests. Calculation showed less than a 1% difference in terms of total energy delivered across the range of different SC sizes. For the high gradient profile, the smallest possible SC size that would allow the route to be traversed without overcharging the SC was found to be 85 F.

Effect of lower thresholds on the FC variation strategy

From the SC size reduction tests carried out, it can be seen that if the SC capacity was below a critical size, the SC may not have enough energy remaining to supplement the FC at the point when the FC variation strategy takes effect. One consideration is to arrange for the FC variation strategy to take effect at a higher SC SoC instead of only engaging when the SoC is reduced to 50%. As discussed in the undercharge and overcharge protection design section, there is a lower threshold to prevent the SoC being fully discharged and an upper threshold to prevent the SoC been overcharged. It was found the SC will be overcharged above the 90% upper threshold only if the SC size is reduced significantly for this particular load profile. Additionally, overcharge protection is not a major issue as simple system switching controls can avoid the SC being overcharged. An additional measure can be added to ensure that no regenerative energy is captured at high SoC. This can be achieved by adding a switch to dump the regenerative energy if required. At the end of a route or if the bus is at a stop for an extended period, the connection to the SC would have to be disconnected. Also, if the bus is on a long downhill run, the regeneration would also have to be disconnected and allow control through the mechanical brake only. As a result this section will focus on investigating the effect of lower thresholds.

Since the previous tests showed the buck/boost converter was unable to operate when the SC SoC drops below 25%, it is important to investigate the ability of the FC variation strategy to prevent the SoC dropping below the lower limit. The FC and boost converter output will start to increase once the SoC reaches the lower threshold. The previous tests of the high gradient profile utilised a 50% lower threshold. This section investigates the effect of changing the lower threshold on the system performance. The same high gradient profile and initial FC and boost converter output base reference setting will be used for tests using different lower threshold settings. The SC capacitance will also been kept constant at 85 F for these tests. A full list of FC and boost converter output reference values based on different lower thresholds for undercharge protection can be found in Appendix Q. Tests at lower thresholds of 40%, 50%, 60%, 70% and 80% were performed. The FC and boost converter output power and SoC change have been plotted in Figure 6.40 and 6.41.

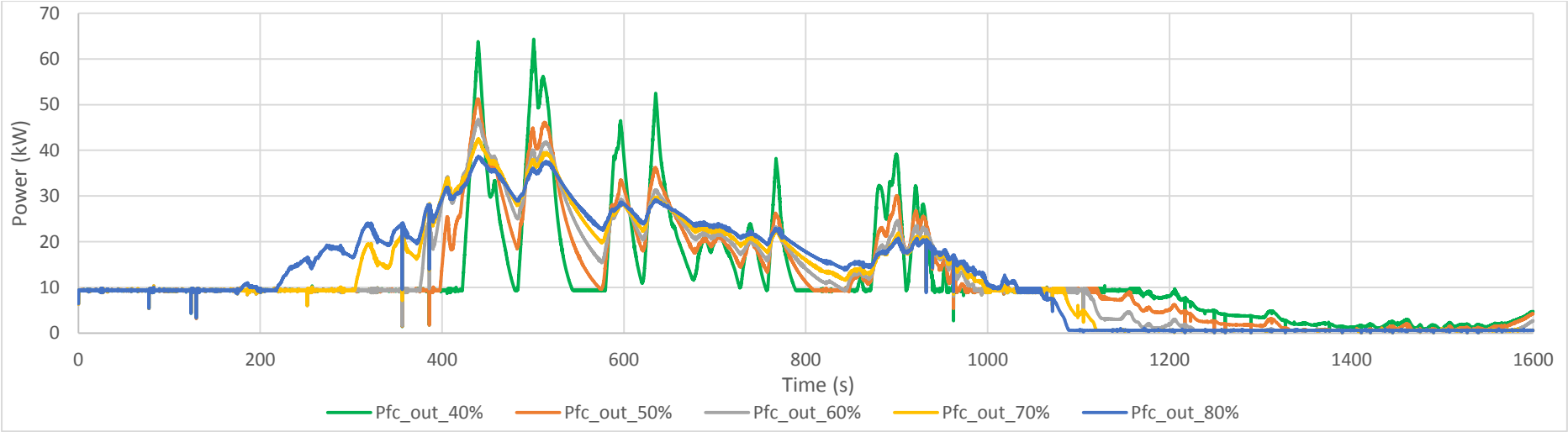

Figure 6.40 FC and boost converter output power change with different lower thresholds

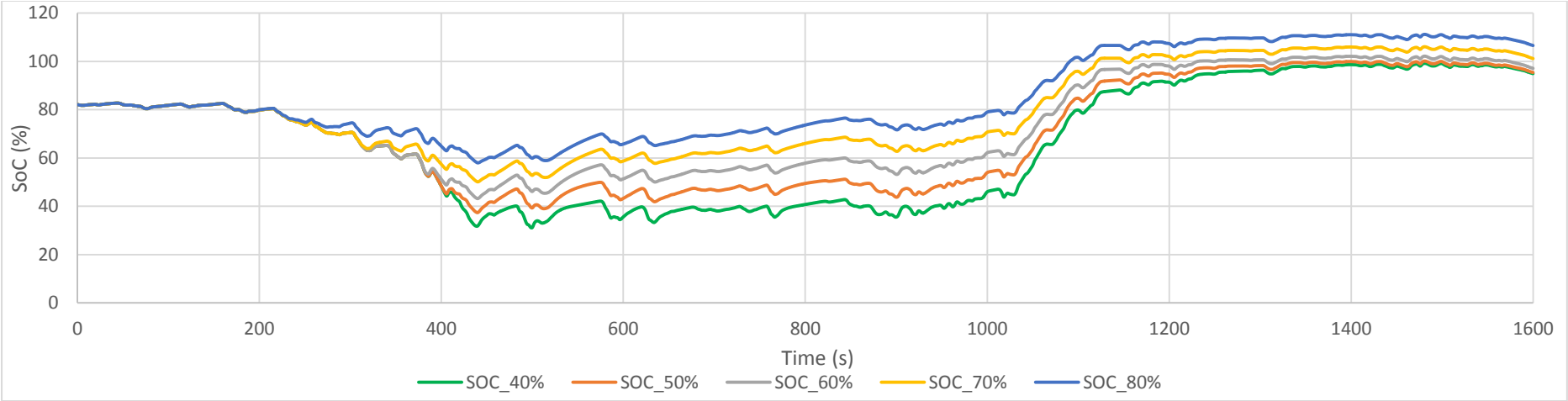

Figure 6.41 SoC change with different lower thresholds

For the 40% lower threshold test, it can be seen the FC and boost converter output reference was adjusted at 422 s when the SoC reached 40%. The reference was increased at a higher rate to quickly charge the SC to prevent the SoC reaching 30%. The reference decreased once the SoC was back to 40%. For the 80% lower threshold test, the FC and boost converter output reference was adjusted much earlier as expected. The reference started to increase at 176 s when the SoC reaches 80%. The rate of variation is much smaller compared with the 40% test.

It can be seen changing the lower threshold will affect the control of the FC and boost converter reference. The total energy delivered for each lower threshold test has also been calculated. The results showed the difference amongst the tests is less than 2%. The difference is mainly caused by the difference in charge and discharge efficiencies within the buck/boost converter operation as a result of the change in ratio of discharge to charge times, resulting from the different FC and boost converter output power once the variation strategy took effect. For the 40% and 50% lower threshold tests the FC and boost converter output needed to be increased at a higher rate to maintain the SoC. On the other hand, the 70% and 80% tests indicated lower rate of change to the reference but overcharged the SC (through this can be solved by adding a switch in practical system as discussed before). As a result, 60% is the most suitable lower threshold limit parameter for the high gradient profile case.

Effect of output saturation on the FC variation strategy

Based on the results obtained in the lower threshold tests, it can be seen the FC and boost converter output power has been varied at a fast rate even with the 60% lower threshold, particularly between 400 s and 600 s. This is because the reduced SoC demanded a higher FC and boost converter output reference as the designed algorithm too effect. For example, if a large load power is demanded due to a bus acceleration when the SoC is at the user defined lower threshold, then the SoC will drop quickly to meet this demand. Consequently the FC would also increase its output power for the reduced SoC. The SC will be charged back to the lower threshold again with the increased FC and boost converter reference. As a result, the FC and boost converter output power will be adjusted back to normal level again. Although the FC output slew rate has been limited by a rate limiter as discussed before, this type of fast “up and down” operation is still not recommended for the FC.

One consideration is to add a saturation on the FC and boost converter output power to prevent large magnitude variations in FC power. The high gradient profile was tested with the model with different saturation levels. The same initial FC and boost converter output base reference, SC size (85F) and the selected lower threshold (60%) were used for this test. Tests at FC and boost converter output current saturation of 40 A, 50 A, 60 A and 70 A were performed. The FC and boost converter output maximum power were limited to 25.2 kW, 31.5 kW, 37.8 kW and 44.1 kW correspondingly. The FC and boost converter output power and SoC change of these tests have been plotted in Figure 6.42 and 6.43.

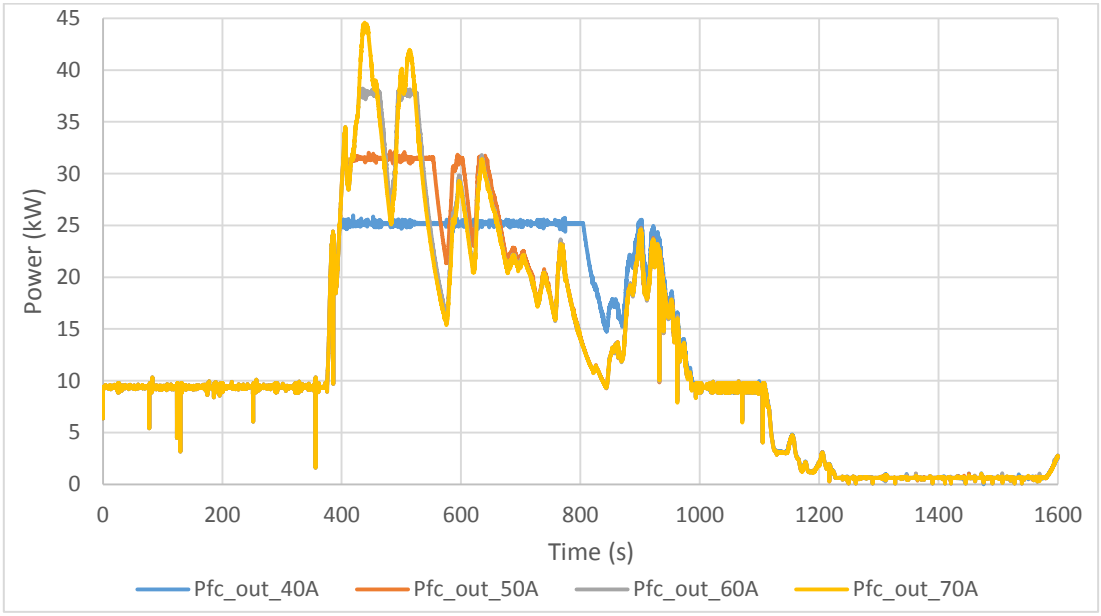

Figure 6.42 FC and boost converter output power change with different saturation level

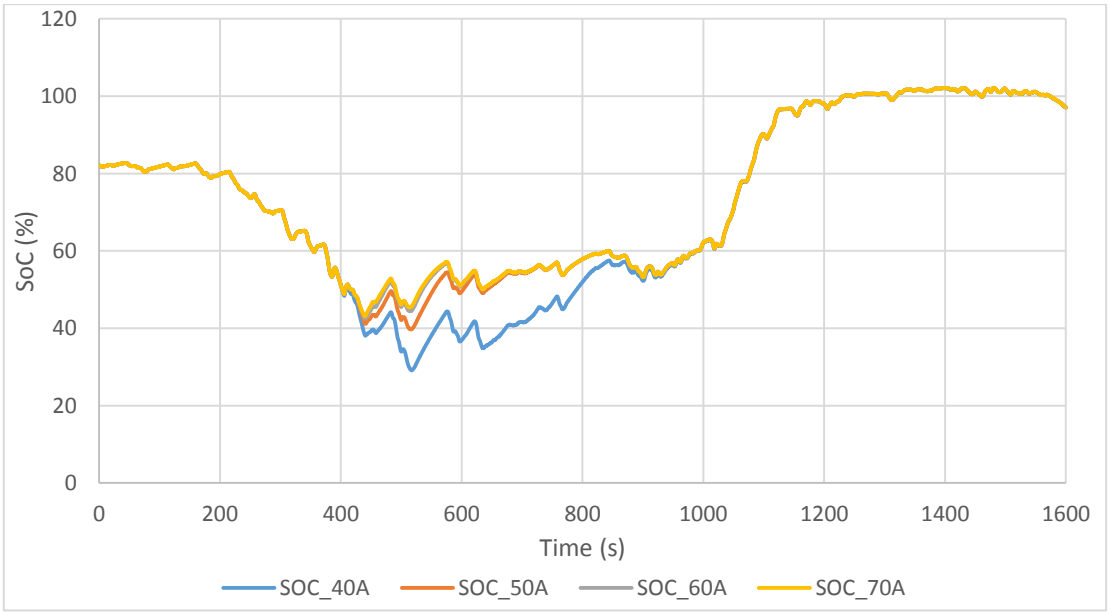

Figure 6.43 SoC change with different saturation level

It can be seen the saturation stopped the FC and boost converter output power going beyond the user defined saturation level. The 40 A saturation kept the output power at 25.2 kW for the longest period of time. The SoC for the 40 A case has the lowest overall value because of the lowest limit to the FC and boost converter output power. On the other hand, the power never reached the saturation limit for the 70 A case.

It can be seen the inclusion of a saturation limit on the FC and boost converter output can effectively limit larger variations in terms of magnitude. However, the required saturation level would be dependent on the power profile of the selected driving cycle. If the saturation level is too high, it would have no effect on controlling the FC output. On the other hand, if the saturation level is too low, it would reduce the ability to charge the SC adequately. It can be seen that the saturation level also needs to be adjusted based on the SoC. Hence an additional strategy to control the saturation limit based on the SoC has been added. The saturation limit has been selected to be 40 A when the SoC is more than 60%. The saturation limit will be 60 A when the SoC is 40%-60%. The saturation limit will be 120 A (peak power) when the SoC is less than 40%. This additional saturation limit control is independent of the undercharge protection calculation equation because it will only affect the maximum power limit. The inclusion of the additional saturation limit control can limit the FC and boost converter output peak while ensuring there is sufficient charging capability for the SC if required. The high gradient profile was tested again with all the identified parameters (85 F, 60% and saturation control). The FC and boost converter output power and SoC change have been plotted in Figure 6.44.

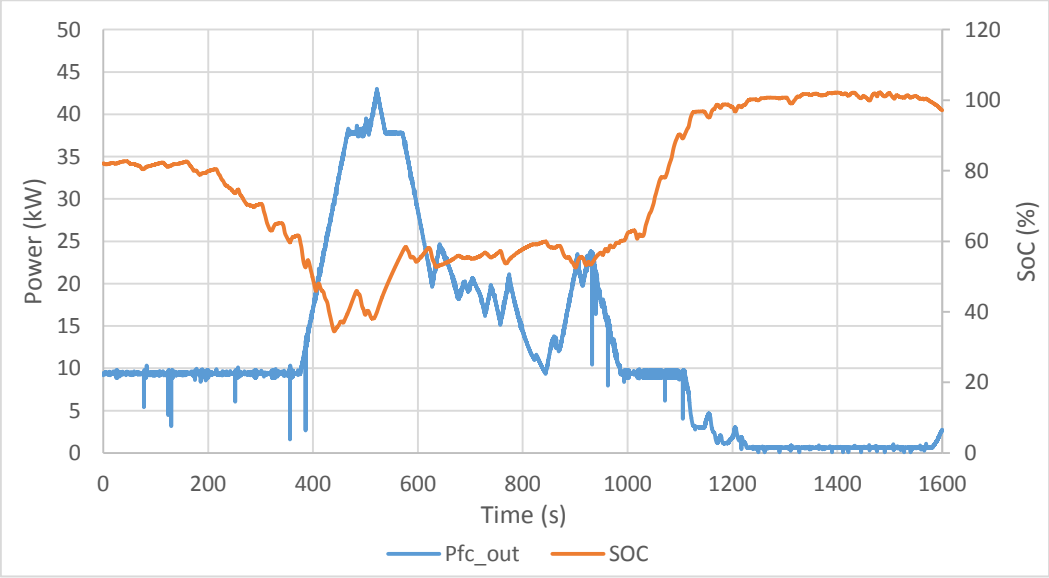

Figure 6.44 FC and boost converter output power and SoC change of the model with saturation control strategy

It can be seen the inclusion of a saturation control strategy limited the FC and boost converter output power between 460 s and 580 s. The saturation limit was increased from 60 A to 120 A between 506 s and 539 s. It can be seen the FC and boost converter output power variation can be reduced with the proposed saturation control strategy. Hence, with the optimised FC variation strategy, the degree of hybridisation for the high gradient route is 42.8 kW of the FC and boost converter output power / 2.72 kWh (85F) SC.

The previous sections investigated how to optimise the FC variation strategy and discussed the effect of varying a number of parameters. The SC size, lower threshold and a saturation limit control strategy have been found for the high gradient profile. It was found varying the SC size and lower threshold will have minor effect on the total energy delivery. Varying the SC size will affect the rate of charge and discharge of the SC SoC which also consequently affects the rate of variation on the FC output. The SC size can be reduced with the inclusion of the FC variation strategy. However, it can only be reduced to a certain minimum capacity beyond which the SC is simply too small. It was also found the smaller the SC size became, the more variation was observed in the FC output. Varying the lower threshold mainly affects the rate of variation, in terms of magnitude, of the FC reference. It will also influence the lowest SoC and highest SoC the SC will attain throughout the driving cycle. Finally, a saturation limit strategy was designed to limit the FC output variation.

6.5 Degree of hybridisation analysis

A strategy to identify a required degree of hybridisation for a certain driving cycle has been identified in section 6.3. The FC and boost converter output base reference power has been determined to be 1.1 times that of the route average power in the degree of hybridisation identification strategy. The required SC size can be determined by calculating the energy difference between the FC and boost converter output power and the load power profile. In section 6.3.5, three driving cycles were tested with the model without the FC variation strategy. The three driving cycles were completed bus routes with the highest average power (32 minutes), the lowest average power (50 minutes) and a longer driving cycle consisting of the first three completed bus journeys (135 minutes). All three tests showed the SoC decreased by the end of the driving cycle because the required constant FC and boost converter output reference had not been identified. The reducing SoC will eventually cause the SC to deplete resulting in the model failing to complete the journey as intended.

To overcome this failing, a FC variation strategy has been designed and optimised in section 6.4 to ensure the identified degree of hybridisation can satisfy the operational requirement under challenging dynamic loads. The previous tests in section 6.4 used the high gradient profile to design and optimise the FC variation strategy. It was found the inclusion of the FC variation strategy provides the facility to adjust the FC and boost converter output reference depending on the driving cycle. With the inclusion of the FC variation strategy, the FC and boost converter output reference does not need to be defined in advance. Hence even if the route power profile has not been given or the bus has been diverted to an unexpected route, the FC and boost converter output reference will adjust its output to meet the required demand. However, the reference identified by the 1.1 times route average power can still be used to define the initial FC and boost converter output as a base reference. The identified SC size has not only been shown to be capable of better controlling the SoC, but also showed potential to further reduce the SC size if required.

It can be seen that the degree of hybridisation identification strategy can also be used for the model with the FC variation strategy. To verify this point, the three driving cycles (driving cycle with the highest power, lowest power and three completed journeys) used in section 6.3.5 have been tested with the model with the FC variation strategy. Using the original parameters derived for the journeys will allow the examination of the model with the FC variation strategy. The results with and without the FC variation strategy have been compared and plotted in Figures 6.45 to 6.47.

Figure 6.45 FC and boost converter output power and SoC change of the highest average power bus journey with and without FC variation strategy

The bus journey with the highest average power used the initial FC and boost converter output power of 17.63 kW and a 2.08 kWh SC. It can be found the final SoC after the driving cycle is reasonably close to the initial SoC with the inclusion of the FC variation strategy at the same degree of hybridisation. It can be seen the FC and boost converter output reference has been reduced a number of times between 100 s and 500 s when the SoC reaches 90%. The FC and boost converter output reference has been increased multiple times as well to prevent undercharge tripped by the 60% threshold, particularly between 1200 s and 1380 s. The highest FC and boost converter output power is 31.5 kW throughout this 32 minute journey. The required FC power would be 35 kW with a 90% average boost converter efficiency. Hence the required degree of hybridisation for this high power journey with the highest average power would be 35 kW FC / 2.08 kWh SC.

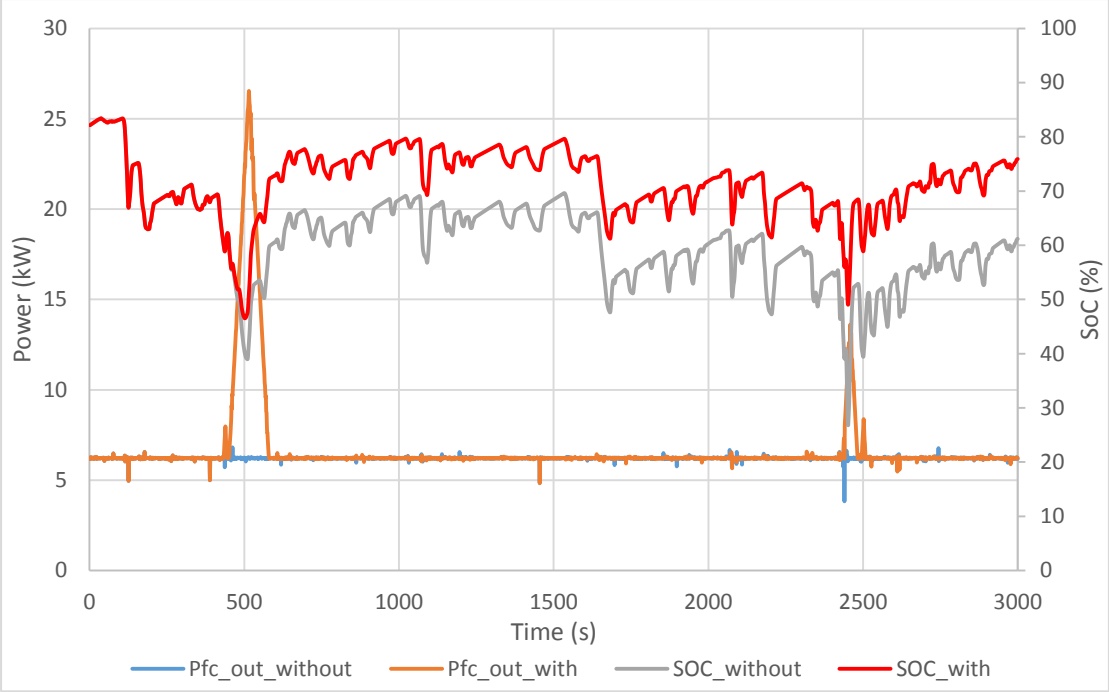

Figure 6.46 FC and boost converter output power and SoC change of the lowest average power bus journey with and without FC variation strategy

The bus journey with the lowest average power used the initial FC and boost converter output power of 6.22 kW and a 1.41 kWh SC. It can be seen the SoC was also maintained at a higher level with the FC variation strategy. The FC and boost converter output was adjusted depending on the SoC. The highest FC and boost converter output power is 26.2 kW which equates to a required FC output power of 29.1 kW with a 90% boost converter efficiency. Hence the required degree of hybridisation for this low power journey would be 29.1 kW FC / 1.41 kWh SC.

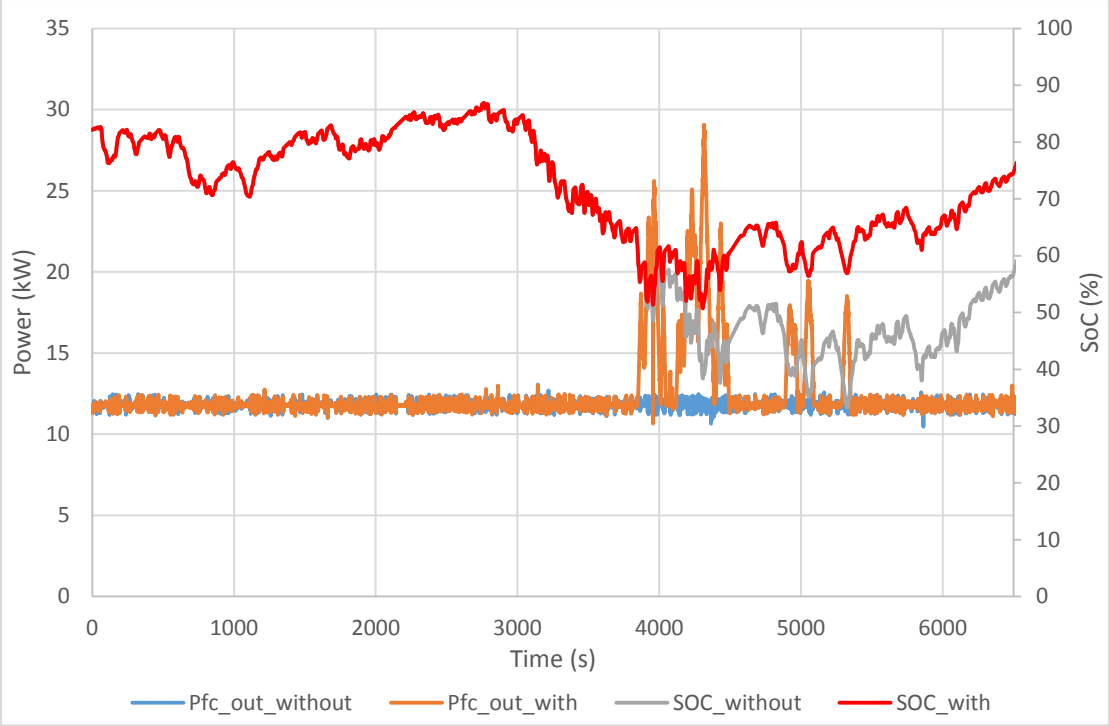

Figure 6.47 FC and boost converter output power and SoC change of the three combined bus journey with and without FC variation strategy

The driving cycle comprising three completed bus journeys used the initial FC and boost converter output power of 11.77 kW and a 3.97 kWh SC. As expected, the SoC change are identical for the model with and with the FC variation strategy until the SoC reaches the threshold value. The SoC was maintained at a higher level as expected. The FC and boost converter output power clearly increased during the second bus journey where higher power operations occurred. The peak power output of the FC and boost converter output power in this driving cycle is 28.7 kW which requires a 31.9 kW FC. Hence the required degree of hybridisation for this longer driving cycle is 31.9 kW FC / 3.97 kWh SC. It can be seen the calculated degrees of hybridisation for all three driving cycles functioned as expected with the inclusion of the FC variation strategy.

The strategy to identify the degree of hybridisation was validated against a number of driving cycles with the inclusion of the FC variation strategy. The model will be used to identify the required degree of hybridisation for the entire day of route 388. The average power of the entire day (without driver breaks) has been calculated to be 9.45 kW as Table 6.2 showed before. That gives the required initial FC and boost converter output power base reference as 10.39 kW. The required SC size has been calculated to be 505 F which has a 16.2 kWh stored energy. The model has been tested with the entire day's power profile (Figure 6.4). The FC and boost converter output power and

the SoC change have been plotted in Figure 6.48.

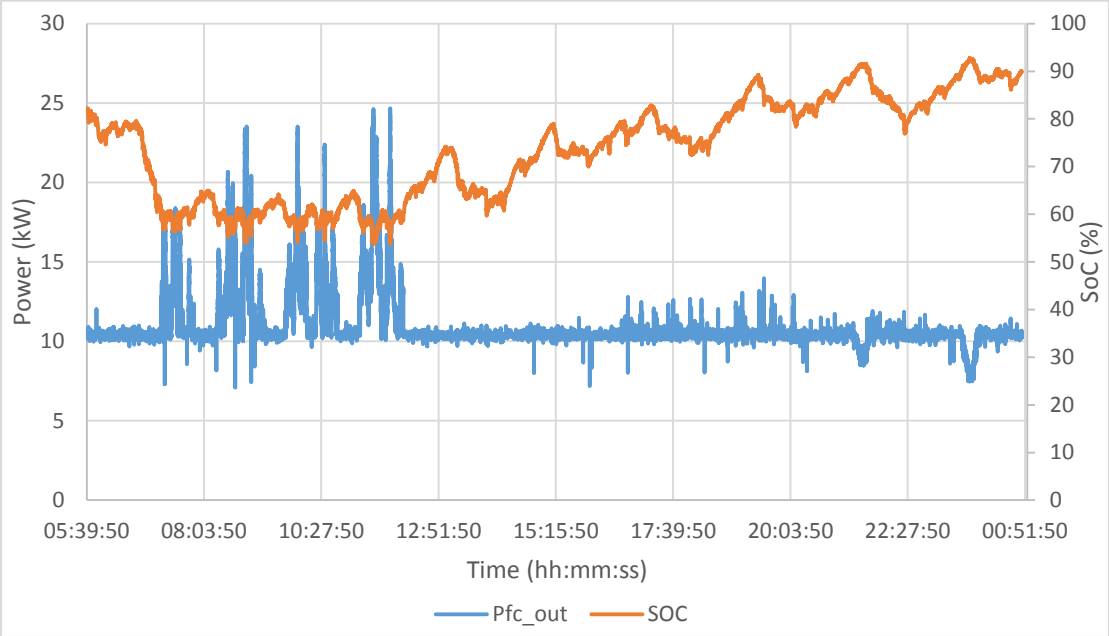

Figure 6.48 FC and boost converter output power and SoC change of the entire operation day of route 388

It can be seen the SC dissipated more energy in the morning driving cycles and was charged more frequently in the afternoon and evening driving cycles. As a result, the FC and boost converter output was increased significantly by the FC variation strategy in the morning operations and then decreased on two noticeable extended occasions in the afternoon and evening operations. This is because morning (rush hour) driving requires a lot of starts which are high load events and rarely will the bus get up to an appreciable speed which would also compromise regenerative energy capture. It was found the average charge effectiveness from regenerative braking throughout the entire day is 82.7% while the discharge efficiency is 90.3%. The SoC was maintained within the desired operational range. The proposed degree of hybridisation proved capable of delivering effective bus operation for the entire day. Since the highest power of the FC and boost converter output is 24.2 kW, this equates to a required FC power of 26.9 kW with a 90% average boost converter efficiency. Therefore, the degree of hybridisation on route 388 bus for the operating day is 26.9 kW FC / 16.2 kWh SC. More measured parameters from the entire day simulation have been plotted in Appendix R.

It can be seen the degree of hybridisation for the route 388 differs from the degree proposed for the high gradient route (42.8 kW / 2.72 kWh). The degree proposed on route 388 bus for the operating day was also tested against the high gradient route. The results have been plotted in Figure 6.49. Although the average power of the high

gradient route is 8.53 kW, the same initial base reference value (10.39 kW) of route 388 was used for the high gradient route. It was found the degree for route 388 bus is more than enough to cover the high gradient route because of the larger SC size. It can be seen the degree proposed for route 388 data has provided a FC SC combination that satisfies route 388 and the high gradient route. Although different driving cycles will result different FC SC combination, it can be found that a universal FC SC combination that satisfies multiple routes could be determined based on the degree of hybridisation identification method proposed in this research.

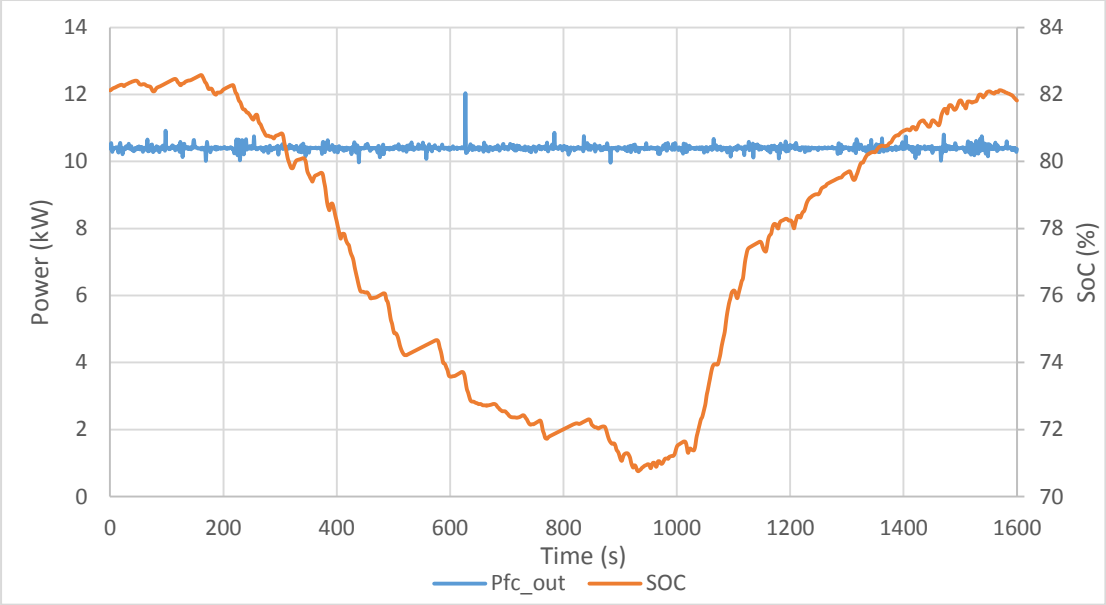

Figure 6.49 FC and boost converter output power and SoC change of the degree proposed for route 388 applied on the high gradient route

6.6 Degree of hybridisation optimisation

The previous sections identified and showed that the proposed degree of hybridisation is capable of operating for the entire day over route 388. It has been shown that the system with the identified degree of hybridisation is capable of meeting the dynamic power demands. The high gradient profile tests carried out in section 6.4.2 showed the potential to reduce the SC size after the inclusion of the FC variation strategy. It can be seen there is potential to further optimise the proposed degree of hybridisation with the FC variation strategy. This section will investigate how would this affect the degree of hybridisation.

The same driving cycle data of route 388 operating day (Figure 6.4) and initial FC and boost converter output base reference (10.39 kW) have been utilised for the following tests. The SC size utilised for the previous test for the full day driving cycle was a 505

F SC (16.2 kWh) with a 60% lower threshold undercharge protection. The same tests have been carried out with different SC size. The required FC power has also been determined by using the highest required power from the FC. Hence a ratio between required FC size and SC size can be obtained. The obtained results have been plotted in Figure 6.50.

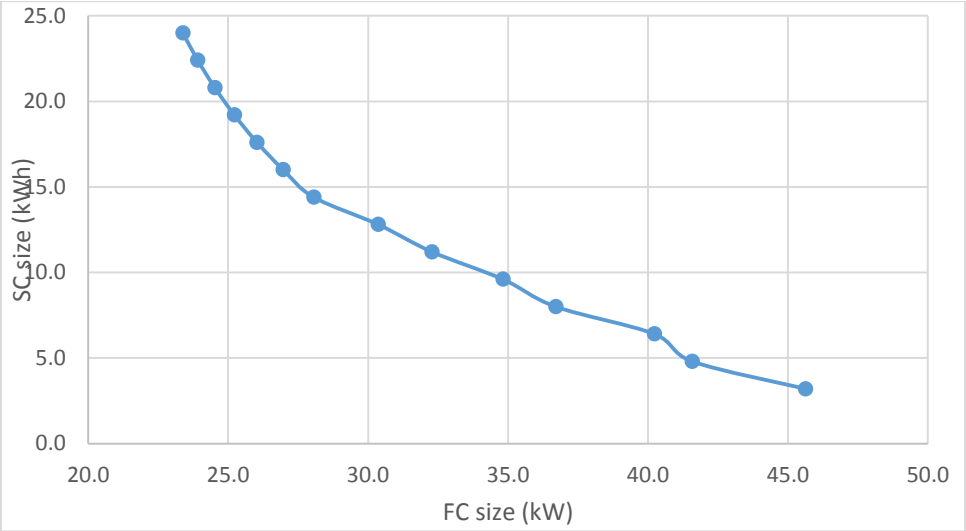

Figure 6.50 Ratio between required FC power and SC size for the full day driving cycle

As expected, it can be seen reducing the SC size would consequently lead to increase in the FC power required. It was also found further reducing the SC size beyond 3.2 kWh will cause the system to fail for this particular profile. The failure was caused by the SoC dropped to quickly for the FC to charge because the SC is too small. It can be seen the SC size can be reduced significantly at the cost of a larger FC.

The 60% lower threshold has also been varied to investigate how such adjustment would affect the degree of hybridisation. The same SC reduction tests have been carried out with 50% and 70% lower threshold. The results have been compared in Figure 6.51.

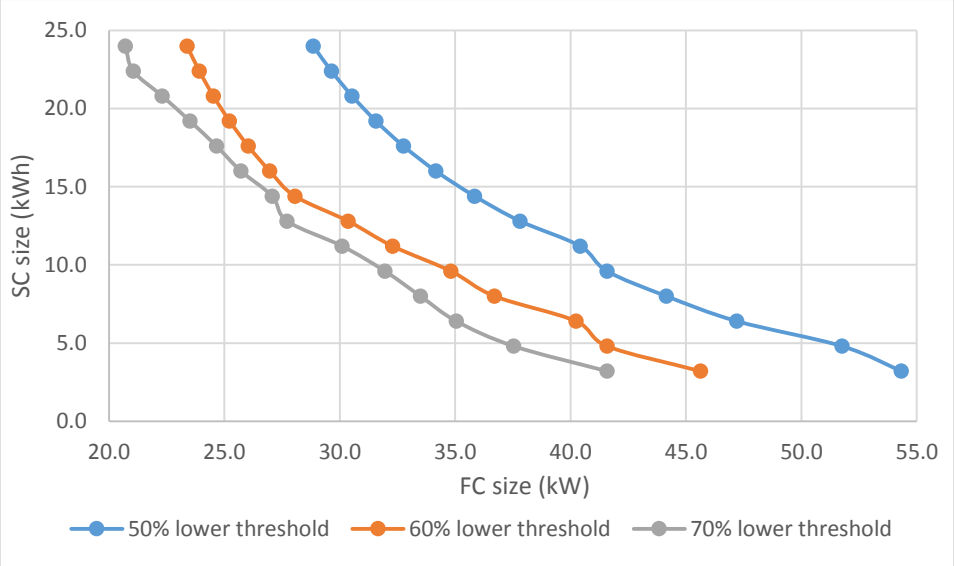

Figure 6.51 Ratio between required FC power and SC size for the full day driving cycle with different lower thresholds

It can also be found reducing the lower threshold to 50% would increase the required size of both the FC and SC. Increasing the lower threshold to 70% would reduce the required size of both the FC and the SC. It has been found there is a trade-off relationship between the SC size reduction and FC size increase. This trade-off relationship would play an important role in optimising the cost of the hybrid system. The cost of the FC system and SC system varies significantly depending on the production scale, power range, market and manufacture. The current market estimated the FC costs approximately £5,000/kW and the SC costs approximately £6,000/kWh [6.1] [6.2]. The total cost of different ratios can be calculated based on the results obtained in Figure 6.51. The total cost of the FC and SC has been plotted in Figure 6.52.

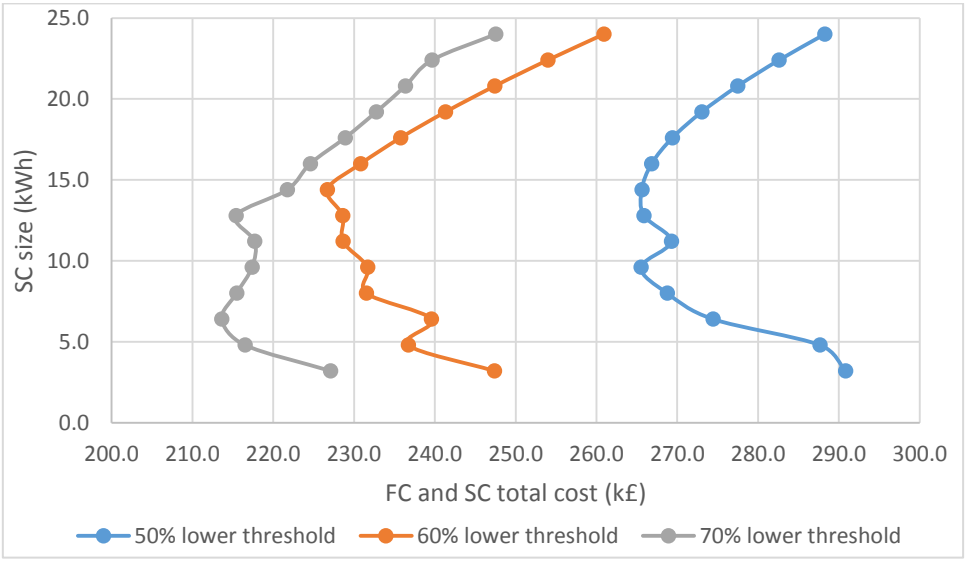

Figure 6.52 FC and SC total cost change with SC size variation

It can be seen the lowest cost for each lower thresholds occurred between 6.4 kWh and 9.6 kWh. There is a middle region where the system achieves the lower costs. However, this can only provide a general estimation of the total cost with different ratios because this is heavily dependent on the cost of the FC and SC. An appropriate cost study of the hybrid model will be required to calculate the exact cost relationship. That would require a detailed cost analysis of the current industry, system scale, manufacturer information and future market change which is beyond the scope of this research. This can be analysed as part of some future work.

The previous tests showed the system having the lowest SC size and lowest total cost had the lowest threshold setting at 70%. At the same time, 70% would cause more frequent adjustment to the FC output, like the first RV1 bus, it is becoming less of a hybrid system. Having a high threshold setting means the bus is not using the SC as an energy storage for boost but merely to attenuate the severity of the ramp change the FC has to undergo. If the FC output has been held constant, the SC was managing all the transient response. Optimisation comes at the cost of using the FC over a wider dynamic power band. To investigate the FC variation frequency, the percentage of the FC output varied has been calculated by using the total time divided by the FC remained at the initial base reference (1.1*average). This will provide the time the FC varied throughout the operational day. The results have been plotted with different lower thresholds as Figure 6.53 shows.

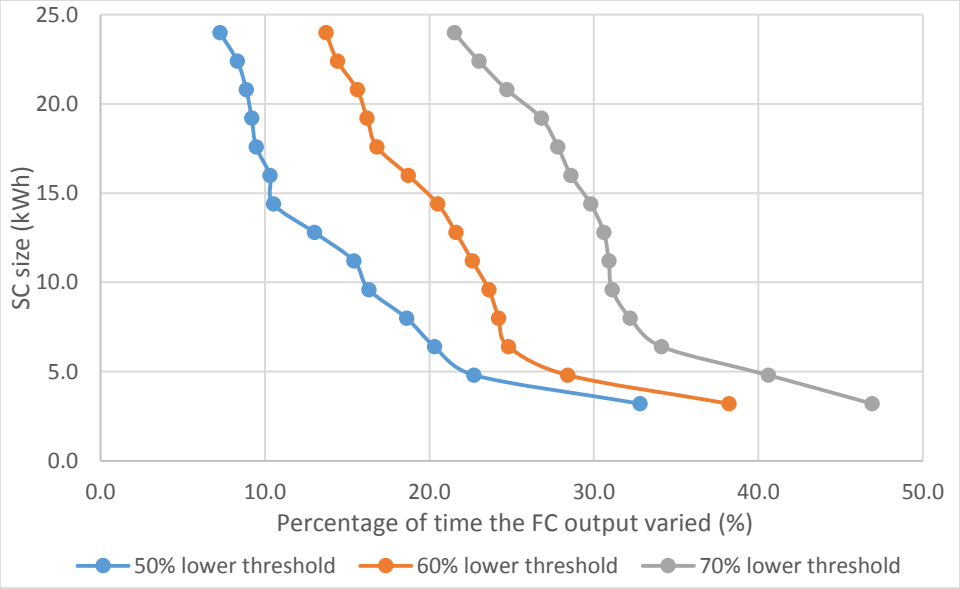

Figure 6.53 Percentage of time the FC output varied against SC size

As can be seen from the figure, the 70% lower threshold was subject to the most FC variation. The FC varied its output for nearly 47% of the day for the worst case scenario. The variation includes the FC and boost converter output being increased to prevent

SoC depletion or being decreased to prevent overcharge. It was found that the average power of the FC and boost converter output for each case is nearly the same with less than 1% variation in results. Since the net power profile of the load and the net power of the FC are the same, varying the SC size and lower threshold will not affect the energy delivery to or from the SC. The minor difference is caused by the charge/ discharge efficiency and slightly different final SoC. The same average FC output power also means the total energy delivered by the FC is always the same.

Discussion with reference to the degree of hybridisation optimisation

It can be seen the degree of hybridisation can be optimised with respect to a number of parameters. However, there is always a trade-off relationship for the parameter that is been optimised. There will be a number of factors involved and optimisation is about finding the “best balance” amongst those factors. Table 6.8 summarises the results obtained from the previous tests.

Table 6.8 Summary of degrees of hybridisation optimisation

	FC (kW)	SC (kWh)	FC varied (%)	Total cost (k£)	Hydrogen consumption (kg)
50% lower threshold	28.8	24	7.25 (Min FC variation)	288.2	11.683
	29.6	22.4	8.31	282.6	11.721
	30.5	20.8	8.86	277.5	11.760
	31.6	19.2	9.19	273.0	11.796
	32.8	17.6	9.46	269.4	11.834
	34.2	16	10.3	266.8	11.872
	35.8	14.4	10.5	265.6	11.910
	37.8	12.8	13	265.9	11.923
	40.4	11.2	15.4	269.3	11.915
	41.6	9.6	16.3	265.5	11.904
	44.1	8	18.6	268.7	11.894
	47.2	6.4	20.3	274.4	11.886
	51.8	4.8	22.7	287.6	11.888
	54.3	3.2	32.8	290.8	11.886
60% lower threshold	23.4	24	13.7	260.9	11.804
	23.9	22.4	14.4	254.0	11.832
	24.5	20.8	15.6	247.4	11.860
	25.2	19.2	16.2	241.3	11.887
	26.0	17.6	16.8	235.7	11.915
	27.0	16	18.7	230.8	11.923
	28.1	14.4	20.5	226.7	11.915
	30.4	12.8	21.6	228.6	11.903
	32.3	11.2	22.6	228.6	11.890
	34.8	9.6	23.6	231.7	11.877
	36.7	8	24.2	231.5	11.865
	40.2	6.4	24.8	239.6	11.861
	41.6	4.8	28.4	236.7	11.858
	45.6	3.2	38.2	247.4	11.861
70% lower threshold	20.7 (Min FC size)	24	21.5	247.5	11.948
	21.1	22.4	23	239.7	11.954
	22.3	20.8	24.7	236.3	11.950
	23.5	19.2	26.8	232.7	11.940
	24.7	17.6	27.8	228.9	11.928
	25.7	16	28.6	224.6	11.915
	27.1	14.4	29.8	221.8	11.902
	27.7	12.8	30.6	215.4	11.888
	30.1	11.2	30.9	217.7	11.875
	32.0	9.6	31.1	217.4	11.864
	33.5	8	32.2	215.5	11.854
	35.0	6.4	34.1	213.6 (Min total cost)	11.844
	37.5	4.8	40.6	216.5	11.834
	41.6	3.2 (Min SC size)	46.9	227.1	11.842

All the degrees of hybridisation in table 6.8 have been shown to be capable of suitably delivering the service for a complete operating day of route 388. The hydrogen consumption has also been estimated based on the full scale model. As can be seen from the table, varying the degree of hybridisation has only a minor impact on the hydrogen consumption because the power profile used is the same for all tests. Since each bus journey is approximately 12.83 km as discussed before, the total distance travelled can be roughly estimated to be 256.6 km (20 journeys). Therefore the systems with the proposed degrees of hybridisation and specific control strategies used 11.683-11.948 kg for 256.6 km which equates 4.55-4.66 kg (~640 MJ) per 100 km with the same initial and final SoC. It can be seen that the hydrogen consumption has been reduced when compared with the 8-9 kg /100 km fuel economy with the London RV1 FC bus. Although the hydrogen consumption cannot be validated at this stage due to lack of information, the results can provide an estimation of the fuel economy of the proposed system. It was acknowledged that the rated power of the selected FC will also have an impact on the hydrogen consumption. A proper validation for the full scale model would need to be carried out for a more accurate hydrogen consumption evaluation which can be carried out as part of the future work.

The four hybrid option results with minimum variation, minimum FC size, minimum total cost and minim SC size have been highlighted. One of these parameters can be maximised for each case, but this would also consequently change the other parameters. It can be seen optimising the degree of hybridisation is not simply finding a “best” number. The factors of optimisation would depend on the specific requirements of the bus designer.

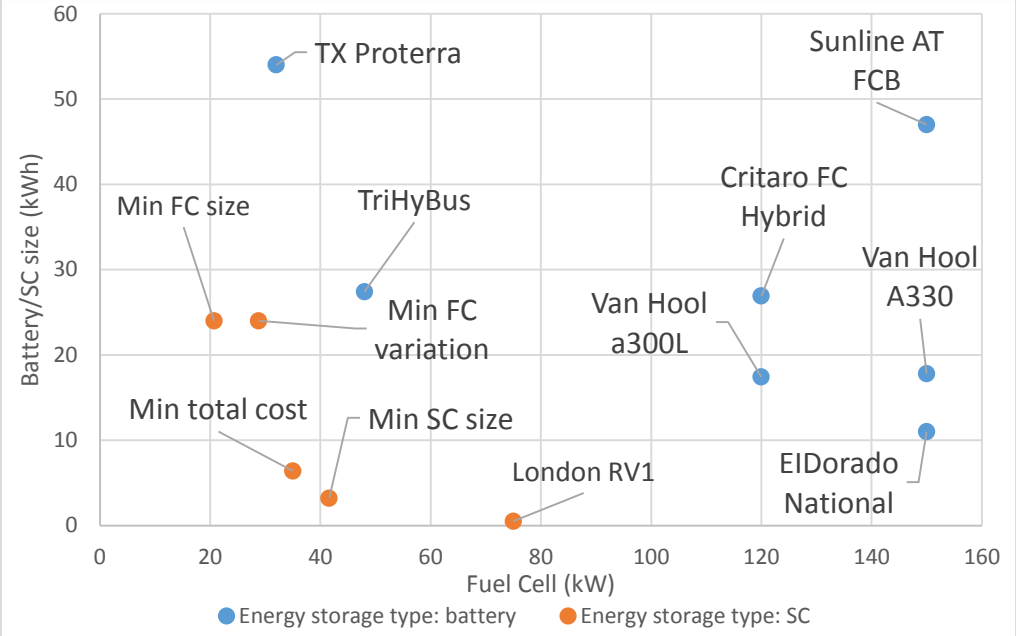

Figure 6.54 FC/SC ratio comparison between route 388 optimised degrees of hybridisation and existing FC buses

Finally, the degrees of hybridisation proposed for route 388 in this research have been compared with other operating FC buses referring back to Chapter 3. The comparison has been plotted in Figure 6.54. The four options optimised in terms of minimum FC size, cost, SC size and FC variation have been plotted in the FC/SC ratio plot.

From the FC point of view, it can be seen the FC size proposed in this research is significantly smaller when compared with those for existing FC buses. However, there is an important point that needs to be addressed for the FC size comparison. The degrees proposed in this research were mainly based on the driving cycle of one operating day. As discussed before, the driving cycle is subject to change based on a variety of factors such as season, weather and other events. Although the proposed FC variation strategy will provide some flexibility for the model to be operated under different driving cycles, the required FC size could be increased to be prepared for possible worst case scenarios. As a result, the degrees identified in this research are more likely to be appropriate for route 388 on that day instead of for route 388 generally. Although more power profiles will be required to properly size the FC for the route 388, the strategy to identify the required degree will be the same which is the most important finding of this research.

From the energy storage point of view, the energy storage size proposed in this research varies over a wider range compared with those installed in existing buses. As discussed in section 3.2, most existing FC hybrid bus models utilise Li-ion batteries as

energy storage with the exception of the London RV1 FC bus. The capacities of the battery used in the existing FC buses are generally larger than proposed in this research. The reason for this is the lower power density of the Li-ion batteries, as discussed in section 2.5.2. More batteries need to be integrated to provide a higher transient power output. The SC used for London RV1 (0.5 kWh) is significantly smaller than the proposed SC capacity in the degree of hybridisation for route 388. There are three reasons for this. First, as discussed in section 2.3.3, route RV1 is a relatively flat route which was specifically selected for the FC bus demonstration. As a result the power variations in the route RV1 in terms of magnitude and frequency are expected to be significantly smaller than for the same bus on route 388. Second, RV1 is a single decker bus while the route 388 bus is a double decker bus. This would further reduce the power demand for RV1 compared to the route 388 bus selected for this research. Third, the FC on RV1 is significantly more powerful than the FC proposed for route 388. This also reduced the requirement of the SC size on-board the RV1 bus.

Based on the discussions, the degree of hybridisation proposed in this research is more appropriate to be the optimum for route 388 on that specific day the data was gathered. The results showed the potential of using a downsized FC with a larger SC in a hybrid bus. The most important finding of this research is the strategy to identify and optimise the degree of hybridisation. The degree of hybridisation identification method can be applied on any other route. The reduced FC size in the present RV1 also greatly improves fuel economy when compared to the FC only RV1 variant, as discussed in section 2.3.3. The downsized FC on buses can reduce fuel consumption and improve system efficiency as they are both directly related to the FC output power. The combination of a downsized FC and a larger SC showed great potential in the FC hybrid model. This type of design holds the advantages of reduced FC stress, improved hybrid performance, and potential to be further optimised in terms of cost, efficiency and fuel consumption.

6.7 Discussion on dynamic power control strategy

Thus far, this research has proposed and showed the FC/SC hybrid controller with the FC variation system can greatly increase bus flexibility. The FC variations system worked by monitoring the SC SoC and reacted by adjusting the FC output to prevent SC depletion. The FC does not modify its output until the lower set threshold SoC is reached through depletion of the SC. To ensure the SoC does not reach the 30% limit (buck/boost converter failure at 25%), protection against depletion has been added by either increasing capacity of the SC or raising the SoC level of the lower threshold trigger point. A higher threshold leads to “shallower” use of the SC and forces the FC to cycle up from its set base reference more frequently and when the SC has an appreciable SoC and low rate of depletion. The FC may also be subjected to steep response or even stepped response depending upon the control mechanism for increasing output from the FC. This is more pronounced at lower threshold settings. Once set, the threshold that is optimised for the most onerous duty of a particular route cannot be simply adjusted for the remainder of the route.

There is a possible improvement on the FC variation strategy and that is to link the FC response to not only SoC of the SC, but also the duty loading on the SC at any particular time during the driving cycle i.e. rate of discharge. The proposal is to implement a response curve as part of the FC control algorithm. The curve relates rate of discharge of SoC to SoC for the SC. Figure 6.55 showed a function response curve as an example.

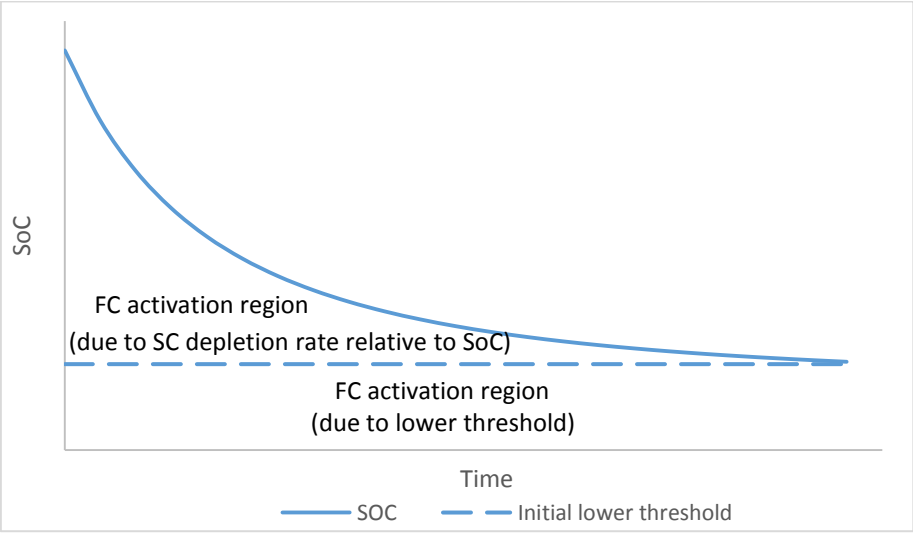

Figure 6.55 Response curve example

As Figure 6.55 shows, at high SoC depletion rate, the FC will be activated to deliver more energy only if that depletion rate is steeper than the response curve at the SoC at that gradient point (shown as the FC activation region). Also, if the depletion rate is less than shown on the response curve for the corresponding SoC, the FC will not be activated to deliver more energy i.e. the FC will continue to deliver the output at its base reference output. The lower the SoC, the lower the rate of discharge required to trigger a response to release more energy from the FC. If the SoC is high, then the rate of depletion must be higher to activate the FC to deliver additional energy above its reference setting. In effect, the response of the FC depends not only on SoC, but also on rate of discharge of the SC.

Using this control strategy, the need for a high SoC threshold to protect against over depletion on a high power route is less critical. In effect, the threshold is being dynamically adjusted depending on the load, SoC and rate of discharge. Not only does the proximity of the threshold SoC activate the FC response but the rate of discharge also determines the limiting SoC for the FC output response. As a result, the threshold is no longer a fixed dumb control setting, but is now a dynamic response parameter.

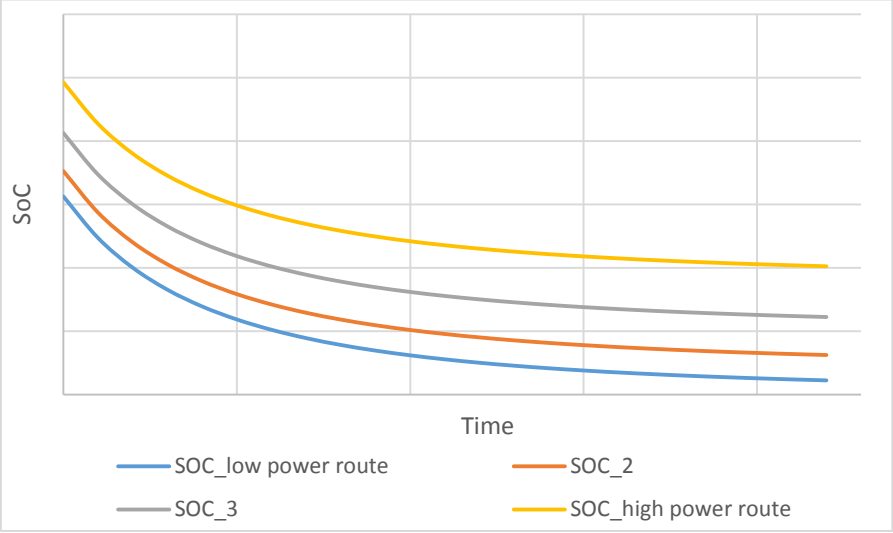

Figure 6.56 Range of FC activation response curves

Figure 6.56 shows a series of FC activation response curves. In reality, the designer would need to consider the dynamics of the route when implementing the dynamic threshold control strategy for the FC hybrid bus. To allow a single optimised design to function over a variety of routes, the algorithm controlling the FC response can be modified to match the route. Of the four response curves shown, the blue curve would applied to a low power route since the instances when the SC would be discharged at a high rate at high SoC would be minimal. With this response curve, the FC will not be activated to respond to provide additional output unless the SC is appreciably depleted.

The yellow response curve denoting the high power route demands increased output from the FC at lower discharge rates even at high SoC. This would allow the FC to contribute to the increasing demand long before the SC is heavily depleted. Using this control strategy, there is a combination between the FC variation strategy and the dynamic threshold control strategy.

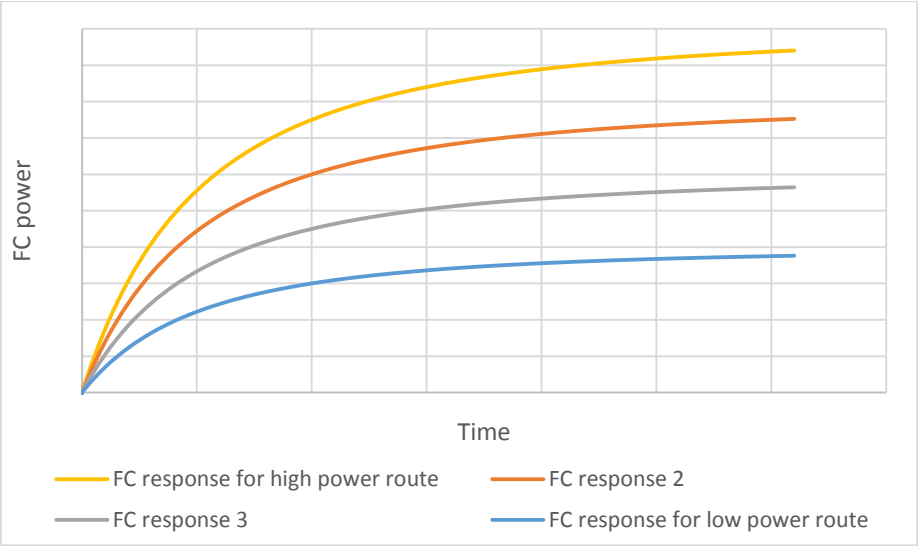

Figure 6.57 FC output response curves

When required, the FC will need to respond to the rate of discharge of the SC. The higher the rate of discharge, the corresponding the higher the rate of output response from the FC. Figure 6.57 shows the required FC activation response generally corresponding to the responses in Figure 6.56. The high power route would require the FC output to respond at a higher rate overall compared to the lower power curves shown. The FC output response curves would be generally matched to the FC activation curves.

There are however limitations with this strategy. If the high power route, for example, occurs in one direction of the journey i.e. mainly uphill, the likelihood is the return journey will be a lower power route i.e. mainly downhill. It is clear setting the control algorithm for uphill will compromise for example regenerative energy recapture and the downhill route. To be able to change the algorithm to be more section of the route specific, there are different means available to manage which control algorithm is used on which part of the route. These could be adjusting the response curve:

1. Based on the bus destination (when the driver changes the display).
2. Programming complete route maps into the FC algorithm.
3. Real time monitoring the bus location using roadside pickups or GPS data.

It is possible to determine an algorithm for each journey (A to B and B to A would be two journeys). However, if the route profile varies significantly within the journey itself,

the algorithm may not achieve optimised efficiencies from the FC for significant parts of the journey since FC efficiency increases as output power decreases.

It may be preferable for the algorithm to be modified en route. For example earlier tests carried out on a high power, low power and combined journeys routes (Figure 6.45-6.47), each of these were optimised at different FC and boost converter base reference output (17.63 kW for high power, 6.22 kW for low power and 11.77 kW for combined journey). For a journey that comprises all three of these journeys, the bus would either have to function using the high power setting which leads to lower FC efficiency across the entire route or adjust the algorithm depending upon which section of the journey the bus is at that specific time. By allowing the FC to function at its best efficiency relative to the route sections, not only do we increase the overall efficiency and improve fuel economy, we also further reduced the stresses applied on the FC by reduce cycling.

The response curve can be modified to allow the “same bus” to function across different general categories of route without amending or modifying the propulsion plant fit for these general categories. This allows a universal FC/SC combination bus for the majority of the city as we now have facility to modify the response curve when unexpected bus operation is required. There is also potential to use fuzzy logic control to better optimise the performance of the propulsion unit and with AI self-learning technology develop a bus suitable for unmanned operation.

6.8 Concluding arguments and recommendations

The aim of this chapter was to develop meaningful discussions around the identification and optimisation of FC/SC degree of hybridisation for bus use. This chapter discussed and formulated arguments from a power system engineering perspective to investigate the FC/SC degree of hybridisation for a FC hybrid bus.

The validated computer model was scaled up to full scale to represent a practical operating London bus. The full scale bus model was evaluated with different actual driving cycles and showed the proposed current control strategy performing as expected. The initial proposal of the FC/SC operation has been designed to keep the FC output always constant while using the SC to supplement the load demands. The control strategy has shown it is capable of keeping the FC output constant while using the SC to satisfy the varying load modelled from actual driving cycles.

The variation of FC output and SC size has been investigated to gain a better understanding of the effect of degree of hybridisation in the bus model. The FC hybrid system was tested with different FC and boost converter current output references. The model showed it is capable of adjusting the FC and boost converter output based on the user-defined reference. It was found varying the FC and boost converter reference will only affect the SC input and output power which changes the SoC. The method to determine a required FC output has been identified to be 1.1 times that of the average power of the driving cycle which would deliver a FC/SC hybrid system with downsized FC.

With regards to the method to identify the SC size, it was found varying the SC size will only affect the SoC change throughout the driving cycle. A number of criteria have been addressed to determine an appropriate SC size based on the results obtained. It has been found that the method to identify the SC size would require the entire selected driving cycle to be simulated in the model which is not an effective method. As a result, a method to estimate the required SC size for a certain driving cycle has been identified based on the cumulative energy calculation throughout the power profile. The calculation method has been validated with the computer model and showed it is capable of providing a reasonable estimation of the required SC size.

Based on the discussions, the method to identify the required degree of hybridisation was summarised in a number of steps. The identified degree of hybridisation has been

tested with various different practical bus collected driving cycles. It was found the SoC will be decrease overall for longer driving cycles because of the losses within the buck/boost converter linked to the SC. The challenge to the initial proposed operation strategy of keeping the FC output always constant has been identified as three limitations. The three limitations are the requirement of more resources to process, inability to identify the real time SC conversion efficiency and no flexibility in bus operations.

Following the identified limitations, the initial proposed strategy of keeping the FC output always constant has been reconsidered. A FC variation strategy has been developed to adjust the FC output depending on the SC SoC. A specific UCL-assigned route with a high gradient profile has been used to analyse the FC variation strategy. The FC variation strategy consist of an undercharge protection system and an overcharge protection system. It was found the inclusion of the FC variation strategy is not only capable of eliminating the three limitations that were identified but also showed potential to further optimise the identified degrees of hybridisation. As a result it has been recommended to integrate the FC variation strategy into the FC hybrid model.

To investigate the potential to optimise the FC variation strategy, a number of parameters have been analysed. It was found the SC size can be further reduced with the consequence of the FC output having to be varied with more frequency and larger magnitude. It was also found varying the lower threshold in the undercharge protection can change the rate of the change of the FC and boost converter reference. An extra saturation control strategy has also been designed and showed capability to limit large magnitude variations of the FC output. An optimised FC variation strategy has been designed and integrated based on the high gradient profile analysis.

The FC/SC model with the optimised FC variation strategy has been tested with more driving cycles and eventually a full day driving cycle of route 388. It was found the model with the FC variation strategy showed good performance in terms of controlling the SoC and meeting the dynamic load demand. The degree of hybridisation has been identified for the operating day of route 388 which also justified and verified the strategy to identify the degree of hybridisation for a driving cycle.

With the degree of hybridisation identified and tested, they have been optimised to explore the potential of an optimum FC/SC ratio. It was found reducing the SC size

would consequently increase the required FC power. The total cost of various FC/SC ratios have also been estimated and the results showed there is a middle range where the minimum total cost occurs. It was also found that raising the lower threshold can reduce the requirement of both FC and SC size. However, the elevated lower threshold will also significantly increase the frequency and magnitude of the FC power output variation. It has been found each parameter in the degree of hybridisation is interlinked with others. As a result, the optimisation of the degree of hybridisation would be dependent on the specific requirement of the bus designer. Four optimised degrees of hybridisation namely minimum FC size, minimum total cost, minimum SC size and minimum FC variation have been proposed for the route 388. The proposed degrees of hybridisation have been compared with degrees of hybridisation of existing FC buses. It has been found that using a downsized FC as power provide and a larger SC to satisfy varying power demand difference is a feasible solution with the proposed control strategy.

A dynamic power control strategy has been proposed to determine the control algorithms for FC activation and response to further optimise the performance of the FC hybrid bus. The control strategy provides the facility to optimise the bus for different routes with the same general bus propulsion system.

FC hybrid system solution recommendation

This research demonstrated the identification and optimisation method for the FC/SC degree of hybridisation for a certain driving cycle. Although the identified degree of hybridisation may not be optimum for other routes, the identification and optimisation method can be applied on other routes. A summary of the FC/SC bus degree of hybridisation identification process from a power system engineering point of view has been presented in a list of steps.

1. **Route selection**. Considering the early stage of FC bus development and the collected driving cycle of this research are all from a double decker bus, the FC bus route for HyFCap project would be expected to be a demonstration route potentially for the first double decker FC bus.

2. **Driving cycle data collection**. This step can be carried out with a conventional bus, preferably with similar specifications to the proposed future FC bus. Since this research focused on the power system point of view, mechanical frameworks, bus design regulations, and system placement (hydrogen cylinder etc.) will not be taken

into consideration at this stage. The most important part of this step would be to collect the power profile as it defines all the power requirements needed to propel or slow the bus regardless of the mechanical design. The driving cycle data needs to be collected for as many different operational scenarios as possible as this data will define the worst case scenarios.

3. **FC output power identification**. Calculate the average route power of the collected driving cycles and using 1.1 times that of the calculated value as the initial FC and boost converter base reference power output.
4. **SC sizing**. Subtract the FC and boost converter output from the power profile to determine the power required from the SC. Calculate the cumulative energy required from and to the SC to determine the required capacitance. Increase the determined capacitance by 20% for efficiency compensation and extra buffer. The SC sized by this method will provide an initial estimation of the SC size.
5. **Model validation**. Run the FC/SC hybrid model with the load simulation system with the identified degree of hybridisation on the driving cycle power profiles to validate the calculation and evaluate the system performance.
6. **Degree of hybridisation optimisation**. Optimise the FC variation strategy by testing the model with different SC size, lower threshold and FC output saturation. Identify a range of different degrees of hybridisation and optimise the degrees depending on the requirement of the bus designer.

The steps summarise the key recommendations for FC bus design from a power system engineering point of view. The outcome of this is expected to be an optimum FC/SC hybrid bus power system design for a specific route that is also capable of operating on different routes.

Chapter 7 Conclusions and further work

7.1 Introduction

This research investigated the use of Fuel Cells for city bus use as part of the HyFCap project and the implementation of the London ULEZ in 2020. Following an extensive literature review into low emission bus propulsion systems and a critical review into FC technology for transportation, it was concluded that the current bus fleet needs to be improved to meet the ULEZ requirements and FC technology has promising performance capabilities for city bus application. Following a gap analysis built upon the literature review and analysis of the current FC bus industry, this research aimed to "explore the potential of integrating a SC with a downsized FC for a FC hybrid bus application and investigate the method to identify an appropriate degree of hybridisation between the constituent power sources".

To conduct research into this field, a scaled model of FC hybrid system was developed in the laboratory with the intention of using the scaled model to develop a computer simulation model that would be used to investigate the optimisation of degree of hybridisation. The results and their examination offered an analytical understanding of the limitations of using a FC only bus system while highlighting the rationale for the use of energy storage technology to supplement the FC as the power source. The hybrid system constructed in the laboratory was used to investigate the practical performance of a FC hybrid bus and through this provide validation tool for the design and development of the computer simulation model. Beyond construction and testing of the basic FC test bench and the hybrid laboratory scale model, the computer simulation model was developed and tested in parallel with the laboratory scale model. This allowed the systems to be validated against each other to provide as accurate a representation of a FC/SC hybrid power system as could be achieved with the available resources. Each constituent sub-system and the fully integrated hybrid computer simulation system were validated against results obtained from the laboratory scale model using the same experimental configuration for validation tests. Both the laboratory scale model and computer simulation were tested with the controller proposed for the hybrid system and the results showed the computer model accurately replicated the practical laboratory scale model. It was concluded that the FC/SC hybrid model was suitable for use in this research and the operation strategy functioned as expected.

The computer simulation model was then utilised to replicate a full scale bus and evaluate, against actual driving cycle data, the performance in more complex dynamic environments. Investigations were undertaken to determine the most appropriate FC and boost converter output reference with a series of tests. The impact of modifying FC output and SC size were investigated and discussed. A method to identify the degree of hybridisation was derived and demonstrated for a number of selected driving cycles. The identified degrees were then optimised with another FC output controlling strategy. The optimised degrees were compared against actual operating FC buses. Finally the degree of hybridisation identification and optimisation method for a FC hybrid bus was provided as a list of steps.

The following sections provide a summary of the research findings and specific recommendations for the HyFCap project when integrating FC systems with bus system. The findings and recommendations have been contributed as a result of this research.

7.2 Summary of the research findings

FC bus technology was being tested and demonstrated as a potential zero emission solution for public transport. The current FC bus industry suffers from high capital cost due to the large FC stack on-board which led to the HyFCap project to specifically investigate a hybrid system comprising a FC and an energy storage. It was found that the current FC bus industry has started to replace the FC only buses with FC hybrid buses. This trend was investigated, tested with the laboratory system and it was found helped overcome four major limitations. These were low efficiency under higher load operations, requirement of a large FC stack, slow response under transient load change and lack of ability to recover retardation energy. Additionally, it was found that the FC size has to significantly increase to be able to cover some of the worst case load scenarios which led to significantly over-sized FCs.

The following conceptual and theoretical analysis indicated that the previously identified drawbacks for FC only bus system can be mitigated by using a hybrid configuration. A scaled FC hybrid system was developed with both laboratory and computer models showing that the FC is capable of being hybridised with an energy storage system. It was also argued that the SC was theoretically more appropriate to be integrated with the FC source than lithium ion batteries because of their performance in terms of power and energy density characteristics.

The initial operation strategy proposed in this research was to use the FC as a constant output power source while using the SC as an energy reservoir to satisfy varying power demand and recover regeneration braking energy. This type of strategy was considered advantageous as it not only mitigates against periods of low FC efficiency operation and dynamic load stress applied on the FC, but also takes advantage of the high power density of the SC. The proposed operation strategy has been designed to utilise a current control strategy applied to the buck/boost converter for the SC. The control strategy has shown its capability to achieve the proposed operation strategy and was validated with the laboratory test bench. The validated control strategy was applied to the computer model. The computer model was used to evaluate a series of actual driving cycles and the control strategy was able to maintain the FC output as required under realistic dynamic loads.

The computer model was used to develop a methodology to identify the optimum FC/SC degree of hybridisation. The consequences of adjusting the FC and boost converter output was found to affect the SoC change throughout the driving cycle compared with other FC reference settings. In order to keep the initial and final SoC of the SC approximately the same after certain driving cycle operations, the initial proposal was to use the average power of the driving cycle to determine the desired output of the FC. However, it was found the difference in charge and discharge efficiency will impact the SoC change throughout the driving cycle. Tests suggested the buck/boost converter losses will vary depending on the power profile and averaged at 90% efficiency. As a result an average 10% increase on the FC and boost converter output was added to compensate for the converter losses. This set the required FC and boost converter reference at 1.1 times the driving cycle average power.

Although the SoC at the start and end of the route will remain approximately constant when using 1.1 times the average driving cycle power as FC and boost converter output reference, it was also found that the SC needs to be properly sized to prevent depletion. The consequences of adjusting the SC size was to affect the maximum and minimum SoC to which the SC would be charged or discharged. A strategy based on calculating the energy required from the SC has been developed. It was found this strategy can provide a reasonable estimation of the required SC size.

It was found that the main factors for identifying the FC/SC degree of hybridisation were the prevention of the SC depletion while being able to cover the entire operation journey/route/day. Increasing the FC output would reduce the transient power

demands from the SC and be able to recharge the SC at a higher rate. Decreasing the FC output would increase the power demands and increase the potential to deplete the SC. The larger the capacity of the SC, the less likely the SC will be to depletion because of the larger capacity, however, this would also increase the cost and space demand on the bus. Thus the optimum FC/SC degree of hybridisation can be identified by using the FC and boost converter output power as 1.1 times the average of the driving cycle power / the SC size where the SoC will never go beyond a certain lower limit throughout the driving cycle.

The initial proposed operation strategy of keeping the FC output always constant has been tested with the identified degree of hybridisation. However, it was found the SoC was unable to be maintained at an expected high level. It was found that in addition to the difference in discharge (power supply) and charge (regeneration) efficiencies significant energy was lost through the necessity of mechanical braking. The 10% increased on the FC and boost converter output reference was unable to compensate fully for the losses, particularly over driving cycle with frequent start stop at low speed which compromises regenerative energy capture. Results suggested the exact required increase on the FC and boost converter reference varies with the driving cycle. It was found keeping the FC output constant was not an efficient and practical solution. As a result, a FC variation strategy was applied that offers the facility to adjust the FC and boost converter output reference through monitoring the SC SoC.

It was found the model with the inclusion of the FC variation strategy can not only eliminate the limitations for the initial proposed operation strategy, but also bring potential benefits of further optimising the identified degree of hybridisation. It was found the degree of hybridisation can be further optimised by adjusting the parameters of the FC variation strategy. It was found reducing the SC size would consequently increase the required FC power as expected. Raising the SoC threshold of the FC variation strategy could reduce the required size of the FC and the SC, but would consequently increase the frequency and magnitude of the FC power output variation. The findings suggest that there will not be a “best” degree of hybridisation for FC hybrid buses, but an optimum degree of hybridisation for the particular driving cycle. Four optimised parameters of hybridisation have been identified for the test route. The computer model can be used by the designer to test and optimise their proposed FC and SC installation. It was concluded the optimisation can be carried with the model based on the requirement of the bus designer. Finally, the comparison between the degrees identified in this research and the existing FC buses suggested that the FC

size can be significantly reduced with the proposed FC hybrid propulsion system.

This research demonstrated that the FC hybrid system with a downsized FC for city bus use is feasible for operating in complex city driving environments and has the potential to be further optimised. This research also demonstrated a method to identify an appropriate degree of hybridisation between the constituent power sources, thus meeting the proposed research aim. Although the degree of hybridisation identification and optimisation have only been carried out with driving cycle data from a single route, the most important outcome of this research is the derivation of a method to identify and optimise an appropriate degree of hybridisation listed as recommendation steps in section 6.8. The output this research delivered can be used to provide an appropriate degree of hybridisation between the FC and SC for any bus route if the driving cycle data can be provided. The FC variation strategy developed in this research allows the bus to be able to operate on other bus routes even if the driving cycle differs from the base reference determined by route average power. However, this strategy limits the depth to which the SC can be explored because of the dumb control of the lower threshold. With this simple control strategy, the bus can be optimised for a particular route, but there is the limitation that this degree of optimised is a compromise across the route.

A dynamic power control strategy has been proposed to further optimise the FC hybrid bus and overcome the limitation of an elevated lower threshold for the FC variation strategy on high power routes. It was proposed that the FC activation was related to not only SoC but also rate of depletion of the SC related to SoC. A series of theoretical FC activation curves have been proposed as well as FC output response curves. Further control strategies have been proposed that would allow this dynamic threshold control to be better tailored across the profile of a route. This would allow improved optimised not only for one specific route, but also for a particular design across a variety of routes. This allows a general FC hybrid bus design to be provided that is capable of operating in the majority of specific city.

7.3 Recommendations for HyFCap project

The findings of this research have been translated into specific recommendations for the FC bus design to the HyFCap project. The resulting recommendations are as follows:

1. An FC only powered bus should not be the considered option for the HyFCap project demonstration bus. A FC with electrical energy storage hybrid system is considered a more appropriate option as a city bus solution.

2. SCs are recommended over batteries to be integrated with the FC as the energy storage device for the FC hybrid bus.

3. The FC size can be significantly reduced in the hybrid bus through the use of energy storage, regenerative braking energy capture and an appropriate power delivery control strategy. This type of downsized FC/SC configuration has been shown to be feasible. The exact amount of FC size reduction would be dependent on the selected route driving cycles.

4. The method to identify an appropriate FC/SC degree of hybridisation has been listed in the recommendation steps in section 6.8.

5. The initial proposed operation strategy of maintaining the FC output constant is not recommended. The inclusion of the FC variation strategy is recommended as an important feature to optimise the degrees and add flexibility. Depending on the requirement of the bus designer, optimisation in terms of a number of parameters can be carried out.

6. Considering integrating the hybrid system into a double decker FC bus from the power system engineering point of view, the FC/SC degree of hybridisation identified following the recommended steps will also work for a double decker FC bus. This research was not concerned with the actual mechanical design of a FC hybrid bus. This would need to be a consideration for the bus designer.

7.4 Recommendations for further work

Throughout this research four areas of further work have been identified as recommendations. The further work is aimed at developing a more complete understanding of the FC hybrid bus development and to provide possibilities for potential further improvements. In each case, extra sources required, proposed strategies and expected outcomes are described.

7.4.1 Explore fuzzy logic control for FC activation response

It would be possible in the future to use fuzzy logic and self-learning control where the bus propulsion system instead of having a finite number of discrete response curves, there would be an infinite number of response curves, in effect a control surface. The bus would through self-learning determines the best point on the control surface map to match the power required, the condition of the power delivery units for that particular position and those upcoming on the route. This would be an important factor for a self-driving bus.

7.4.2 Investigate impact of mechanical braking

It was stated in section 6.2.2 that the mechanical impact on the bus braking operation was not included in this research. This is because the braking characteristics of the bus were not supplied as part of the bus data. However, it was found in section 6.3.5 that the mechanical braking will have an impact on the bus, particularly for low speed bus operations due to the more frequent requirement of mechanical braking. Thus, it is recommended that the mechanical impact of mechanical braking be investigated. Bus braking characteristics and modification of the computer model would be required to complete an assessment of the impact on the bus caused by mechanical braking.

7.4.3 Explore hybrid energy storage

This research selected a high power density SC over batteries to be integrated with the FCs which generally has higher energy density. As identified in the system optimisation sections, the energy storage for the FC hybrid system would require a larger capacity. However, SCs are still significantly more expensive than batteries. There has been recent work into combining SCs and batteries (particularly Li-ion) to build a hybrid energy storage system. The concept is similar to the FC/SC hybrid model which is to use a SC to cover larger transient power changes while using batteries to slowly charge the SC. This type of hybrid energy storage could improve efficiency optimisation and be used to reduce the electrical energy capacity demand of the

energy storage on-board the FC bus. This type of FC/battery/SC design would likely reduce the required SC on-board which can reduce the high cost associated with SCs because SCs are generally significantly more expensive than batteries. The feasibility and investigation needed would be the design of the controller between the FC, the SCs, the batteries and the load demands.

7.4.4 Mechanical design of the FC double decker bus

The mechanical design for integrating the FC and SC on a double decker bus was outside the scope of this research. As such, the conclusions drawn on the degree of hybridisation identification strategy are limited to the electrical power perspective only. The main issue associated with a double decker FC bus would be the placement of hydrogen cylinders. Currently the London single decker RV1 bus has the cylinders on the roof of the bus. However, it would be difficult to put the cylinders on the roof for the double decker buses because of the vehicle height limit in cities. As a result, a lighter and smaller design of hydrogen storage could be a key component for a double decker FC bus. This would require the studies on bus mechanical design, operation regulation and hydrogen storage placement.

7.4.5 Investigate scaling impact on fuel consumption

As discussed in section 6.2.1, the scaling of the model will have an impact on the fuel consumption and efficiency. This research focused on optimising the system in terms of power. Optimising hydrogen consumption and efficiency can also be carried out based on the research outcome in terms of power obtained in this work. The optimised hydrogen consumption can be used for comparison with conventional diesel engines in terms of energy content. The full scale model would have to be validated in order to determine accurate hydrogen consumption and efficiency values. This would require validation of the performance curves for the components in the full scale model or the construction of a full scale laboratory system. Optimising the fuel consumption would be another important parameter for the bus designers.

References

Chapter 1

[1.1] F Birol, 2016, Energy and air pollution world energy outlook special report, International energy agency, [online] available at https://www.iea.org/publications/freepublications/publication/WorldEnergyOutlookSpecialReport2016EnergyandAirPollution.pdf accessed 30/01/2018.

[1.2] P Jones, C Cavoli, 2014, Roads to a Carbon Free Transport, UCL Transport Institute, [online] available at https://www.ucl.ac.uk/transport-institute/pdfs/roads-to-carbon-free accessed 30/01/2018.

[1.3] TfL, 2015, Cleaner air for London progress report on the delivery of the Mayor's air quality strategy, [online] available at https://www.london.gov.uk/sites/default/files/maqs_2015_progress_report_final_for_publication.pdf accessed 30/01/2018.

[1.4] Greater London urban area agglomeration zone, 2015, Air quality plan for the achievement of EU air quality limit value for nitrogen dioxide in greater London urban area (UK0001), Department for Environment Food & Rural Affairs, pp. 31.

[1.5] L Langton, H Pinner, H Ho, 2016, Lethal and illegal solving London's air pollution crisis final report, Institute for Public Policy Research, [online] available at https://www.ippr.org/files/publications/pdf/lethal-and-illegal-solving-londons-air-pollution-crisis-Nov2016.pdf accessed 30/01/2018.

[1.6] T Bush, S Eaton, S Gray, C Jephcote, A Kent, A Loader, 2013. Air pollution in the UK 2013, Department for environment food & rural affairs [online] available at https://uk-air.defra.gov.uk/assets/documents/annualreport/air_pollution_uk_2013_issue_1.pdf accessed 30/01/2018.

[1.7] Transport for London, 2014. Transport emission roadmap, cleaner transport for a cleaner London, [online] available at http://content.tfl.gov.uk/transport-emissions-roadmap.pdf accessed 30/01/2018.

[1.8] G Hitchcock, B Conlan, D Kay, C Brannigan, D Newman, 2014, Air quality and road transport impacts and solutions, Royal Automobile Club Foundation, [online] available at https://www.racfoundation.org/wpcontent/uploads/2017/11/racf_ricardo_aea_air_quality_report_hitchcock_et_al_june_2014.pdf accessed 30/01/2018.

[1.9] C Holman, L Grant, 2016, Clearing the air priorities for reducing air pollution in the UK, The Chartered Institution of Water and Environmental Management, [online] available at , http://www.ciwem.org/wp-content/uploads/2016/02/Clearing-the-Air.pdf accessed 30/01/2018.

[1.10] R Howard, S Beevers, D Dajnak, 2016, Up in the air, how to solve London's air quality crisis: part 2, King's College London, [online] available at https://policyexchange.org.uk/wp-content/uploads/2016/09/up-in-the-air-part-2.pdf accessed 30/01/2018.

[1.11] TfL, 2016, Health, safety and environment report 2015/16, [online] available at http://content.tfl.gov.uk/health-safety-environment-report-2015-16.pdf accessed 30/01/2018.

[1.12] Greater London Authority, 2015. Mayor confirms world's first ultra low emission zone and welcome more money for cleaner taxis, [online] available at https://www.london.gov.uk/press-releases/mayoral/ultra-low-emission-zone accessed 30/01/2018.

[1.13] R Calderwood, 2015, City of London air quality strategy 2015-2020, [online] available at https://www.cityoflondon.gov.uk/business/environmental-health/environmental-protection/air-quality/Documents/city-of-london-air-quality-strategy-2015.pdf accessed 30/01/2018.

[1.14] Department of Environment, 2015, Draft plans to improve air quality in the UK, tackling nitrogen dioxide in our towns and cities, Department for Environment Food and Rural Affairs, pp. 25.

[1.15] R Jardine, 2013. Bus services in London, London Assembly Transport committee [online] available at https://www.london.gov.uk/sites/default/files/Bus%20Services%20in%20London%20Report%2C%20Transport%20Committee_0.pdf accessed 30/01/2018.

[1.16] TfL, 2015, Ultra Low Emission Zone report to the Mayor, [online] available at https://consultations.tfl.gov.uk/environment/ultra-low-emission zone/user_uploads/ulez-consultation-report-to-the-mayor.pdf accessed 30/01/2018

[1.17] M Cottrell, M Baker, 2014, Ultra Low Emission Zone integrated impact assessment, [online] available at https://consultations.tfl.gov.uk/environment/ultra-low-emission-zone/user_uploads/ulez-iia-report_final.pdf accessed 30/01/2018.

[1.18] Environment Committee Members, 2016. Driving away from diesel Reducing air pollution from diesel vehicles, London Assembly, pp. 20-23.

[1.19] Low Carbon Vehicle Partnership, 2016. The journey of the Green Bus A revolution in introduction of greener, cleaner buses in the UK is helping deliver on climate and air quality objectives, [online] available at https://greenerjourneys.com/wp-content/uploads/2016/02/Journey-of-the-Green-Bus-FINAL.pdf accessed 30/01/2018.

[1.20] TfL, 2015, Ultra low emission zone portfolio, [online] available at http://content.tfl.gov.uk/board-20151217-pt1-item12-ulez.pdf accessed 30/01/2018.

[1.21] S Curtin, J Gangi, 2015, Fuel Cell technologies market report, U.S. Department of Energy Efficiency and Renewable Energy [online] available at https://energy.gov/eere/fuelcells/market-analysis-reports accessed 30/01/2018.

[1.22] Y Kwon, D Jeong, 2015, Analysis on technology competitiveness in Fuel Cell field, Journal of Clean Energy Technologies, Vol.3, No.1, pp. 1-6 DOI: 10.7763/JOCET.2015.V3.158.

[1.23] A Korner, C Tam, S Bennett, 2015, Technology roadmap hydrogen and fuel cells, International Energy Agency [online] available at https://www.iea.org/publications/freepublications/publication/TechnologyRoadmapHydrogenandFuelCells.pdf accessed 30/01/2018.

[1.24] Z X Guo, J Evans, R Bucknall, M Emes, P Hall, N Tyler, 2013. HyFCap Track Record, Case for Support and Management Plan, UCL.

[1.25] EPSRC, 2016. HyFCap – reducing the cost and prolonging the durability of hydrogen fuel cell systems by in-situ hydrogen purification and technology hybridisation. [online] available at: http://gow.epsrc.ac.uk/NGBOViewGrant.aspx?GrantRef=EP/K021192/1, accessed 30/01/2018.

Chapter 2

[2.2.1] J Reed, 2000, *London Buses – a Brief History*, Capital Transport Publishing, pp. 17, ISBN-10: 185414233X.

[2.2.2] D Mais, 2017, Annual bus statistics: England 2016/17, Department for Transport [online] available at https://www.gov.uk/government/uploads/system/uploads/attachment_data/file/666759/annual-bus-statistics-year-ending-march-2017.pdf accessed 26/01/2018.

[2.2.3] TfL, 2016, London buses performance financial year 2015/16, [online] available at http://content.tfl.gov.uk/tfl-annual-report-2015-16.pdf accessed 30/01/2018.

[2.2.4] TfL, 2016, London bus network statistics TfL surface transport – buses directorate, [online] available at http://content.tfl.gov.uk/london-bus-network-statistics.pdf accessed 30/01/2018.

[2.2.5] TfL, 2015, Health, safety and environment report 2014/15, [online] available at http://www.betterbuildingspartnership.co.uk/sites/default/files/media/attachment/TfL-health-safety-environment-report-2015.pdf accessed 30/01/2018.

[2.2.6] D Anderson, 2015, Transport Statistics Great Britain 2015, Department for Transport, [online] available at https://www.gov.uk/government/uploads/system/uploads/attachment_data/file/489894/tsgb-2015.pdf accessed 30/01/2018.

[2.2.7] TfL, 2014, Transport emission roadmap cleaner transport for a cleaner London, [online] available at http://content.tfl.gov.uk/transport-emissions-roadmap.pdf accessed 30/01/2018.

[2.2.8] S Knight AM, 2014, Driving away from diesel reducing air pollution from diesel vehicles, [online] available at https://www.london.gov.uk/sites/default/files/Driving%20Away%20from%20Diesel%20final%20report.pdf accessed 30/01/2018.

[2.2.9] London datastore, 2016, Average Air Quality in London, King's College London [online] available at https://data.london.gov.uk/dataset/london-average-air-quality-levels accessed 30/01/2018.

[2.2.10] D Carslaw, S Beevers, E Westmoreland, M Williams, 2011, Trends in NO_x and NO_2 emissions and ambient measurements in the UK, King's College London, pp. 15-22.

[2.2.11] Greater London urban area agglomeration zone, 2015, Air quality plan for the achievement of EU air quality limit value for nitrogen dioxide in greater London urban area (UK0001), Department for Environment Food & Rural Affairs, pp. 20-27.

[2.2.12] TfL, 2015, Have your say on ultra low emission zone Air quality improvement [online] available at https://consultations.tfl.gov.uk/environment/ultra-low-emission-zone accessed 30/01/2018.

[2.3.1] J Q Li, 2014, Battery electric transit bus developments and operations: a review, International journal of sustainable transportation, volume 10, issue 3, 2016, DOI: 10.1080/15568318.2013.872737.

[2.3.2] M Hawes, 2016, UK bus sector sees threefold rise in new low emission vehicles, SMMT driving the motor industry [online] available at http://www.smmt.co.uk/2016/01/uk-bus-sector-sees-threefold-rise-in-new-low-emission-vehicles/ accessed 30/01/2018.

[2.3.3] S Carrol, 2015, Green fleet technology study for public transport, Cenex for the public procurement of innovation in action network [online] available at http://www.cenex.co.uk/resources/green-fleet-technology-study-public-transport/ accessed 30/01/2018.

[2.3.4] London Datastore, 2015, Number of buses by type of bus in London, [online] available at https://data.london.gov.uk/dataset/number-buses-type-bus-london accessed 30/01/2018.

[2.3.5] London bus engineering team, 2016, Bus fleet data and audits, [online] available at https://tfl.gov.uk/corporate/publications-and-reports/bus-fleet-data-and-audits accessed 30/01/2018.

[2.3.6] Low Carbon Vehicle Partnership, 2015, The journey of the green bus: A revolution in the introduction of greener, cleaner buses in the UK is helping deliver on climate and air quality objectives, Green Journeys.

[2.3.7] Frost and Sullivan, 2014, Strategic analysis of global hybrid and electric heavy-duty transit bus market [online] available at http://www.frost.com/sublib/display-report.do?id=NC7C-01-00-00-00 accessed 30/01/2018.

[2.3.8] Y Zhou, M Wang, H Hao, L Johnson, H Wang, 2014, Plug-in electric vehicle market penetration and incentives: a global view, Springer science and business media Dordrecht, DOI: 10.1007/s11027-014-9611-2.

[2.3.9] M Mahmoud, R Garnett, M Ferguson, P Kanaroglou, 2016, Electric buses: a review of alternative powertrains, Renewable and sustainable energy reviews, volume 62, pp. 673-684, DOI: 10.1016/j.rser.2016.05.019.

[2.3.10] FCU JU, 2016, Urban buses: alternative powertrains for Europe a fact-based analysis of the role of diesel hybrid, hydrogen fuel cell, trolley and battery electric power trains, [online] available at http://www.gppq.fct.pt/h2020/_docs/brochuras/fch-ju/20121029%20urban%20buses,%20alternative%20powertrains%20for%20europe%20-%20final%20report_0.pdf accessed 30/01/2018.

[2.3.11] J Miles, S Potter, 2014, Developing a viable electric bus service: the Milton Keynes demonstration project, Elsevier, Research in transportation economics, Volume 48, pp. 357-363, DOI: 10.1016/j.retrec.2014.09.063.

[2.3.12] M Broussely, G P Eds, 2007, Industrial applications of batteries from cars to aerospace and energy storage, Elsevier Science, pp. 208-212, ISBN: 9780080471273.

[2.3.13] M Chris, M Masrur, D Gao, 2011, *Hybrid electric vehicles: principles and applications with practical perspectives*, John Wiley Ltd, pp. 385-387, ISBN-10: 0470747730.

[2.3.14] A Lajunen, 2013, Energy consumption and cost benefit analysis of hybrid and electric city buses, Transportation research Part C: emerging technologies, Volume 38, pp. 1-15, DOI: 10.1016/j.trc.2013.10.008.

[2.3.15] L Gaines, P Weikersheimer, 2015, Status and isses for idling reduction in United States alternative fuel and advanced vehicle technology market trends, [online] available at https://cleancities.energy.gov/files/u/news_events/document/document_url/93/2015_strategic_planning_idling_reduction.pdf accessed 30/01/2018.

[2.3.16] J M German, 2011, *Hybrid powered vehicles*, second edition, SAE international technology profiles, pp. 9, ISBN-10: 143981175X.

[2.3.17] W Wu, J Partridge, R Bucknall, 2016, Development and modelling of a lab scaled PEM Fuel Cell drive system for city driving application, 51th International Universities Power Engineering Conference, Coimbra, Portugal, DOI: 10.1109/UPEC.2016.8114036.

[2.3.18] S Ranganathan, 2006, Hybrid buses costs and benefits, National renewable energy laboratory [online] available at http://www.eesi.org/files/eesi_hybrid_bus_032007.pdf accessed 30/01/2018.

[2.3.19] M Ehsani, 2014, *Alternative fuels and advanced vehicle technologies for improved environmental performance*, Towards zero carbon transportation, pp. 632-654, ISBN: 9780857097422.

[2.3.20] S Bruno, G Jurgen, T Wener, 2015, *Advances in battery technologies for electric vehicles*, Introduction to hybrid electric vehicles, battery electric vehicles and off road electric vehicles, Woodhead publishing, pp. 6-10, ISBN: 978-1-78242-377-5.

[2.3.21] H Y Li, G R Zhang, 2011, Hybrid electric vehicle drive control, International conference on environmental science and information application technology, Procedia environmental science 10 pp. 403-407, DOI: 10.1016/j.proenv.2011.09.066.

[2.3.22] ucsusa.org, 2015, Series vs parallel vs series/parallel drivetrains, Union of concerned scientists, [online] available at http://www.ucsusa.org/clean-vehicles/electric-vehicles/series-vs-parallel-drivetrains#.V2Ep97srKUm accessed 30/01/2018.

[2.3.23] J Larminie, J Lowry, 2012, *Electric vehicle technology explained second edition*, John Wiley Ltd, pp. 19-23, ISBN: 978-1-119-94273-3.

[2.3.24] R Muncrief, M Harold, 2012, Impact of auxiliary loads on fuel economy and emission in transit bus applications, SAE 2012 world congress & exhibition [online] available at http://papers.sae.org/2012-01-1028/ accessed 30/01/2018.

[2.3.25] M Ehsani, Y Gao, A Emadi, 2010, *Modern electric, hybrid electric and fuel cell vehicles*, CRC Press, pp. 108, 218, 322, ISBN-10: 1420053981.

[2.3.26] Low carbon vehicle partnership, 2016, The low emission bus guide, [online] available www.lowcvp.org.uk/assets/reports/LowCVP+LEB+Guide+2016+interactive+V3.pdf accessed 30/01/2018.

[2.3.27] M Dolan, 2015, Driving away from diesel reducing air pollution from diesel vehicles, [online] available at https://www.london.gov.uk/sites/default/files/Driving%20Away%20from%20Diesel%20final%20report.pdf accessed 30/01/2018.

[2.3.28] Gatwick group, 2015, South east region London buses: past present and future, Chartered institute of logistics and transport, [online] available at https://ciltuk.org.uk/About-Us/Nations-Regions-Groups/South-East/Gatwick-Group accessed 30/01/2018.

[2.3.29] A Robb, 2014, The new bus for London – diesel/electric hybrid clean fleets case study, [online] available at http://www.cleanfleets.eu/fileadmin/New_Bus_for_London_Case_Study_for_Clean_Fleets_-_final.pdf accessed 30/01/2018.

[2.3.30] P White, 2015, Impacts of bus priorities and busways on energy efficiency and emissions, University of Westminster, [online] available at https://greenerjourneys.com/wp-content/uploads/2015/09/Binder2.pdf accessed 30/01/2018.

[2.3.31] TfL, 2014, Annual report and statement of accounts 2013/14, Mayor of London, [online] available at https://www.gov.uk/government/uploads/system/uploads/attachment_data/file/330456/IPCC_annual_report.pdf accessed 30/01/2018.

[2.3.32] V Everitt, 2015, Annual report and statement of accounts, Transport for London, pp. 91 [online] available at http://content.tfl.gov.uk/tfl-annual-report-and-statement-of-accounts-2016-17.pdf accessed 30/01/2018.

[2.3.33] TfL, 2015, Cleaner air for London progress report on the delivery of the Mayor's air quality strategy, Greater London Authority, [online] available at https://www.london.gov.uk/sites/default/files/maqs_2015_progress_report_final_for_publication.pdf accessed 30/01/2018.

[2.3.34] LowCVP, 2016, A green bus for every journey, Low carbon vehicle partnership, [online] available at https://greenerjourneys.com/wp-content/uploads/2016/11/LowCVP-A-Green-Bus-for-Every-Journey-FINAL.pdf accessed 30/01/2018.

[2.3.35] G Esposito, 2016, The low emission bus guide interactive version, Low carbon vehicle partnership, [online] available at https://www.lowcvp.org.uk/assets/reports/LowCVP%20LEB%20Guide%202016%20interactive%20V3.pdf accessed 30/01/2018.

[2.3.36] F Coyle, 2014, London buses emissions reduction, TfL, [online] available at https://www.dtpm.cl/descargas/estudios/workshop/London%20Buses%20Emissions%20Reduction%20-%20Chile_V2.pdf accessed 30/01/2018.

[2.3.37] P Atkins, R Cronwell, N Tebbutt, N Schonau, 2013, Preparing a low CO_2 technology roadmap for buses, LowCVP, [online] available at http://www.apcuk.co.uk/wp-content/uploads/2015/10/LowCVP-Ricardo-Bus-Roadmap-FINAL.pdf accessed 30/01/2018.

[2.3.38] TfL, 2015, Emissions from the TfL bus fleet, Safety, Accessibility and Sustainability panel, [online] available at http://content.tfl.gov.uk/sasp-20151015-part-1-item08-transport-emissions-road-map.pdf accessed 30/01/2018.

[2.3.39] U Chong, H Steve, L Yim, A Boies, 2013, Air quality and climate impacts of alternative bus technologies in greater London, Environmental science and technology, 48 (8) pp. 4613-4622, DOI: 10.1021/es4055274.

[2.3.40] D Gregory, O Mclaughlin, S Mullerder, N Sundararajah, 2016, New solutions to air pollution challenges in the UK, [online] available at https://www.imperial.ac.uk/media/imperial-college/grantham-institute/public/publications/briefing-papers/New-solutions-to-air-pollution-challenges-in-the-UK-LFSP-BP.pdf accessed 30/01/2018.

[2.3.41] P Hoffmann, B Dorgan, 2012, *Tomorrow's energy: hydrogen, fuel cells and the prospects for a cleaner planet*, MIT Press, pp. 149-154, ISBN-10: 0262516950.

[2.3.42] Chic-project.eu, 2015, History of CUTE and HyFLEET: CUTE, FCH JU, [online] available at http://chic-project.eu/ accessed 30/01/2018.

[2.3.43] C Stockford, N Brandon, J Irvine, etc. 2015, H2FC supergen: an overview of the hydrogen and fuel cell research across the UK, International journal of hydrogen energy, Volume 40, issue 15, pp. 5534-5543, DOI: 10.1016/j.ijhydene.2015.01.180.

[2.3.44] T Hua, R Ahluwalia, L Eudy, etc. 2015, Status of hydrogen fuel cell electric buses worldwide, Journal of power sources, Volume 269, pp. 975-993, DOI: 10.1016/j.jpowsour.2014.06.055.

[2.3.45] Department for transport statistics, 2016, Average new car fuel consumption, Great Britain: 2000 to 2016, [online] available at https://www.gov.uk/government/uploads/system/uploads/attachment_data/file/661674/env0103.ods accessed 26/01/2018.

[2.3.46] Honda, 2017, Honda celebrates national hydrogen and fuel cell day with continued investment in hydrogen fuel cell technology and infrastructure, [online] available at https://www.prnewswire.com/news-releases/honda-celebrates-national-hydrogen-and-fuel-cell-day-with-continued-investment-in-hydrogen-fuel-cell-technology-and-infrastructure-300531660.html accessed 27/01/2018.

[2.3.47] T Tyler, 2011, Fuel Cell bus workshop San Francisco CA, Bluways, [online] available at http://gofuelcellbus.com/uploads/Bluways_IFCBW_2011.pdf accessed 30/01/2018.

[2.3.48] International energy agency, 2011, Hybrid and electric vehicles the electric drive plugs in, IEA energy technology network, pp. 113, [online] available at http://www.ieahev.org/assets/1/7/IA-HEV_Annual_Report_May_2013_3MB.pdf accessed 30/01/2018.

[2.3.49] R Ahluwalia, X Wang, R Kumar, 2012. Fuel Cell Transit Buses, Argonne National laboratory, Argonne, IL, [online] available at http://www.ieafuelcells.aeat.com/ documents/Fuel_Cells_for_Buses_Jan_2012.pdf accessed 30/01/2018.

[2.3.50] D Hayter, 2016, London: a capital for hydrogen and fuel cell technologies, Hydrogen London and Mayor of London, [online] available at https://www.london.gov.uk/sites/ default/files/london_-_a_capital_for_hydrogen_and_fuel_cell_technologies.pdf accessed 30/01/2018.

[2.3.51] Ballard, 2016, Fuel Cell electric buses, a solution for public transport, Group exhibit hydrogen fuel cell batteries, H2FC, [online] available at www.h2fc-fair.com/hm16/images/forum/pdf/01monday/1240.pdf accessed 30/01/2018.

[2.3.52] CHIC, 2016, London hydrogen buses and the CHIC project, FCH JU, [online] available at http://www.hydrogenlondon.org/wp-content/uploads/2015/11/CHIC-Emerging-Conclusions__short_Oct2015.pdf accessed 30/01/2018.

[2.3.53] D Yorke, 2012, Practical experience of the hydrogen bus fleet, London, First London buses, TfL [online] available at http://www.sustainabilitywestmidlands.org.uk/wp-content/uploads/GTC_Conf_Hydrogen_Bus_Presentation.pdf accessed 30/01/2018.

[2.3.54] Element energy limited, 2012, Post-2014 London hydrogen activity: options assessment, TfL [online] available at http://www.hydrogenlondon.org/wp-content/uploads/2013/10/HydrogenBuses-Post-2014-221012.pdf accessed 30/01/2018.

[2.4.1] R O Hayre, S W Cha, W Colella, F B Prinz, 2016, *Fuel Cell Fundamentals*, Hoboken, New Jersey pp. 273, ISBN: 9781119191766.

[2.4.2] F Barbir, 2005, *PEM Fuel Cells Theory and Practice*. Elsevier Academic Press, pp. 7-11, pp. 24, pp. 45, ISBN: 978-0-12-078142-3.

[2.4.3] W Wu, R Bucknall, 2013, Conceptual Evaluation of a Fuel-Cell-Hybrid Powered bus, IEEE pp. 1-5, University College London, DOI: 10.1109/UPEC.2013.6714968.

[2.4.4] J M German, 2011, *Hybrid-Powered Vehicles, second edition*, SAE international technology profiles, pp. 9, ISBN-10: 143981175X.

[2.4.5] Antig Fuel Cell Innovation, 2008, Technology: Types of Fuel Cells, Antig Technology, [online] available at http://www.antig.com/technology/technology_fuel_cell_types.htm accessed 30/01/2018.

[2.4.6] N G Moreno, M C Molina, D Gervasio, J F P Robles, 2015, Approaches to polymer electrolyte membrane fuel cells (PENFCs) and their cost, Elsevier, Rewable and Sustainable Energy Reviews, Volume 52, pp. 897-906, DOI: 10.1016/j.rser.2015.07.157.

[2.4.7] U Eberle, B Muller, R V Helmolt, 2012, Fuel cell electric vehicles and hydrogen infrastructure: status 2012, Energy & Environment Science 2012,5, pp. 8780, DOI: 10.1039/C2EE22596D.

[2.4.8] N N Li, A G Fane, W S Winston, T Matsuura, 2008, *Advanced Membrane Technology and Applications*, John Wiley Library, pp. 757-758, ISBN: 978-0-471-73167-2.

[2.4.9] F Gao, B Blunier, A Miraoui, 2013, *Proton exchange membrane fuel cells modelling,* John Wiley and sons, pp. 13-16, DOI: 10.1016/j.renene.2004.11.015.

[2.4.10] R Heck, R Farrauto, S Gulati, 2012*, Catalytic air pollution control, third edition*, John Wiley and sons, pp. 492-499, ISBN: 9781118397749.

[2.4.11] P Corbo, F Migliardini, 2011, Hydrogen fuel cells for road vehicles, Springer, pp. 77-79, pp. 138, pp. 150-155, ISBN 978-0-85729-136-3.

[2.4.12] S Bent, 2013, Hydrogen and fuel cells – merging technologies and applications, 2nd edition, Elsevier, pp. 163, ISBN: 9780123965035.

[2.4.13] Greet, 2010, The greenhouse gases, regulated emissions and energy use in transportation model, Argonne national laboratory [online] available at https://greet.es.anl.gov/publications accessed 30/01/2018.

[2.4.14] Essom, 2013, Heating values of hydrogen and fuels, Bangkok metropolis, [online] available at http://www.essom.com/upload/eng_data/22.pdf accessed 30/01/2018.

[2.4.15] J Larminie, J Lowry, 2012, *Electric vehicle technology explained second edition*, John Wiley Ltd, pp. 19-23, pp. 91, ISBN: 978-1-119-94273-3.

[2.4.16] F Barbir, 2013, *PEM Fuel Cells theory and practice, 2nd edition*, Elsevier, pp. 17-30, pp. 39-52, ISBN: 9780123983725.

[2.4.17] S Srinivasan, 2006, *Fuel Cells from fundamentals to applications*, Springer, pp. 208-211, ISBN 978-0-387-35402-6.

[2.4.18] Hyper Physics, 2009, Thermodynamic properties of selected substances, Georgia state university, [online] available at http://hyperphysics.phy-astr.gsu.edu/hbase/tables/therprop.html#c1 accessed 30/01/2018.

[2.4.19] J Beretta, 2013, *Automotive electricity: electric drives*, ISTE, pp. 223-229, ISBN: 978-1-848-21095-0.

[2.4.20] K Harrison, R Remick, G Martin, A Hoskin, 2010, Hydrogen production: fundamentals and case study summaries, National renewable energy laboratory, [online] available at https://www.nrel.gov/docs/fy10osti/48269.pdf accessed 30/01/2018.

[2.4.21] I Pilatowsky, R Romero, C Isaza, S Gamboa, P Sebastian, W Rivera, 2011, *Cogeneration fuel cell sorption air conditioning systems*, Springer, pp. 29, ISBN 978-1-84996-028-1.

[2.4.22] NPTEL, 2012, Modelling of the fuel cell: current-voltage predictions, Indian institutes of technology, [online] available at http://nptel.ac.in/courses/103102015/10 accessed 30/01/2018.

[2.4.23] C Kunusch, P Puleston, M Mayosky, 2012, *Sliding mode control of PEM fuel cells*, Springer, pp. 15-18, ISBN 978-1-4471-2431-3.

[2.4.24] A Husar, S Strahl, J Riera, 2013, Experimental characterisation methodology for identification of voltage losses of PEMFC: applied to an open cathode stack, International journal of hydrogen energy, volume 37, issue 8, DOI: 10.1016/j.ijhydene.2011.11.130.

[2.4.25] S Colleen, 2011, *PEM fuel cell modelling and simulation using MATLAB*, Elsevier, pp. 64-66, ISBN: 9780080559018.

[2.4.26] N Benchouia, A hadjadj, A Derghal, 2013, Modelling and validation of fuel cell PEMFC, Renewable energy development centre, Vol 16, pp. 365-377.

[2.4.27] I S Martin, A Ursua, P Sanchis, 2014, Modelling of PEM fuel cell performance: steady-state and dynamic experimental validation, Energies ISSN 1996-1073, DOI:10.3390/en7020670.

[2.4.28] S Dushyant, S Berry, 2011, Fuel cells technologies for fuel processing, Elsevier, pp. 18-20, ISBN: 978-0-444-53563-4.

[2.4.29] H T Pu, 2014, *Polymers for PEM Fuel Cells*, John Wiley and sons, pp. 14-17, ISBN: 9781118329405 .

[2.4.30] J H Wee, A Dong, S Gu, 2007, Applications of proton exchange membrane fuel cell systems, Elsevier, Renewable and sustainable energy reviews 11 pp. 1720-1738, DOI: 10.1016/j.rser.2006.01.005.

[2.4.31] H M Frank, 2009, *Hydrogen and fuel cell – advances in transportation and power*, Fairmont press, pp. 168, ISBN-10: 1420071564.

[2.4.32] D M Tagare, 2011, Electric power generation: the changing dimensions, IEEE press, pp. 220, ISBN: 9780470600283.

[2.4.33] L Giorgi, F Leccese, 2013, Fuel cells: technologies and applications, The open fuel cell journal, 2013, Vol. 6, pp. 1-20, DOI: 1875-9327/13.

[2.4.34] D Feroldi and M Basualdo, 2012, Description of PEM fuel cell systems, Springer-Verlag London Limited, pp. 51, DOI: 10.1007/978-1-84996-184-4_2.

[2.4.35] P Gianfranco, 2012, *Electric and hybrid vehicles – power sources, models, sustainability, infrastructure and the market*, Elsevier, pp. 242, ISBN: 9780444535665.

[2.4.36] K Murugesan, V Senniappan, 2013, Investigation of water management dynamics on the performance of a Ballard mark-V proton exchange membrane fuel cell stack system, International journal of electrochemical science 8, pp. 7885-7904, DOI: 10.1177/0957650914539306.

[2.5.1] P Grbovic, 2013, *Ultra-capacitor in power conversion systems*, John wiley and sons, pp. 2-5, ISBN: 9781118356265.

[2.5.2] A Andrijanovits, H Hoimoja, D Vinnikov, 2012, Comparative review of long term energy storage technologies for renewable energy storage, Electronics and electrical engineering, No.(2) 118, DOI: 10.5755/j01.eee.118.2.1168.

[2.5.3] G Pistoia, 2010, *Battery operated devices and systems – From portable electronics to industrial products*, Elsevier, pp. 348, ISBN: 9780080932545.

[2.5.4] P W Parfomak, 2012, *Energy storage for power grids and electric transportation: a technology assessment*, Congressional research service, pp. 7, ISBN-10: 1490945148.

[2.5.5] X Luo, J Wang, M Donner, J Clarke, 2015, Overview of current development in electrical energy storage technologies and the application potential in power system operation, Applied energy, volume 137, pp. 511-536, DOI: 10.1016/j.apenergy.2014.09.081.

[2.5.6] N Kularatna, 2015, *Energy storage devices for electronic systems*, Academic press, Chapter 2.4, pp. 2, ISBN: 9780124081192.

[2.5.7] N N Clark, 2009, Assessment of hybrid electric transit bus technology, Transportation research board, pp. 25, DOI: 10.17226/22983.

[2.5.8] H Chen, T Cong, W Yang, C Tan, Y Ding, 2009, Progress in electrical energy storage system: a critical review, Prog Nat Sci, 19, pp. 291-321, DOI: 10.1016/j.pnsc.2008.07.014.

[2.5.9] J Whartman, I Brown, 2016, Zinc air battery-battery hybrid for powering electric scooters and electric buses, [online] available at https://www.electric-fuel.com/wp-content/uploads/2016/03/Zinc-Air-Powering-Electric-Scooters-and-Buses-1998.pdf accessed 30/01/2018.

[2.5.10] Beliveau M, Rehberger J, Rowell J, Xarras A, 2010, A study on hybrid cars: environmental effects and consumer habits, Faculty of Worecester Polytechnic Institute [online] available at https://www.rsm.nl/fileadmin/Images_NEW/ECFEB/pdf/ Wilmink__2015__A_study_on_the_factors_influencing_the_adoption_of_Hybrid_and _Electric_Vehicles_in_The_Netherlands.pdf accessed 30/01/2018.

[2.5.11] M Lu, F Beguin, E Frackowiak, 2013, *Supercapacitors: materials, systems and applications*, Wiley, P232, ISBN: 978-3-527-32883-3.

[2.5.12] Namisnyk A, 2003, A survey of electrochemical supercapacitor technology, University of Technology, [online] available at http://services.eng.uts.edu.au/cempe/ subjects_JGZ/eet/Capstone%20thesis_AN.pdf accessed 30/01/2018.

[2.5.13] Berkeley Energy & Resources Collaborative, Storage wars: batteries vs supercapacitors, 2013, [online] available at http://berc.berkeley.edu/ storage-wars-batteries-vs-supercapacitors/ accessed 30/01/2018.

[2.5.14] M S Whittingham, 2012, History, evolution and future status of energy storage, IEEE, vol 100, pp. 1520, DOI: 10.1109/JPROC.2012.2190170.

[2.5.15] K Lu, 2014, *Materials and energy conversion, harvesting and storage*, John Wiley and sons, pp. 236, ISBN: 978-1-118-88910-7.

[2.5.16] M Das, I Das, N K Bhattacharyya, D Mukherjee, H Saha, 2013, Application of supercapacitor to power small electronic appliances, IOSR Journal of electrical and electronics engineering, volume 4, issue 3, pp. 28-32, e-ISSN: 2278-1676.

[2.6.1] M Nilsson, K Hillman, A Rickne, T Magnusson 2012, *Paving the road to sustainable transport: governance and innovation in low carbon vehicles*, Routledge – Business and Economics, pp. 184, ISBN-10: 113824130X.

[2.6.2] J Wang, Y Chen, Q Chen, 2006, A fuel cell city bus with three drivetrain configurations, Journal of power sources, volume 159, issue 2, pp. 1205-1213, DOI: 10.1016/j.jpowsour.2005.12.031.

[2.6.3] Y Li, J Li, Z Qin, Z Wang, 2014, Development of fuel cell hybrid electric city bus, Transportation electrification Asia-Pacific IEEE Conference and Expo, DOI: 10.1109/ITEC-AP.2014.6940811.

[2.6.4] N Kularatna, 2015, Energy storage devices for electronic systems, Academic press, chapter 2.7, chapter 5.8, ISBN: 9780124081192.

[2.6.5] A Panday, H O Bansal, 2014, A review of optimal energy management strategies for hybrid electric vehicle, International journal of vehicular technology, volume 2014 article id 160510, pp. 19, DOI: 10.1155/2014/160510.

[2.6.6] P Garcia, L M Fernandez, J P Torreglosa, F Jurado, 2012, Comparative study of four control systems for a 400 kW fuel cell battery powered tramway with two dc/dc converters, International transactions on electrical energy systems, volume 23, issue 7, pp. 1028-1048, DOI: 10.1002/etep.1636.

[2.6.7] P Garcia, J P Torreglosa, L M Fernandez, F Jurado, 2013, Control strategies for high power electric vehicles powered by hydrogen fuel cell, battery and supercapacitor, Expert systems with applications, volume 40, issue 12, pp. 4791-4804, DOI: 10.1016/j.eswa.2013.02.028.

[2.6.8] P Garcia, L M Fernandez, J P Torreglosa, F Jurado, 2013, Operation mode control of a hybrid power system based on fuel cell/battery/ultracapacitor for an electric tramway, Computers & Electrical Engineering, volume 39, issue 7, pp. 1993-2004, DOI: 10.1016/j.compeleceng.2013.04.022 .

[2.6.9] L Xu, J Li, M Ouyang, J Hua, G Yang, 2013, Multi-mode control strategy for fuel cell electric vehicles regarding fuel economy and durability, International journal of hydrogen energy, volume 39, issue 5, pp. 2374-2389, DOI: 10.1016/j.ijhydene.2013.11.133.

[2.6.10] O Kra,, H Ghodbane, R Saadi, M Becherif, 2015, Energy management of fuel cell/supercapacitor hybrid source based on linear and sliding mode control, Energy Procedia, 74, pp. 1258-1264, DOI: 10.1016/j.egypro.2015.07.770.

[2.6.11] B Vural, A Boynuegri, I Nakir etc. al, 2010, Fuel cell and ultra-capacitor hybridisation: a prototype test bench based analysis of different energy management strategies for vehicular applications, International journal of hydrogen energy, volume 35, issue 20, pp. 11161-11171, DOI: 10.1016/j.ijhydene.2010.07.063.

[2.6.12] L Xu, J Li, J Hua, X Li, M Ouyang, 2009, Optimal vehicle control strategy of a fuel cell/battery hybrid city bus, International journal of hydrogen energy, volume 34, issue 17, pp. 7323-7333, DOI: 10.1016/j.ijhydene.2009.06.021.

[2.6.13] L Xu, J Li, M Ouyang, 2015, Energy flow modelling and real time control design basing on mean values for maximising driving mileage of a fuel cell bus, International journal of hydrogen energy, volume 40, issue 43, pp. 15052-15066, DOI: 10.1016/j.ijhydene.2015.08.104.

[2.6.14] J Zhang, C Lv, M Qiu, Y Li, D Sun, 2013, Braking energy regeneration control of a fuel cell hybrid electric bus, Energy conversion and management, volume 76, pp. 1117-1124, DOI: 10.1016/j.enconman.2013.09.003.

[2.6.15] C C Chan, 2007, The state of the art of electric, hybrid and fuel cell vehicles, Proceeding of the IEEE ISSN 0018-9219, pp. 704-718, DOI: 10.1109/JPROC.2007.892489.

[2.6.16] C Zheng, G Xu, J Jeong, S Cha, Y Park, W Lim, 2014, Power source sizing of fuel cell hybrid vehicles considering vehicle performance and cost, International journal of prevision engineering and manufacturing, volume 15, issue 3, pp. 527-533, DOI: 10.1007/s12541-014-0367-0.

[2.6.17] L Xu, M Ouyang, J Li, F Yang, L Lu, J Hua, 2013, Optimal sizing of plug-in fuel cell electric vehicles using models of vehicle performance and system cost, Applied energy, volume 103, pp. 477-487, DOI: 10.1016/j.apenergy.2012.10.010.

[2.6.18] E Hosseninzadeh, M Rokni, S G Advani, A Prasad, 2013, Performance simulation and analysis of a fuel cell/battery hybrid forklift truck, International journal of hydrogen energy, volume 38, issue 11, pp. 4241-4249, DOI: 10.1016/j.ijhydene.2013.01.168.

[2.6.19] P Melo, J Ribau, C Silva, 2014, Urban bus fleet conversion to hybrid fuel cell optimal powertrains, Procedia social and behavioural sciences 111, pp. 692-701, DOI: 10.1016/j.sbspro.2014.01.103.

[2.6.20] J Ribau, R Viegas, A Angelino, A Moutinho, C Silva, 2014, A new offline optimisation approach for designing a fuel cell hybrid bus, Transportation research part C: emerging technologies, volume 42, pp. 14-27, DOI: 10.1016/j.trc.2014.02.012.

[2.6.21] J Ribau, C M Silva, J M C Sousa, 2014, Efficiency, cost and life cycle CO2 optimisation of fuel cell hybrid and plug-in hybrid urban buses, Applied energy, volume 129, pp. 320-335, DOI: 10.1016/j.apenergy.2014.05.015.

[2.6.22] R Cipollone, D D Battista, M Marchionni, C Villante, 2014, Model based design and optimisation of a fuel cell electric vehicle, Energy procedia 45, pp. 71-80, DOI: 10.1016/j.egypro.2014.01.009.

[2.6.23] L Xu, C D Mueller, J Li, M Ouyang, Z Hu, 2015, Multi-objective component sizing based on optimal energy management strategy of fuel cell electric vehicles, Applied energy, volume 157, pp. 664-674, DOI: 10.1016/j.apenergy.2015.02.017.

[2.6.24] I Lachhab, L Krichen, 2014, Impact of Ultra-capacitor sizing optimisation on fuel cell hybrid vehicle, International journal of renewable energy research, [online] available at http://dergipark.gov.tr/download/article-file/148100 accessed 30/01/2018.

[2.6.25] P Bubna, S G Advani, A K Prasad, 2012, Integration of batteries with ultracapacitors for a fuel cell hybrid transit bus, Journal of power sources, volume 199, pp. 360-366, DOI: 10.1016/j.jpowsour.2011.09.097.

[2.6.26] C Xie, X Xu, P Bujilo, D Shen, H Zhao, S Quan, 2015, Fuel cell and lithium iron phosphate battery hybrid powertrain with an ultracapacitor bank using direct parallel structure, Journal of power sources, volume 279, pp 487-494, DOI: 10.1016/j.jpowsour.2015.01.029.

[2.6.27] F Odeim, J Roes, A Heinzel, 2015, Power management optimisation of an experimental fuel cell/battery/supercapacitor hybrid system, Energies 2015, 8(7), pp. 6302-6327, DOI:10.3390/en8076302.

[2.6.28] B Wu, M A Parkes, V Yufit, etc.al, 2014, Design and testing of a 9.5kW proton exchange membrane fuel cell supercapacitor passive hybrid system, [online] available at https://docslide.com.br/documents/design-and-testing-of-a-95kwe-proton-exchange-membrane-fuel-cellsupercapacitor.html accessed 30/01/2018.

[2.6.29] Q Li, H Yang, Y Han, M Li, W Chen, 2016, A state machine strategy based on droop control for an energy management system of PEMFC battery supercapacitor hybrid tramway, International journal of hydrogen energy, volume 41, issue 36, pp. 16148, DOI: 10.1016/j.ijhydene.2016.04.254.

[2.6.30] P Bubna, D Brunner, J J Gangloff, J Suresh, G Advani, 2010, Analysis operation and maintenance of a fuel cell/battery series hybrid bus for urban transit applications, Journal of power sources, volume 195, issue 12, pp. 3939-3949, DOI: 10.1016/j.jpowsour.2009.12.080.

[2.6.31] F Sergi, 2013, Development and realisation of a hydrogen range extender hybrid city bus, Journal of power sources, volume 250, pp. 286-295, DOI 10.1016/j.jpowsour.2013.11.006:.

Chapter 3

[3.2.1] HyFLEET:CUTE team, 2009, Hydrogen transport bus technology and fuel for today and for a sustainable future, Energy and transport European Commission, [online] available at http://gofuelcellbus.com/uploads/HyFLEETCUTE_Brochure_Web.pdf accessed 30/01/2018.

[3.2.2] B Madden, 2007, London fuel cell bus trail operational experience and learnings, H2NET summer meeting, technical consultant to London buses, [online] available at http://gofuelcellbus.com/uploads/London_HyFLEET.pdf accessed 30/01/2018.

[3.2.3] M Binder, M Faltenbacher, M Kentzler, M Schuckert, 2006, Clean urban transport for Europe final report, [online] available at https://trimis.ec.europa.eu/sites/default/files/project/documents/20090917_155253_20956_CUTE%20-%20Final%20Report.pdf accessed 30/01/2018.

[3.2.4] J M Kunberger, 2010, The TriHyBus and its triple hybrid drive train for city buses, Proton Motor, [online] available at www.h2fc-fair.com/hm10/images/pdf/proton-motor04.pdf accessed 30/01/2018.

[3.2.5] A Doucek, L Janik, 2011, TriHyBus: the first fuel cells hydrogen bus in new EU countries, ECS Transations 32 (1), pp. 49-53, DOI: 10.1149/1.3641838.

[3.2.6] L Eudy, M Post, 2016, Fuel cell buses in U.S. Transit fleets: current status 2016, National renewable energy laboratory, [online] available at https://energy.gov/sites/prod/files/2016/12/f34/fcto_2016_fuel_cell_bus_report.pdf accessed 30/01/2018.

[3.2.7] L Eudy, K Chandler, 2011, National fuel cell bus program: Proterra fuel cell hybrid bus report, Columbia demonstration, Federal transit administration, [online] available at https://www.nrel.gov/hydrogen/assets/pdfs/fta_report_no_0003.pdf accessed 30/01/2018.

[3.2.8] Mercedes-Benz, 2009, The Citaro fuel cell hybrid generation zero emission, bus specification, Mercedes-Benz technical data brochures, [online] available at https://www.mercedes-benz.co.uk/content/unitedkingdom/mpc/mpc_unitedkingdom_website/en/home_mpc/bus/home/new_buses/models/regular_service_busses/_Citaro_c2/facts/technical_data_e6.html accessed 30/01/2018.

[3.2.9] L Eudy, K Chandler, 2012, Sunline transit agency advanced technology fuel cell bus evaluation: third results report, National renewable energy laboratory, [online] available at https://www.nrel.gov/docs/fy12osti/52349-1.pdf accessed 30/01/2018.

[3.2.10] G Pistoia, 2013, *Lithium-ion batteries: advances and applications*, Elsevier, pp. 190-193, ISBN: 978-0-444-59513-3.

[3.2.11] J Slavik, 2014, Electric buses in urban transport – the situation and development trends, Journal of traffic and transportation engineering, pp. 57, ISSN 2328-2142.

[3.2.12] T Lipman, A L Stewart, J Lidicker, 2015, Driver response to hydrogen fuel cell buses in real world setting, Transportation research record 2502, DOI: 10.3141/2502-06.

[3.2.13] L Eudy, M Post, 2015, Zero emission bay area (ZEBA) fuel cell bus demonstration results: fourth report, National renewable energy laboratory, [online] available at https://www.nrel.gov/docs/fy15osti/63719.pdf accessed 30/01/2018.

[3.2.14] N Hoelzinger, N L Geoffroy, 2013, CHIC influencing factors to the acceptance process of FCH technologies in public transport (CHIC project), EU Fuel Cells and hydrogen joint technology initiative, [online] available at http://chic-project.eu/wp-content/uploads/2015/03/CHIC_Social-assessment_final.pdf accessed 30/01/2018.

[3.2.15] A Zaetta, B Madden, 2011, Hydrogen fuel cell bus technology state of the art review, NexthyLights, Element energy, [online] available at http://s3.amazonaws.com/zanran_storage/nexthylights.eu/ContentPages/2481166193.pdf accessed 30/01/2018.

[3.2.16] T Tyler, R D Core, 2011, Fuel cell bus workshop san Francisco, CA, Bluways [online] available at http://gofuelcellbus.com/uploads/Bluways_IFCBW_2011.pdf accessed 30/01/2018.

[3.2.17] CHIC team, 2015, Presentation of emerging conclusions, Fuel cells and hydrogen joint undertaking, [online] available at http://3emotion.eu/sites/default/files/documents/CHIC%20Emerging%20Conclusions__for%203Emotion.pdf accessed 30/01/2018.

[3.2.18] J Ally, T Pryor, A Pigneri, 2015, The role of hydrogen in Australia's transport energy mix, International journal of hydrogen energy, volume 40, issue 13, pp. 4426-4441, DOI: 10.1016/j.ijhydene.2015.02.022.

[3.2.19] K Chandler, L Eudy, 2009, National fuel cell program: accelerated testing report, AC Transit appendices, National renewable energy laboratory, [online] available at https://www.nrel.gov/docs/fy10osti/48106-2.pdf accessed 30/01/2018.

[3.2.20] Van Hool, 2013, Van Hool A330 fuel cell hybrid bus specification, Van Hool technical data, [online] available at https://www.nrel.gov/docs/fy06osti/39441.pdf accessed 30/01/2018.

[3.2.21] L Eudy, M Post, 2017, American fuel cell bus project evaluation: third report, National renewable energy laboratory, [online] available at https://www.afdc.energy .gov/uploads/publication/fc_bus_project_eval_3rd_rpt.pdf accessed 30/01/2018.

[3.2.22] T Hua, R Ahluwalia, L Eudy, etc al. 2014, Status of hydrogen fuel cell electric buses worldwide, Journal of power soruces, volume 269, pp. 975-993, DOI: 10.1016/j.jpowsour.2014.06.055.

[3.2.23] D Stolten, B Emonts, 2012, *Fuel cell science and engineering: material processes, systems and technology*, Wiley-VCH Verlag, pp. 1081, ISBN: 978-3-527-33012-6.

[3.2.24] Fuel Cells Bulletin, 2015, Ballard in $17m deal to deploy 300 buses in China, launch modules, Elsevier, FC Bulletin volume 2015, issue 10, pp. 2, DOI: 10.1016/S1464-2859(15)30301-1.

Chapter 4

[4.2.1] Hydrogenics, 2015, Shift power and energise your world, about the company, [online] available at http://www.hydrogenics.com/about-the-company/who-we-are accessed 30/01/2018.

[4.2.2] Y C Liu, R Bucknall, C K Tam, 2011, PEM Fuel Cell installation and performance testing, University College London.

[4.3.1] M Wens, M Steyaert, 2011, *Design and implementation of fully integrated inductive DC-DC converters in standards CMOS*, Springer, pp. 49-53, ISBN 978-94-007-1436-6.

[4.3.2] A Ioinovici, 2013, *Power electronics and energy conversion systems: fundamentals and hard switching converters*, Wiley library, Volume 1, pp. 402, ISBN: 9781118443040.

[4.8.1] R Liu, L Zhang, X Sun, H Liu, 2012, *Electrochemical technologies for energy storage and conversion*, volume 1 and 2, Wiley online library, pp. 69, 317, ISBN: 978-3-527-32869-7.

[4.8.2] K Lu, 2014, *Materials in energy conversion, harvesting and storage*, Wiley online library, pp. 323, ISBN: 9781118892374.

[4.8.3] H Hsuan, W CHien, 2012, An integrated optimisation approach for a hybrid energy system in electric vehicles, Apply energy, 98:479-90, DOI: 10.1016/j.apenergy.2012.04.012.

[4.8.4] C Clemente, V Ottorino, 2014, Experimental analysis on the performance of lithium based batteries for road full electric and hybrid vehicles, Applied energy 2014.04.013, pp. 2, DOI: 10.1016/j.apenergy.2014.04.013.

[4.8.5] J Warner, 2015, *Handbook of lithium-ion battery pack design – chemistry, components, types and terminology*, Elsevier 978-0-12-801456-1, pp. 194-196, ISBN: 9780128016688.

[4.8.6] V Musolino, E Tironi, 2010, A comparison of supercapacitor and high power lithium batteries, IEEE 978-1-4244-9034-3, pp. 5, DOI: 10.1109/ESARS.2010.5665263.

[4.8.7] A Burke, H Zhao, 2015, Applications of supercapacitors in electric and hybrid vehicles, 5th European symposium on supercapacitor and hybrid solutions, [online] available at https://steps.ucdavis.edu/wp-content/uploads/2017/05/2015-UCD-ITS-RR-15-09-1.pdf accessed 30/01/2018.

[4.8.8] T D Atmaja, A Min, 2012, PEMFC optimisation strategy with auxiliary power source in fuel cell hybrid vehicle, [online] available at iptek.its.ac.id/index.php/jts/article/view/17 accessed 30/01/2018.

[4.8.9] X S Hu, L Johannesson, N Murgovski, B Egardt, 2014, Longevity-conscious dimensioning and power management of the hybrid energy storage system in a fuel cell hybrid electric bus, Applied energy volume 137, pp. 913-924, DOI: 10.1016/j.apenergy.2014.05.013.

[4.8.10] D Perrotta, B Ribeiro, R Rossetti, J Afonso, 2012, On the potential of regenerative braking of electric buses as a function of their itinerary, Social and behavioural sciences, pp. 10, DOI: 10.1016/j.sbspro.2012.09.830.

[4.8.11] X Wu, C Hu, J Du, M Zhou, 2014, The fuel economy analysis of series hybrid electric bus with different energy storage devices, Internal journal of control and automation vol. 7, pp. 210-213, DOI: 10.14257/ijca.2014.7.4.18.

[4.8.12] Y Zhu, S Murali, M D Stoller, K Ganesh, 2011, Carbon-based supercapacitors produced by activation of graphene, Science vol. 332, issue 6037, pp. 1537-1541, DOI: 10.1126/science.1200770.

[4.8.13] D B Murray, J G Hayes, 2015, Cycle testing of supercapacitor for long life robust applications, IEEE Transactions on power electronics, vol.30, pp. 2505-2515, DOI: 10.1109/TPEL.2014.2373368.

[4.8.14] T Bartley, 2005, Ultracapacitors and batteries for energy storage in heavy duty hybrid electric vehicles, [online] available at http://formulahybrid.ru/Books/new/technical_paper_ultracaps.pdf accessed 30/01/2018.

[4.8.15] B Scrosati, K M Abraham, W V Schalkwijk, 2013, *Lithium batteries: advanced technologies and applications*, Wiley online library, pp. 265, ISBN: 9781118615515.

[4.8.16] Y Brunet, 2011, *Energy storage*, Wiley online library, pp. 219, DOI: 10.1002/9781118557808.ch5.

[4.8.17] M C Pera, D Hissel, H Gualous, C Turpin, 2013, *Electrochemical components*, Wiley online library, pp. 213, ISBN10 1848214014.

[4.8.18] F Beguin, E Frackowiak, 2013, Supercapacitors: materials, systems and applications, Wiley online library, pp. 69, ISBN: 978-3-527-32883-3.

[4.8.19] K M Khyrul, 2013, 48V Supercapacitor power management unit, Tampere university of technology, [online] available at https://dspace.cc.tut.fi/dpub/bitstream/handle/123456789/22085/Kabir.pdf?sequence=1 accessed 30/01/2018.

[4.8.20] W Hofmann, J Schalabbach, W Just, 2012, *Reactive power compensation: a practical guide*, Wiley online library, pp. 147-156, ISBN: 9781119967286.

[4.8.21] A Nadeau, G Sharma, T Soyata, 2014, State of charge estimation for supercapacitors, a kalman filtering formulation, 2014 IEEE international conference on acoustic, speech and signal processing, pp. 2194, DOI: 10.1109/ICASSP.2014.6853988.

[4.8.22] A Nadeau, M Hassanalieraph, 2015, Energy awareness for supercapacitors using kalman filter state of charge tracking, Journal of power sources, volume 296, pp. 383-391, DOI: 10.1016/j.jpowsour.2015.07.050.

[4.8.23] M Wens, M Steyaert, 2011, *Design and implementation of fully-integrated inductive DC-DC converter in standard CMOS, Analog circuits and signal processing*, Springer science and business media, pp. 28, ISBN 978-94-007-1436-6.

[4.8.24] S Misra, D Mahapatra, S K Patro, 2013, Performance estimation of tristate DC-DC buck converter with fixed frequency and constant switching hysteresis control, International journal of application or innovation in engineering and management, volume 2, issue 6, pp. 213, ISSN 2319 - 4847.

Chapter 5

[5.4.1] N Benchouia, A E Hadjadj, A Derghal, L Khochemane, B Mahamah, 2013, Modelling and validation of fuel cell PEMFC, [online] available at http://www.cder.dz/vlib/revue/pdf/v016_n2_texte_14.pdf accessed 30/01/2018.

[5.4.2] R Seyezhai, B Mathur, 2001, Mathematical modelling of proton exchange membrane fuel cell, International journal of computer applications, volume 20, pp. 2, DOI: 10.1016/S0378-7753(01)00798-4.

[5.4.3] M N Souleman, O Tremblay, L A Dessaint, 2009, A generic fuel cell model for the simulation of fuel cell vehicles, IEEE engineering 978-1-4244-2601, pp. 1723-1726, DOI: 10.1109/VPPC.2009.5289692.

[5.4.4] H Najafizadegan, H Zarabadipour, 2012, Control of voltage in proton exchange membrane fuel cell using model reference control approach, [online] available at http://www.electrochemsci.org/papers/vol7/7086752.pdf accessed 30/01/2018.

[5.4.5] A E Monem, A M Azmy, S Mahmoud, 2014, Dynamic modelling of proton exchange membrane fuel cells for electric vehicle applications, Petroleum and environmental biotechnology volume 5 issue 2, pp. 2-4, DOI: 10.1109/VPPC.2011.6043131 .

[5.4.6] J L Zhang, J F Wu, H M Zhang, J Zhang, 2013, *PEM Fuel cell testing and diagnosis*, Elsevier, pp. 15-32, ISBN: 9780444536891.

[5.4.7] L H Seim, 2011, Modelling, control and experimental testing of a supercapacitor/battery hybrid system – passive and semi-active topologies, Norwgian University of life sciences, [online] available at https://brage.bibsys.no/xmlui/bitstream/handle/11250/188829/M_Thesis_L_H_Seim_Brage.pdf?sequence=1 accessed 30/01/2018.

[5.4.8] A B Cultura, Z M Salameh, 2015, Modelling, evaluation and simulation of a supercapacitor module for energy storage application, International conference on computer information systems and industrial applications, pp. 876-879, DOI :10.2991/cisia-15.2015.235.

[5.4.9] R Drummond, D A Howey, S R Duncan, 2014, Low order mathematical modelling of electric double layer supercapacitors using spectral methods, University of Oxford, pp. 3-7, DOI: 10.1016/j.jpowsour.2014.11.116.

[5.4.10] A Balakrishnan, K R V Subramanian, 2013, *Nanastructured ceramic oxides for supercapacitor applications*, CRC press Tylor & Francis group, pp. 59, ISBN 9781138072671.

[5.4.11] D Wu, 2013, Control of a supercapacitor based energy storage system, University of Manchester, [online] available at https://www.research.manchester.ac.uk/portal/files/54547989/FULL_TEXT.PDF accessed 30/01/2018.

Chapter 6

[6.1] A Korner, 2015, Technology roadmap hydrogen and fuel cells technical annex, International energy agency IEA, [online] available at https://www.iea.org/publications/freepublications/publication/TechnologyRoadmapHydrogenandFuelCells.pdf accessed 30/01/2018.

[6.2] C Hall, M Kothari, Y Sharma, 2014, Ultracapacitors, MMcGraw hill education publisher, Chapter 12, pp. 7, ISBN-10: 0071841679 .

Appendix

[A.1] J Gallo, T B Rubin, J Tomic, 2014, Peak demand charges and electric transit buses, US department of transportation federal transit administration, [online] available at http://www.calstart.org/Libraries/Publications/Peak_Demand_Charges_and_Electric_Transit_Buses_White_Paper.sflb.ashx accessed 30/01/2018.

[A.2] M Mahmoud, R Garnett, M Ferguson, P Kanaroglou, 2016, Electric buses: a review of alternative powertrains, Renewable and sustainable energy reviews, volume 62, pp. 673-684, DOI: 10.1016/j.rser.2016.05.019.

[B.1] G Masiero, M H Ogasavara, A C Jussani, M L Risso, 2015, Electric vehicles in China: BYD strategies and government subsidies, RAI-Journal of management and innovation, volume 13, issue 1, DOI: 10.1016/j.rai.2016.01.001.

[B.2] J Grutter, 2015, Real world performance of hybrid and electric buses, Rewable energy and energy efficiency promotion in international cooperation, pp. 29-32, DOI: 10.1016/j.energy.2015.12.041.

[B.3] M Payne, 2014, New generation transport, sub mode options investigation, Mott Macdonald, [online] available at http://democracy.leeds.gov.uk/documents/s149482 /App%20H%20C-1-16%20Sub%20Mode%20Options%20Report.pdf accessed 30/01/2018.

[B.4] Transport news brief, 2013, Chinese electric buses enter service in London, Society of motor manufacturers and traders [online] available at http://www.transportnewsbrief. co.uk/news/chinese-elelectric-buses-enter-service-london/ accessed 30/01/2018.

[B.5] M Weston, 2015, ZeEUS project London demonstration, [online] available at http://zeeus.eu/uploads/publications/documents/zeeus-london-leaflet.pdf accessed 30/01/2018.

[B.6] T Brown, 2015, First-ever electric double decker London red bus, The Manufacturer available at http://www.themanufacturer.com/articles/first-ever-electric-double-decker-london-red-bus/ accessed 30/01/2018.

[B.7] M poulton, 2014, Electric buses, London electric vehicle partnership meeting city hall, [online] available at http://www.triangle.eu.com/wp-content/uploads/2014/07/LEVP-070714-Electric-Buses-Mark-Poulton.pdf accessed 30/01/2018.

[B.8] A Barkow, 2015, Unplugged final report: Wireless charging for electric vehicles, Project unplugged, [online] available at http://unplugged.enide.eu/wordpress/wp-content/uploads/2015/12/UNPLUGGED-Publishable-Final-Report.pdf accessed 30/01/2018.

[C.1] R Berger, 2015, Fuel cell electric buses – potential for sustainable public transport in Europe, Fuel cell and hydrogen joint undertaking, [online] available at http://www.fch.europa.eu/sites/default/files/150909_FINAL_Bus_Study_Report_OUT_0.PDF accessed 30/01/2018.

[C.2] S Curtin, J Gangi, 2014, The business case for fuel cells 2014: powering the bottom line for businesses and communities, Breakthrough technologies institute, [online] available at https://energy.gov/sites/prod/files/2015/02/f19/fcto_2014_business_case_fuel_cells.pdf accessed 30/01/2018.

[C.3] E Klaassen, 2014, International comparison of fossil power efficiency and CO2 intensity, ECOFYS, [online] available at https://www.ecofys.com/files/files/ecofys-2014-international-comparison-fossil-power-efficiency.pdf accessed 30/01/2018.

[C.4] P Corbo, 2011, *Hydrogen fuel cells for road vehicles*, Green energy and technology, Chapter 2 pp. 34, ISBN 978-0-85729-136-3.

[C.5] J Partridge, W Wu, R Bucknall, 2017, Development of bus drive technology towards zero emissions: a review, *Hybrid electric vehicles*, Intech open access, pp. 15, ISBN 978-953-51-3298-1.

[D.1] Chic-project.eu, 2015, History of CUTE and HyFLEET: CUTE, FCH JU, [online] available at http://chic-project.eu/ accessed 30/01/2018.

[D.2] C Carnevali, R Genova, P Jenne, M Mazzuchelli, M Reijalt, G Priano, 2012, Fuel cell electric buses and perspectives: Hign VLO city project authors, Energy conference and exhibition, IEEE, DOI: 10.1109/EnergyCon.2012.6347722.

[D.3] 3emotion.eu, 2016, About the project environmentally friendly efficient electric motion, FCH JU, [online] available at http://www.3emotion.eu/about-project accessed 30/01/2018.

[D.4] M Dolman, 2017, Zero emission public transport fuel cell buses in Europe, [online] available at http://hydrogenvalley.dk/wp-content/uploads/2017/09/FCB-CPH17_ELEMENT-ENERGYZero-emission-transportation-for-Europe.pdf accessed 30/01/2018.

[D.5] FCHJU, 2017, Joint initiative for hydrogen vehicles across Europe, [online] available at http://www.fch.europa.eu/project/joint-initiative-hydrogen-vehicles-across-europe accessed 30/01/2018.

[E.1] Gofuelcellbus.com, 2015, International fuel cell bus collaborative all active demonstrations [online] available at http://gofuelcellbus.com/index.php/the-collaborative/all-active-demonstrations/ accessed 30/01/2018.

[F.1] Londonbusroute.net, 2013, Route RV1, London bus services limited, [online] available at http://www.londonbusroutes.net/photos/RV1.htm accessed 30/01/2018.

[F.2] B Madden, 2007, London fuel cell bus trail operational experience and learnings, H2NET summer meeting, [online] available at gofuelcellbus.com/uploads/London_HyFLEET.pdf accessed 30/01/2018.

[F.3] D Raine, 2009. Bringing hydrogen to London's streets, Air products & TfL [online] available at http://www.airproducts.com/~/media/downloads/case-study/t/en-tfl-case-study.pdf accessed 30/01/2018.

[F.4] D Snauwaert, 2016, Van Hool delivers two fuel cell buses for London, Vanhool, [online] available at https://www.vanhool.be/ENG/actua/2fuelcellbuseslo.html, accessed 30/01/2018.

[F.5] J Aldous, 2012, Fuel Cell power generating electricity, heat and hydrogen, cleanly, quietly and efficiently transport issue, [online] available at https://fuelcellpower.files.wordpress.com/2017/09/fcpsummer12final1.pdf , accessed 30/01/2018.

[G.1] F Gao, B Blunier, A Miraoui, 2013, *Proton Exchange Membrane Fuel Cells Modelling*, Wiley online library, pp. 5-9, ISBN: 978-1-848-21339-5.

[G.2] J Larminie, A Dicks, 2013, *Fuel Cell Systems Explained, Second Edition*, Wiley online library, pp. 14-16, ISBN: 978-0-470-84857-9 .

[G.3] A S Acrico, V Baglio, V Antoucci, edited by H Liu, J Zhang, 2009, *Electrocatalysis of Direct Methanol Fuel Cells*, Verlag GmbH & Co KGaA, Weinheim, chapter 1, pp. 1-4, ISBN: 9783527627707.

[G.4] V S Bagotsky, 2012, *Fuel Cell: Problems and Solutions*, Second Edition, The electrochemical society series, pp. 71, ISBN: 978-1-118-08756-5.

[G.5] M Ehasani, Y M Gao, A Emadi, 2009, Modern Electric, *Hybrid Electric, and Fuel Cell Vehicles: Fundamentals, Theory and Design, Second Edition*, CRC Press, pp. 444-447, ISBN-10: 1420053981.

[G.6] S Bent, 2013, *Hydrogen and Fuel Cells – Emerging Technologies and Applications, Second Edition*, Elsevier, pp. 159-161, ISBN: 9780123965035.

[G.7] F Holcomb, M Blinder, W Taylor, J Torrey, J Westerman, 2000, Phosphoric acid fuel cells, US Army Engineer Research and Development Centre, [online] available at http://www.dtic.mil/dtic/tr/fulltext/u2/a386669.pdf accessed 30/01/2018.

[G.8] C Zuo, M F Liu, M L Liu, 2012, Solid Oxide Fuel Cells, Georgia Institute of Technology, pp. 8, DOI: 10.1007/978-1-4614-1957-0_2.

[G.9] S Mcphail, A Aarva, H Devianto, R Bove, A Moreno, 2010, SOFC and MCFC: Commonalities and opportunities for integrated research, Elsevier, International Journal of Hydrogen Energy, DOI: 10.1016/j.ijhydene.2010.09.071.

[G.10] M M Mench, 2008, *Fuel Cell Engines Introduction to Fuel Cells*, John Wiley Library, pp. 10, pp. 14-16, ISBN: 9780470209769.

[K.1.] K B Liu, C Y Liu, Y H Liu, 2016, Analysis and controller design of a universal bidirectional DC-DC converter, Energies 2016, 9, 501, pp. 3-7, DOI:10.3390/en9070501.

[K.2.] A D Patel, 2014, Analysis of bidirectional buck boost converter by using PWM control scheme, International journal of engineering development and research, pp. 80, ISSN: 2321-9939.

Appendix A
Selection of operating battery electric bus models

Table A-1 Selection of operating electric bus models worldwide [A.1]

Manufacturer	Length	Capacity	Battery type	Battery capacity	Range	Deployment location
ABB TOSA	18 m	135	Lithium Titanate oxide	38 kWh	Trolley, on-route	Switzerland
BYD	12 m	40	BYD Iron Phosphate	324 kWh	250 km	Worldwide
Complete Coach Works	12 m	37	Lithium-iron Phosphate	213 kWh	145 km	US
EBusco	12 m	76	Lithium-iron Phosphate	242 kWh	250 km	China, Finland
Hengtong EBus	12 m	70	Lithium Titanate	60 kWh	38 km	China
New Flyer	12 m	40	Lithium-Ion	120 kWh	72 km	US, Canada
Primove	12 m	44	Lithium-Ion	60 kWh	Wireless, on-route	Germany
Proterra	10 m	35	Lithium Titanate	74 kWh	42 km	US
Siemens	8 m	40	Lithium-iron Phosphate	96 kWh	Trolley, on-route	Austria
Sinautec	12 m	41	Ultra-Cap and Battery	5.9 kWh	Trolley, on-route	China

Table A-1 shows a selection of operating battery electric buses in different locations. As the table shows, both overnight and opportunity e-buses development has been carried out worldwide. There is no simple answer which strategy is best as they are dependent on the application. Mahmoud [A.2] carried out a detailed comparison study of different electric powertrains and concluded that a single technological choice would not satisfy the varied operational demands of transit services because electric buses are highly sensitive to the energy profile and operational demands.

Appendix B

London battery electric bus development

London has been working on overnight e-bus operation since 2012 and are also investigating the potential of opportunity e-bus technologies. From the overnight e-bus perspective, TfL has also been working with BYD, which is one of the largest electric bus manufacturers in the world, to test the potential of fully electric buses in London since 2012. The first two battery electric buses were handed over to TfL in 2013 and then entered daily service on two central London routes, number 507 and 521 which were the first fully electric buses in London [B.1]. These single-decked 12-metre BYD buses are powered by a Iron-phosphate battery and have demonstrated that their range can comfortably exceed 250 km on a single charge in actual city driving conditions [B.2]. Those two trial buses were operating on routes 507 and 521, which are relatively short commuter service routes. Hence these electric buses can start service in the morning peak alongside the diesel bus fleet and return to the depot to recharge in the evening for an overnight operation [B.3]. The electric bus battery takes four to five hours to recharge from totally exhausted. The BYD electric bus battery has been designed for a life of more than 4000 cycles which translates to 10 years battery lifetime under normal operating conditions [B.4]. The trial fleet was extended to 6 buses in summer 2014. The trial buses in London not only provide zero emission environmental benefit but have also shown promising results in both technical and economic terms, and have convinced TfL to take further steps towards adopting this new clean technology in the capital. The development timeline and future plans for London electric buses have been plotted in Figure B-1.

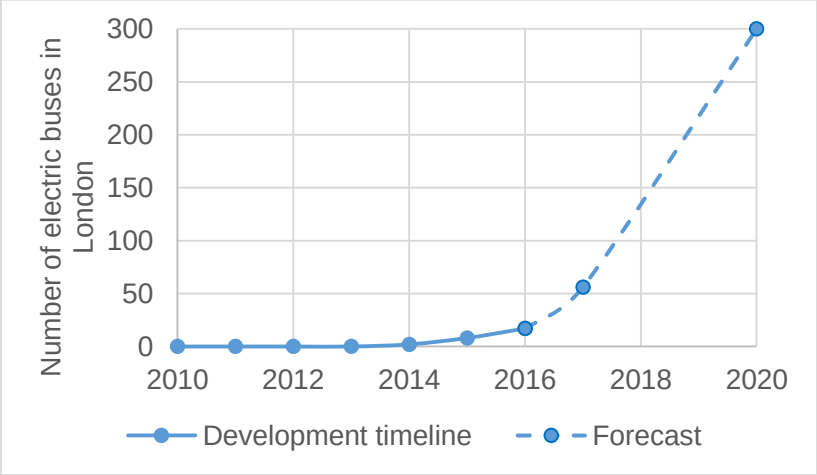

Figure B-1 Number of electric buses in London and TfL forecast (300 buses in 2020 represent all single decker zero emission buses including FC, electric etc. and excluding double decker ones)

The latest data in 2017 showed there are currently 22 electric buses operating in London including 17 single decker BYD electric buses and 5 double decker pure electric buses [B.5] [B.6]. TfL has set a goal to achieve a 300 zero emission buses (mainly FC and electric) milestone by 2020 to supplement the ULEZ. These buses will serve as pilot projects for the coming innovative recharging method projects for the opportunity strategy, which is to utilise fast wireless charging at passenger stop points. The recent first-ever double decker electric buses use wireless charging technology as part of an innovative charging technology development. However, this is still far from a mature technology and requires a recharging network infrastructure [B.7]. The electric buses in London have shown good performance on the short commuter routes. Pure e-buses are still best suited for shorter routes with operational flexibility and scope to recharge them in inter-peak periods due to the limits of present battery capacity and recharging technology [B.8]. To sum up, recent battery electric bus development in London has shown that electric buses are technically feasible. It would seem that electric buses will also have an important role to play in the coming ULEZ implementation in 2020. However, more time is needed to evaluate the actual performance and address the key challenges of electric buses over time.

Appendix C
High level comparison between battery electric bus and FC bus

FC buses and battery electric buses have both been developed as long term solutions for zero emission bus system, which is the ultimate objective for a clean transportation network. Therefore, this section will mainly compare battery electric buses (opportunity, overnight and trolley) and FC bus technologies as the two most promising zero emissions solutions. A summary of the discussion has been provided in Table C-1.

Daily range: Opportunity e-buses have a smaller energy storage system that requires frequent recharging, which equates to poor performance in terms of daily range. Overnight e-buses utilise a much larger battery which increases the range with reported values of over 300 km per charge. Trolley e-buses are continuously powered with electricity by overhead lines along the route which effectively gives unlimited range. FC buses use hydrogen cylinders as fuel tanks which allows the range to be greatly extended (up to 450 km) for as much as the hydrogen fuel cylinder weight and size allows [C.1].

Route flexibility: Opportunity and trolley e-buses require recharging infrastructures along the route which greatly limits their route flexibility. This is somewhat dependant on the size of the on-board battery and will likely be more acute for trolley e-buses. The Overnight e-buses and FC buses are expected to be able to operate for an entire day's service without recharging or refuelling. As such this allows for much greater route flexibility. This appears to be easily achieved for FC buses, however for Overnight e-buses this is not always the case and will again be dependent on the size of the battery.

Refuelling time: Opportunity e-buses require frequent recharging throughout the entire route. Although each recharges for the opportunity e-bus only takes up to 15 minutes, it is still considered as a drawback due to the requirement for regular recharging. Overnight e-buses require a longer recharging time (average >4 hours) after each operation due to the increased battery capacity. The recharging time is heavily dependent on the charging power. Trolley e-buses are powered through overhead wires so that they require no refuelling time. FC buses are refuelled with gaseous hydrogen, which can be completed quickly (< 10 minutes) [C.1].

Infrastructure: Opportunity e-buses and trolley buses require corresponding infrastructure along the route and at each end of the routes. Therefore, opportunity e-buses and trolley buses require a comprehensive infrastructure network. Overnight e-buses and FC buses both require infrastructure to recharge/refuel at the end of daily operation. This can however be centralised at the service depot and hence does not need to be as comprehensive. It appears however that the current recharging times for overnight e-buses presents a problem since it is likely that a significant number of recharging points would be needed to recharge the batteries of a large fleet in time for the next day's service. This could potentially be an issue if the number of buses grows significantly, while this wouldn't be a problem for FC buses because of their short refuelling time [C.2].

Fuel availability: All three battery electric bus technologies use electricity to recharge their batteries. This electricity could be central managed and distributed locally through the local electricity grids, however widespread electric bus deployment could significantly stress this infrastructure. FC buses will likely require the development of a comprehensive distribution network for hydrogen, although on-site hydrogen production has been demonstrated. Additionally, hydrogen fuel storage would also create additional cost.

Clean source: Real zero emissions bus technology needs to be clean throughout the manufacturing process, fuel production and bus operation. Currently, battery electric and FC bus technologies can achieve zero operating emission but the lifetime emissions are much harder to quantify. It is hard to forecast how the emissions from new technology manufacturing will change, but the fuel production method can be roughly estimated. In 2015, 67% of electricity was made from fossil fuels and 16% of electricity was from renewable energy sources [C.3] while about 96% of hydrogen was made from fossil fuels [C.4]. Therefore, from the current status, electricity for battery electric buses comes from a cleaner fuel than hydrogen for FC buses.

Cost: FC buses are currently generally the most expensive in terms of the capital costs of the buses. Although it is hard to determine how the infrastructure costs will compare for widespread deployment. Although overnight e-buses require a larger battery on-board, the infrastructure requirement from opportunity and trolley e-buses are still considered more expensive than the overnight e-buses.

Table C-1 High level comparison of zero emission bus concepts [C.5]

Zero emission option	Opportunity E-bus	Overnight E-bus	Trolley E-bus	Fuel Cell bus
Daily range	4	3	1	2
Route flexibility	3	1	4	1
Refuelling time	2	3	n/a	1
Infrastructure	3	2	4	1
Fuel availability	1	1	1	4
Clean source	1	1	1	4
Cost	3	1	2	4

(1-best, 4-worst)

Appendix D

European main FC bus demonstration project 2001-2019

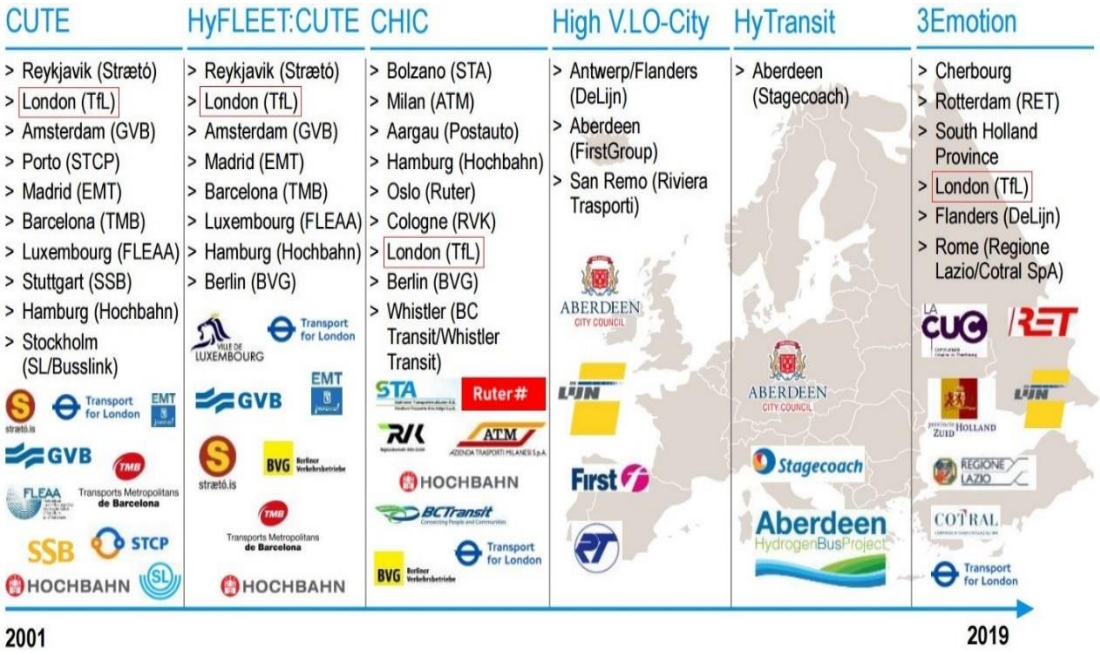

Figure D-1 Former and ongoing FC bus demonstration projects in Europe (Figure edited from FCH JU, 2015)

CUTE (Clean urban transport for Europe, 2001-2006) was the first major European project initiated for the deployment and testing of FC buses. There were 27 Citaro fuel cell buses operating in nine European cities (3 per city) along with the corresponding refuelling infrastructure. This project proved to be a valuable pilot to determine the feasibility of FC buses for a clean urban public transport system [D.1].

HyFLEET: CUTE (2006-2009) was based upon the information garnered from the CUTE and was the world's largest FC bus demonstration and research project. The project involved 47 FC buses in regular public transport service in 10 cities across three continents. This project diversified the technology and reduced fuel consumption in FC buses by developing more efficient hydrogen powered bus technology [D.2].

CHIC (Clean H_2 in European Cities Project, 2010-2016) is a project initiated by the EU, aimed at full market commercialisation of FC hydrogen powered buses. This project involved 36 FC buses operating in seven European cities. Following the CHIC project, London has deployed a fleet of Hydrogen Buses operating in Central London and managed by TfL. This will be explained in detail later.

High V.LO-City (2012-2018) is a project that involves 14 FC buses deployed in three cities across Europe. This project aims to assess if FC buses can operate at the same level as conventional diesel buses in terms of efficiency and flexibility. Additionally, hydrogen, from two of the refuelling sites, is produced from sustainable energy sources to demonstrate the sustainability potential [D.1] [D.2].

HyTransit (2013-2018) is a project supported by the FCH JU involving 6 FC buses operating daily services in Aberdeen to contribute to the assessment for the adoption of hydrogen buses in Europe. The project seeks to achieve some technical targets in terms of hydrogen consumption, availability and daily operation hours.

3Emotion (Environmentally friendly efficient electric motion, 2015-2019) project will bridge the gap between current FC bus pilot projects and larger scale commercialisation studies. This project involves the deployment of 21 new and 8 existing FC buses in 5 European cities. The project aims at enhance the technical side of FC buses and move towards cost effective integration in local bus fleets [D.3].

JIVE (Joint initiative for hydrogen vehicles across Europe, 2017-2022) project will pave the way to commercialisation of fuel cell bus fleets through the deployment of 142 fuel cell buses across 9 locations, more than doubling the number of FC buses operating in Europe. This project is the latest project which has just been confirmed in Jan 2017 and will be the first large scale validation project of fuel cell bus fleets. The project aims to demonstrate the technical readiness of FC buses to bus operators and the economic viability to policy makers [D.4] [D.5].

Appendix E

Active FC bus demonstration project

Table E-1: Active fuel cell bus demonstration project in 2016

(Reorganised from [E.1])

Project	Fleet	Year	Location	Length (m)	FC size (kW)	Battery type	Battery size (kWh)	Drive type
JHFC	2	2006	Tokoname, Japan	10.5	180	Nickel Metal Hydride	Not available	FC dominant hybrid
University of Delaware	2	2007	Dewark, US	6.7	40	NiCad	60	Battery dominant hybrid
TriHyBu	1	2009	Neratovice, Czech Republic	12	48	Lithium Ion	26	Battery dominant hybrid
BurbankBus	1	2010	Burbank, US	10.7	32	Lithium Titanate	54	Battery dominant hybrid
HySUT	2	2010	Tokyo, Japan	10.5	180	Nickel Metal Hydride	Not available	FC dominant hybrid
NFCBP	1	2010	San Francisco, US	12.2	32	Lithium Ion	n/a	FC APU Compound
Toyota FCHV	1	2010	Toyota City, Japan	10.5	180	Nickel Metal Hydride	Not available	FC dominant hybrid
NFCBP	4	2010	Hartford, US	12.2	120	Lithium Ion	17.4	FC dominant hybrid
CHIC	8	2010	London, UK	12	75	Supercapacitor	0.5	FC dominant hybrid
CHIC	3	2011	Milan, Italy	11.9	120	Lithium Ion	26	FC dominant hybrid
SunLine	6	2011	Thousand Palms, US	12.2	150	Nanophosphate Li-ion	11	FC dominant hybrid
NFCBP	12	2011	Multi-city, US	12.2	120	Lithium Ion	17.4	FC dominant hybrid
CHIC	4	2011	Cologne, Germany	18.4	150	NiMeH and Supercapacitor	23 and 0.6	FC dominant hybrid
CHIC	5	2011	Aargau, Switzerland	11.9	120	Lithium Ion	26.9	FC dominant hybrid
CHIC	5	2012	Oslo, Norway	13	150	Lithium Ion	17.5	FC dominant hybrid
NIP, CHIC	6	2012	Hamburg, Germany	12	120	Lithium Ion	26	FC dominant hybrid
CHIC	5	2013	Bolzano, Italy	11.9	120	Lithium Ion	26	FC dominant hybrid
HyTransit, HighVLO City	14	2014	Aberdeen, UK	12.2	150	Not available	Not available	FC dominant hybrid
HighVLO City	5	2014	Brussels, Belgium	12.2	150	Not available	Not available	FC dominant hybrid
NFCBP	1	2014	Austin, US	10.7	30	Lithium Titanate	54	Battery dominant hybrid
NFCBP	1	2014	Birmingham, US	9.8	75	Lithium Titanate	54	Battery dominant hybrid

Appendix F

Development history of London FC bus RV1

In April 2002, a new route, RV1, began to operate between Tower Gateway and Covent Garden via the South Bank. The route is aimed at tourists since the route goes past various attractions with the majority of the route having riverside views (thus the RV prefix) [F.1]. The first RV1 buses were conventional diesel powered buses manufactured by Mercedes Citaro from 2002 to 2004. TfL, as part of the CUTE project from 2001, started working with Citaro on development of FC trial buses. The first three experimental FC buses went into service in 2004. The first trial FC buses in 2004 used a direct electrical FC drivetrain using 2 x 125 kW FCs directly driving the electric motor [F.2]. The trial buses operated from 2004 to 2006 and could only be operated in the morning due to poor availability and efficiency [F.2].

From 2007, as part of the HyFLEET: CUTE project, the FC bus fleet in London was extended to a five bus fleet with the upgraded Citaro system. The five bus fleet was operated on route RV1 from 2007 to 2009. Following the completion of the trial (2009), the buses were decommissioned and the components returned to the manufacturers for further research [F.3]. Following on the assessment of recorded improvement during the project, TfL decided to order a full fleet of FC buses which led to the start of the CHIC project.

As part of the CHIC project in 2010, TfL unveiled the first FC bus fleet covering a complete route, the same route RV1, in the UK. There are currently eight FC buses servicing the route RV1 since 2011 and this is the first time a whole route has been fully operated by hydrogen powered buses in the UK [F.3]. The eight new FC buses have been retrofitted from Wright pulsar/VDL chassis and have proven to be much more durable and reliable. From the customer feedback, the only noticeable difference between the RV1 FC buses and conventional buses is that the former have reduced noise and less vibration [F.3].

Two more buses will be added to the RV1 bus fleet in 2017 which is part of the 3emotion project. The new buses will be constructed from independent bus designer, Van Hool. These two FC buses are hybrid Van Hool A300 model 12-metre bus with two axles [F.4]. They are equipped with the latest FC module from Ballard and optimised hybrid technology. This project aims at to deliver the next-generation FC bus

system offering improved durability and reliability along with significant cost reduction for the coming 2020 London ULEZ [F.5]. The details of system design and technical information of these new FC buses have not yet been unveiled, so this research will only focus on the existing eight FC bus fleet from 2011 to 2016. Figure F-1 summarise the London FC bus development timeline from 2001 to 2020.

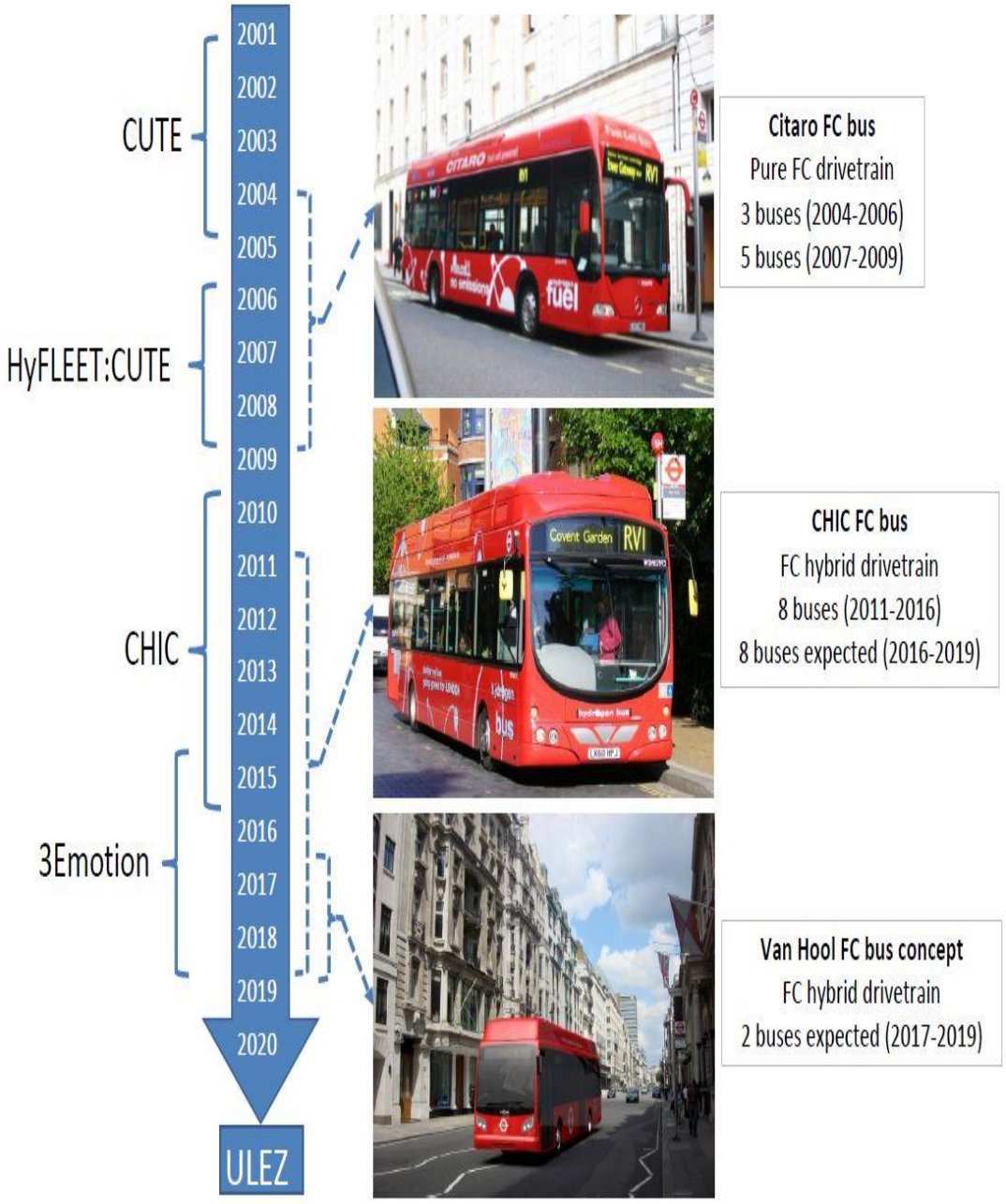

Figure F-1 London FC hydrogen bus development timeline
(Bus photos edited from Citaro, TfL, Van Hool, 2016)

Appendix G

Operation and theory of six common FC types

Proton Exchange Membrane Fuel Cell: The PEMFC uses a thin proton conductive polymer membrane as the electrolyte. The PEMFC functions at a low operating temperatures and has a fast start up time which makes this technology particularly well adapted to transportation and portable applications. The solid polymer membrane electrolyte can prevent electrolyte leakage risk which is especially important for public transportation applications [G.1]. The PEMFC holds the additional benefits of high specific power (compared to other fuel cell technologies) and high efficiency (average of 50%). However, the catalyst of the PEMFC is typically platinum which is considered as an expensive material. The other drawback of the PEMFC is the slow reaction rate, which causes significant problem for transportation applications. Another critical issue of the PEMFC is the requirement for high hydrogen purity level which creates the need of additional fuel processing [G.2].

Direct Methanol Fuel Cell: The DMFC is a similar technology to the PEMFC in that it uses the same electrolyte and catalyst. Instead of pure hydrogen, the DMFC uses liquid methanol as the fuel which makes this technology attractive. Methanol is a low cost liquid fuel that is easily produced, stored, transported and distributed; furthermore, it can be supplied with present infrastructure without further significant investment. Additionally, methanol can also be produced from agricultural products to make it “green” [G.3]. Unfortunately, the DMFC has very low power density and low efficiency [G.4]. The DMFC is typically used in applications requiring slow and steady power consumption over long periods [G.2].

Alkaline Fuel Cell: The AFC is one of the oldest FC technologies developed for aerospace since the 1960s and was used on the Apollo and Shuttle Orbiter craft to generate electricity and water. The AFC uses an alkaline as the electrolyte and a nickel-based anode catalyst. This reduces production costs compared with the platinum-based PEMFC. The AFC has a wide range of operating temperature and also high efficiency because of the fast kinetics allowed by the hydroxide electrolyte. Because of the high risk of liquid leakage of AFC technology, it is not suited for domestic transportation but has been mainly used in aerospace. Potassium hydroxide, the electrolyte, is a highly corrosive chemical, which is difficulty to contain as it causes leaks [G.5] [G.6]. The common conditions during transportation application, such as

acceleration and vibration, could increase the risk of leakage, which makes the AFC not well suited for domestic public transportation. Another reason is the AFC requires advanced hydrogen and oxygen purification processes to eliminate carbon monoxide production which incurs additional cost and complexity [G.1].

Phosphoric Acid Fuel Cells: The PAFC technology utilises a chemical reaction similar to that of the PEMFC which uses platinum as the catalyst and phosphoric acid as the electrolyte. The PAFC was the first commercially available FC and is widely used for static applications. The PAFCs are very efficient in terms of generating electricity and heat which makes them well suited for larger scale power plants [G.1]. However, the PAFC is rarely used in transportation applications for two primary reasons. The first one, which is probably the more important one, is that the phosphoric acid electrolyte has a freezing point of 42 °C which means the PAFC must always be kept above 42 °C to prevent stressing the stack [G.5]. This process will greatly increase the operational cost of transportation applications. The second reason is that the PAFC has a relatively slow start-up time, which can be crucial for transportation application [G.7].

Solid Oxide Fuel Cell: The SOFC uses a solid nonporous metal oxide as the electrolyte and operates at high temperature (800-1000 °C). The high temperature operation can make the FC achieve very high efficiency (~80%) with cheap non exotic catalysts [G.2]. On the other hand, the high temperature operation has also caused problems such as safety issues, fuel economy concerns, thermal stress of materials, complicated cooling and pre-heater systems being some of the most significant. Static applications for the SOFC can not only minimise the problem addressed before, but also take full advantage of the high temperature operation [G.8]. However, because of the high operating temperature and long start-up time, the SOFC is difficult to use in transportation applications, both technically and economically.

Molten Carbonate Fuel Cell: The MCFC uses a combination of alkali carbonates as the electrolyte and relies on a molten carbonate salt to conduct ions [G.1]. The MCFC also operates at high temperature, around 650 °C which makes the MCFC also capable of high efficiency and has no need for a precious metal catalyst. Hydrocarbon reformation can also occur in the MCFC which avoids the need for purified hydrogen [G.1]. Stephen [G.9] provides a detailed study of the differences and applications of the SOFC and the MCFC. The authors summarised that the primary difference between the MCFC and the SOFC is that the MCFC requires carbon dioxide

recirculation. The MCFC also exhibits the same problems caused by high temperature operations as the SOFC. The MCFC also has an extremely long start-up time which makes it unsuitable for transportation applications [G.10].

Appendix H

HyPM HD 8 FC system further information

Detailed technical specifications of HyPM HD 8 FC system have been summarised from the installation and operation manual and presented in Table H-1.

Table H-1 HyPM HD 8 FC system technical specifications (@ 21℃ 101.3 kPa)

Property	Unit	Value
Product information		
Model number		HyPM HD 8
Part number		1036617
Physical		
Dimensions (L*W*H)	mm	785*446*301 (±3)
Mass	kg	78 (±1)
Volume (based on inner dimensions)	L	105
Performance		
Rated electrical power	kW	8.5
Maximum electrical overload		None permitted
Operating current	A_{dc}	0-380
Operating voltage	V_{dc}	20-40
Peak efficiency	%	51
Time from off mode to idle	s	≤25
Time from idle to rated power	s	≤5
Fuel system requirement		
Gaseous hydrogen	%	≥99.99
CO	μmol/mol	≤0.2
Sulfur (total, ex. H_2S, COS)	μmol/mol	≤0.004
Total hydrocarbons	μmol/mol	≤2
Supply pressure (absolute)	kPa	515-690
Stack operating pressure (absolute)	kPa	≤120
Consumption	L/min	≤130
Hydrogen temperature	℃	2-40
Air delivery system		
Maximum air flow rate	L/min	≤800
Air filtration		Chemical and particulate
Composition		Ambient air
Sulfur	μmol/mol	≤0.004
Air inlet temperature	℃	2-40
Operating environment		
Storage air temperature (with freeze preparation procedure)	℃	-20-46
Ambient air temperature	℃	2-40
Maximum FCPM interior temperature	℃	46
Relative humidity (operation and storage)	%	≤95
Altitude range	m	0-400
Orientation	°	±30

Property	Unit	Value
Emissions		
Allowable pressure drop of customer cathode exhaust	kPa	≤3
Water collected at anode @25℃	mL/min	≤12
Water collected at cathode @25℃	mL/min	≤23
Relative humidity (operation and storage)	%	≤95
Noise (at full power, measured at 1 m distance)	dBA	≤70
Cooling system requirements		
Heat rejection	kW	≤13
FCPM coolant outlet temperature	℃	50-60
Coolant type		
De-ionised water (DI H_2O)	%	100
Ethylene glycol (EG) / De-ionised water (DI H_2O)	%	40/60
Resistivity	kΩ*cm	≥200
Coolant flow rate (DI H_2O only)	L/min	≥30
Maximum pressure drop of customer coolant system	kPa	≤20
Maximum coolant inlet pressure	kPa	≤170
Electrical input		
Signal (FCPM enable and E-stop)		12-13 V_{dc}, ≤1 A
Start-up		12-13 V_{dc}, 300 W ≤ 25 s
Cool down mode		12-13 V_{dc}, 200 W
Diagnostics		12-13 V_{dc}, 300W ≤ 6.5 min
Freeze preparation (if required by integrator)		12-13 V_{dc}, 300 W ≤ 25 s
Communication interfaces		
CAN Bus v2.0 A (standard 11 bit), Baud rate 250 kbit/s		

Figure H-1 shows the physical dimensions of the HyPM HD 8 FC. Figure H-2 shows the component and interface connection drawing from the underside view of HyPM HD 8 FC.

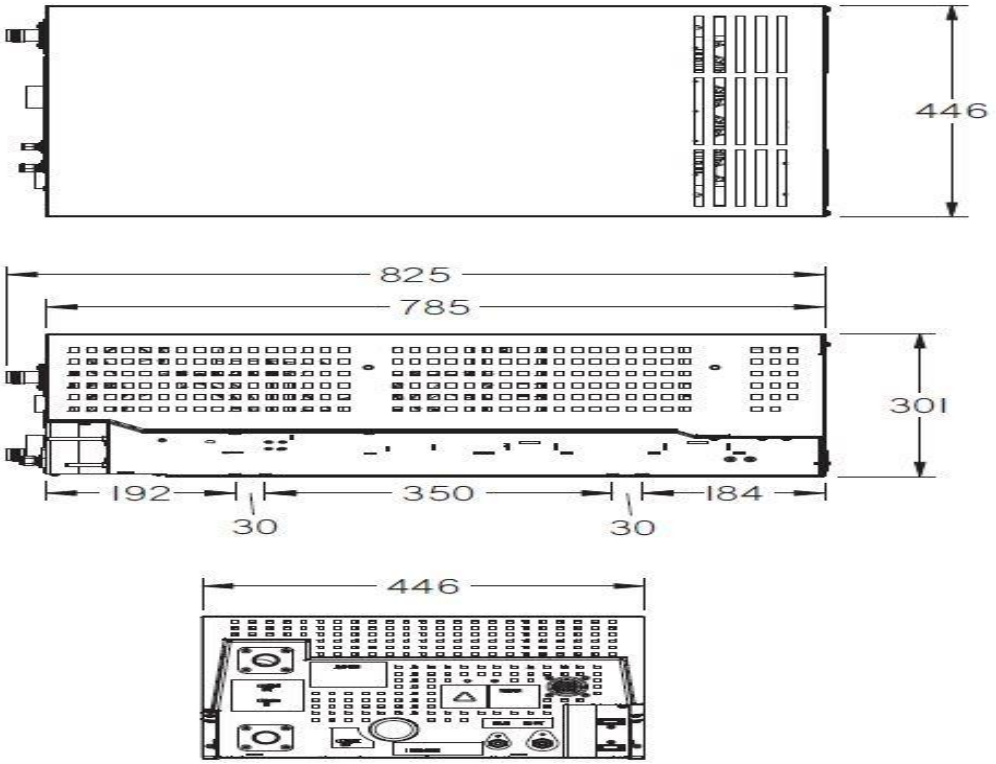

Figure H-1 HyPM HD 8 Fuel cell physical dimensions

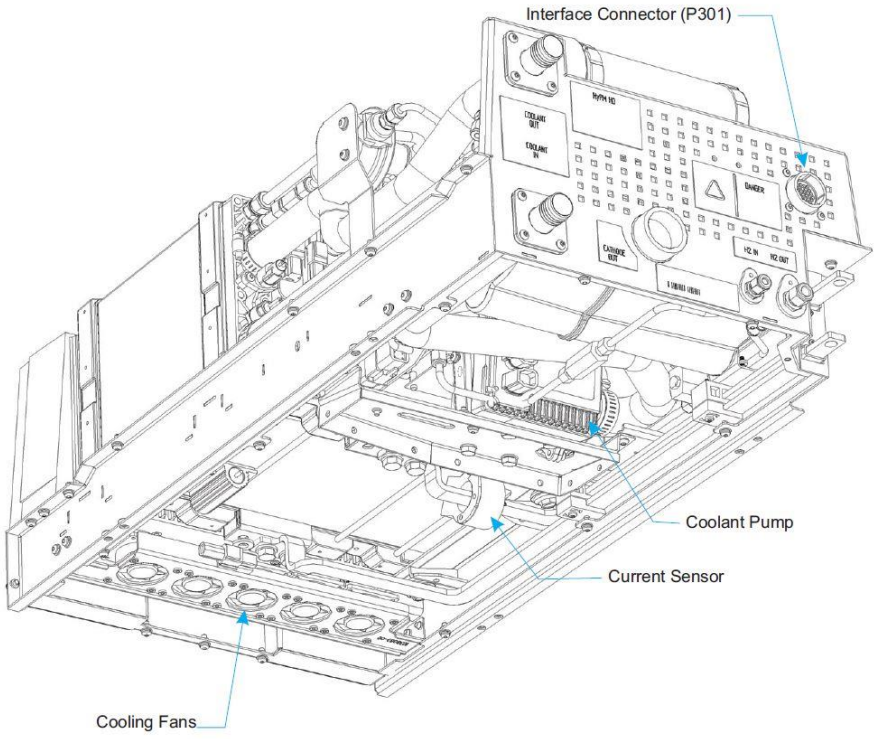

Figure H-2 HyPM HD 8 FC drawing from underside view

Appendix I

Boost converter datasheet and schematics

CUSTOM POWER DESIGN

ELECTRONICS CONSULTANTS PROVIDING CUSTOM DESIGN, DEVELOPMENT, TEST & SUPPORT

Tel: + 44 (0)118 930 2299 *A DIVISION OF SMET LTD* *Fax: +44 (0)118 930 2206*

www.custompsudesign.com Unit 19, The Markham Centre, Station Road, Theale, Berks. RG7 4PE. custom@custompsudesign.com

WIDE RANGE DC-DC HYDROGEN STACK CONVERTERS.

UP TO 1500W INPUT, WITH WIDE STACK VOLTAGE RANGE.

Model Number Selection (other input and output voltages available).

OUTPUT	INPUT: 12-36V	18-48V	24-60V	30-84V
5.0V at 250A (750W)	SM5550	SM5560	SM5570	SM5580
9.0V at 140A (1260W)	SM5551	SM5561	SM5571	SM5581
12.0V at 125A	SM5552	SM5562	SM5572	SM5582
15.0V at 100A	SM5553	SM5563	SM5573	SM5583
18.0V at 83.3A	SM5554	SM5564	SM5574	SM5584
21.0V at 71.4A	SM5555	SM5565	SM5575	SM5585
24.0V at 62.5A	SM5556	SM5566	SM5576	SM5586
48.0V at 31.3A	SM5557	SM5567	SM5577	SM5587
13.8V at 108.7A	SM5558	SM5568	SM5578	SM5588
27.6V at 54.4A	SM5559	SM5569	SM5579	SM5589

- HIGH OUTPUT POWER IN COMPACT SIZE.
- FEATURES 'STACKLIMIT'© CONTROL.
- REMOTE ON / OFF CONTROL FACILITY.
- MANUAL OR PROCESSOR BASED VERSIONS.

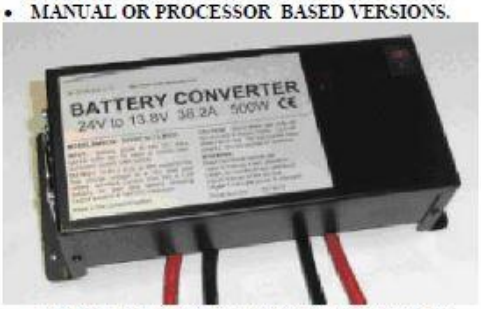

TEMPORARY PICTURE REPRESENTATIVE OF SHAPE AND CONNECTIONS.

GENERAL DESCRIPTION. A small converter handling up to 1500W from a hydrogen stack, with various dc outputs, model dependent. The input and output are ohmically isolated, making installation very simple. The output has a constant current limit and the unit can be turned on/off remotely, via a logic compatible / stack voltage control input. Note that connection terminals are underneath.

The unit is intended for use with fuel cell stacks, where maximum power is available at a well defined stack voltage, typically 45% of the stack's open circuit voltage. By setting the 'STACKLIMIT'© of the converter to this voltage, the unit will start to fold back with high load, balancing the stack at maximum possible stack output.

A fixed output current limit applies, but normally the stack will limit before the current limit is reached.

Other units available for N x 12V battery charging.

The output impedance of the unit is deliberately degraded to permit parallel use, with reasonable load sharing.

Power input and output is via 5mm female terminal posts, underneath the raised base of the unit.

SPECIFICATION.

INPUT VOLTAGE: See model listing above.
The 'STACKLIMIT'© is variable by potentiometer, from mininmum input voltage to 55% of maximum input, see text.

OUTPUT:

Voltage (10% Load): -	Nominal + 100mV ±50mV.
Line Regulation: -	<± 0.05V for a 10% input change.
Load Regulation: -	<-0.1V for a 10% to 90% change.
Low Frequency Ripple: -	Less than 100mV pp.
Current Limit: -	Nominal plus 10%, ± 7%.
On/Off Control: -	The unit will draw less than 0.1mA until voltage (3V to 84V) is applied to the control input.

GENERAL:

Protection:	Over-current output limit with input fusing.
Size:	295mm x 133mm x 88mm.
Weight:	2400 grams.
Storage Temp Range:	-40 to +70C.
Operating Temp Range:	-40 to +40C.
Manufacturer	Made in UK.

CAUTION: This adaptor is supplied on the basis of the user determining the suitability for the purpose for which it is to be used. Do not use in a moving vehicle without the consent of the vehicle manufacturer. Do not use for aviation or marine applications without our written agreement. Do not use for life dependent applications.

Made in the UK

We reserve the right to change the specification without notice. Document 5550-993

Figure I-1 Proposed boost converter datasheet

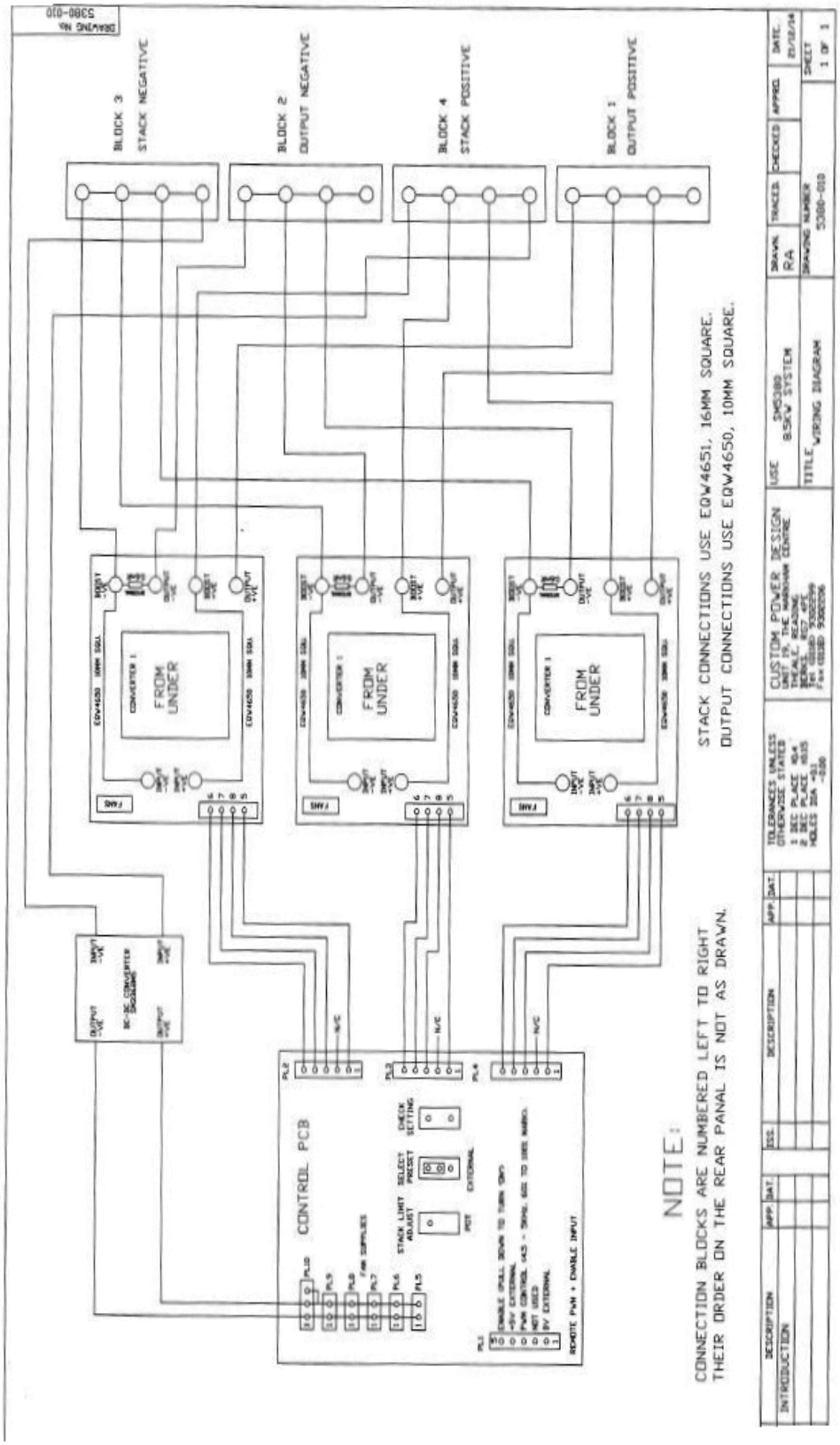

Figure I-2 Proposed boost converter configuration

Appendix J

Plots of FC under large step transient load

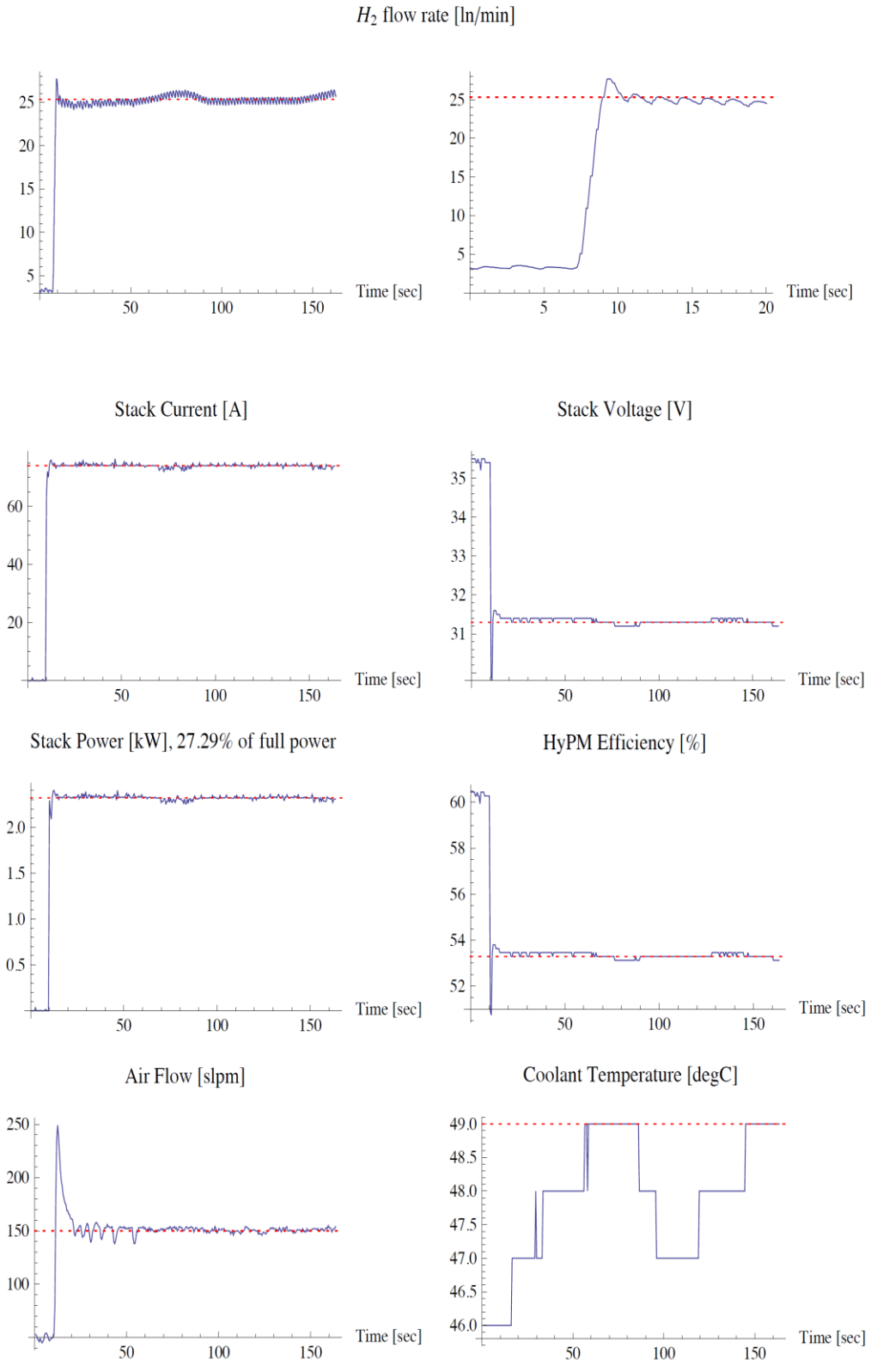

Figure J-1 FC under 0-25% increment load

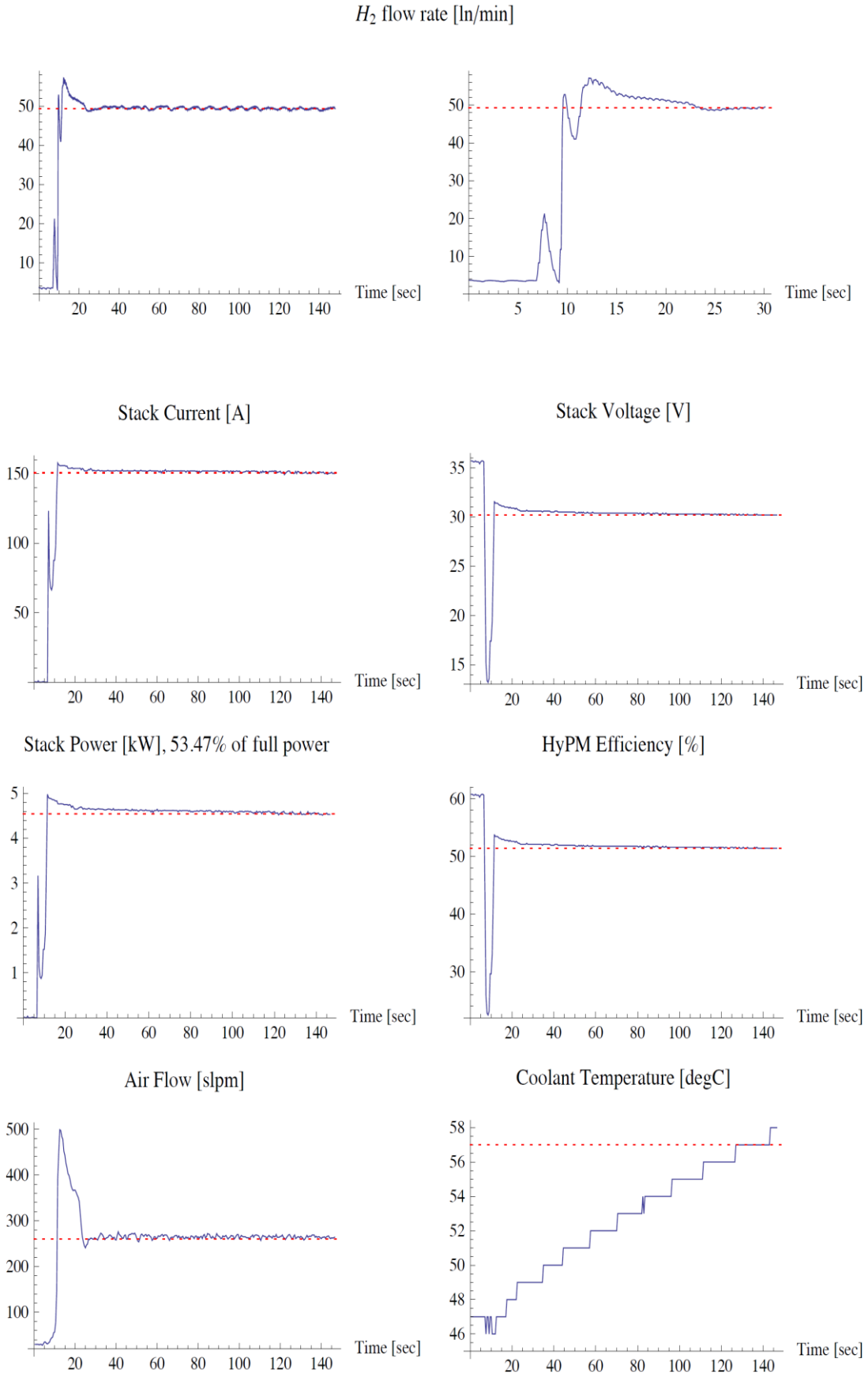

Figure J-2 FC under 0-50% increment load

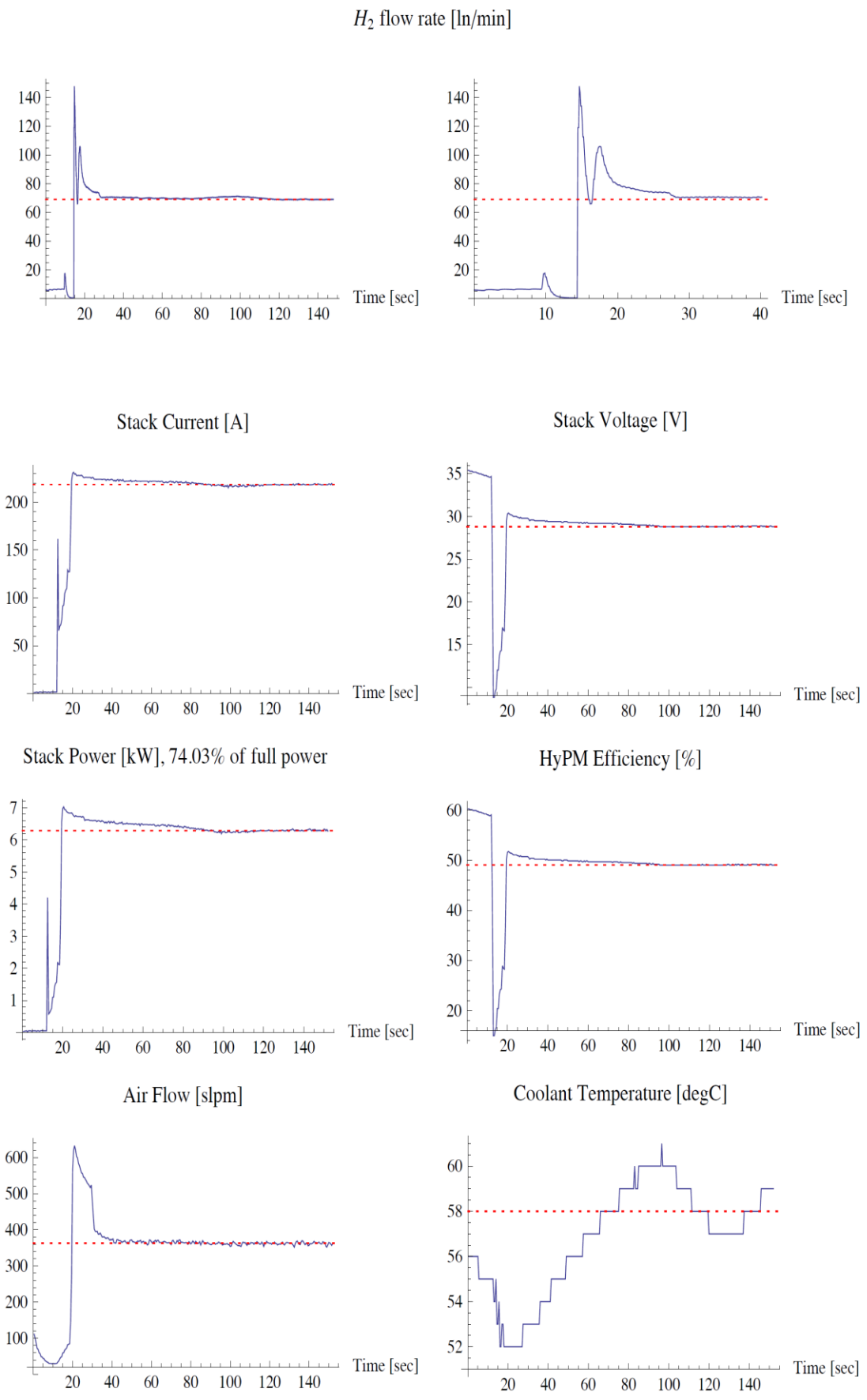

Figure J-3 FC under 0-75% increment load

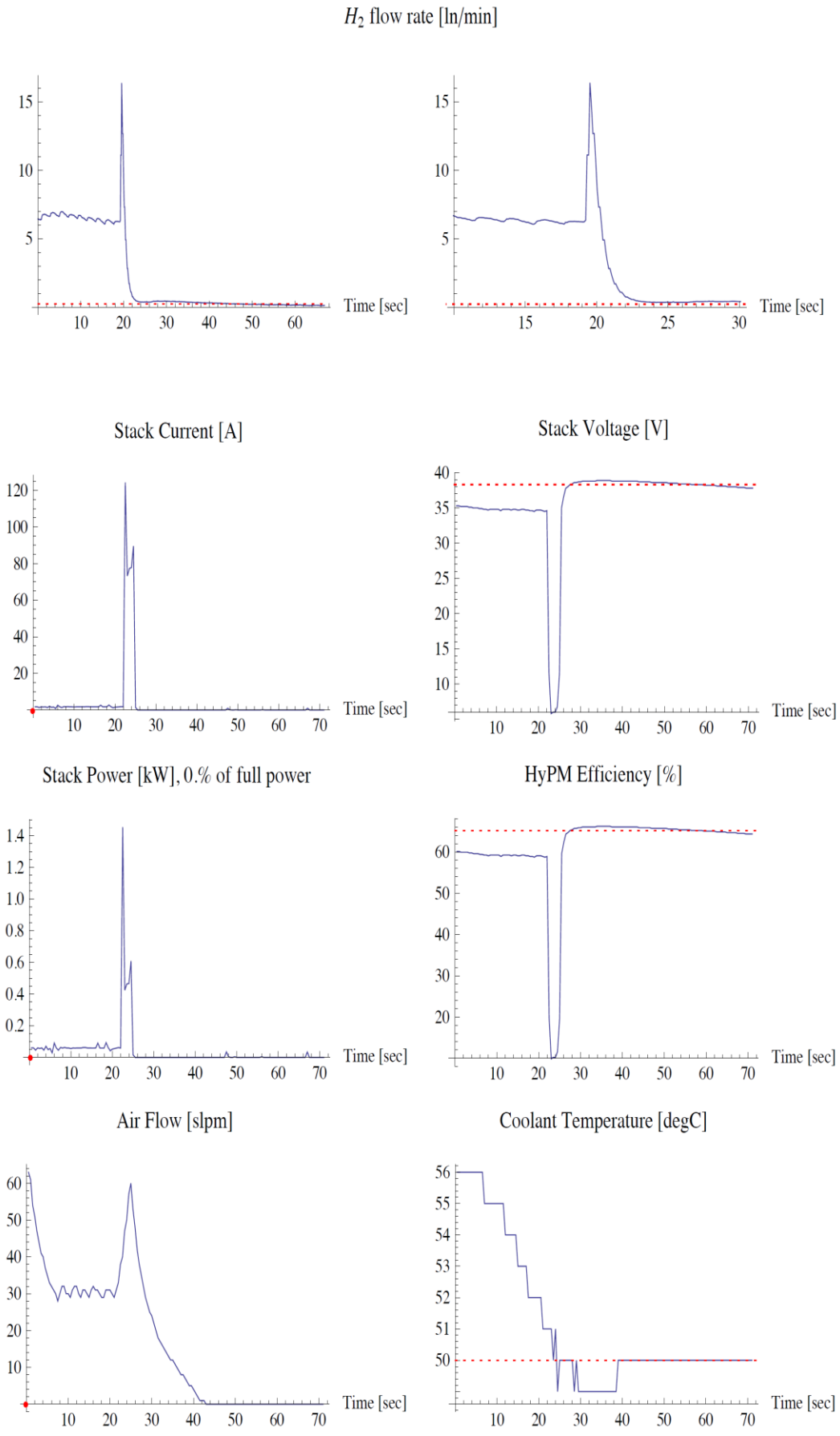

Figure J-4 FC under 0-100% increment load

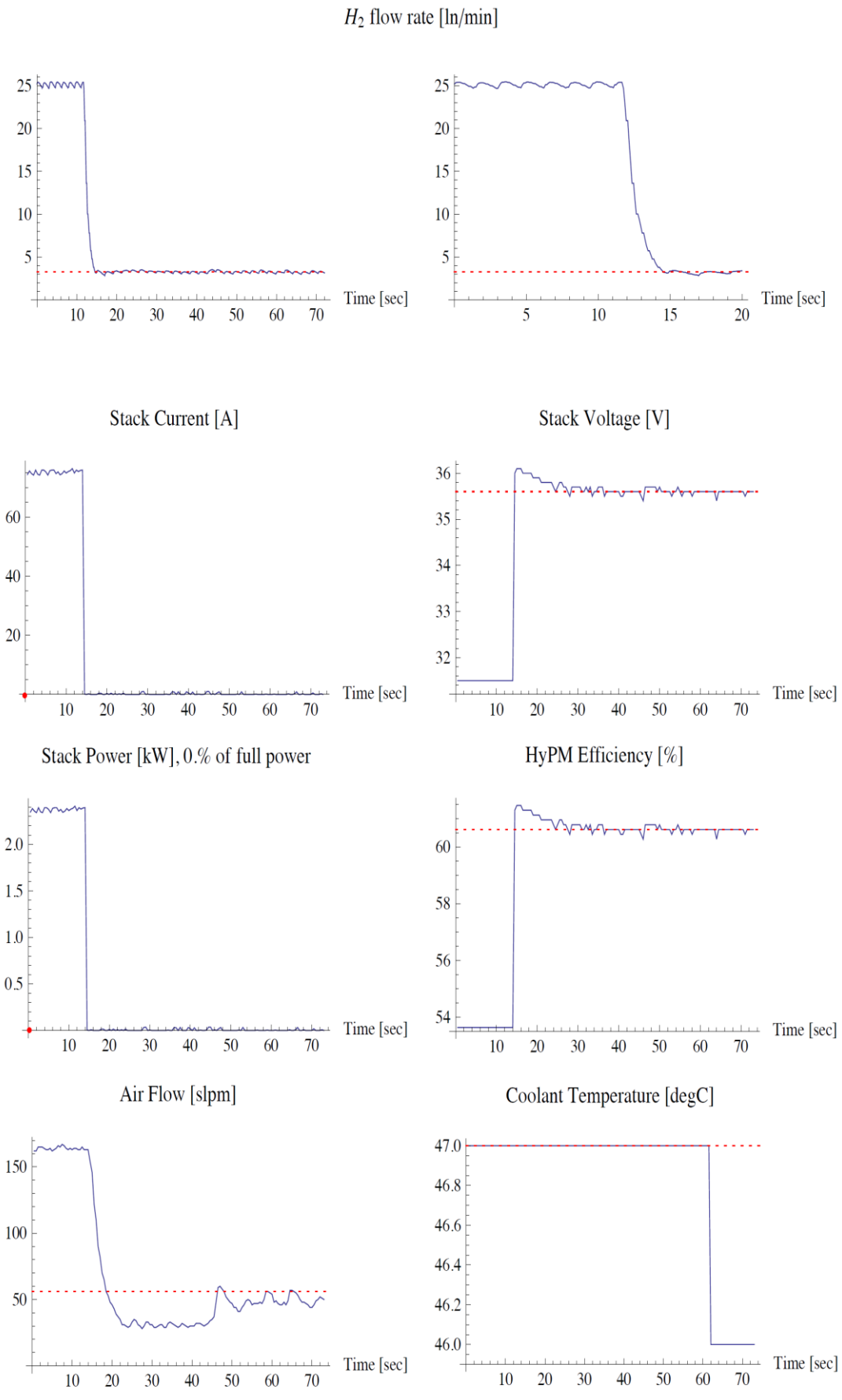

Figure J-5 FC under 25-0% decrement load

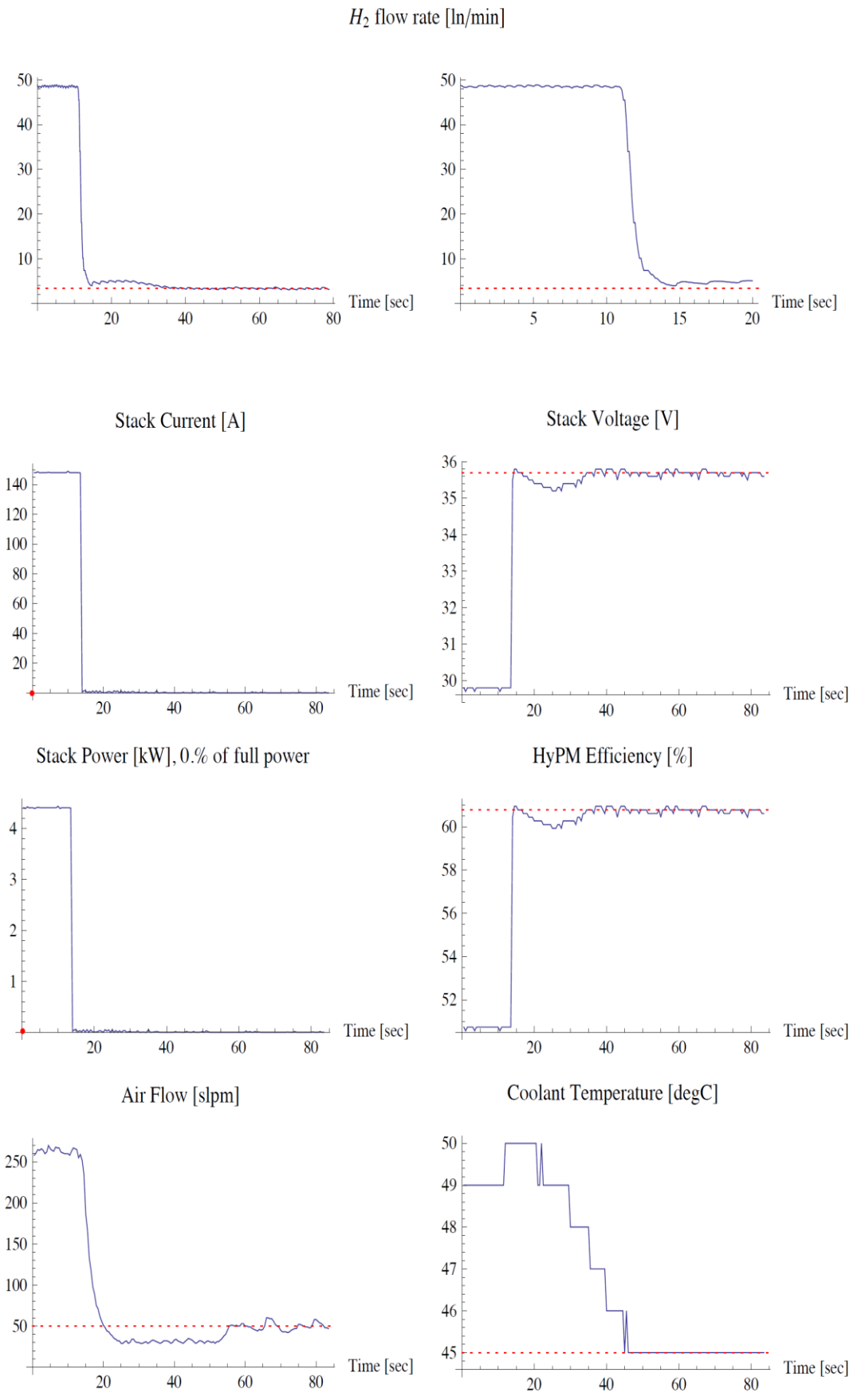

Figure J-6 FC under 50-0% decrement load

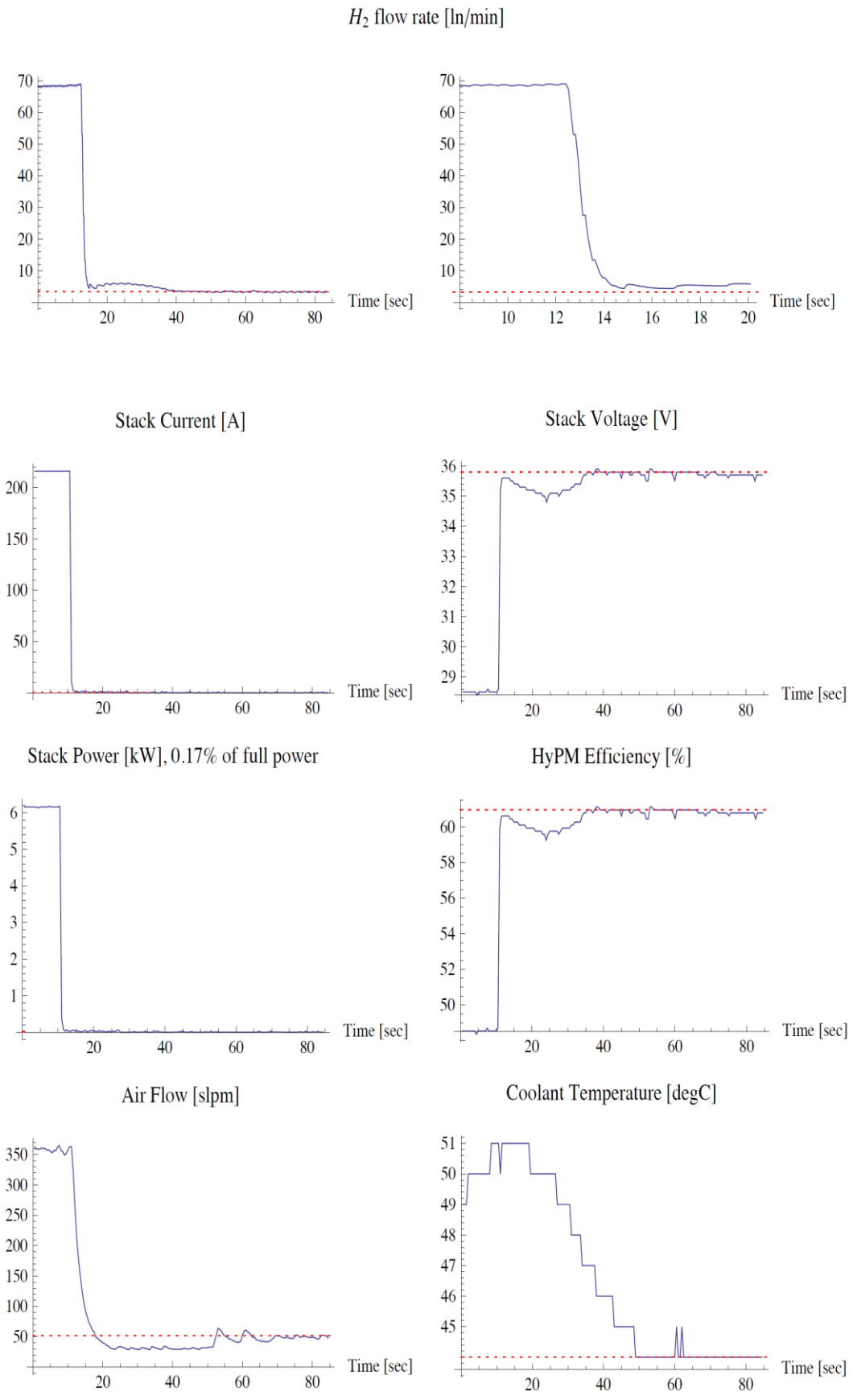

Figure J-7 FC under 75-0% decrement load

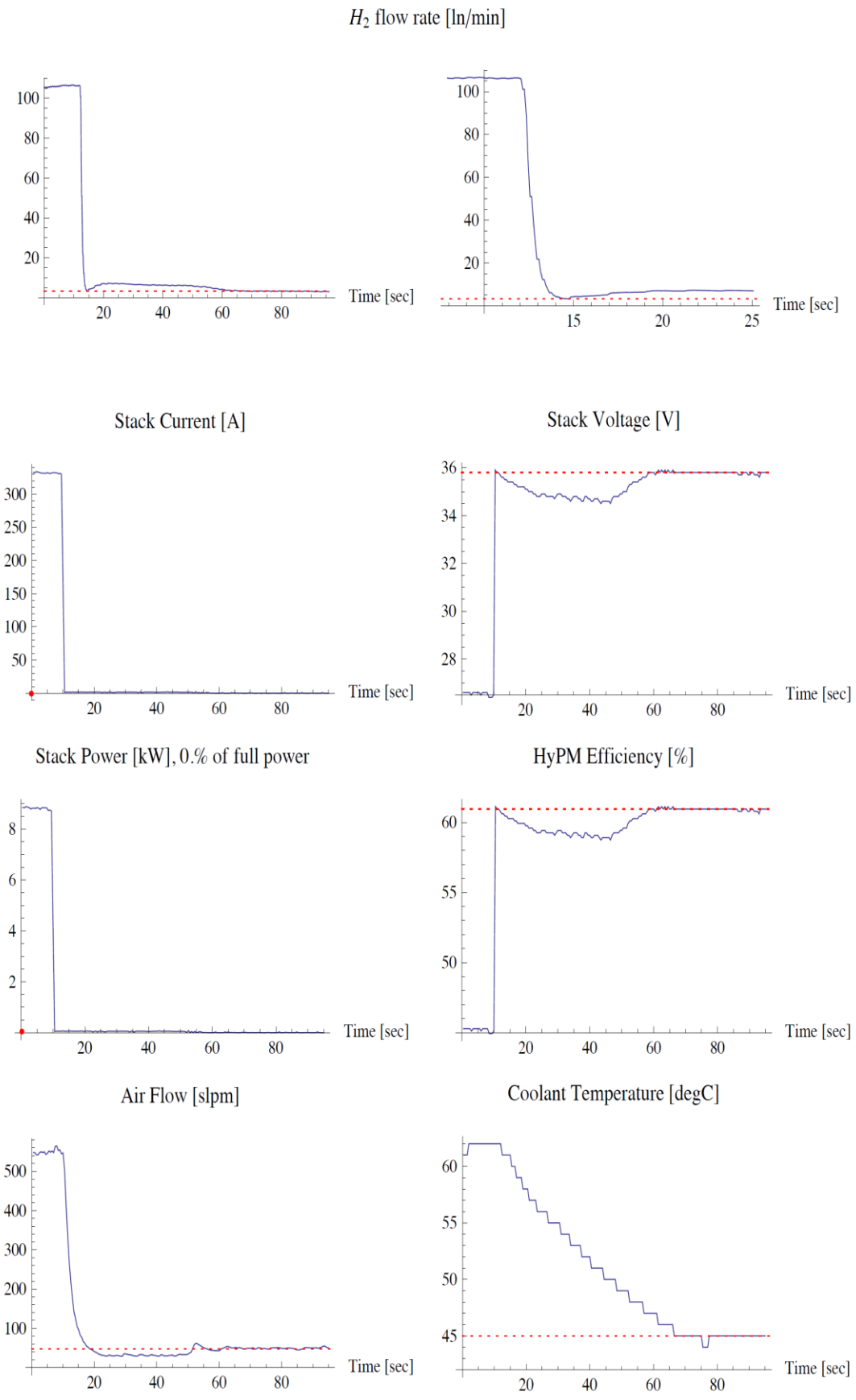

Figure J-8 FC under 100-0% decrement load

Appendix K

H bridge buck/boost converter operation

A bidirectional buck/boost converter utilised an adapted H-bridge converter configuration has been used for the SC buck/boost converter that was produced by AEP hybrid. The converter is capable of operating in either buck mode or boost mode. The buck/boost converter configuration and its operation modes have been shown in Figure K-1 to K-4.

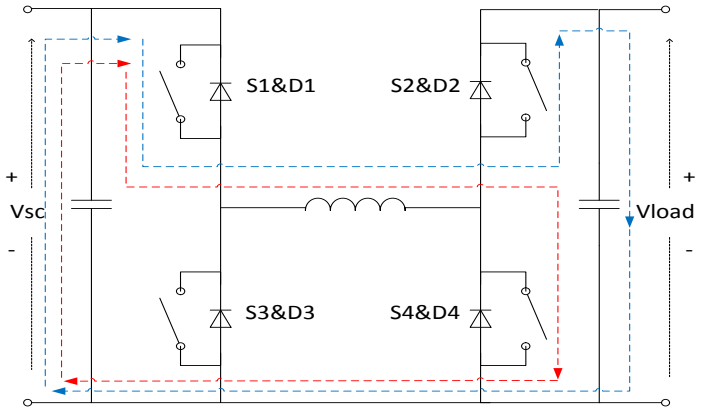

Figure K-1 Bidirectional buck/boost converter configuration and operation modes (SC discharge, step up mode)

In the boost mode during SC discharging, the IGBT S1 will be closed and S4 will be switched at a controlled frequency to constantly make the inductor charge or discharge to boost the output voltage or current. In this mode, the buck/boost converter operates exactly the same as a boost converter.

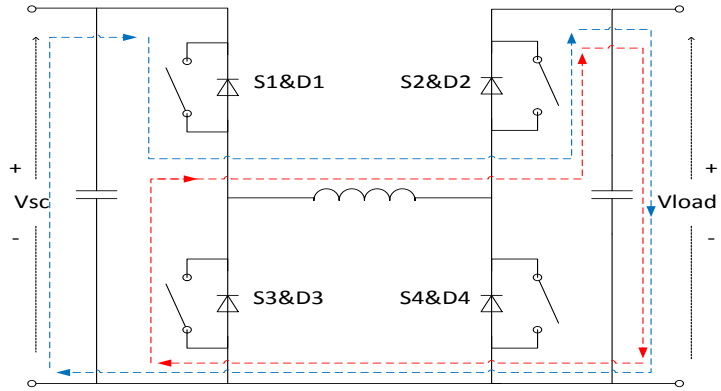

Figure K-2 Bidirectional buck/boost converter configuration and operation modes (SC discharge, step down mode)

In the buck mode during SC discharging, the IGBT S1 will be switched at a controlled frequency. In this mode, the buck/boost converter operates the same as a typical buck converter to step down the output voltage or current. Therefore this H-bridge buck/boost converter configuration can be operated in either boost mode or buck mode

by controlling the switch S1 and S4 in the circuit. Since this converter will be used to control the discharge and charge of the SC, the converter would have to be able to operate in the opposite way as well.

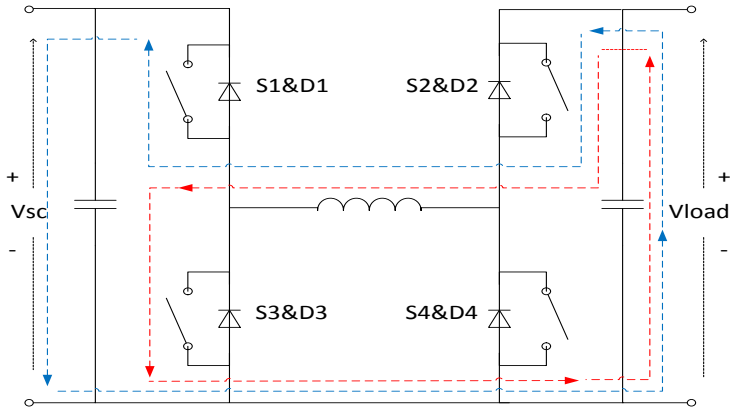

Figure K-3 Bidirectional buck/boost converter configuration and operation modes (SC charge, step up mode)

During SC charging operations, the power flow would be expected to be going from the load back to the SC. In the step up mode of SC charge, the switch S2 will be closed and S3 will be switched at a controlled frequency. The buck/boost converter in this operation is basically the same as a typical boost converter except the load and SC side has been swapped.

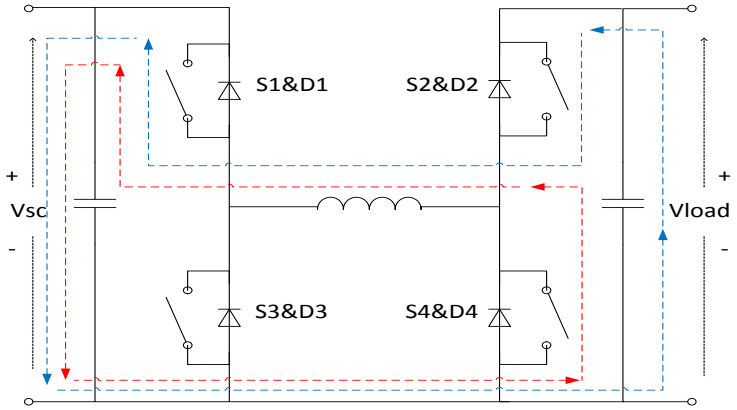

Figure K-4 Bidirectional buck/boost converter configuration and operation modes (SC charge, step down mode)

In the step down mode of SC charge, the switch S2 will be switched at a controlled frequency. This operation is also the same as in the buck converter modes with the power sources exchanged. Therefore this H-bridge buck/boost converter is capable of operating in bidirectional boost and buck mode. More details of the derivation and calculation of this type of buck/boost converter can be found in literature [K.1] and [K.2].

Appendix L

Buck/boost converter structure for SC control

The converter for SC is controlled via the PowerPanel software where the reference value and control mode can be selected.

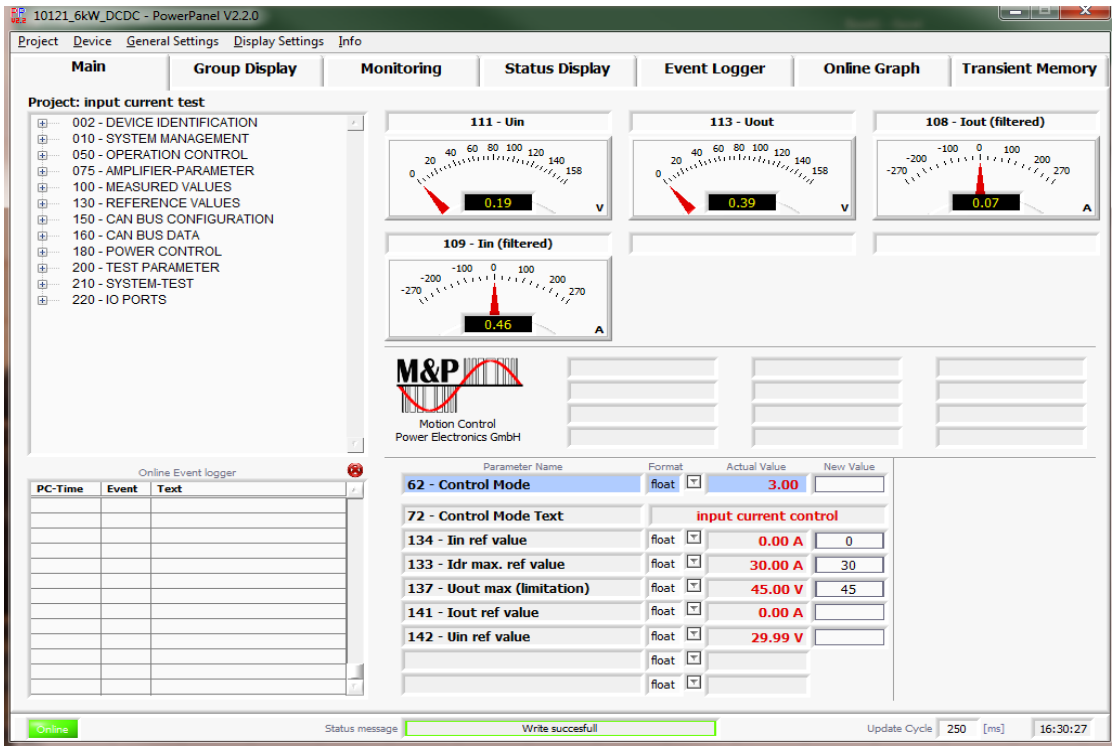

Figure L-1 Power Panel software control interface for the buck/boost converter

Table L-1 presented the parameters for difference control modes within the PowerPanel software.

Table L-1 Control mode selections of the Power Panel software

Mode	Control	Parameter	Maximum values
Idr-Reg	Coil current	131-Idr ref value	±150 A
Uout-Reg	Output voltage	135-Uout ref value	70 V
Iout-Reg	Output current	141-Iout ref value	±150 A
Iin-Reg	Input current	134-Iin ref value	±150 A
Pin-Reg	Input power	181-Pin ref value	±6000 W

An overview of the control structure and algorithm with all belonging parameters for those control modes can be found. The control structure provided a brief explanation of the operation and functions for each control mode.

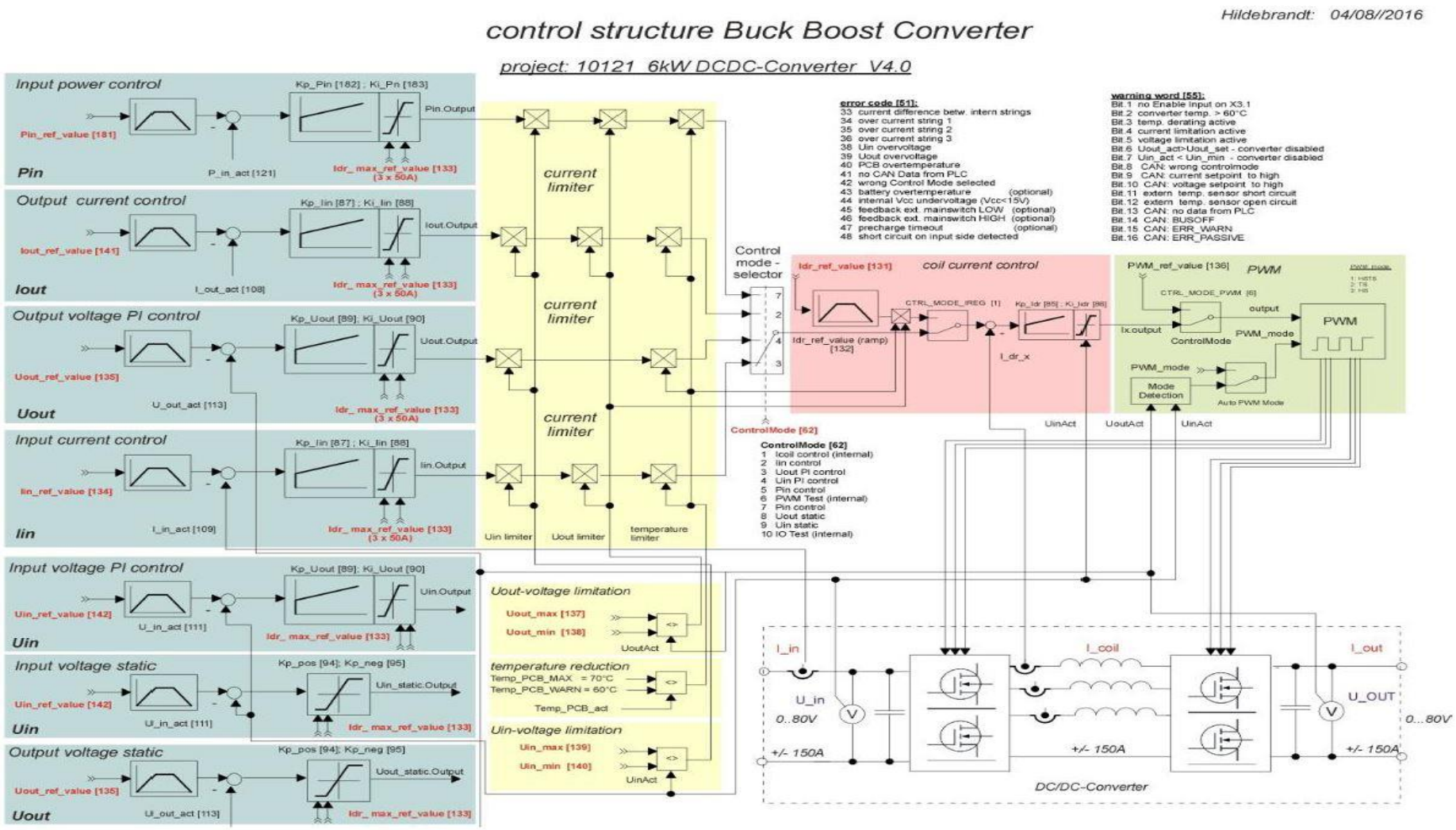

Figure L-2 Control structure of the buck/boost converter for the SC

Appendix M

Simulink generic FC model extra information

Figure M-1 shows the expanded model schematics of the Simulink generic FC model. This section shows the schematics of the calculation of air consumption and fuel consumption. The left corner “Cell Voltage” block indicates anther sub-system that is being used to calculate the FC voltage which has been shown in Figure M-2.

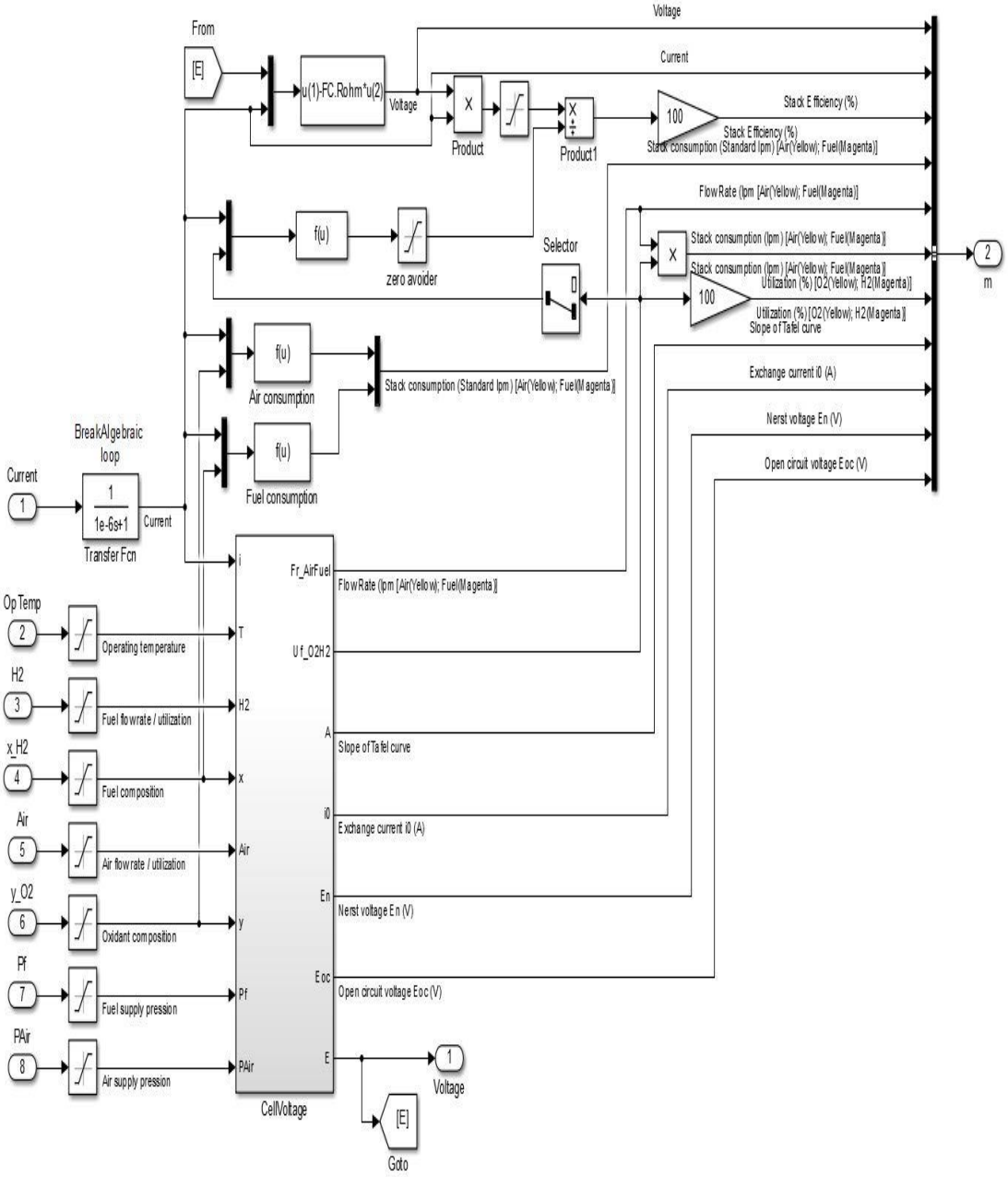

Figure M-1 Model schematics of the Simulink generic FC model

Figure M-2 shows the schematics of the cell voltage subsystem. In the sub-system, the Nernst voltage, activation loss, concentration loss and Ohmic loss have been calculated and exported as port connectors. Two more sub-systems have been used to calculate the partial pressure and fuel/air utilisation flowrate corresponding to determine the real time cell voltage. Further details of the Simulink FC block can be found in the FC block description on the Mathworks website.

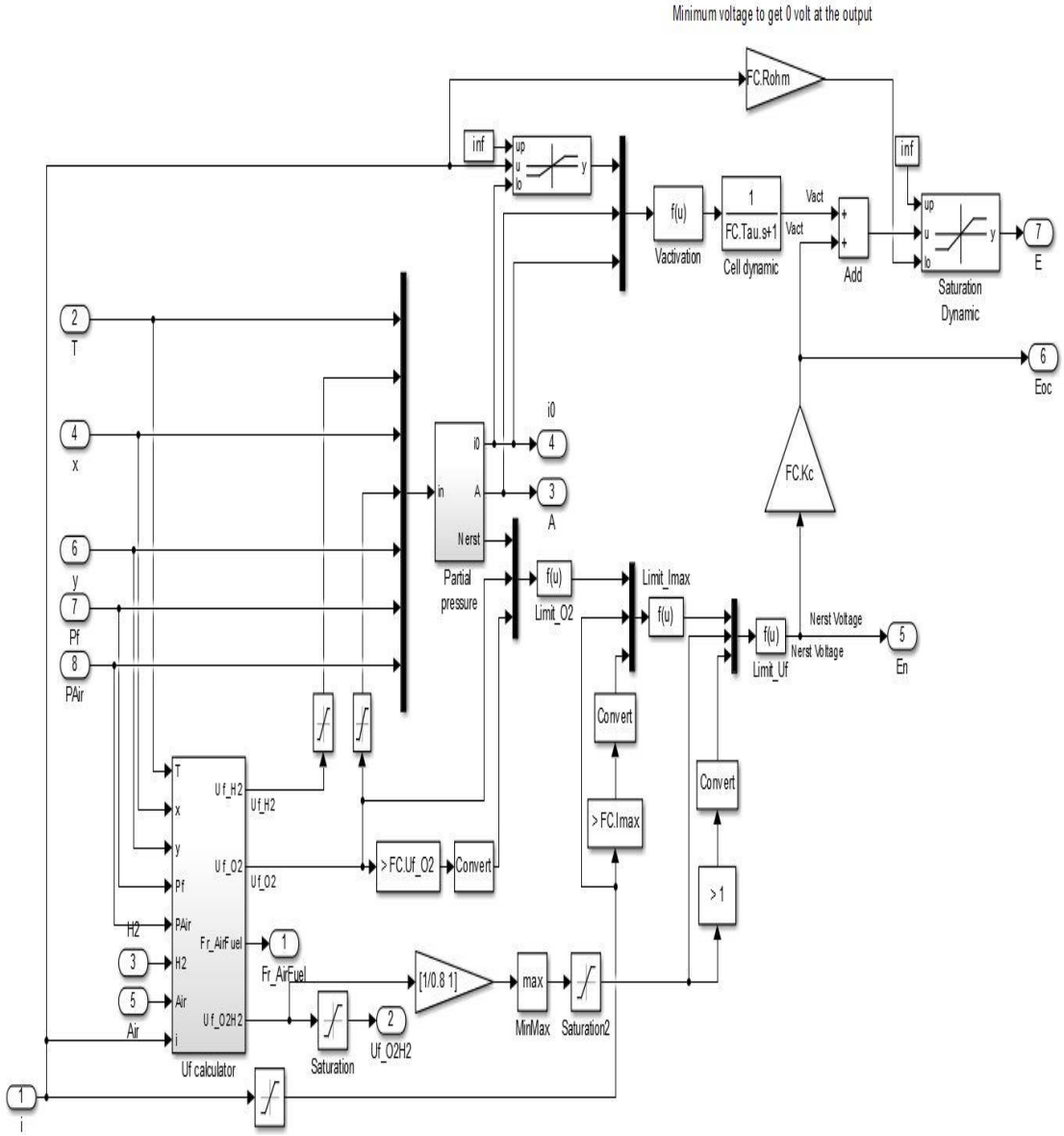

Figure M-2 Model schematics of cell voltage calculation

Appendix N

Ballard 85 kW PEMFC product specification

Table N-1 Datasheet of the 85 kW Ballard FC

Description	Model	Ballard FCveloCity-HD
Technology	Fuel Cell	Proton exchange membrane
Performance	Net power	85 kW
	Operating DC voltage range	280-420 V
	Rated net current	288 A
	Idle power	4 kW
Physical	Dimensions	1130*869*506 mm
	weight	256 kg (fuel cell module) 125 kg (air and cooling sub-systems)
Fuel	Type	Gaseous hydrogen
	Composition	As per SAE specification J2719
Operation	Oxidant	Air
	Stack coolant	50/50 pure ethylene glycol and deionized water WEG 60 to 70 °C
	Fuel supply pressure	8 bar nominal
	Fuel flow rate	1.7 g/s maximum
Safety compliance	Certifications	ISO 6469-2:2009
	Enclosure	IP55
Monitoring	Control interface	CAN bus
Emissions	Exhaust	Zero emissions
	Sound level	Less than 75 dBA
Support	Sub-systems	Coolant sub-system
		Air sub-system

Appendix O

HyFCap bus data collection and analysis

The data collection and analysis of the bus data collected under the HyFCap project was mainly carried out by David Ashmore and Cedrick Lin from UCL. A brief description of the data collection and analysis has been provided in this section.

The bus data collection was carried out by an Enviro 400H diesel-battery hybrid double decker bus owned by UCL as Figure O-1 shows. The bus usually operates in daily service on route 388 and is occasionally driven out for different driving tests assigned by UCL. During the tests, various devices has been used to log the required information as Table O-1 shows. The bus has been operated on various routes selected for different route conditions. The number of passenger was manually counted to briefly estimate the mass change during the bus operations.

Figure O-1 UCL diesel electric hybrid bus

Table O-1 Data logging devices for the UCL bus

Data type	Device	Record freq (Hz)
Bus	Logger	0.36-0.83
Video	GoPro	Continuous
GPS	Phone	1

Although this bus was constantly operating in London's daily services, the data was not always logged by the bus loggers (because of BAE regulations). There is only a limited amount of logged data that has been sent by BAE for UCL research purposes. Figure O-2 shows one of the route information from the operation on 03/02/2015. The bus operated on the 388 bus route which is a 7 miles (11 km) route from Stratford city bus station to Blackfriairs station. The researcher used GPS and a video camera to record the entire route to align the bus traffic and route conditions against the logged power/speed profiles. Figure O-3 shows the analysis interface of the collected bus data.

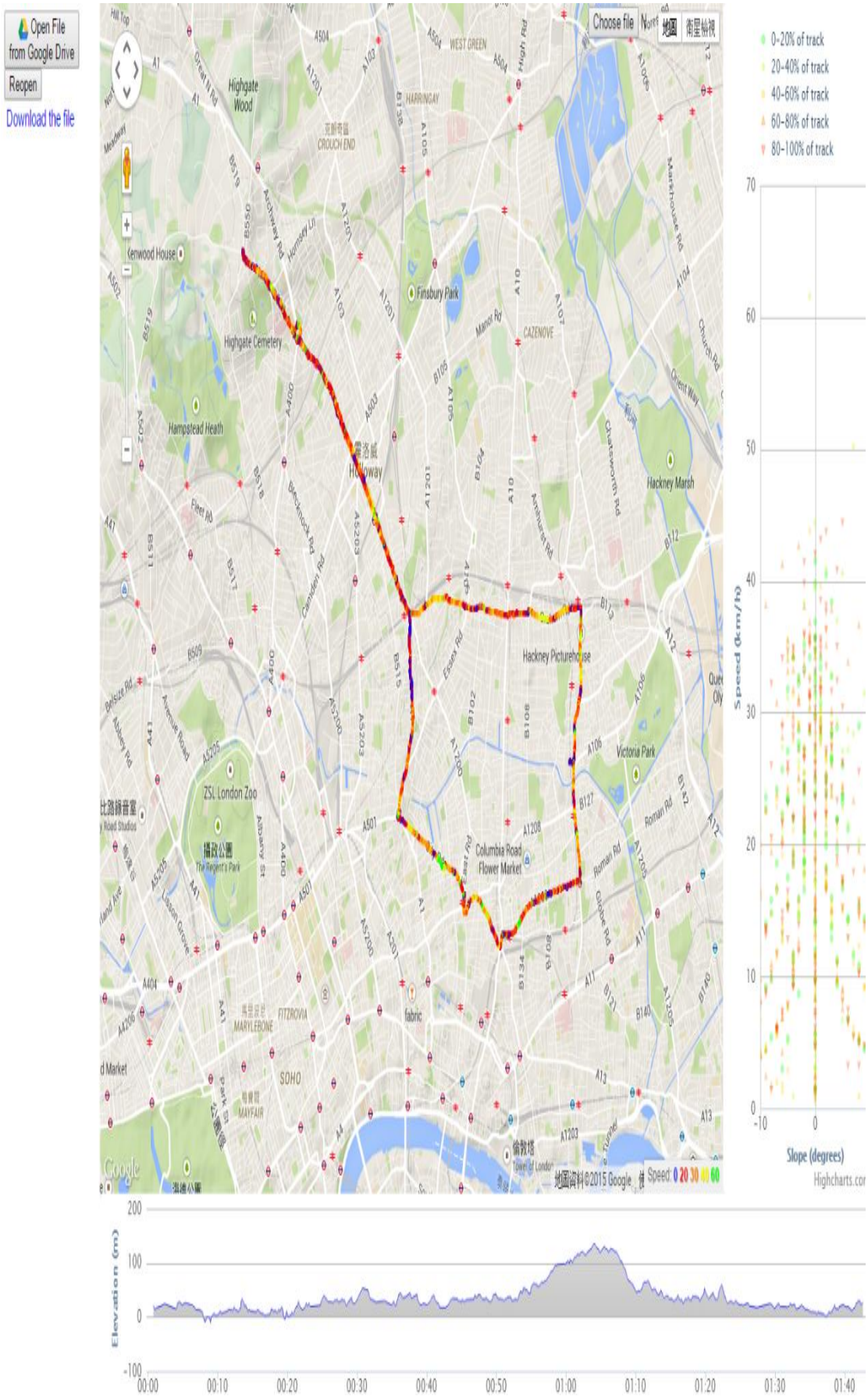

Figure O-2 Data analysis of elevation, route and speed profile of the UCL bus

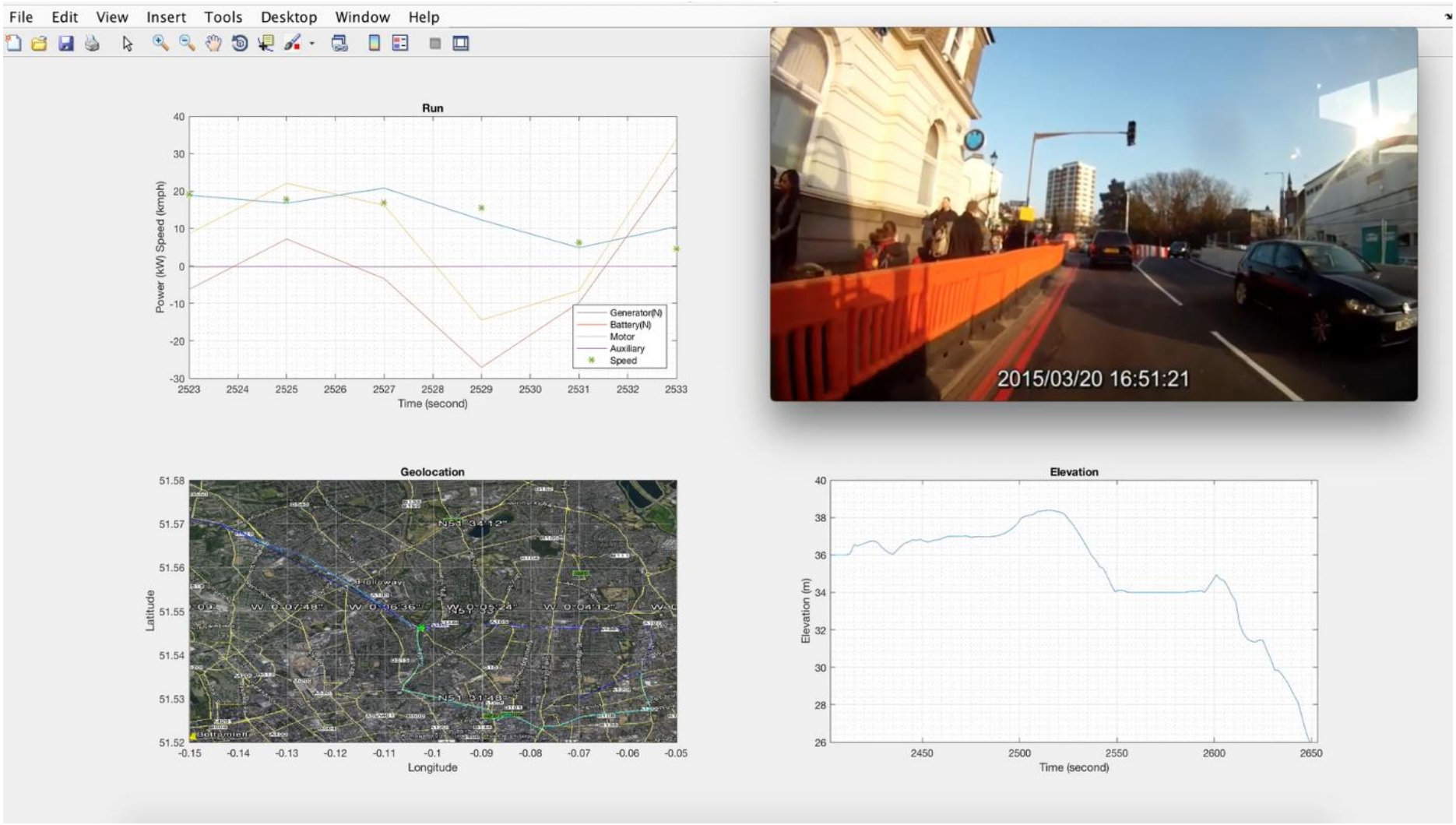

Figure O-3 Data analysis interface of the collected bus data

Appendix P

Simulink sampling frequency justification

In the peak power profile test, transient overshoot and undershoot has been observed in the FC and SC output current and voltage (Figure 6.6 and 6.8). As discussed before, the transient overshoot and undershoot are caused by the PID tuning delay. When the power changed quickly, the PID controller needs to calculate the new error and use the feedback loop to keep the same output. All PID controller in the FC/SC hybrid model utilised the same sampling frequency which is one sample every 1^-5 s. Increasing the sampling frequency is expected to be able to speed up the PID tuning and consequently reduce the transient overshoot and undershoot. To verify this argument, a series of test with different sampling frequency has been carried out. Since it was found that increasing the sampling frequency will dramatically slow the simulation speed, only the first 60s of the peak power profile has been tested with different sampling frequencies. Figure P-1 showed the Pfc_out with 1^-5 sampling frequency against the first 60 s of the peak power profile.

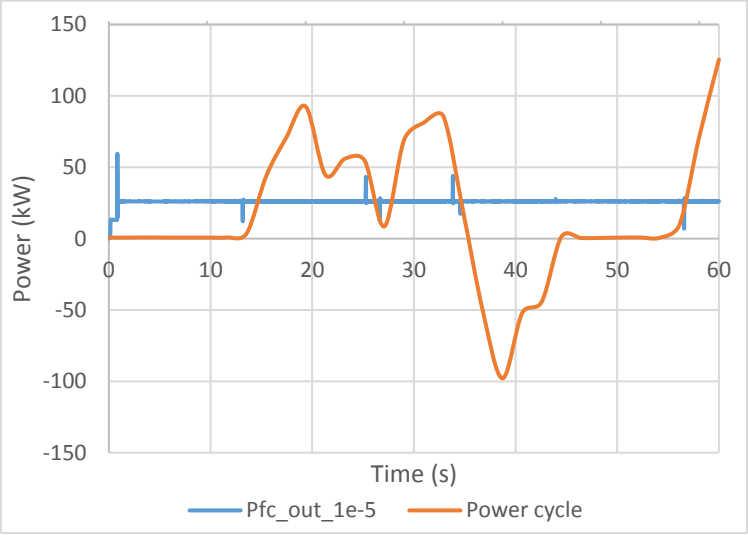

Figure P-1 First 60 s of the peak power profile with 1^-5 s sampling frequency

An initial overshoot has been observed for the PID controller to set the required amount of power from the FC (25 kW for this case). Then a number of short transient overshoots and undershoots (recovered in less than 0.05 s) have been observed when the power profile crosses over the Pfc_out. This is caused by the SC switching between charge and discharge which caused a different error on the load side. As a result the boost converter for the FC has to reset the new PID value to keep the constant output. Figure P-2 shows the same 60 s power profile with different sampling frequencies.

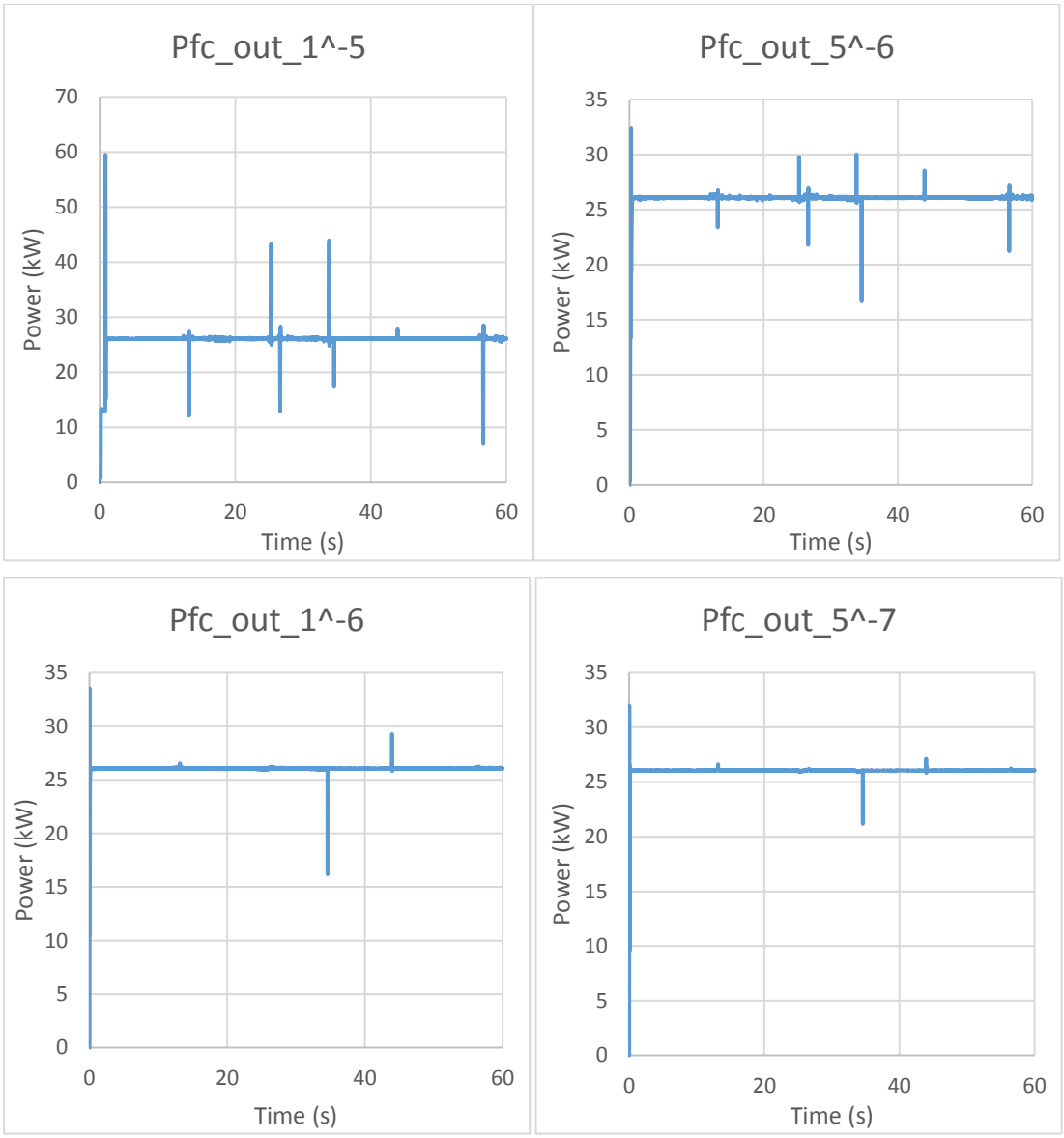

Figure P-2 First 60 s of the peak power profile with different sampling frequency

As it can be seen from the figures, the quicker the sampling frequency is the lesser transient overshoot and undershoot have been observed. The PID controller is capable of regulate the output quicker with a higher sampling frequency. Although the higher sampling frequency can provide more stable output, due to the constraint of the PC computing power, all the other simulations have to be carried out with the 1^-5 sampling frequency. The transient overshoot and undershoot should have minor effect on the total FC and boost converter output power. After calculating the total energy the FC provided for each sampling frequency, it was found the total energy difference between the four sampling frequencies is less than 0.6%. This difference is deemed to be acceptable in this research.

Appendix Q
Undercharge protection calculation with various lower thresholds

As discussed in section 6.4.1, the equation to calculate the new Ifc_out reference has been identified to be:

$$Ifc\_out\_new = Ifc\_out + \frac{120 - Ifc\_out}{(lower\ threshold \times 100) - 30} \times 100 \times (lower\ threshold - SOC)$$

The new Ifc_out can be calculated if the lower threshold has been provided. Table Q-1 provides an example of the new Ifc_out references when the Ifc_out is 10 A at different lower thresholds. As the table shows, the higher the lower threshold becomes, the smaller the increase of rate on the FC and boost converter output.

Table Q-1 Undercharge protection example

SoC	90% lower threshold	80% lower threshold	70% lower threshold	60% lower threshold	50% lower threshold	40% lower threshold
0.9	**10**	n/a	n/a	n/a	n/a	n/a
0.89	11.83333	n/a	n/a	n/a	n/a	n/a
0.88	13.66667	n/a	n/a	n/a	n/a	n/a
0.87	15.5	n/a	n/a	n/a	n/a	n/a
0.86	17.33333	n/a	n/a	n/a	n/a	n/a
0.85	19.16667	n/a	n/a	n/a	n/a	n/a
0.84	21	n/a	n/a	n/a	n/a	n/a
0.83	22.83333	n/a	n/a	n/a	n/a	n/a
0.82	24.66667	n/a	n/a	n/a	n/a	n/a
0.81	26.5	n/a	n/a	n/a	n/a	n/a
0.8	28.33333	**10**	n/a	n/a	n/a	n/a
0.79	30.16667	12.2	n/a	n/a	n/a	n/a
0.78	32	14.4	n/a	n/a	n/a	n/a
0.77	33.83333	16.6	n/a	n/a	n/a	n/a
0.76	35.66667	18.8	n/a	n/a	n/a	n/a
0.75	37.5	21	n/a	n/a	n/a	n/a
0.74	39.33333	23.2	n/a	n/a	n/a	n/a
0.73	41.16667	25.4	n/a	n/a	n/a	n/a
0.72	43	27.6	n/a	n/a	n/a	n/a
0.71	44.83333	29.8	n/a	n/a	n/a	n/a
0.7	46.66667	32	**10**	n/a	n/a	n/a
0.69	48.5	34.2	12.75	n/a	n/a	n/a
0.68	50.33333	36.4	15.5	n/a	n/a	n/a
0.67	52.16667	38.6	18.25	n/a	n/a	n/a
0.66	54	40.8	21	n/a	n/a	n/a

0.65	55.83333	43	23.75	n/a	n/a	n/a
0.64	57.66667	45.2	26.5	n/a	n/a	n/a
0.63	59.5	47.4	29.25	n/a	n/a	n/a
0.62	61.33333	49.6	32	n/a	n/a	n/a
0.61	63.16667	51.8	34.75	n/a	n/a	n/a
0.6	65	54	37.5	**10**	n/a	n/a
0.59	66.83333	56.2	40.25	13.66667	n/a	n/a
0.58	68.66667	58.4	43	17.33333	n/a	n/a
0.57	70.5	60.6	45.75	21	n/a	n/a
0.56	72.33333	62.8	48.5	24.66667	n/a	n/a
0.55	74.16667	65	51.25	28.33333	n/a	n/a
0.54	76	67.2	54	32	n/a	n/a
0.53	77.83333	69.4	56.75	35.66667	n/a	n/a
0.52	79.66667	71.6	59.5	39.33333	n/a	n/a
0.51	81.5	73.8	62.25	43	n/a	n/a
0.5	83.33333	76	65	46.66667	**10**	n/a
0.49	85.16667	78.2	67.75	50.33333	15.5	n/a
0.48	87	80.4	70.5	54	21	n/a
0.47	88.83333	82.6	73.25	57.66667	26.5	n/a
0.46	90.66667	84.8	76	61.33333	32	n/a
0.45	92.5	87	78.75	65	37.5	n/a
0.44	94.33333	89.2	81.5	68.66667	43	n/a
0.43	96.16667	91.4	84.25	72.33333	48.5	n/a
0.42	98	93.6	87	76	54	n/a
0.41	99.83333	95.8	89.75	79.66667	59.5	n/a
0.4	101.6667	98	92.5	83.33333	65	**10**
0.39	103.5	100.2	95.25	87	70.5	21
0.38	105.3333	102.4	98	90.66667	76	32
0.37	107.1667	104.6	100.75	94.33333	81.5	43
0.36	109	106.8	103.5	98	87	54
0.35	110.8333	109	106.25	101.6667	92.5	65
0.34	112.6667	111.2	109	105.3333	98	76
0.33	114.5	113.4	111.75	109	103.5	87
0.32	116.3333	115.6	114.5	112.6667	109	98
0.31	118.1667	117.8	117.25	116.3333	114.5	109
0.3	120	120	120	120	120	120

Appendix R

Extra plot of route 388 operating day simulation

Figure R-1 showed the power balancing of the model throughout the operating day of route 388. Although the plot is too compressed to see the details, it can still be observed the Psc_out is always slightly smaller than the load power profile. The difference is been covered by the FC and boost converter output as expected.

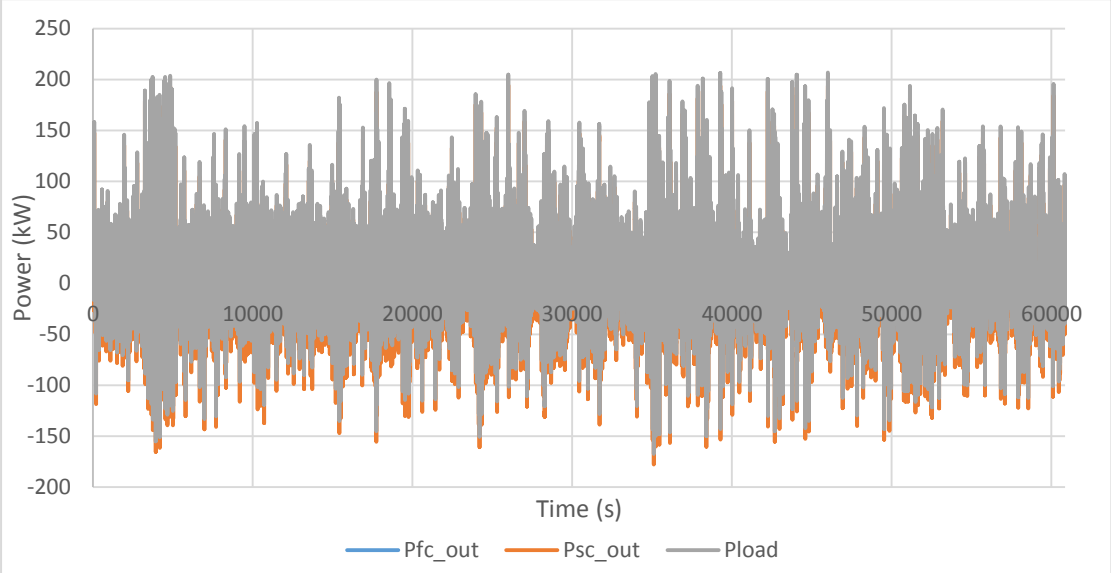

Figure R-1 Power balancing of the FC/SC hybrid for the entire operating day

Figure R-2 showed the FC output power (Pfc_in) throughout the operating day. The FC output power responds to the FC and boost converter output reference (Pfc_out) because FCs are passive power sources. The boost converter has been found to have a 97% average efficiency throughout the entire day.

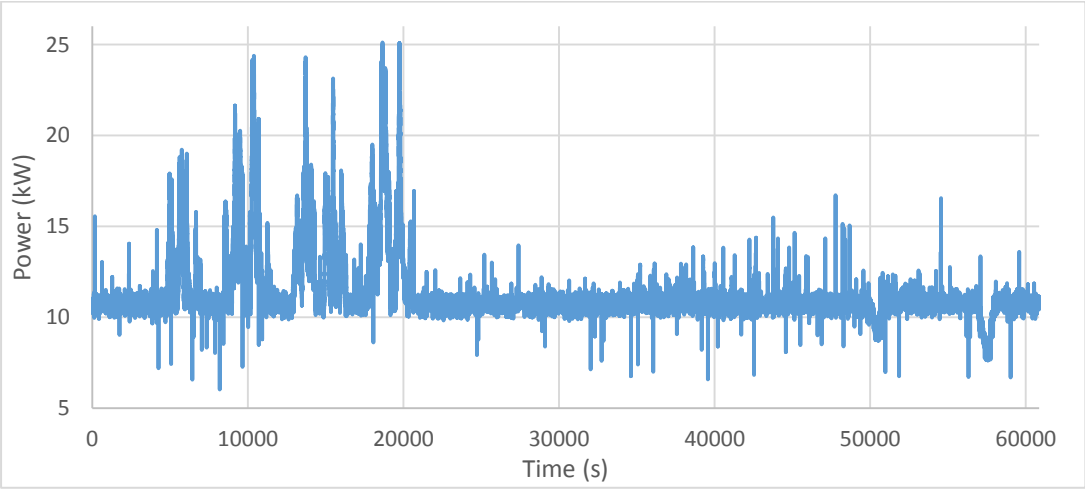

Figure R-2 FC output power of the FC/SC hybrid for the entire operating day

The efficiency of the FC and the hydrogen consumption have been plotted in Figure R-3 and R-4.

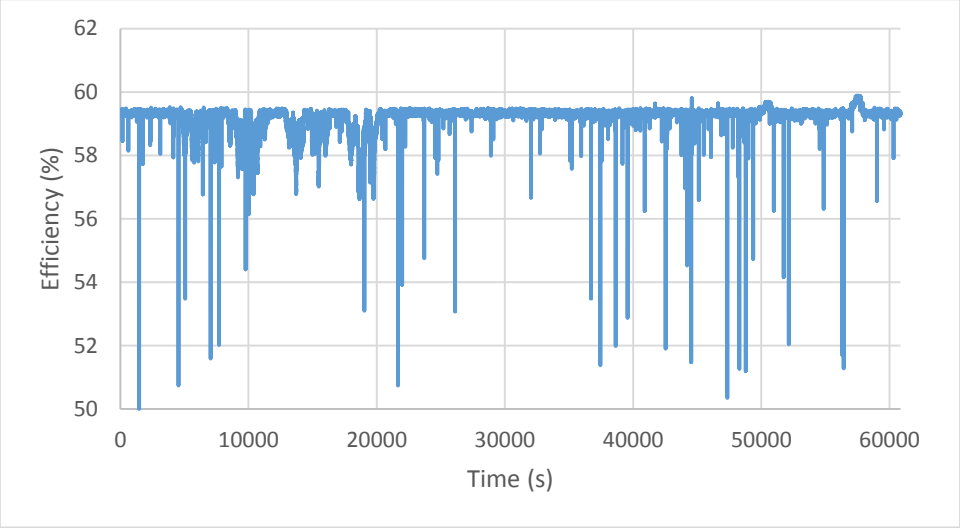

Figure R-3 FC efficiency of the FC/SC hybrid for the entire operating day

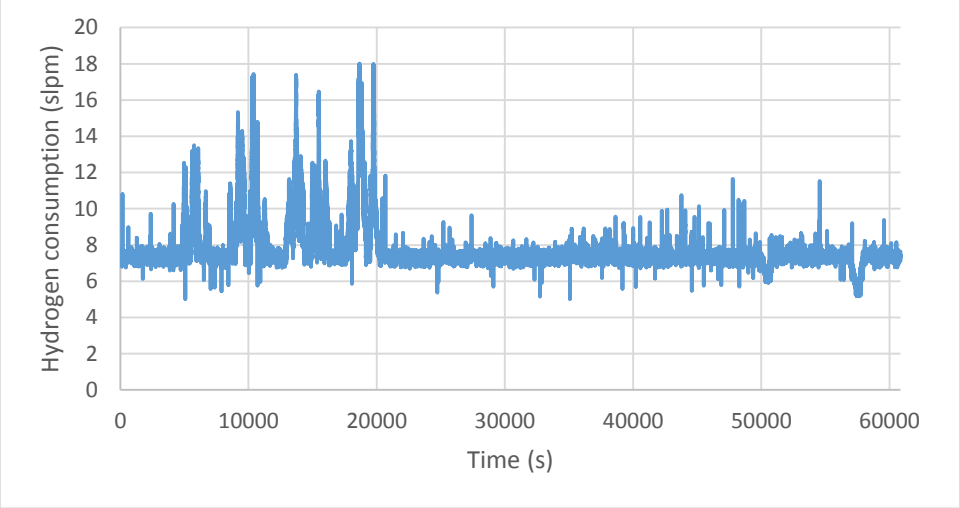

Figure R-4 FC hydrogen consumption of the FC/SC hybrid for the entire operating day

Since no graphs were provided for the 85 kW FC selected for the full scale model study in this research, the efficiency and hydrogen consumption of the 85 kW FC can be subjected to change. The 85 kW full scale FC model was unable to be validated. As a result, the FC efficiency and hydrogen consumption were not included in this research. Although the exact numbers might be different, it can be observed the FC followed the expected trend addressed in this research. The FC efficiency dropped as the required power increased. The increased power would also increase the hydrogen consumption. Those two parameters can be analysed as part of the future work once the full scale FC can also be validated.